MATTHIAS-PETER SCHÖPFER

TACTILE PERCEPTION OF COGNITIVE ROBOTS

DISSERTATION ZU ERLANGUNG DES AKADEMISCHEN GRADES EINES

Doktors der Ingenieurswissenschaften

DER TECHNISCHEN FAKULTÄT UNIVERSITÄT BIELEFELD

Vorgelegt von
Matthias-Peter Schöpfer
Technische Fakultät
Universität Bielefeld

Dezember 2011

Gedruckt auf säurefreien und alterungsbeständigen Papier nach DIN/ISO 9706

Contents

List of Figures

List of Tables

Part I

Introduction

Robots are on the verge of leaving the capsuled and structured working environments of factory assembly lines. Flexible work cells[1] allow cooperation of humans and robots at a new level. Safe interaction between often quite powerful manipulators and men without the need for classical safeguarding equipment or safety light curtains are within reach. This factory scenario is, however, still a very constrained one compared to robots entering not only the working environment of trained experts, but also into people's homes. Up until now, specialized niche robotic devices have been available that can clean floors and windows, or serve as toys or entertainment robots. Without degrading the accomplishments of these robotic tools, the goal of general purpose robots in the homes remains yet an illusive one.

[1] In modern flexible manufacturing the robots' workspace and task are highly reconfigurable and allow fast adjustments to new component parts and work flows

The broad propagation of robotic assistance systems is in part held back by the inability of present systems to dexterously manipulate objects in unstructured and unknown environments. Of course, other factors like the pricing, reliability, usability and maintainability are inhibiting the popularity of the few already available devices even further. To cope with the challenge of dexterous manipulation, most scientists pursue a strategy of replicating the functionality of the most versatile tool known: the human hand.

The Key components of dexterous manipulation are: a high number of degrees of freedom, compliance and haptic sensing. In the human hand, both kinesthetic and tactile perception are important for solving tasks. In this thesis, we investigate the artificial tactile and haptic sensing in robotic devices, with a particular focus on tactile sensing.

The combination of tactile and kinesthetic sense, is called haptic perception. Tactile perception includes pressure, vibration, thermoreception and the nociceptive sense [215].

"Tactile sensing for robotics is still in its infancy" [350].

There is a growing interest in the robotic community in tactile sensing. The number of publications in the most important robotic journals and conferences regarding tactile sensing have more than doubled during the last six years (see Fig. 1). Compared to other modalities like vision, however, tactile sensing has been neglected by robotic researchers. Research in robotic tactile sensing can be divided into two main fields: the development of tactile sensing devices and the processing of tactile data. At the time of writing, tactile sensing devices that can just approach the performance of the human sense of touch seem out of reach. Further research and development in this area is definitely needed. Despite this fact, however, the use and exploitation of available sensors should not be neglected. Tactile sensing is indispensable for in-hand manipulation and can reveal object properties that cannot be acquired by optical sensors.

A tactile sensor is "a device or system that can measure a given property of an object or contact event through physical contact between the sensor and the object" [202].

Material properties that need haptic sense include compliance, texture and friction, weight as well as temperature or rather thermal conductibility.

It is important to explore the properties of artificial tactile sensing and to study the resulting tactile data. We are investigating all of the essential challenges in dexterous manipulation: recognition, grasping and the manipulation and modification of grasped objects; with a strong emphasis on the artificial sense of touch. In this thesis we present state of the art tactile robotics. We also highlight current

shortcomings with a view to steering the design and development of new sensing devices.

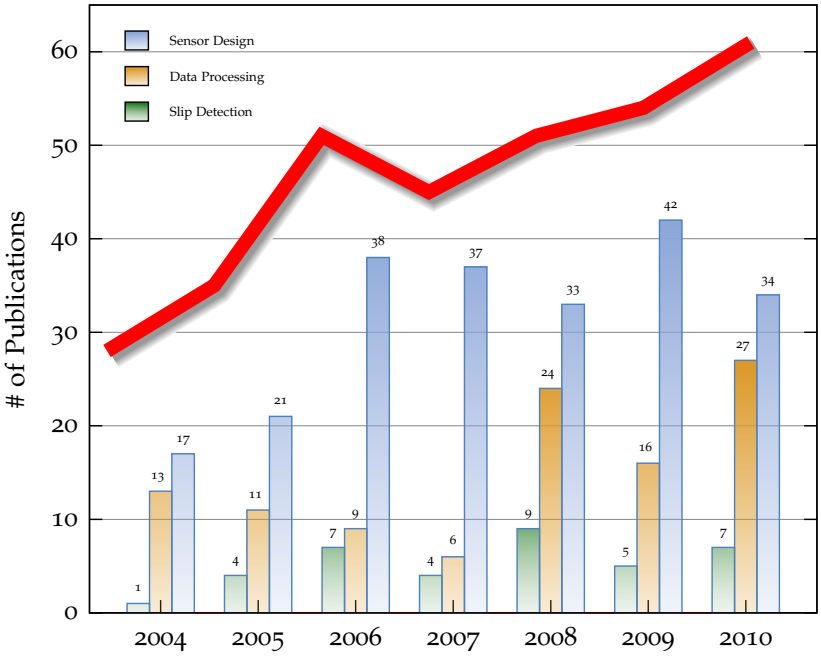

Figure 1: During the last years, an increase of publications dealing with artificial tactile sensing can be noted. Still, most publications investigate sensor designs. The conference proceedings and journals thoroughly investigated include, but are not limited to, IEEE/RSJ International Conference on Intelligent Robots and Systems, IEEE International Conference on Robotics and Automation, IEEE Transactions on Robotics, 2010 IEEE Haptics Symposium, The International Journal of Robotics Research, IEEE Sensors Journal, Proceedings of IEEE Sensors, IEEE Transactions on Haptics.

IMPORTANT LESSONS CAN ALSO BE LEARNED from psychophysical and neurophysiological experiments. A deeper understanding of human tactile sensing allows for the development of biologically inspired algorithms and should help to build systems that can perform better in general situations. However, these insights could prove interesting for the neurophysiological community. Since the processing of tactile stimuli in humans is not completely understood, artificial architectures may give inspiration back to the field of human studies.

A recent study shows that touch is considered the second most important modality in evaluating products [299].

THE AIM OF THIS DISSERTATION is to exploit tactile sensing in robotic setups, especially cognitive robotics, and to enrich and augment commonly used modalities and methods. To this end, different aspects of tactile perception have been covered. We begin by providing a summary of interesting findings from the neurophysiological community. We then present solutions to a number of challenging technical issues that had to be overcome in order to work at the frontier of this uncharted territory. The next chapters deal with the artificial sense of touch. Tactile object recognition is one of the most matured areas of applied tactile sensing in robotics. Two very different and novel approaches in this domain are presented. The first one introduces the idea of entropy in tactile stimuli. The primary goal is not classification, although the results are very competitive, but rather to gain some insights into artificial tactile processing and possibly relevant feature vectors. In the second approach, an artificial robot hand equipped with tactile sensors

The three main aspects of this thesis include:

- Tactile Object Recognition
- Tactile Determined Grasp Force Adaption
- Handling of Deformable Material

was used to probe previously unseen objects. A well known probabilistic method was employed to enhance the gathered information. The acquired 3-D point clouds open up many new possibilities to improve the perception of the robotic system, for example through sensor fusion with 3-D vision systems. Object recognition is a welcome by-product of this method.

Tactile sensing can contribute in many different ways to enhance the overall performance of robotic systems.

We continue in this thesis focusing on optimal grasp force determination through slip detection with a static tactile sensor. Detection of incipient slippage is a very important aspect of tactile sensing as it allows for the adjustment of the grasp force without any prior knowledge about the weight and friction of the object. Furthermore, a quick reaction to changes of initial conditions (think of the filling of a glass) has become possible making it an indispensable component of a cognitive robotic system. That may also be the reason why slip detection has drawn such great attention in the tactile robotics community recently. Finally we use touch to deal with one of the great challenges in robotics: the handling of deformable material. Relatively little research has been carried out in this new and demanding field. This is why we decided to take some first steps in the direction of tactile guided manipulation of deformable objects. Even though the handling of deformable materials was not solved in all its generality, the conducted experiments are an initial move towards tactile driven acting and reasoning.

Structure of the Thesis

This thesis is divided into six parts. In part I, a general introduction into the topic of this thesis is given. The following sections give the reader background information on important findings in the human studies and then continue to discuss related work that had the most impact on this work and the robotics community. The chapter closes with a short section where the author gives some acknowledgments. Part II is dedicated to all the technical issues that arise when working with such complex technical systems. We discuss some of the invented solutions that build the strong foundation the rest of this thesis is based upon. In the next three chapters, namely part III,IV and V, tactile perception of cognitive robots is investigated from three different perspectives. Each chapter starts with an in-depth review of related work, providing a broader image of this aspect of tactile based robotics. We investigate tactile object recognition, the adaptation of grasp force in combination with the detection of incipient slippage, as well as the handling of deformable material. In part VI, a conclusion is given.

Short Table of Contents:

The summary of some interesting findings from the neurophysiological community is meant as an introduction to the sense of touch. The aim of this dissertation is to exploit tactile sensing in robotic setups, especially in cognitive robotics, and to enrich and augment commonly used modalities and methods. To this end, different aspects in tactile perception are covered in this thesis.

This thesis about tactile perception of cognitive robots is supported by three pillars: object recognition, slip detection and manipulation of deformable material.

When working with new, innovative hardware, like the robots and tactile sensors used throughout this thesis, inventive solutions to arising problems have to be found. The solutions found here comprise an engineering accomplishment that shall not be skipped, as the rest of this thesis would not have been possible without tackling the questions of hardware control first.

In the following, Tactile object recognition is addressed as one of the most matured areas of application of tactile sensors in robotics. The two presented approaches focus on aspects of tactile object recognition that have not been investigated before. At first, an entropy based method is used for classification of objects based on tactile views of the object. The proposed architecture enables us to analyze a large number of tactile features and their contribution to the task at hand. The second approach facilitates a robot hand

equipped with tactile sensors. A tactile based grasping procedure is used to acquire haptic data from the test objects. This data is processed with a well known probabilistic method which is successfully adapted to the tactile data domain. The resulting 3-D point clouds allow for a seamless data fusion with other modalities. The object recognition task serves to prove the validity of the method.

We continue on analyzing the optimal grasp force without any knowledge about the objects friction or weight. To this end, a slip detection algorithm for the used high-speed tactile sensor arrays is implemented and validated. In addition, an experiment for the dynamic detection of fine surface features, i.e. textures, is made. The results are highly relevant to any real world grasping application.

Finally, touch is used to handle one of the great remaining challenges in robotics: the handling of deformable material. In the presented experiment, the properties of materials regarding their elasticity and plasticity are investigated. In addition, arbitrary shaped pieces of plasticine are deformed to a ball.

A picture sometimes says more than a thousand words. This is even more true for moving pictures. Hence, where appropriate, a reference to a video on the enclosed storage medium is added.

Previous Work

In the preparation of this work and during the process of experimenting and evaluating, quite some research was done in this area and adjacent fields. In addition, this thesis investigates three neighboring but yet distinct aspects of tactile sensing. Therefore, this thesis is arranged in such a way, that every chapter will give a detailed review of strongly related publications in this specific area of tactile based robotics. In this section, however, a broader overview shall be given, mentioning those beacons in robotics research that have a strong association to the research questions addressed here. In addition, a diligent review of the most important findings from the neurophysiological and psychophysics community will provide interesting insights into the human sense of touch, giving us crucial cues to some of the technical challenges we experienced in this work.

The remainder of the chapter will give a broad overview of related work. Each part, however, will give an additional in-depth review on related work.

Human Sense of Touch

The skin fulfills several important functions to the human body in a remarkable fashion. It provides mechanical protection against heat and cold, fluids, radiation and infections [104]. It is also an essential part of our metabolism and important for our heat regulation. Skin provides the important sense of touch, consisting of tactile, thermal, painful and pruritic submodalities. The sense of touch is not only important in a vast number of everyday activities but it also has a social, affective aspect to it - in contrast to the sensation of pain [90, 115, 231, 245]. The following paragraphs focus on the tactile submodality (sensation of pressure, texture and vibration) and summarizes results that can be found in a number of publications [314, 230, 54, 197, 31, 69, 81, 172, 73, 84, 240, 316, 215]. Individual references were given, where appropriate.

The human sense of touch includes:

- Tactile Sensation
  - Pressure
  - Texture
  - Vibration
- Thermal Sensation
- Pain
- Pruritic Sensation

The skin consists of three layers: the epidermis, the dermis or corium and subcutis or hypodermis (cf. Fig. 2). The epidermis is mostly composed of keratinocytes and is 0.03 – 4 [mm] thick. The dermis mainly consists of papillae but also accommodates capillary blood vessels, the lymphatic system and receptors for temperature, pain and the tactile senses (pressure and vibration). In a fully

grown adult, the skin covers a surface area of approximately 2 [m^2]. The skin contains about 2 million sweat glands and 5 million hair follicles, covering almost all surfaces except for the soles of the feet and the palms of the hands. These areas are referred to as glabrous skin [230].

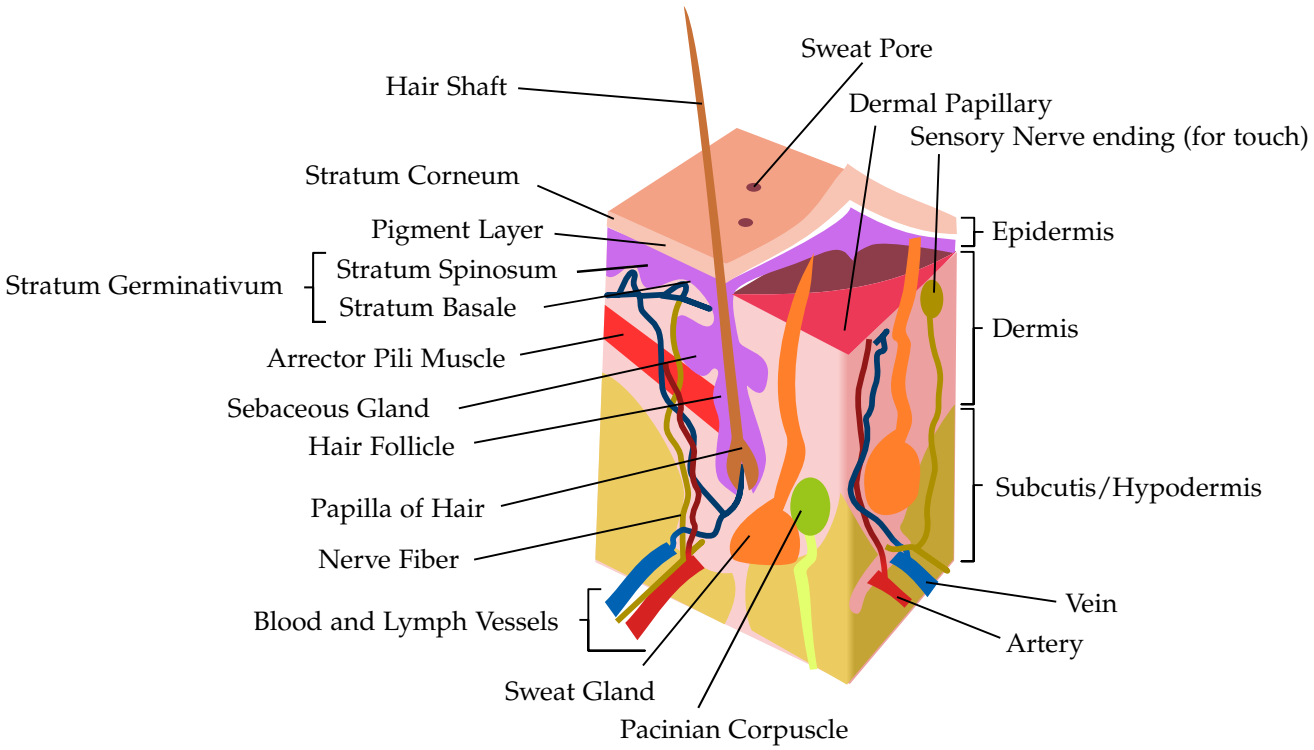

Figure 2: Schematic drawing of the human skin. Source: US Government (Public Domain).

Receptors

THE TACTILE ASPECT OF THE SENSE OF TOUCH is composed of four receptors. These act for the perception of pressure, vibration and texture.

I. Pacinian corpuscles
II. Meissner's corpuscles
III. Merkel disks
IV. Ruffini endings

While the Meissner's corpuscles and Merkel disks are found in the upper part of the dermis, the Pacinian corpuscles and Ruffini endings are located in the lower parts of the dermis. As a consequence, they differ in their receptive fields. The most discriminating feature though is the difference in adaption, i.e. the impulse output of the cells. While the receptors of the fast adapting type will drop to zero or a baseline activity, as long as the stimulus does not vary,

the slow adapting mechanoreceptors will respond to the stimulus for its full duration (cf. Fig. 4). Whenever the stimulus changes, the slow adapting receptors will change the frequency of the output spikes. Both types are further differentiated into type I and II depending on the receptive field (type II receptors have a larger receptive field).

An overview of the receptors is given in Table 1. Depending on the body area, the distribution of the different mechanoreceptors differs. The figures listed in Table 1 are typical for the fingertips, where the highest density of mechanoreceptors is found. The density in the back of the hand is about 60 – 75 % lower. Other parts of the body (e.g. the back) are more sparsely covered with mechanoreceptors. This is also found in the somatosensory cortex [267], where hands and lips (e.g. areas with high density of mechanoreceptors) are overrepresented while the torso and arms are underrepresented.

Figure 3: A visualization of the somatosensory cortex: the body-parts are scaled to reflect their representation in the human brain.

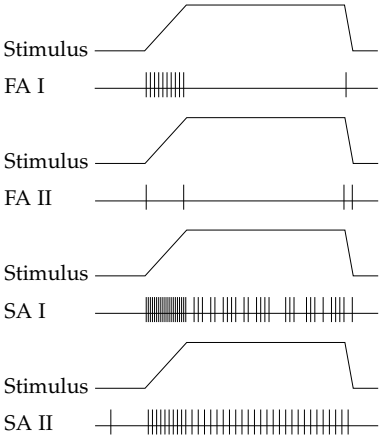

Figure 4: The simplified response behavior of the different mechanoreceptors to a stimulus. Adapted from [230, 240, 197, 371].

Throughout decades of research, the psychopysical model suggested in [29] holds valid until today. In this model, the frequency range of 40 – 500 [Hz] or sense of "vibration" is mainly perceived with the Pacinian corpuscles [221]. Meissner corpuscles operate in the range of 2 – 40 [Hz], what is perceived as "flutter". Merkel disk are most sensitive at frequencies in the range of 0.4 – 2.0 [Hz] and account for the perception of static pressure. The Ruffini end organs are receptive at 100 – 500 [Hz], which produces a "buzzing" sensation. Please note a deviation from the ranges given in Table 1. This is mostly because the precise measurement of the spiking and response behavior of single receptor cells is extremely hard, if not almost impossible. Also this model, of course, refers to the "sweet spots" of the receptors. This does not mean that the receptor is completely unresponsive beyond the given frequencies.

Receptor Type	Afferent Fiber	Receptive Field [mm^2]	Frequency Range	Receptors [$1/cm^2$]	Sensitive to
Meissner's Corpusle	FA I (RA)	1 – 100	10 - 200	140	Dynamic light touch, Motion & Vibration
Pacinian Corpuscle	FA II (PC)	10 – 1000	40 – 800	21	Dynamic touch, Vibration
Merkel Disk	SA I	2 – 100	0.4 – 100	70	Static light touch, Texture
Ruffini Endings	SA II	10 – 500	7	49	Static touch, Skin stretch

Table 1: A listing of the mechanoreceptors contributing to the tactile aspect of the sense of touch with description of the function and receptive field. Adapted from [69, 197, 31].

Information Processing In [180], an upper bound for the skin as an information channel is determined. A pulsatile stimulation is used in the experiment. The upper bound limit for the tactile sense is set to 100 [$\frac{\text{bit}}{\text{s}}$], and is backed by normal reading speed of braille, which is reported at about 60 [$\frac{\text{words}}{\text{min}}$]. These numbers, however, must be read with care, since they are very task-specific. The sense of touch operates very quickly regarding various material properties but needs a considerably longer time for spatial features, for example those found in braille [195]. Tactile perception in search tasks can

The information rate of the tactile sense is 100 [$\frac{\text{bit}}{\text{s}}$].

be significantly boosted by using the whole hand instead of one finger or by using two hands instead of one [260].

Spatial Acuity To reveal the spatial resolution of the human skin, different tests have been employed. The two point touch threshold presents two stimuli to the subject and the minimal distance is determined where the two stimuli could subjectively be discriminated. The alternative is the point localization threshold, where two stimuli are presented one after the other. The subject has to distinguish if the stimuli was presented at the same or at a different spot [153].

Spatial resolution at the fingertip is about 1 – 1.7 [mm]. The tactile sense therefore performs better than the auditory sense, but worse than vision.

Another approach facilitates braille patterns, Landolt C symbols or handcrafted relief patterns in different sizes. The spatial resolution at the fingertip is determined in the range of 1 – 1.7 [mm] [371, 297, 207, 372, 374, 364, 62]. The only area yielding better resolution is the lip (0.55 [mm]) [297]. A decrease in the performance is noticed from index to the little finger [374, 297] with a significant decrease in the little finger compared to the other digits. The spatial acuity decreases with the age of the subjects. An approximate decrease of 1 % per year is noted [363, 364]. This holds only true for sighted individuals. Blind subjects did not only exhibit a higher resolution but also suffer from significantly lower deficits in their spatial acuity when growing older [204, 251, 372, 364]. The spatial resolution at other parts of the body may be up to 10 times lower [189].

It has been found that women are able to perceive finer surfaces than men in a passive tactile acuity experiment. Furthermore, this phenomenon could be explained since it was proven that the finger size is directly related to the spatial resolution of the fingertips. This correlation explains why women outperform men as they tend to have smaller hands than men [268]. Spatial acuity decreases substantially if the stimulus used vibrates at frequencies above 5 [Hz], although the spiking behavior of the FA I and SA I cells are not affected [17]. In addition, the spatial resolution is independent from the amplitude of the stimulus [16].

Temporal Acuity The temporal resolution of the human skin can be approached from two different perspectives: the perception of vibrations and the discrimination of two consecutive taps on the skin. The latter is reported to be about 10 – 12.5 [ms] (according to [93, 316]). This data is generally confirmed [269], where a mean interval of 13.23 [ms] is reported for young subjects. The elderly group had a considerable higher interval (avg. 28.50 [ms]). This effect is notable not only with the sense of touch, but also in vision and hearing [134].

The temporal resolution is around 12.5 [ms] or 80 [Hz]. Hence, the sense of touch performs better than vision, but worse than hearing.

To put these figures in comparison with other modalities, touch performs better than vision (25 – 30 [Hz] [184, 379]), but worse than the auditory sense (in the order of 1 [ms] [287]). It is therefore consistent with findings, that also the cross-modal temporal resolution of audio-tactile perception outperforms audio-visual and visual-

tactile perception (∼10 [Hz] vs. ∼4 [Hz]) [88].

Perception of Roughness, Textures and Fine Surface Features While the temporal and spatial acuity of the human sense of touch are interesting and important figures for engineers and provide some quantitative measures, there are other effects interacting with spatial and temporal responses. This is especially true when it comes to the perception of roughness or texture[2] or even fine surface features. To illustrate this, a small experiment on oneself may be conducted: different materials with an optimally great range of surface roughness shall be scanned with the fingertip at intentionally *varying speeds*. A resulting experience should be, that diverse materials, at different speeds reveal the optimal feel for the surface.

[2] For simplicity, we define texture as a patterned surface roughness, as for example in cloth

The recognition of spatial features decreases if temporal cues are removed and vice versa [91]. Moreover, three parameters for the perception of roughness were determined: Given R as the ridge width and G as the groove width (cf. Fig. 5) as two parameters in regular roughness patterns, the scanning speed S is then the third factor. The effects of R and G are found uniform at spatial ranges from 0.75 – 3 [mm]. The groove width G affects the perceived roughness more than R. The role of S seems to be stronger than the role of R, while G tends to dominate the roughness perception [38]. The relation of R and G are explained by the proportional displacement of the skin and its ridges, which is potentially higher at large values of G. With coarse surfaces (spatial distance > 200 [μm]), lateral movement is not always necessary [349, 198]. With movement, however, spatial periods could be discriminated down to 18 [μm]. There are strong indications that surface features below 200 [μm] are sensed solely through vibrations [123], which are likely encoded by the Pacinian corpuscles [19, 20, 18]. Therefore, movement is necessary to perceive fine surface features or finer degrees of roughness, but even with more coarse surfaces, vibrotactile effects contribute to the perception. For a thorough review on roughness perception and encoding see [122].

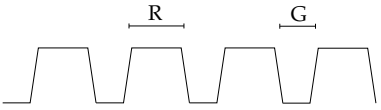

Figure 5: The roughness perception is influenced by the groove width G and the ridge width R.

Besides these findings on the performance of the human tactile sense on the perception of roughness, another interesting result could be retrieved in a series of experiments with 24 different car seat materials [272]. In contrast to the previous cited works, a more 'natural' stimulus was used. The participants were asked to perform free sorting tasks and describe their sensation. As a result, 4 continuous and orthogonal perceptual dimensions for textures were found: soft/harsh, thin/thick, relief and hardness.

Exploratory Procedures Lederman and Klatzky investigated the question of how humans facilitate the sense of touch to interact with objects to elicit certain properties [191]. The focus were the stereotypical patterns of hand movements the subjects executed to reveal different object qualities. In their work, Lederman and

Klatzky gave distinction to the term *Exploratory Procedure* (EP). An EP is a specific action that reveals object properties like contour following, pressing, lateral motion and so forth. The EPs were analyzed for necessity, sufficiency, optimality and specialization for different object properties, for example weight, hardness or temperature. For a complete list of the optimal EPs consult Table 2. A general note about EPs is that they are not disjoint as contour following involves lateral motion and vice versa [170].

Somewhat unexpectedly, enclosure just performs above chance level in the determination of the global shape of objects. Apart from that, enclosure is the least specialized EP. Even young children of 4 – 5 years of age are able to use the optimal EPs to determine whether the properties of objects make them suitable for a certain task [173]. Regarding the recognition of shapes, it could be shown that haptically acquired shapes are biased towards simple and/or symmetric geometric objects [72]. Also if subjects were constrained to certain EPs in a categorization task, they tended to prefer using the primary object property associated with the specific EP. For example when constrained to lateral motion, texture was dominant but when using enclosure, shape was the preferred object category [56].

For a good summary of the findings on EPs, see [193] and especially [194], which also points out some implications to robotics.

Property	Optimal EP
Texture	Lateral Motion
Hardness	Pressure
Temperature	Static Contact
Weight	Unsupported Holding
Volume	Enclosure
Global Shape	Contour Following
Exact Shape	Contour Following

Table 2: Optimal Exploratory Procedures for different object properties according to [191]

In the domain of haptic figure/ground segmentation, that is separating a 3-D object (figure) from its supporting structure (ground) very good performances were noted. In particular, when the object was not fixed to the supporting surface, small micro-movements were sufficient for humans to detect the object [265, 266]. If the object was fixed, usually texture was the cue that led to fast and robust recognition rates.

Tactile Grasp Force Control Various studies have been made to investigate how humans estimate and control the grasp force, for example when grasping unknown objects. This apparently simple action which we fulfill countless times a day involves the correct estimation of different physical properties, and when examined closely, it turns out it is a complicated task. Although, experience and learning from previous lifts, as well as vision, gives important cues [101, 99, 98], the excessively good human performance cannot be explained by experience and vision alone. When determining the optimal grasp force, which is something humans are remarkably good at, it is noted that the force should be sufficient, so the object cannot slip out of the hands. At the same time, it should yet not be excessively more force than necessary to maintain force closure. For one to be able to grasp fragile objects, but also to prevent fatigue in the muscles. This force is dependent on the weight of the object as well as the friction between the surface of the object and the human hand. While the weight of the object can be estimated from visual or haptic experiences [100, 150], humans are prone to misjudgments. The so called size-weight illusion[3] is a clear

[3] A bigger object of the same weight is perceived as being lighter than the smaller object. Or, with same-sized objects of different masses, the lighter object is perceived as bigger.

indication that the grasp force is not solely dependent on the perception of the objects' weight. The second parameter, friction, is much harder to quantify, and highly constrained by external conditions like moisture. Also the transition from stick to slip condition is highly non-linear and therefore hard to predict at times.

So given the difficulty of the task, how does the human achieve such excellent results in grasping? Ronald S. Johansson found evidence that the human sense of touch is involved in the grasp force adaption [381, 147, 371, 382]. In the conducted experiments, the participants had to grasp the apparatus with a precision grasp of the thumb and index finger [63]. The weight of the apparatus could be varied, as well as the surface (sandpaper, silk or suede). The outcome of these experiments was that subjects needed only 0.1 [s] to adapt the grip force to the load and friction circumstances. It was also found that particular the FA Type I and II as well as the SA I are involved in this process. Astonishingly, when slips where provoked, adaption took as little as 0.06 – 0.08 [s] [148, 149]. This leads to the conclusion that this process is highly automated and may not run solely in the somatosensory cortex. In a later study, the finger was stimulated with a vibrotactile display. There, 30 [Hz] was the frequency that most responsively triggered an increase in the grip force, which leads to the assumption that mainly the Meissner's corpuscles (FA I) are responsible for the detection of incipient slippage [225]. When the skin was anesthetized, the task could still be fulfilled, albeit with much higher grip forces. This leads to the conclusion that proprioception also has its part in this concert of receptors to solve this task. When subjects grasp, they exceed the minimal necessary force by a certain safety margin. This margin remains constant across tries but changes inter-subject. Hence, it can be assumed that this behavior is learned, see [84] for more support.

Through particularly the FA I, but also FA II and SA I mechanoreceptors, humans are able to determine the optimal grip force in 0.1 [s] and react to slippage events within 0.06-0.08 [s]. The safety margins in the grip force can always be found, but vary from subject to subject.

Vision and Touch

In an early study on the relation of vision and touch subjects were presented with objects. The visual size appearance of these objects, through the use of a lens, differed from the haptic impression [285]. The task was to draw or to identify the object later. The experiment showed that the visual impression dominated the haptically acquired. Very few subjects were reported to have noticed a conflict between the different modalities. It should be noted, however, that the task, since the objective was to identify the size of the object, was biased towards visual perception and hence not a fair choice to gain true insights in this conflict [174].

Early studies showed the predominance of vision over touch. This was put into perspective by later works.

In another study, it is shown that visual recognition of miniaturized objects outperforms haptic recognition with 2.5 and 5-year old subjects [27]. These two results suggest that touch is not the preferred modality for 3-D shape and size perception. Interestingly, a very recent work compares the perceptual spaces of vision and

touch [89]. In this experiment, subjects are asked to discriminate artificial (with 3-D-printing) shells that have been varied along three dimensions in the space of shell variations. In an additional experiment with real sea shells it was shown that the results generalize well. The authors found a high correlation between haptical and visual similarity perception. This points to similar object representations across the modalities.

When subjects interact with products, the relative importance of modalities is found to depend on the type of the object as well as the task at hand [299, 77]. Although vision was rated overall the most important modality in judging a number of products, touch was more important than smell, sound and taste. Interestingly, the subjects thought they would miss the auditory sense more than touch, which the authors account to the social aspects of hearing (speech). Also they add that it would be hard to imagine having no sense of touch, and that it is even "doubtful whether any person could survive without being able to perceive [touch]", which might be taken into account when looking at these results.

In [214] it is shown that visual and tactile perception are at roughly equal performance, if the visual spatial resolution is reduced to the level of touch. The author presents a counterexample to the hypothesis that a functional similarity exists between the two modalities. In an experiment, it was found that vision was prone to a certain masking effect while touch responded in the opposite manner.

Extending their work on Exploratory Procedures [191], the authors (Lederman & Klatzky) state that vision can be regarded as another Exploratory Procedure [174]. It is argued that every EP has costs, in terms of time needed for the execution and cognitive processing, with each EP yielding a specific portfolio of object information, e.g. shape and size through vision, or temperature through haptic interaction. Therefore, a weighting of the EPs is proposed. The results of the conducted experiment, which consisted of a comparison of two objects along a scale of roughness, hardness, temperature, weight, size or shape and their semantically accessibility, lead the authors to propose three models for the exploratory control in humans (cf. Fig. 6). The results suggest that the "Visual Preview Model" conforms best, although the other models could not be disproved. Another finding of the study is that touch was frequently used when material properties like roughness, weight, temperature and hardness were in question, and considerably less often when geometric properties were asked for. The haptic interactions used conform to the suggested EPs in [191]. In an additional experiment where haptic exploration was extrinsically delayed, it was shown that vision generally cannot serve as a substitute for haptic exploration. The hypothesis, that material properties are relatively more

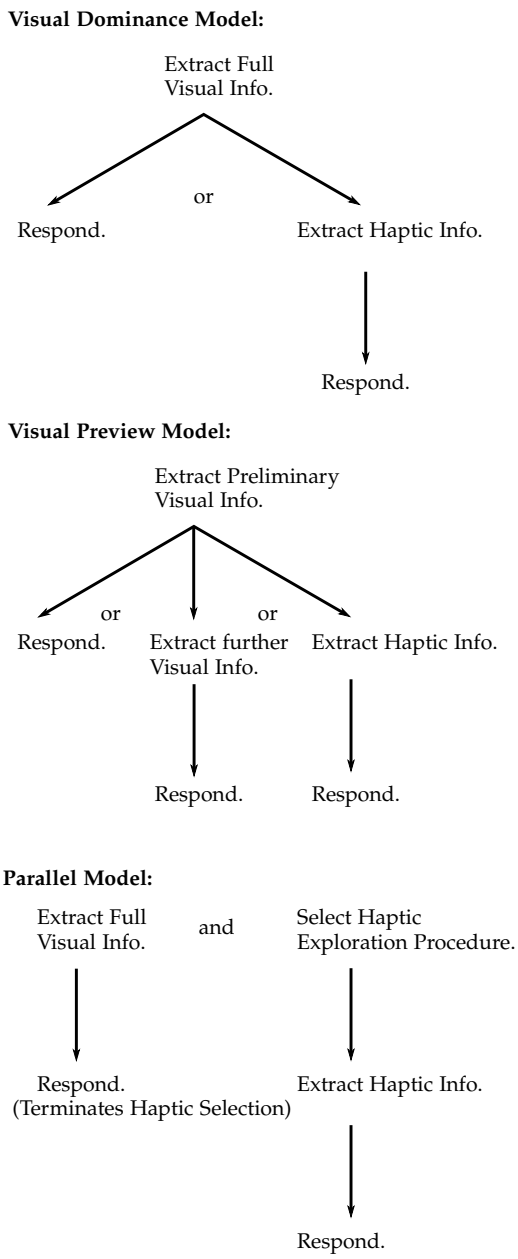

Figure 6: These are the models of exploratory control as proposed in [174]. Although the authors state that all three models are in principle consistent with the results from their experiments, the Visual Preview model seems to fit best to the findings from the experiments.

important than shape and size under haptic exploration, is made and supported by [176]. If available, visually explorable properties like shape and size became more salient than those haptically acquired, which can be explained by the lower effort that is usually required to gain this information. In the conducted experiments, however, we see, that haptic exploration is very goal-directed in terms of unveiling the objects' material properties.

If only vision is used, shape tends to dominate object categorization. If haptic interaction is also permitted, shape and texture are at equal level with shape.

In a recent study, the influence of vision and touch were investigated in a task where subjects had to judge the similarity of objects as well as to categorize them [55]. The objects in question were all novel to the subjects. The test set was generated with a 3-D printing device. The objects varied in shape as well as in their texture. The range in texture is somewhat limited since all objects were made from the same material and the spatial resolution of 3-D printers is restricted. When using vision, shape clearly dominated the outcomes, but when using haptics or allowing bimodal interaction with the objects, texture and shape were at equal levels.

Object interaction with vision present is faster than pure haptic interaction.

The performance of manipulation tasks with, without or only partial vision has also been examined [278]. All manipulation tasks could be performed without vision, but, of course, at the cost of a longer execution time (approximately $\frac{1}{3}$ longer compared to using vision). Once a model of the task was learned, the execution times could be decreased getting close to the time archive with vision. Hence, a (learned) task model can somewhat be substituted for visual perception.

Texture sensing requires dynamic object scanning.

Regarding the perception of texture there are indications that information is encoded qualitatively different across the modalities [385]. It is stated that both senses require dynamic scanning for texture perception; for the tactile sense either actively or passively dynamic (i.e. in the latter case, the finger is fixed and the sample is moved). The differences, however, are that the active eye movement and fixations were not affected by different textures, while the active dynamic tactile exploration is affected. Visual perception yields important cues for the haptic exploration of the objects' surface, nevertheless, cross-modal performance is often not better.

Influence of the size-weight illusion.

Vision cues are used for preshaping and grasping, but also for programming of the initial load force.

Through a number of studies, the influence of visual cues on the parametrization or programming of the load force of the grasp were analyzed [145, 146]. In [101] subjects are confronted with the size-weight illusion (for details on the size-weight illusion, see [8]). Three boxes of different size, yet having the same weight are presented to the subjects. Although all subjects concordantly reported that the smallest box was the heaviest, which is consistent with the size-weight illusion, the initial grasp force and vertical acceleration increased with the box size.

Interestingly, no difference in the grip forces during the static

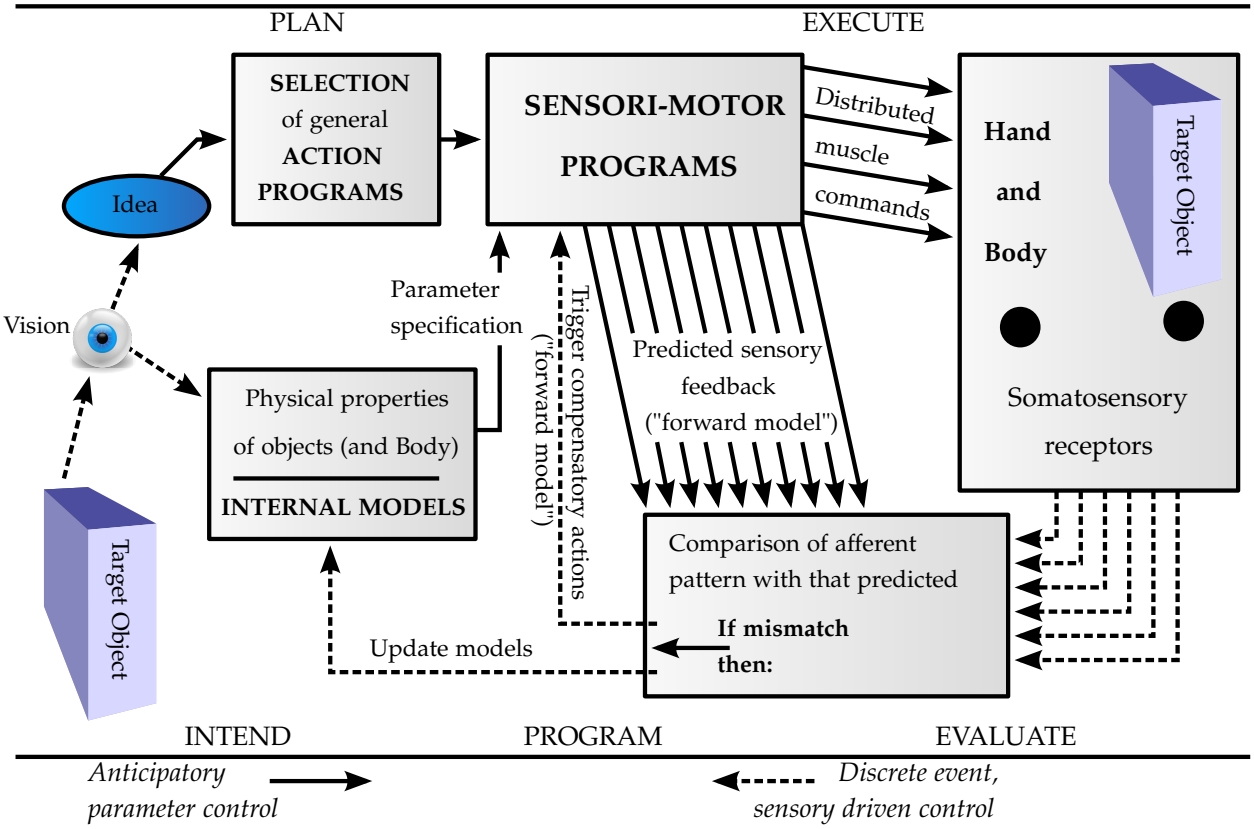

Figure 7: A model of the predictive feed-forward sensory control of manipulation according to Johansson [146]. Depicted is the anticipatory parameter control, where internal models of motor commands, which conform to visual and haptical percepts, are specifically parametrized prior to execution. If a mismatch between the anticipated and actual input occurs (e.g. a novel object), "single trial learning" is triggered, including pre-programmed corrective motor patterns. This behavior is called discrete event, sensoydriven control.

phase of the lift could be verified. This leads to the conclusion, that visual cues are used to parametrize initial grasp forces, while the grasp itself is influenced strongly by somatosensory input. A correlation of size, isometric and load forces is developed approximately at the age of 3-4 years [98]. In younger children, no programming effect was found. Visual information at that age is primarily used to preshape their hand and close the hand when close to the object. In addition, the visual influence on programming a grasp is larger at the age of 6-7 than in adults [98].

A MORE COMPLEX STUDY ON THE INFLUENCE OF VISION AND TOUCH was done in [142]. Here, an apparatus with a long horizontal elongation was developed that had to be grasped with a precision grip at one end. The task was to lift the object vertically while keeping the object level and in a horizontal plane. In addition, the device presented a curved surface at the grasp position. The curvature was varied, therefore requesting for different load forces to prevent rotational slip. These experiments were done with and without vision as well as with and without digital anesthesia, hence with and without cutaneous sensibility. Among other things, grip force, torque load, object position and twist were recorded. One finding was, that both vision or digital sensibility can be used to effectively scale the grasp force to the curvature. Another result was that the rotational elasticity of the fingertip pulp was an

The influence of curvature on the grasping task has been investigated, i.e. how humans adapt to different curvatures in the presence and absence of vision and cutaneous receptors.

important control variable in dexterous manipulation as not only rotational slip was tried to be prevented, but also the compliance of the fingertips was compensated and taken into account. When subjects had neither vision nor digital sensibility, they were still able to produce adequate motor commands for the task at hand but generally failed in adapting to the curvature of the apparatus. When vision was available and the subjects were allowed to see the curvature of the grasped surface, the use of internal models let the subjects perform well, giving a good judgment of the objects size and weight. Nevertheless, the digital anesthesia had great impact when vision to the curved surface was disallowed. Although it was possible for the subjects to fulfill the task through corrective motor commands with the vision feedback, actions were delayed in comparison to when full somatosensory information was available. Blindfolded, but not anesthetized individuals were able to adapt within 0.1-0.2 [s] to new curvature conditions. Despite that, the authors suggest a feedforward model of motor control in which mismatches of expected and actual somatosensory information result in a model change. The authors do not address the role of non-anesthetized parts of the somatosensory system, like muscles, joints, tendons, etc. which might also give important information in this task and which would explain the relatively good performance with anesthetized digits and while being blindfolded.

Beyond what has already been reported, other cross-modal effects between vision and touch are possible. For instance, one popular example for a cross-modal illusion would be the McGurk Effect [232], where seeing the lips of the speaker influences the audible perception. In this spirit, the aspects of cross-modal *illusory conjunctions* (ICs) between tactile perception and vision are subject to a study in [52]. In this context, an IC is perceived when a felt perception is experienced as being seen and vice versa. The authors were able to show the existence of cross-modal ICs, which had been reported first and foremost within one modality, in both directions, e.g. tactile to visual and visual to tactile. They could also support previous findings that ICs primarily happen under the condition of divided attention. Another result from the six conducted experiments was that frequency of recognized ICs increased if the stimuli fell into the same hemispace, i.e. the same side of space relative to the body. Regarding the origin of the ICs, namely if they resulted from failures in memory or from not correctly encoded or perceived features, the authors could not account for a single IC resulting from failures in memory. One has to deduct from this empirical data that ICs primarily or even exclusively result from impaired perceptual processing.

Cross-modal illusory conjunctions can be experienced with vision and touch, when felt perceptions are expressed to be seen and vice versa. Tactile illusions are also reported in [190].

Tactile Robotics Review

Tactile feedback has been experimented within robotics for quite some time, albeit with yet limited advertence and effort towards broader acceptance of the importance of tactile stimuli in cognitive robotic setups. However, tactile as well as proprioceptive sensing is very recently becoming more and more the focus of attention in the robotics community (cf. Fig. 1). The journal with the highest impact factor in robotics, the IEEE Transactions on Robotics, has recently published a special issue on the robotic sense of touch. This has to be considered a milestone in robotic tactile sensing and punctuates the development of the past years in this sector. But why has the robotic community neglected this subject for so long? Explanations for this deferment in tactile sensing research are:

IEEE Transactions on Robotics 2011, Volume 27, Issue 3 features a special Issue on Robotic Sense of Touch.

- While audio or vision is perceived through a single, local and small sensor, tactile sensing is distributed over larger areas, and the stimulus is also spread over that area.
- In contrast to other modalities, tactile sensing is not only the transfer of a physical property into a digital signal. Characteristics like texture, shape, force, friction are to be captured into meaningful representations, which is not straightforward. As a consequence, scientists are still searching for an artificial skin that is able to provide the desired data.
- In contrast to other modalities, that can be passively acquired, tactile sensing often involves active and potentially invasive maneuvers to gain data. Therefore, sophisticated algorithms and safety measures have to be taken prior to the usage of tactile sensors [218].
- In fields like computer vision, it is clear that images are to be processed and interpreted. There is little, if any, development of completely novel camera or recording principles. With tactile sensing, the opposite is true. The majority of research is done on tactile sensing mechanisms.
- One of the problems that also has to be approached is the tactile inversion problem, i.e. which stimuli is responsible for causing the tactile perception. This problem arises foremost on sensors with limited dimensions of perception, like tactile sensing arrays that can only quantify forces perpendicular to the surface, or stretch- or flexible sensors, where stress from bending produces signals that can be misinterpreted as strain.

Nevertheless, tactile sensing is and has been considered important among roboticist[4]. Although this thesis is mostly concerned with the processing and understanding of tactile sensor output, a short overview of the most common designs and

[4] "Touch sensing [is] an essential concomitant of vision", "It was felt that [...] touch sensing [is] indispensable, at least for all but the grossest manipulation." [108]

principles in artificial tactile sensing will be given. For detailed information on the different sensing principles, the reader is directed to [246, 247, 244, 64].

Capacitive Sensors

Sensors of this type use a capacitor, or more commonly an array of capacitors with a deformable dielectric. If d, the distance of the two plates is much smaller than A, the area of the plates, the capacity is given as:

$$C = \varepsilon_0 \varepsilon_r \cdot \frac{A}{d} \tag{1}$$

where ε_0 is the permittivity and ε_r is the dielectric constant of the dielectric layer (cf. Fig. 8). Therefore, the distance d can be measured and hence the force acting on the sensor element can be estimated. Sensors of this kind usually allow multiplexing of the sensor cells which reduces wiring. Capacitive arrays usually have good sensitivity and only moderate hysteresis, depending on the specific design and production. Capacitive sensors may suffer from measurement gaps between the sensor elements. Depending on the implementation, the scan rates are limited due to the multiplexing of the sensor cells. Also, capacitive arrays are prone to electro-magnetic fields, which can not always be avoided, especially in a robotic context. Because of their simplicity and robustness, various implementations exist [107, 106, 50, 211, 370]. It was possible to produce a stretchable capacitive sensor with silicon embedded thin gold films [59] or to use flexible printed circuit boards [187, 44, 333]. Since the presence of dielectrics (like for example the human hand) influence the capacity of the sensors, they are usually more sensitive to human touch, and may even be exploited with little more effort for range/proximity sensing [199, 138, 95]. An extremely small and yet flexible sensor with sensing elements of only 250 [μm] radius could be produced [275] with a gap of 1 [mm] center-to-center spacing. Recently, an universal robot skin was developed for the humanoid robot iCub [295] which is also based on the capacitive principle and is also modular [303, 302, 301, 37]. It has been used for full body sensing as well as fine manipulation task in the fingertips. The nowadays very popular "multi-touch" transparent tactile sensors employed in displays of smartphones and touchpads are often also based on the capacitive principle [164].

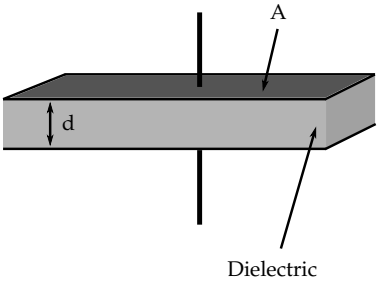

Figure 8: The capacitive sensing working principle: A capacitor consisting of two plates and a dielectric, deformable material is charged.

Optics based Sensors

Sensors that use light in some way to measure the contact forces are probably the most diverse category in tactile sensing. One of the major advantages of optical sensors is the immunity to external electric-magnetic fields[5] [9], and more often than not they are waterproof at the point of measurement. Through the

[5] It is desirable to have tactile sensors available under Magnetic Resonance Imaging (MRI) for certain medical examinations

usage of optical fibers, the necessary electronics must not be on-site [276, 277, 402, 401, 3, 262]. This has its applications in minimal invasive surgery, where space near to the point of measurement is very constricted. The disadvantages of optical tactile sensors are that the temporal resolution is often limited due to CCD-cameras and that the post-processing of the data is time consuming. Also optical sensors tend to be complex and therefore prone to errors. Nevertheless optical sensors offer special abilities that often cannot be achieved with other designs and therefore niche a market, like for example 3 degree-of-freedom (DOF) sensors [400, 397, 399, 252, 253].

An exoskeletal sensor was developed with very high temporal resolution of 5 [kHz] albeit low spatial resolution [28, 264]. Special designs are to be found in [139], where optical tactile sensors were implemented in tracks of a mobile robot to improve locomotion. In [185], slippage is detected by tracking a human fingertip. Custom slip sensors use the working principle of an optical computer mouse [235]. Due to advances in electronics, combinations of LED and light receiver can attain high temporal frequencies [293, 289, 288, 114, 155].

The most prominent working principle can be seen in Figure 9. An interesting concept is presented in [157], where two layers of point patterns allow 3-D force reconstruction.

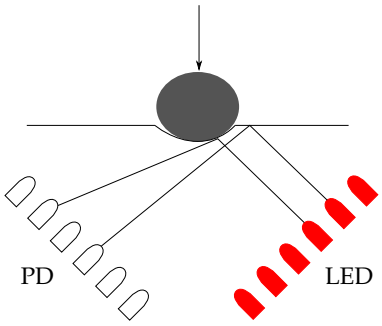

Figure 9: Different optical sensing working principle have been developed. Here, Light Emitting Diodes (LEDs) illuminate a reflective surface. An array of Photo Diodes (PDs) is used to measure the distractions on the reflexions to estimate the force on the sensing element.

Piezo-Resistive Sensors

One of the most common sensor designs is to use a piezo-resistive material, i.e. a material that changes its electrical resistance when pressure is applied. Often, the material is an elastomer (e.g. silicone) with some conductive additive like carbon but also special printed ink or fabrics are used. Since only a voltameter is needed this design is simple. The robustness of the elastomer and carbon fibers make this design very durable. In addition, piezo-resistive sensors have – depending on the material used – low hysteresis and creep [380]. On the downside, the foam has non-linear properties, which makes it difficult to get precise measurements. The cheapest, and also simplest variant are Force-Sensitive Resistors (FSR), which are available for less than 10 €. While basic tactile perception is possible with FSRs, they have a low sensitivity, coarse spatial resolution and suffer from a number of issues, for example they are much less sensitive to pressure from a sharp point than when the pressure is distributed over a larger area. For details, refer to the very recent analysis in [188, 263]. However, some work has been done with FSRs [1, 67, 375, 121, 284], for example in [373], where a sensing array of FSRs was constructed. To compensate for the low spatial resolution of the pad, a super-resolution algorithm from computer vision was employed, which exploits a series of tactile images for that purpose.

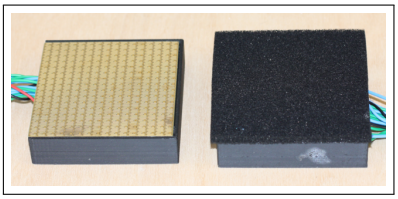

Figure 10: The sensor mainly used in this thesis uses a piezo-resistive elastomer as seen on the right side. On the left, the optimized M-shaped voltameters of the sensor can be seen.

Basically two ways to measure the resistance can be employed. In the two-sided setup, a semi-circle or pyramid shaped elastomer is placed between the two electrodes. When force is applied, the contact area increases and thus the resistance decreases. In the one-sided design, the electrodes are covered by the sensor material as seen in Figure 11. When pressure is applied to the elastomer, the conductivity increases due to a higher contact area and the compression of the carbon fibers that thicken the path of the electricity and therefore cause a lower resistance of the material. The latter is used in advanced sensor designs, like those employed in this thesis [312, 311, 161]. They still suffer from non-linearity, but show a linear behavior over a large area of the stimuli. The newer design allows a temporal resolution of up to 1.9 [kHz], with a spatial resolution of 5 [mm] and a sensing range from 0.5...30 [kPa]. Alternative implementations also exist [329, 358, 36, 182, 357].

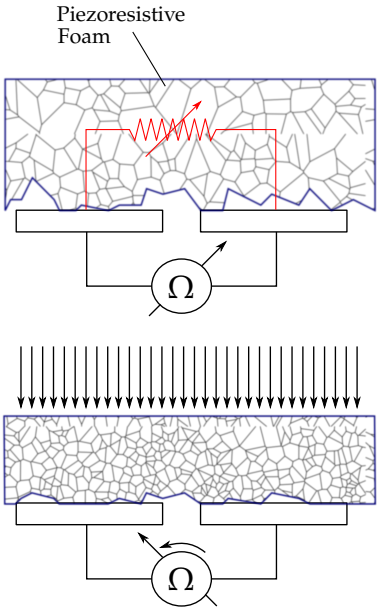

Figure 11: One-sided piezo-resistive sensor working principle. When force is applied, the resistance decreases due to more carbon fibers compressing and virtually increasing the conductive path.

Piezo-Electric Sensors

One of the first tactile sensors exploited the piezo-electric effect which is found foremost in some crystals and ceramics. If a piezo-electric material is subjected to stress or deformation, an electric dipole forms and a voltage is applied. This is, of course, only the case during the deformation of the crystal. Piezo-electric materials deform when a voltage is impressed. The most common piezo-electric material used in tactile sensor design are polyvinylidene fluoride (PVFD), a plastic material. They are popular because of their high bandwidth and since they are simple to put into application. On the downside, piezo-electric sensors are *dynamic* sensors in the sense that they can only detect changes in stress but measuring absolute forces is not feasible, hence they are somewhat similar to the FA Type I and II afferent nerve endings in the human skin. Due to their high bandwidth, they are well suited for the perception of vibrations. Some successful implementations can be found in [47, 51, 66, 348, 87, 335].

Piezo-electric sensors are only sensitive to dynamic touch, but offer high bandwidths and are well suited to detect changes in contact conditions or vibrations.

Other Designs

Various different designs and ideas exist but not all will be covered in great detail here. Of course traditional strain gauges that are commonly used in force/torque sensors can be used in tactile sensing. A most promising area of development is in the field of Micro-Electro-Mechanical Systems (MEMS), where most often strain gauges, but also resistive designs, are employed to produce tactile sensing arrays [217, 318, 331, 273]. Interesting designs with shear sensing have also been presented [45]. The downside of the MEMS technology is that the resulting sensors are fragile. On the other hand if protective coatings are used, sensitivity decreases.

Furthermore, a few designs exploiting the hall effect can be found [332]. More promising are the designs based on fluid coupling though. While good measurement of the applied forces are possible [347, 345, 346, 162, 383] and even some hybrid designs allow thermal sensing [384], a decent spatial resolution is still very hard to obtain.

Another interesting idea is the use of acoustic wave diffraction for tactile perception, as such a method would enable full body sensing on the casing of robots. This method, however, is very novel and suffers from a high amount of noise in the data [210].

Combined Sensing Modalities To mimic the sensing abilities of the human skin, considerable effort has been done to combine tactile and thermal sensing [42, 367, 165, 2, 342, 75, 324, 396, 393, 298]. Even though significant progress has been made, certain difficulties remain. For one, most designs use a special thermal sensor (e.g. PVDF) which makes it hard to obtain tactile information at the same location. Measuring the temperature is an inert process. To gain information about the material, not only the temperature but the thermal conductivity must be found, which calls for a source of heat on the artificial skin. In addition, sensors with combined static and dynamic sensing principles have been fabricated [300, 229, 96, 250].

Tactile Data Processing

A FEASIBLE STARTING POINT IN THE HISTORY of robotic tactile sensing is marked by [168], where a five-fingered robot hand was equipped with 22 digital switches. The authors were able to discriminate two different shapes (cylindrical and square) using hyperplanes in the tactile space. The main contribution of this paper is the solely tactile view on the classification problem. A similar approach is found in [255]. In this paper a robotic hand is equiped with tactile sensors as well (again with only micro switches). The hand is used to grasp different objects. The micro switches, one at each of the phalanges, provide contact information. With the joint positions and data from the switches, a machine learning algorithm could be used to discriminate 5 different objects depending on their shape and size with admissible precision.

Tactile Sensors has been subject in robotics research since 1975.

Despite the increased hopes and expectations in tactile sensing in the 1980's and 1990's, it took until today for the dawn of a period of tactile enthused robotic sector.

IN [108] AN INQUIRY WAS CONDUCTED among 55 scientists asking for the requirements and applications for tactile sensing devices. Beside other things, "[a]pproximately 90% of the respondents felt strongly that tactile sensing is needed." The requirements were features like skin-like behavior in flexibility as well as a high spatial and temporal resolution. Of course, 'out-of-the-box' designs would be helpful or devices with preprocessing on the sensor. Almost 30 years later, many of the wishes are still being tackled quite inten-

sively by researchers today. Although quite some improvements have been achieved, the quantum leap in tactile sensing has up until today not occurred.

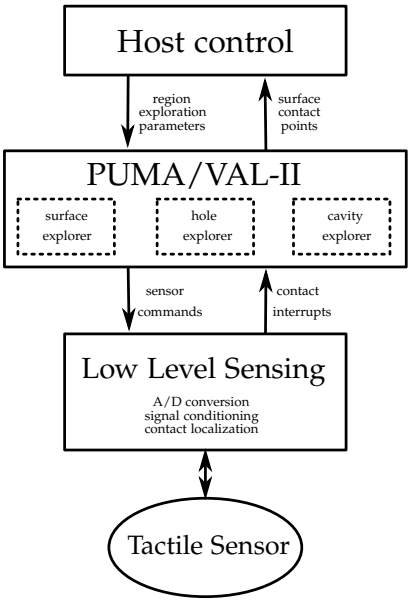

Figure 12: This is a schematic drawing of the tactile sensing system according to [5]. Although this is a feasible and especially with the hardware available probably optimal approach, a closer integration of tactile sensing data into the trajectory generation would be preferable from todays perspective.

Peter K. Allen describes a robotic setup at Columbia University where vision and touch were used to discriminate a set of household objects [5]. The work focuses on the visual perception which is accomplished with a passive stereo camera setup. The tactile sensor used in these experiments had the shape of an octagonal cylinder (length: 228 [mm], diameter: 40 [mm]) with a total of 133 sensing elements. The sensitivity of the sensor was considerably poor, at least approx. 1.7 [N] where needed to get a sensor reading, the sensor is saturated at around 11 [N] with a resolution of 8 bit. The sensor was mounted on a robot's end-effector. In the experiments, the different test objects were first converted into elaborate 3-D object models. Every object was filed into a hierarchical database. Since this procedure needed heavy user interaction and involved some hand-tuning at certain parameters (e.g. importance of parts of objects, like handles, to the classification algorithm), this approach is time-consuming and does not scale well with the number and complexity of the objects. In addition, one shortcoming of all model-based approaches is that novel objects are - if at all possible - hard to cope with. Nevertheless, the system was able to detect and recognize different objects and match the models successfully. Also, the tactile sensor was used to explore parts of the objects that were occluded. Different procedures for the exploration of holes, cavities and surfaces are presented. Despite the promising results, there is no information given on how long object exploration took. It has to be assumed, that the tactile object exploration was quite time-consuming and also that the objects had to be fixed to the table to resist the forces needed to get sensor readings. The tac-

tile exploration system (cf. Fig. 12) represents a feasible approach, yet raises the question if a closer integration of tactile sensor data into the (then real-time) trajectory generation would yield better performances. The presented architecture here just interrupts the movement of the end-effector, which puts unnecessary constraints on the trajectory and will not allow for smooth contour following. The exploratory programs used a sample of the assumed structure (i.e. surface, hole or cavity) in a predefined pattern. Other tactile based shape matching algorithms were developed later [154]. An interesting fusion of vision and tactile data was done in [291] using tactile and visual saliency maps.

In [248] a comprehensive survey of the advances in robotic tactile sensing from 1977 – 1989 is given.

AT THE DAWN OF THE 1990S, TACTILE SENSING came more into focus of the robotic community. In [248] a review is given which covers the advances in tactile sensor design and also in tactile sensing processing up to that date. The author states that the field of tactile sensor data processing is underdeveloped and compares the situation to the early days of computer vision. In addition, a comprehensive survey of the most common sensing principles, on which most tactile sensors still rely today, is given here and in [247] respectively. In the considered period, more publications cover new tactile sensing devices. When looking at the papers on tactile data processing, one has to critically state that most problems are still in existence today, in some areas, the concluding answer has yet to be found.

A textbook on robotic tactile sensing [246] with contributions from Howard R. Nicholls, Peter K. Allen and Susan J. Lederman was written in 1992.

A PURELY HAPTIC APPROACH to 3-D object modeling and recognition was taken in [7], in this case without tactile feedback though. To gain contact information, a robotic hand was used to enclose objects and the contact points were inferred from forward kinematics of the joint position sensors. This work was extended in [6], where in addition the 4-fingered hand was equipped with tactile sensors in the phalanges. Both works were based on superquadrics[6] [12, 10], which represent a family of geometric shapes like ellipsoids, cylinders, cubes and many more. Some simple examples can be seen in Figure 13. Generally speaking, these geometric shapes can be combined to model arbitrary objects and are well suited for tactile and haptic shape modeling, since with very sparse data, bounding boxes can be obtained and further refined in the process of exploration. In the mentioned work, only a single superquadric is used per object, which of course limits the precision significantly. Nevertheless, an object database of six different objects (e.g. box, cylinder, pyramid, light bulb) and a set of four different bottles was haptically explored. The authors were able to implement some of the exploratory procedures (EP) first described by Lederman [191] in her experiments on human haptic exploration strategies. In total three EPs were implemented: enclosure, lateral motion and contour following. While enclosure already had been done in [7], with the object fixated to the table with the robot hand grasping

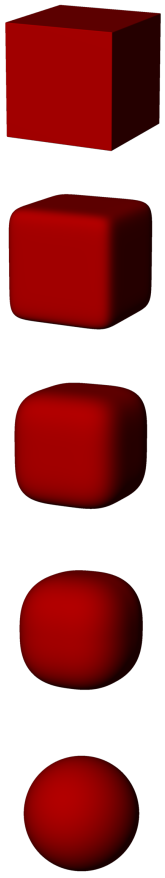

Figure 13: General superquadrics obey the implicit formula of $|x|^r + |y|^s + |z|^t = 1$. Here, as an example, superellipsoids with shape parameter varied from $e = n \in \{0.01 \ldots 0.99\}$ from top to bottom are given. Superellipsoids are formed via $(|x|^{\frac{2}{e}} + |y|^{\frac{2}{e}})^{\frac{e}{n}} + |z|^{\frac{2}{n}} = 1$.

[6] In the following, the definition according to Barr shall be used, where superquadrics are seen as an inclusion of both superellipsoids and supertoroids

from different angles, the other two EPs were based on an rough volumetric estimate from the enclosure operation. In the lateral motion ('surface explorer') a finger was used to repeatedly probe the assumed surface until contact could be established. After probing, the contact would be released and the next spot (straight line scanning) was probed. The contour following task was solved similarly, as the supposed shape of the object was probed with a two finger pinch grasp. To this end the central axis of the object and the rough or estimated contour must be known. Of course, these estimates can be acquired through a vision system, but this was not done in this work. In [390] visually acquired models in the form of superquadrics are refined with the use of tactile sensors. Unfortunately, this very interesting idea has only been carried out in simulation.

Another work worth mentioning can be found in [74], where the question of the next best view in terms of the path planning to the next sensing location is tackled. The very interesting question is, what the optimal exploration path would be to resolve ambiguities in pose or object recognition. While a suitable algorithm for polyhedral objects in 2-D could be found, the general problem in 3-D, even more with arbitrary objects, is found too complex for analytical solving. Some heuristic methods are presented, but are only evaluated in simulation. This problem remains to be solved in its generality in the real world.

The advantages of dynamic tactile sensing are advocated in [129, 127]. Dynamic tactile sensing in this case has to be understood as tactile sensing *through* movement of the sensor, not the moving of the sensor as such (i.e. to different positions to acquire static touch images). The presented tactile sensing mechanism consists of a finger which is equipped with an accelerometer and piezo-electric polymer elements. Since the piezo-electric sensor will only emit a electric tension on changes of pressure, the finger is moved over the surfaces in question. The advantages of the referenced design is the possibility to perceive very small surface features (it is reported that ridges of only 6.5 [μm] were detected), as well as textures and slippage. The downside is, however, a low precision in the absolute pressure measurement, since this can only be accomplished through integration of the signals over time. Since all sensors suffer from noise and inaccurate readings, the error will add up leading to a growing error. Another problem found in the texture detection is, that the output signal is strongly influenced by the relative speed of the object in relation to the sensor. Therefore, a proper motion of the object must be prevented to gain evaluable data. It is also mentioned, that the surface of the sensor (i.e. the micro- and macro-structure such as material/friction, ridges) plays a major role in the resulting signals, although no comparative data is given. In [65], the problems of using dynamic tactile sensing in manipulation control

Detection of extremely fine surface features through dynamic tactile sensing with piezo-resistive sensors.

are addressed. While dynamic tactile sensors are capable of detecting incipient slippage, which in principle allows to stabilize grasps through the adaption of the grasp force, two main challenges are expressed: (i) the need for additional force/torque sensors to get information on the absolute, static contact forces and (ii) the observation that movements to establish contact and/or force adjustments can also cause the same signals as if the object is in the process of slipping. To overcome the latter challenge, a phase/event/transition language is proposed. The paper regrettably lacks an evaluation of the proposed approach through experiments.

Force based control versus Position based control.

In this line of dynamic tactile sensing [25, 130], the use of an artificial neural net to detect incipience of slippage was employed in simulation [34] as well as an extension to that work as an experimental study [35]. This raises the question on how to model contact situations, beyond what classical mechanics can contribute to the matter. The authors state: "Even if it was possible to describe friction by Newton's law, contact between two bodies in the presence of friction is one of the most complex problems of contact mechanics, and the direct problem never admits a closed-form solution." Hence, a simulation using finite element method (FEM) was employed, with Gaussian noise added for training the neural net and also to generate a test set. For their experiments, a dynamic tactile sensor was used which consisted of two layers of piezo-electric plastic material (Polyvinylidenfluorid, short PVDF). The second layer was mounted in such a way, that the tangential stress on the sensors surface was measurable. Although a high success rate could be achieved on the raw tactile data fed to the neural net, several shortcomings of the presented results must be stated. The sensor layout does not allow static sensing, has both low spatial and temporal resolution and has not been used on a robotic arm, i.e. it has not been shown that the approach can filter the oscillations coming from the controllers. It is also not clear how precise the movement of the object against the sensor was measured and which samples were used to train the network. This is an important aspect, as one would like to detect slippage very early, when the object has not moved significantly. In the presented work, a lever detects the passive movement of the object and might not detect the early stage of slippage during the transition of stick to slip.

Some more work on the finite element method for modeling contacts can be found [158, 135, 179], general limitations especially in unstructured of simulations remain, of course.

Strongly related to the aforementioned results and to some findings within this thesis, are two different approaches on slip detection and how they were tested on two different piezo-resistive setups [124]. The first algorithm uses the fast fourier spectrum of the center of mass on the tactile array. The position of the center of mass was transformed into polar coordinates (r, θ), with θ being disregarded. This way, only a 1-D fourier transformation had to be calculated. Due to the low temporal resolution in the scanning of the tactile sensor, the maximal detectable frequency was limited

Center of mass in the discrete case is given as $C = \frac{\sum m_i r_i}{\sum m_i}$.

to 32. In the case of early slippage, the spectrum, which normally was dominated by noise, not only showed generally higher amplitudes but also peaked at very low and very high frequencies. The approach was found to be effective in detecting incipient slip, but not slippage as such. Also very fast slips would not be detected, due to the low temporal resolution. In a second experiment, the power spectrum density (PSD) of the total force on the sensor was evaluated. The authors describe a "catch and snap" effect on the piezo-resistive rubber material which they claim to be detectable, both by simple threshold or by a neural net, the latter yielding better results. Both algorithms were experimentally verified on two different setups; one being a specialized setup, the other consisting of a sensor mounted on a robot's end-effector. The low temporal resolution of the employed sensors suggests that the results are highly subject to aliasing effects. It is not clear how the results are affected by different materials and forces.

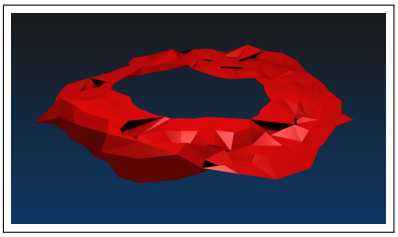

Figure 14: Tactile acquired data can be transfered into 3-D model, as seen here. One idea to solve the tactile inversion problem is using FEM methods.

A very interesting approach worthwhile of further investigation using FEM to model tactile contact is the numerical construction of a tactile Jacobian [43]. A scalar function is used for a forward model from the tactile data to the contact information, and therefore avoiding the difficulties associated with tactile inversion. This function is used to find a tactile Jacobian, with which the robot is able to track unknown objects maintaining certain contact conditions. This work is further extended in [404], where a similar approach is used, but developed in a more general fashion. Here, the central moments of the tactile data are used for the construction of a forward model and the tactile Jacobian. Extensive experiments underline the feasibility of the general idea, although shortcomings in the principle exist. This is related to the tactile inversion problem: Given a stimulus, one can deduct the tactile image, but given a tactile image, one cannot generally deduct the stimuli, since this mapping is not unambiguous. The authors suggest to overcome the deficits with additional sensing such as force/torque and joint torque sensors.

In his review paper [128], Robert D. Howe states that since in the human skin several different mechanoreceptors are found to especially respond to different stimuli, "[t]his suggests that creating a robot hand with dexterous manipulation skills will require a range of sensors for different parameters." He developed models on how different sensors are to be integrated into a holistic representation, depending on the task at hand, from constrained and structured to completely unstructured. The more complex the environment is and the more unconstrained the setting, the incorporation of more sensors is needed and more models have to be generated. An example of the data flow in a haptic processing layout can be found in Figure 15.

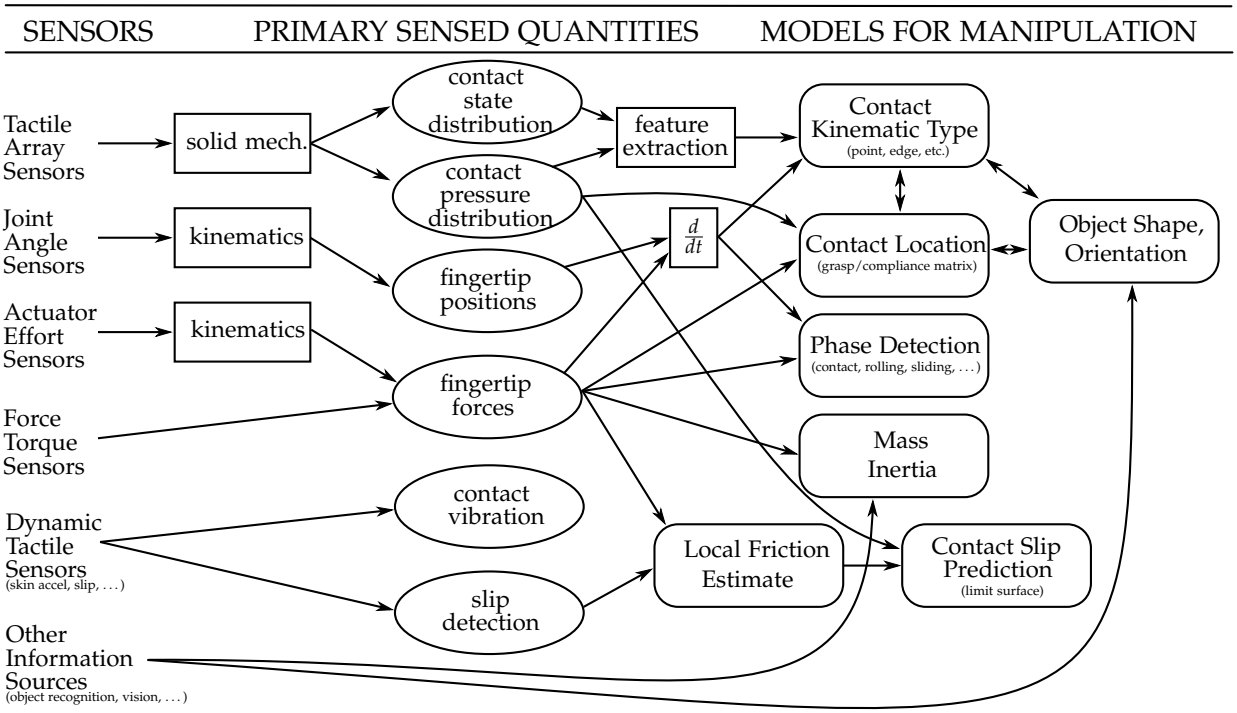

Figure 15: This figure is adapted from [128]. It shows from left to right the generally possible sensors and a sensible way of interconnecting and fusing the available data to get a number of different models for an overall object representation. It is a good illustration on why tactile sensing in robotics can be regarded as a hard problem, as direct contact with the environment is inevitable for tactile sensing. This, however, puts high demands on both hardware and sensors as well as the software and modeling.

In his two review papers [202, 203], Mark H. Lee gives a very dense aggregation on the most important developments in the 1990's. While tactile sensing in the 1970's was almost not existent and only very little work was done in the 1980's, a significant growth in publications dealing with the sense of touch in the robotic community can be found from approximately the beginning of the 1990's. Although it is stated that tactile sensing has matured, an overwhelming majority of publications still deal with the sensor design. Generally, touch is seen as complementary to vision and is considered important in the community, but also the problems arising from tactile sensing, i.e. the need for modeling contact situations as well as the need for real-time sensing and processing are recognized as a challenge to the roboticists. In addition, novel areas of application are examined, for example the agriculture and food processing industry and the health care sector, especially in minimal invasive surgery and teleoperation/telepresence.

Lee summarizes the developments and applications in tactile sensing in the 1980's and 1990's and pronounces new areas of application in the field of minimal invasive surgery.

A taxonomy on haptical sensed surface features is developed in [257, 256]. These features may be acquired without tactile sensing but some kind of contour following must be employed. The work is based on the use of a spherical fingertip that is employed to explore a surface. The 3-D points data gained through forward kinematics of the fingertip are then examined for features like bumps, pits, ridges or ravines. The detectability of these features is dependent on the diameter of the sphere. Also, the quality of the contour following clearly influences the usability of the data. A Wiener filter was used to smooth the data and outliers were deleted

when constructing the initial surface estimates which is necessary to detect the features.

Acknowledgments

It would not have been possible to write this doctoral thesis without the help and support of the kind people around me, to only some of whom it is possible to give particular mention here.

First of all, I would like to thank Prof. Dr. Helge Ritter for his support, inspiration, patience, motivation and for providing a pleasant working environment. Without his trust in my abilities, this thesis would not have been possible. I would like to show my gratitude to Prof. Dr. Gunther Heidemann for his indispensable advice and for being a great mentor. He opened the door to science for me.

I would also like to thank Dr. Michael Pardowitz for his advice and motivation when I needed it most.

I am indebted to many of my colleagues for their support. I owe my gratitude to Carsten Schürmann for building such great tactile sensors, Florian Schmidt for many nice discussions, Risto Kiova for his advice in all technical issues and Martin Meier for his ideas and fruitful collaboration. I would like to thank all members of AG Neuroinformatik and Central Labs for the countless discussions and ideas. Thanks to Dr. Sven Wachsmuth for the nice working environment.

I would like to show my gratitude to Jonathan Maycock and Kathlyn Varno for proof reading large parts of this thesis.

I would also like to express my great appreciation for all my friends for their continuing support.

Above all, I would like to thank my wife Katrin for her never ending encouragement, love and faith in me. For my parents, who always supported my unconditionally, and my sisters, I feel deep gratitude.

Part II

Framework for Tactile Robot Control

In the context of the different experiments and studies that are described in detail in the following chapters, software packages that may have a broader area of application were written. Since the development took a considerable amount of time and software engineering skills, a short description of the most important aspects will be presented in this chapter.

The selected software here may contribute to the research in this field or in a broader robotics context since it addresses problems that are common to a number of research questions. It should be mentioned, however, that the presented work is not the only viable solution to the encountered challenges.

At the time of writing, two big open source robotics frameworks exist. Willow Garage has been pushing their Robot Operating System (ROS) [279] forward for the last years. ROS is not so much an operating system in the classic computer science sense, but rather a communication middleware that allows the easy integration of different packages (or "stacks", as they are called) into one system. That may be why it offers support for a wide variety of platforms.

The second big framework, and older than ROS is the Orocos project from the University of Leuven [32]. Orocos has in the meantime its own driver to support the Kuka/DLR LWR, which is the robot used throughout most of this thesis. When the experiments were conducted, however, the driver was not available and indeed does not offer all the features the OpenKC software presented here has.

The section on the control framework for the Kuka/DLR Light-Weight Robot presumes some basic knowledge of robot control, kinematics, trajectory and path planning. The reader may refer to any robotics text book, e.g. [321, 325, 249, 259].

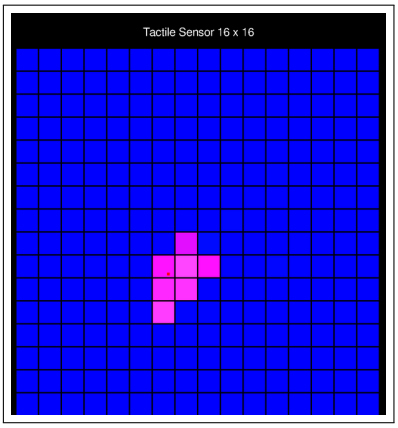

Figure 16: A visualization of a 16×16 sensor image. The pink dot marks the center of gravity.

libtact

Tactile sensors have not yet become a standardized product like cameras, microphones or general human device interfaces for example. This of course has an impact on the interface designs that are currently in use for tactile sensing arrays. In this work, three different kinds of sensors were used, two of them use a proprietary RS-232[7] protocol while one adapted the standard USB video device class (UVC[8]) specification to transmit the data to the computer.

[7] RS-232 has become a standard for serial binary communications in the computer domain. The standard defines the physical layout of the connection, e.g. the voltage levels.

[8] The USB video device class is supported by many operating systems, including Linux and Microsoft Windows.

Common to all tactile sensors are a number of tasks, like of course the acquisition of the data, buffering of the data as well as the recording of the data. Often, the data has to be synchronized with other sensors or modalities. Therefore, each acquired sensor frame has to have a time stamp attached to it. Also, the visualization of the data is important, both on- and offline. Especially in real-time applications, it can be important to monitor sensor data from a remote location or external process. Therefore, efficient network access to the data is also a nice feature to have. These are all tasks, that are handled by the libtact library and the programs that come with the library, respectively.

The software package offers a standard C interface with an easy function set. It provides means to start a background thread that handles the data flow from the sensor. The library is highly optimized to have minimal memory consumption and a low demand on computing time. Once the thread is started, and therefore all necessary memory has been allocated, the remaining operation is real-time capable. It is thread safe, i.e. the tactile data can be accessed from many different threads. From the C-API[9] the following functions are accessible:

[9] Application Programming Interface

Active frame Immediate access to the last grabbed or acquired frame with or without a time stamp is possible both with low latency and completely thread safe. Therefore, different threads have transparent access to the tactile sensor data. Access to the frame can be blocking, i.e. waiting for the next frame to become ready, or non-blocking, and thus returning the latest buffered data from the sensor.

Ring buffer history The libtact library allows to define an arbitrary

window size n, where the last n frames are kept in memory. This reduces the update costs on newly acquired data frames from the sensor. It also allows fast access to the last n tactile frames. This is important for algorithms that work on sliding windows, i.e. require a time series of data to do calculations on. Since in a typical setup, insertions and deletions of data are quite frequent (as they run at the frequency of the sensor), it is important to be able to do these operations quickly. It is also of great importance to the real-time capabilities of the library that this update operation does not issue an allocation and freeing of memory, as this would add the possibility of being interrupted for an unpredictable amount of time by the kernel. Through the API, a linear chunk of memory is returned. The data from the ring buffer is copied in one block to a provided memory location. This operation is thread safe to grant low latency.

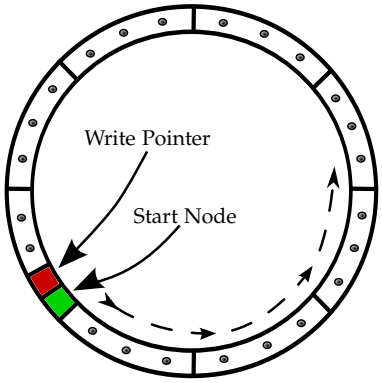

Figure 17: A ring buffer of size n allows efficient access to the last n data samples. It avoids time consuming allocation and de-allocation of memory. The typical case of replacing the oldest frame with the most recent only required one write operation and one increment operation of the write pointer.

Recording It is also possible to record longer segments of data for later evaluation. To ensure that no frames are dropped, the user is able to suggest a desired buffer size. If, however, the buffer size is exceeded, the library will try to allocate additional memory. Since the recorded frames are kept in memory, unexpected delays from disk operations are avoided. It is therefore possible to record previously unknown length of tactile data. In the event of reallocation, however, real-time constraints may be violated.

Setting of marks In addition, where required, the libtact library allows to set different start and stop marks during recording. Thus it is possible to keep track of several events and analyze these segments in a subsequent step. These marks all facilitate the same string in memory, hence, act as pointers to the data and therefore no needless doubling of memory and data will occur.

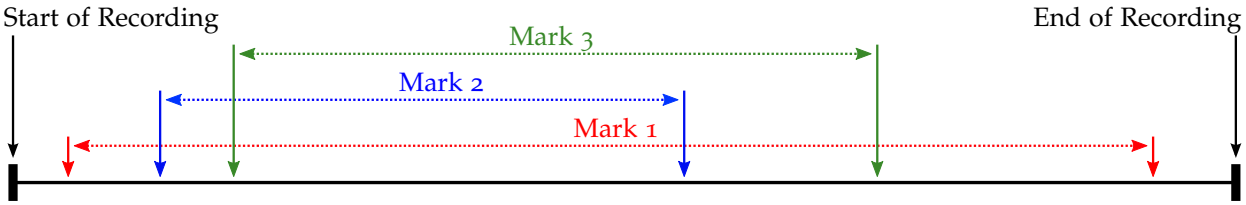

Figure 18: The library provides means to set arbitrary start and stop marks to extract different segments from the time series. Since only pointers are used, setting of many marks scales very well.

Network support The library offers the possibility to start a server thread, which will run independently from the data acquisition thread instance. It acts as a consumer of the data provided by the acquisition thread and handles incoming client connections. A client may connect using the Unix TCP/IP socket interface. An implementation of a client application and functions to connect to a tactile sensor over the network are included in the libtact package. The transmission format is a simple binary format which allows fast access to the data, since time-consuming data conversions are avoided. On the downside, however, the format

The Transmission Control Protocol (TCP), operates at the Open Systems Interconnection (OSI) layer 3 and 4 respectively and incorporates error detection. Therefore, transmission errors should not be encountered in the higher layers.

may be prone to errors. But since a TCP connection is used, transmission errors should generally not occur.

Multi Sensor Support At the time of writing, three different tactile sensors are supported with the same basic set of functions, like getting a sensor frame or getting the dimensions of the sensor. These sensors are the DSA100-256IS and the tactile sensor modules in the SDH-2 hand. Both sensors were developed by Weiss Robotics. The other supported sensor type is the myrmex sensor developed by Carsten Schürmann in the context of the Excellence Cluster Cognitive Interaction Technology in Bielefeld [312, 311]. Some functions are not supported by all sensing devices. In that case, an appropriate error code is returned.

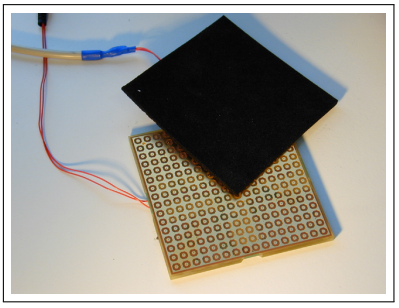

Figure 19: The DSA100-256IS Tactile Sensor produced by Weiss Robotics.

Concurrent Sensor Usage Several sensors may be used at the same time. The library is constructed in a way that different handles allow the separate access to the underlying hardware.

Visualization There are viewer applications that come with the library that allow the display of the tactile data on a graphic display and in a terminal respectively. The viewer can directly connect to the sensor or connect to a possibly remote sensor over the network.

Save & Restore Another feature is the saving and restoring of recorded data. During an experiment, usually the data will be stored in memory. When the recording has finished, the data is written to disk for later evaluation and documentation.

To maximize the impact of this software package to the tactile sensing community, the software was released as Open Source and published under the GNU General Public License. The library has been used throughout all the work and is stable and mature. It is build to support different hardware with a consistent interface.

OpenKC

Robots in Research

A COMMON PROBLEM AMONG ALL ROBOTIC RESEARCHERS is that most robots are build for industrial applications, since, of course the principal customers for the robot manufacturers are coming from the industry. The market for manipulators for research applications is just too small for the robot manufacturing industry to develop a specific robot for this area of application. While the hardware side of the developed robots could often be reused, the needs on the software side for the industry and sciences are contradictory in many aspects.

The robot manufacturing industry provides interfaces that are well suited for the traditional and highly structured use case of a robot arm on a production line; doing exactly one task repeatedly with high accuracy with seldom or no external sensor input. These interfaces are often not open and versatile enough to be used in a robotics research context. For applications in research, more often than not, direct and real-time[10]control of the robot is important. It must be possible to define a distinct trajectory and it must also be possible to immediately react to incoming sensor events. This is of course only manageable if direct real-time control over the robot can be attained.

Therefore an appropriate software interface is needed – which most of the time does not exist and is not profitable to build. The disclosure of the internal controls of the manipulator is another possibility, although more cumbersome for the scientists. In that case, a whole interface for the robot must be developed by the scientific community. Since this is a time consuming task with, at least at the first level minimal scientific impact, from the viewpoint of academia not the preferred option. Once, however, this work is done the enormous flexibility of the manipulator can be unleashed.

This is, however, quite often not even an option to the scientist. With the robot market being very competitive, most manufacturers were not willing to take any risks in publishing internals of their work to competitors. As a consequence, most robot platforms cannot be fully exploited in a scientific context, since reverse engineering is even more work and also considerably more dangerous.

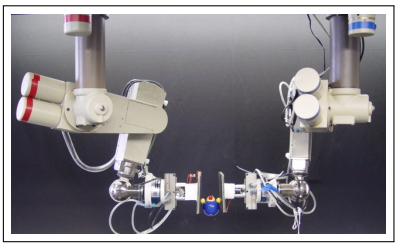

Figure 20: Up until 2008 a bimanual setup consisting of two PUMA 260 robot arms was used. At the end-effectors, a tactile sensor array was mounted with the pneumatic grippers. The robots were controlled using RCCL, the robot control C library.

[10] If a program or system must react within a set response time, it is said to have real-time constraints. Three levels of real-time exist:

Hard A violation of the real-time constraints results in a total system failure

Firm Like hard real-time, except that rare violations of the real-time constraint can be tolerated

Soft Violation of the real-time constraint will result in degraded service quality

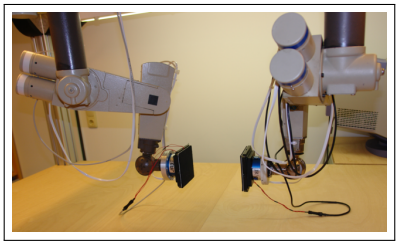

Figure 21: From 2008 to 2009, the pneumatic grippers were removed from the setup to allow a firmer and directer control of the tactile paddles.

IT HAS BEEN THE PUMA (see also Figures 20 and 21) robots, originally build by Unimation in the late 1970's and throughout the 1980's, which could first be found most in robotic research labs around the world. From that time on, robot manufactures have often been neglecting the needs of researchers and aiming their products strictly on the industrial market.

Although the PUMA robots seem to be by todays standards somewhat outdated, many of them are still in use in research facilities, partly because they still satisfy the requirements, partly because an alternative was lacking for quite some time. One reason for the popularity of PUMA robots in the research laboratories around the world is that the Unimate Controllers consist of standard hardware (VAX PDP-11) and is therefore well documented. It enabled the scientists to circumvent Unimations own VAL programming language. Thanks to standard interfaces, the manipulators could also be controlled in real-time with standard Unix workstations [213, 212].

The PUMA (Programmable Universal Machine for Assembly) line of robots derived from the Stanford Arm, the first all-electrical mechanical manipulator, originally developed by Victor Scheinman in 1969.

Figure 22: Rendered picture of a PA-10 6C. The PA-10 7C has an additional joint between joint 2 and 3 counting from the robots base.

[11] To clarify, a 6C and a 7C version exist, with 6 or 7 joints respectively

[12] The control cycle is 10 [ms]

[13] German Aerospace Center

THE POLITICS OF THE ROBOT MANUFACTURERS STARTED to change in 1999, when Mitsubishi Heavy Industries released the PA-10 series of robot manipulators. They offered, through a separate available motion control board and the PA-Library, the possibility to externally control the redundant 7-DOF[11] robot in real-time[12] using a regular PC or workstation. The PA-10 series were also very popular due to their redundant degree of freedom that let scientist work on new path planning algorithms. These algorithms exploit the redundant kinematics allowing to avoid singularities, joint limits as well as collisions.

AT THAT TIME (2002), THE DLR[13] had presented their new Light-Weight Robot (LWR) [117]. It is the third generation release and the result of an endeavor to develop a light weight arm for space missions that had started in 1992. The outcome is a robotic arm, that is truly unique in its features and design. First of all, the arm weights only 15 [kg] with a payload of 7 [kg], or even 14 [kg] under certain constraints regarding the velocity and acceleration. It has, like the human arm, 7 joints and therefore 7 DOF. The drives are highly integrated and modular.

Property	Puma 260	PA-10 7C	Schunk LWA 3	Kuka/DLR LWR
Weight [kg]	13	40	18.7	15
Payload [kg]	1	10	5	7 (14)
# Joints	6	7	7	7
Length [mm]	890	1317	1076	1178

Table 3: Some specifications of the most popular robots in robotics research

The joints are commanded by an actuating torque. To be able to control the torque commanded, every joint is equipped with torque sensors in addition to classical position encoders. The light weight design and the remarkable high weight/power ratio called for a

special control strategy. Because of the low mass, special care has to be taken not to hit the natural frequency of the arm during operation. Therefore, a dynamic model was implemented [4]. Through this model, the torques and forces (like gravitation) acting on the robots joints are estimated. This allows for impedance control or work in gravitation compensation mode, where the robot arm virtually hoovers in its position and can easily be moved by external forces.

Figure 23: Rendered picture of a Schunk Light-Weight-Arm (LWA) with 7-DOF.

As of today, over 60 Kuka/DLR light-weight robots have been sold to research facilities worldwide.

The DLR found with the Kuka Roboter GmbH a commercial partner who was willing to push the development of the arm towards mass production. As of today, a pre-series of the Kuka/DLR Light-Weight Robot (LWR)is released and mainly sold to research facilities. The second generation of the Kuka/DLR LWR IV, the Kuka/DLR LWR IV+ is now available. The manipulator comes with the Kuka control software (KSS) and the Kuka Robot Controller (KRC2). This is the same software and hardware that Kuka uses for robots in the small and medium sized robot sector. With this, the standard programming language for Kuka robots, the Kuka robot language (KRL), has been extended to support the new features of the lightweight arm. The KRL is an imperative *PASCAL* [387] like programming language with robotic specific statements for motion planning and using tools. Through the user interface the four modes of operation of the LWR are accessible:

I. Position Control

II. Axis Impedance Control

III. Cartesian Impedance Control

IV. Gravitation Compensation Control

In modes II. and III., the active compliance of the robot can be parametrized. This is done in setting stiffness[14] and damping parameters[15] in an ideal spring-damper model, either at joint level, or in Cartesian mode for specific directions of arbitrary coordinate systems (e.g. tool, base, world). When the robot is run in mode IV., it simply holds its position compensating for gravitational forces. In this mode, the robot can be guided by direct interaction.

In an ideal mass-spring-damper model, is derived from the differential equation:

$$\ddot{x} + \frac{c}{m}\dot{x} + \frac{k}{m}x = 0.$$

with x being the displacement, m the mass, k is the spring constant and c is the damping coefficient.

[14] corresponds to k

[15] corresponds to $\zeta = \frac{c}{2\sqrt{mk}}$

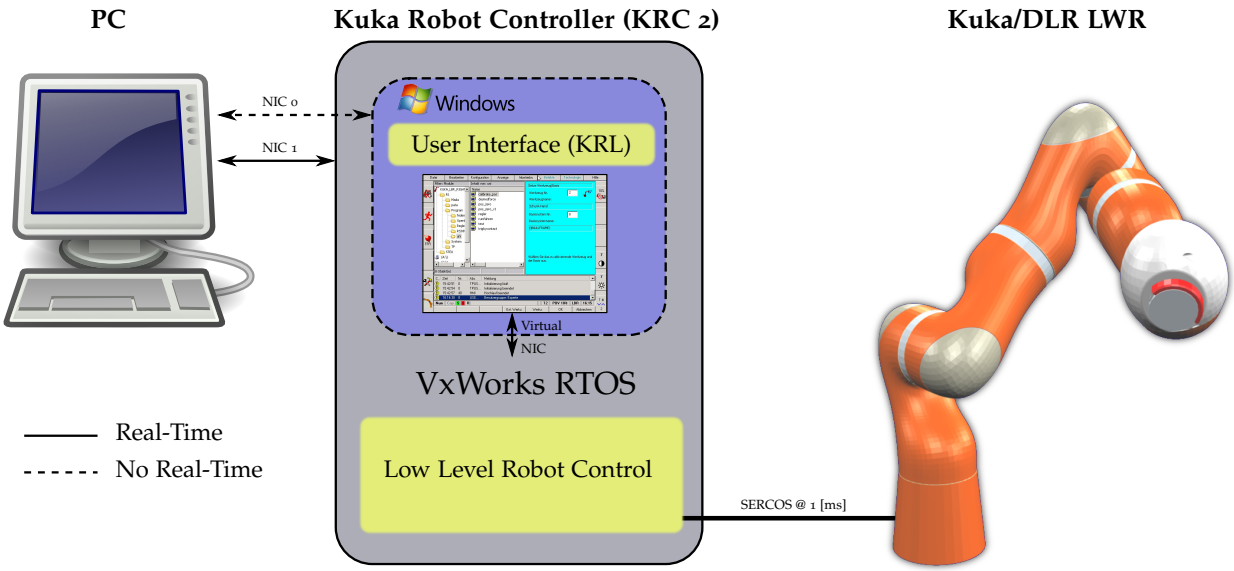

Figure 24: Schematic Drawing of the Interfaces of the Kuka Robot Controller (KRC2). The Controller has a SERCOS Interface to the joint drives and internal sensors of the robot, as well as two network interfaces. Various other interface options, such as Profibus, exist but are intentionally left out in this figure.

While most remained the same on the hardware side of the robot, the LWR was now integrated into the standard control architecture of the Kuka robot company, which specializes in industrial applications. The control scheme of the robot is shown in Figure 24.

The robot is attached to the controller via the SErial Realtime COmmunication System (SERCOS). It is a time-slice based communication bus, which transmissions suffice real-time constraints. On the controller, a Mind River VxWorks Real-Time Operating System (RTOS) does the low level control of the robot. The modeling, kinematic calculations and communication are all found here. Within the VxWorks Operating System (OS), a Microsoft Windows XP Embedded runs as non-privileged client, i.e. the Windows OS is neither real-time capable nor does VxWorks grant real-time privileges to the guest. The main purpose is to provide a familiar user interface to the operator.

From the user interface the robot can be manually operated as well as programmed. The communication of the selected commands to the real-time VxWorks layer, and therefore to the robot, is done through a virtual network controller, which is implemented as a chunk of shared memory between the two OSs. The employed controllers have two Ethernet Network Interface Cards (NIC). Hence, it is possible to access the controller externally. One NIC is associated to the VxWorks OS, while the other is assigned to the Windows client OS. To externally control the robot in real-time, only the NIC dedicated to VxWorks can be used, since the other NIC is assigned to the non real-time OS and therefore is not real-time capable.

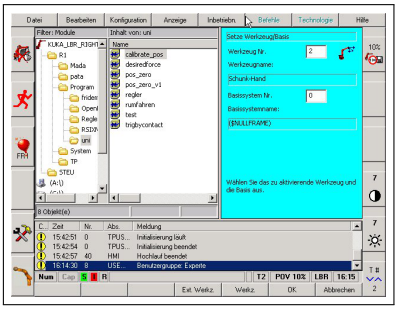

Figure 25: The user interface of the Kuka System Software. It allows various modes of moving the robot arm, for example with a space mouse attached to the Kuka Control Panel (KCP).

Limitations of KRL

The Kuka Robot Language, which natively runs on the Kuka controllers, offers an easy-to-use interface for industrial applications and allows for the generation of trajectories and procedures in very little time. It has its limitations though when it comes to the scientific scope. The major shortcomings are:

Limited set of functions While KRL supports the generation of a variety of different trajectories in both task and configuration space, the total function set compared to more common programming languages is limited[16]. While Boolean logic and basic mathematics operations are supported, functions regarding I/O are rare and advanced math functions are missing.

[16] Some of the modern programming languages like C or C++ also come with a small set of build in functionality, but usually come with a rich repertoire of extensions like the C standard library or the Standard Template Library (STL)

Import of Libraries One of the crucial disadvantages of KRL is that there are no mechanisms for including third party libraries. The research community has developed and optimized many software packages on topics that are highly relevant for roboticists. Libraries for machine learning, kinematics, mathematics, including fast linear algebra packages, are available and serve as the toolbox for today's and tomorrow's scientific applications. Besides that, those libraries and frameworks often combine the work, knowledge and effort of a whole community and therefore are hardly reproducible by one institution or group, let alone an individual; reimplementing even parts of those libraries in KRL is not feasible nor reasonable.

Control of Trajectories KRL has many ways of generating trajectories[17] and is able to trigger events at certain parts of the trajectory as well as respond to external inputs. Thus it allows the combination of trajectories in many ways. Albeit the roboticist cannot influence the joints nor Cartesian position of the end-effector in real-time with KRL primitives alone. In some applications, it might become necessary to generate trajectories that fulfill certain constraints utilizing the redundancy of the manipulator in one way or another. This can hardly be accomplished from within the KRL.

[17] Linear and arc movements in Cartesian space as well as straight movements in joint space are natively supported in KRL

Analytical Inverse Kinematics In KRL, the 7-DOF arm is treated as a 6-DOF arm with an additional axis[18]. The inverse kinematics are therefore analytically solved. Once the arm configuration[19] is determined, all solutions are disambiguated and movements are done totally agnostic of the redundant joint. On one hand, this approach allows for researchers to repeatably and deterministically find *one*[20] solution for the motion planning. On the other hand, singular configurations, which could easily be avoided with the additional axis, pose a problem. The enhanced dexterity that a 7-DOF arm offers remains unused and therefore somewhat wasted.

[18] This approach is comparable to a 6-DOF robot on a linear axis

[19] Traditionally, a 6-DOF manipulator with revolute joints is in a configuration

$$C = (S, E, W)$$

with:

$S \in$ *{Shoulder Left | Shoulder Right}*

$E \in$ *{Elbow up | Elbow down}*

$W \in$ *{Wrist flip | Wrist no flip}*

[20] Opposed to the theoretical infinite set of solutions with 7-DOF kinematics

Concurrency and Timing KRL programs are executed on the Vx-

Works part of the controller and thus are running in a real-time context. Unfortunately, the programmer has no means to influence the timing of the program. While it is possible to wait a specific amount of time, there is no way of knowing how much time (neither cycles nor wall clock time) has passed. Also, it seems that no mechanisms to run tasks concurrently or controlling concurrent access (i.e. mutexes) exist. This complicates the programming of complex applications, especially if interrupts are used, since the programmer has to find other ways to safely avoid race conditions. To concurrently monitor an external sensor, an interrupt on one of the physical input channels (e.g. Profibus, D/A-Channels) has to be invoked, which further complicates the system.

Limited I/O Although KRL has ways for input and output of data, these mechanisms suffer from the lack of functions to ensure synchronous data transfer. Also, only a very limited number of I/O ports exist, which significantly limits the available data that can be exchanged from or to the KRL context. The transfer of more complex data structures can be especially difficult to accomplish (there is no way to serialize and deserialize complex data types). The experienced programmer will also miss the advantages of remote procedure calls (RPC) or similar mechanisms.

Editor The editor does not support code completion and cannot come up with the same comfort as modern integrated development environments. Also because the editor supports so called inline forms, which allow generation of movement commands with just a few mouse clicks, it can at times be very cumbersome to write large portions of code. This is of course not really a shortcoming of the language itself but does make development of large portions of KRL code really cumbersome, especially if one is spoiled by Unix-like operating system, where the freedom of choice is held in high esteem. Since the KSS software also manages the communication between the Windows and VxWorks layer, certain precautions have to be obeyed when external editors are employed[21].

[21] To avoid race conditions, the file has to be written in the windows file system and then an update in the KSS software has to be triggered

IT HAS TO BE MENTIONED that these problems are quite common among industrial manipulators. Also, to the best knowledge of the author, no open standard for such a programming language exist. And as long as knowing how to program a robot is bringing additional revenue to the robot manufacturer, very few attempts to change the status quo will be made. Nevertheless, first steps in this direction are underway [241].

IN THE FOLLOWING, WE PRESENT the development of an Open Source library[22] that will allow the real-time remote control of the robot as well as parametrization and switching to all supported modes of operation. The library is written in ANSI C and can there-

[22] Available at http://opensource.cit-ec.de

fore easily be used from a broad variety of programming languages and POSIX [137] conforming operating systems. The software package uses the GNU autotools and is hence easy to configure, build and install. It consists of a shared (dynamic) library and some test and example programs. It has been tested with Gentoo Linux as well as Ubuntu Linux.

The library exploits two remote interface methods provided by Kuka: (i) Remote Sensor Interface – Extensible Markup Language (RSI-XML) and (ii) Fast Research Interface (FRI). At first, only the RSI-XML interface was available. The original intended use case of this interface was, however, different from what was needed in academia. The pledges of the customers were not unheard by Kuka, so now Kuka also provides the FRI, which overcomes most of the limitations of RSI-XML. Although, as a result of the new interface, a complete rewrite of the code was necessary, we tried to keep the changes in the API at a minimum. Nevertheless, due to changes in the control flow, some additional functions had to be provided.

In order to ensure a flawless operation, the communication between the robot and the remote computer must not be interrupted nor delayed. Since the robot control resides on the KRC, the real-time requirements are not hard, but firm. RSI-XML allows to configure the robots behavior in case an answer is not received in time[23], and thus a single, or even a few late packages, might not necessary bear fatal consequences. A strong degradation in the robots behavior or even an interruption of the movement may occur on late packages and should be clearly prevented. To achieve this, as a first measure the Ethernet connection between the robot and the remote computer should be run on a separate Ethernet switch. Ethernet as such is not real-time capable since it cannot guarantee maximal latencies. It is designed for high throughput. It is reasonable to prevent any other network traffic on the network card and the net itself to reduce packet collisions and competing access on the physical Ethernet layer. In practice, sufficient real-time behavior can be obtained[24].

[23] In case a correction is missed, either the last correction will be assumed again or a zero correction (stop) will be driven

[24] The author managed to run three robots concurrently over one Ethernet switch

It should be taken care that the Ethernet device immediately causes the server process on the remote computer to wake up and process the data. This can be accomplished by using only a small buffer size on the network interface. It was our interest to be able to use an operating system that ensures good interoperability with the Ubuntu GNU/Linux[25] environment and at the same time yields an excellent performance with low administrative overhead. The authors used a Gentoo GNU/Linux distribution with a standard kernel configured for low latency (PREEMPT) with high precision timer and a timer frequency of 1,000 [Hz]. Also a patched kernel with the RT_PREEMPT extensions was tested without significant improvement of the run-time behavior, yielding a slightly less jitter

[25] This is the standard platform used in the working environment of the faculty of technology in Bielefeld

in the timing.

Although an explicit real-time operating system might have ensured a slightly more robust execution, the benefits of using a standard GNU/Linux environment outweigh the minimal gains from using such a considerably more complicated environment, especially when it comes to updates and maintenance.

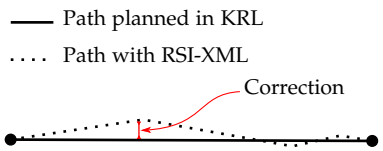

Figure 26: The intended field of application of RSI-XML: a path is planned and executed from within KRL. External corrections to the path are transmitted in real-time. For example, if the robot was to do a force guided movement, corrective movements could be generated with the help of a force sensor at the robots end-effector.

Robot Sensor Interface

KUKA PROVIDES A SOFTWARE PACKAGE, that allows real-time control of the manipulator, the Robot Sensor Interface (RSI). We are using the XML-edition (RSI-XML). With the use of this software interface, an TCP connection via Ethernet to a remote computer can be established. The robots controller starts to send messages in a given cycle time (usually 12 [ms]), the remote computer has to answer with an appropriate packet within the given cycle time. The intended area of application is to be able to do minor corrective movements or deviations from the original path based on for example force or distance readings (cf. Fig. 26). That basically means, that the main path is still planned and executed in KRL, with all the limitations listed above. To gain maximal control over the movements of the arm, however, the movement issued in KRL was to hold the position, and we used RSI-XML to drive the robot, i.e. the path in KRL was just a point and the correction was the actual trajectory.

RSI-XML is available for all industrial robots from Kuka. The interface has predefined objects for joint angles and position data and also a limited set of free variables that can be used either in messages from the robot or messages to the robot. We are using these variables to read the torques from the joints as well as the estimated forces and torques at the robots end-effector. The latter are calculated on the controller with the help of the dynamic model of the robot. We are also using these variables to send control parameters to the robot and to trigger the switching of controller modes. The number of free variables is quite limited, so unfortunately there are not enough of them to send both stiffness and damping parameters in a single message cycle. Therefore, to set stiffness and damping through OpenKC in RSI-XML mode, two API calls are needed.

IN A SIMPLE SETUP, THE ROBOT might send its actual joint position values and the remote computer would answer with the corrections of the joint angles that the robot should accomplish within the next control cycle (cf. Fig. 27). Using this construction enables the user to do velocity control at either joint or position level, depending on the control mode that was chosen.

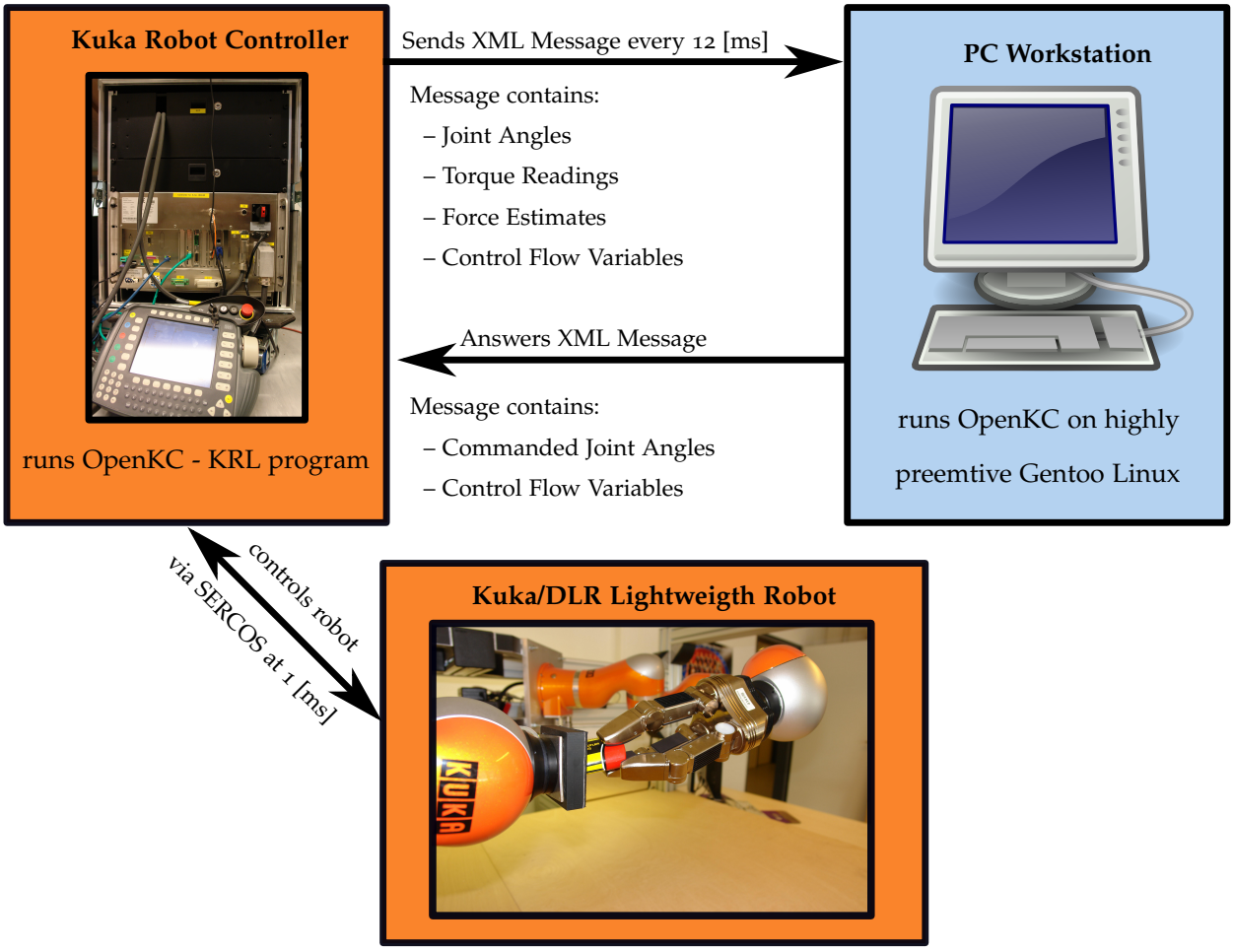

Figure 27: Control Scheme of the Kuka/DLR LWR using the RSI XML interface. The XML messages are sent over Ethernet and allow real time control over the Kuka/DLR Robot

OpenKC RSI-XML Edition

To allow the processing of the messages from the robot on the remote computer a server thread is started. The thread is scheduled with real-time priority (RT_FIFO), if sufficient permissions are given to the executing user. The server will listen on the configured TCP port and serve all incoming connections. On the reception of a message, the contents will get parsed using the libxml2[26] library package, which allows both fast and reliable parsing of XML content. The internal structures are updated according to the recent information from the robot. At this time either a previously registered callback function gets activated, which will return a set of corrections to be sent to the robots, or an internal set of corrections are sent to the robot. This represents the two available methods of setting a desired correction for the robot:

I. Register a callback function, which will get called on each IPO cycle. This callback routine will run in the real-time context and thus should avoid lengthy calculations or I/O, so that the real-time constraint is not set at jeopardy. This is the preferred

[26] http://xmlsoft.org/

approach for tight closed loop control, for example during sensor guided motions.

II. Use a setter function, that will set the corrections asynchronous to the real-time task. This is the preferred way to control the robot if the timing constraints cannot be satisfied. It should be noted, that the caller is in charge of handling the correct timing for the desired trajectory, i.e. the user has to be aware of timing constraints in the setting of the desired trajectory.

BESIDES CONTROLLING THE POSITION of the joints or the end effector, the OpenKC framework provides means to set the parameters for stiffness and damping in both, the Joint-space and Cartesian impedance control modes. The parameters are transmitted using free variables from the RSI-XML context. Through a control variable, an interrupt in the KRL program on the Kuka controller gets called. In this interrupt routine, the parameters are copied to a local variable in the KRL programs context. A handshake is used to signal the successful transfer of the variables back to the OpenKC framework. To activate the new settings, the current movement must be interrupted by a call to a switch controller routine, even if the control mode remains the same. During this procedure, the arm cannot be moved. A simplified sequence diagram can be found in Figure 28.

The OpenKC framework also enables the use of the KRL trajectory generator through calls to KRL routines. Parameters for the KRL Point-to-Point movement can be transfered to the KRL context and an adequate KRL call is made.

Evaluation To test the performance of the framework a special ping[27] like application was written. The application generates XML messages just like the ones the Kuka controller would and measures the time needed for the framework to answer the message. The program uses high resolution timers and runs with real-time priority to measure the round-trip time very precisely. Even when the OpenKC server was under heavy load and the ping cycle was at 1 [ms] (opposed to the fixed 12 [ms] used by the real Kuka controller) an average round-trip time of 0.5 [ms] with a maximum response time of 0.85 [ms] could be accomplished. The measurement ran over a 12 hour period, experiencing no packet losses. The test were run on two Core 2 Quad PCs running at 2.8 [GHz]. In the experimental environment two real robots and a simulated robot could be simultaneously controlled via a single PC using OpenKC without a significant performance drop[28].

[27] A program above all known in the TCP/IP domain. It sends an ICMP message to a host an measures the round-trip time

[28] It should be noted though, that depending on the run-time of the callback function, the responsiveness of the system might decrease

THE LIBRARY HAS A LOW MEMORY footprint (approx. 1 MB on 64bit GNU/Linux) which favors good real-time performance. The library has been audited with memory checkers to ensure safe and high performance run time behavior. Especially in the parsing of

the XML messages (through libxml2) and the conversion from and to XML all operations are carefully checked for error conditions.

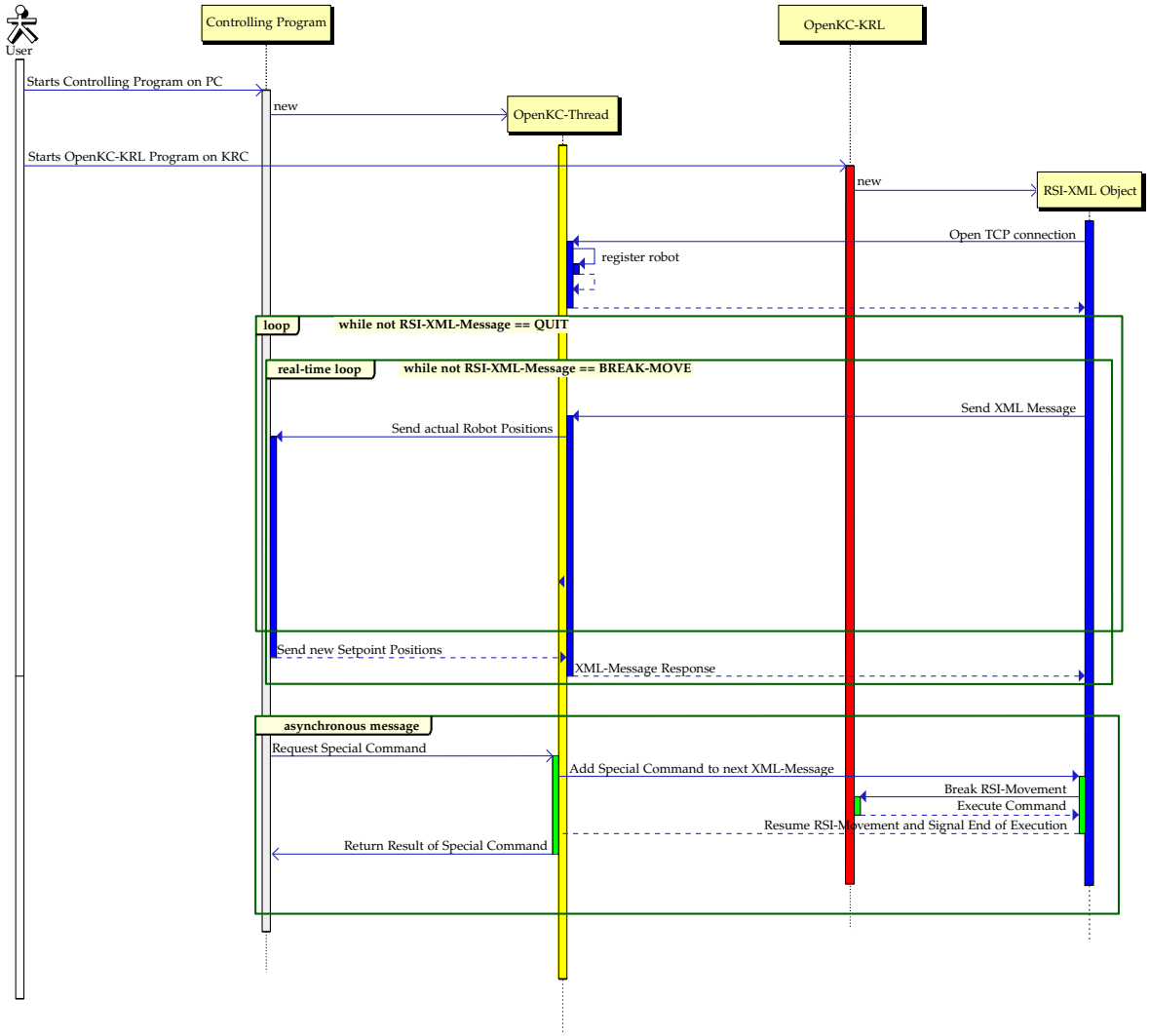

Figure 28: In this sequence diagram, the simplified course of action during control of the Kuka/DLR LWR is shown. In this case, OpenKC is used in the RSI-XML callback mode, i.e. in the real-time loop, a tight sensor integration and real-time trajectory planning is possible. This may be interrupted by asynchronous calls to special functions like changing settings for stiffness and damping.

Most of the limitations of KRL can be overcome since the OpenKC library can easily be integrated in any C/C++ program or any programming language that have bindings for C code. The programmer is exempt from the cumbersome work of making the communication from and to the robot real-time capable. All what is left is the generation of the desired trajectories, which then of course have to be supplied within the real-time cycle.

At the time of writing, OpenKC does not only support the real-time trajectory control, but also certain KRL commands like the so called PTP (Point to Point) movements, can be triggered remotely. During this triggered movement, the trajectory of the robot can still be influenced and the position and joint values are available as well. With this mechanism, OpenKC might even be interesting if no real-time trajectory control is desired, but simple remote operation is

sufficient.

Fast Research Interface

In 2010 a new interface for the Kuka/DLR LWR became available: the Fast Research Interface (FRI). It follows a different approach than the RSI-XML interface. It bypasses the KRL level and therefore does not suffer from most of the problems that are to be associated to KRL. The interaction with KRL is, nevertheless, still possible and allows the almost complete remote operation of the robot. FRI was designed with real-time control and the special architecture of the LWR in mind and hence brings some changes, some of which are listed in Table 4. It was neither tried nor achieved to be compatible with the RSI-XML interface – thus, the only common aspect that unites both approaches is the principle to send messages in the robots cycle via an Ethernet interface that has to be answered within a given time frame to steer the robots movements.

Property	RSI-XML	FRI
Joint Angles	DEG	RAD
IP-Protocol	TCP	UDP
Distance	[mm]	[m]
Angles	RPY	Rotational Matrix
Joint Order	A1-A2-A3-A4-A5-A6-E1	A1-A2-E1-A3-A4-A5-A6
Cycle Time	12 [ms]	1-100 [ms]
Message Format	ASCII XML	Binary
Offset A2	+90°	–

Table 4: The new FRI interface is not meant to be backward compatible

OpenKC FRI Edition

Due to the high number of incompatibilities, we decided to completely rewrite the OpenKC framework to now perfectly suit FRI, while keeping the API as constant as possible. As a consequence of this decision, two separate versions of the OpenKC framework exist at the benefit of a clean and lean implementation. Mixing the interfaces would have blown up the code in an unreasonable manner, making it much harder to read and maintain. Nevertheless, there are important points in which the RSI-XML and the FRI versions differ. For one, the callback interface uses the corrected joint order and radians, to avoid potentially unnecessary conversions.

Other changes are accounting to the new state model that was introduced with FRI. Now, once the FRI is started, either by a KRL call to `FRIOPEN()` or by pressing a softkey on the control panel, the robot enters the Monitor Mode. In this mode, control of the robot is not yet possible, but UDP-packets with various information

Information Provided by FRI
Handshake & Header Data
Statistics of Connection
Robot State (Drives, etc.)
FromKRL, ToKRL Variables
Measured Positions
Commanded Positions
Measured Forces
Jacobian Matrix
Mass Matrix

Table 5: The information provided by FRI in Monitor and Command Mode.

concerning the status of the robot (cf. Table 5) are sent continuously. By answering the messages within the previously defined cycle time (1 – 100 [ms]), it is possible to sequentially alter the connection status until one is found eligible to enter Command Mode. This has to be triggered by a KRL call to `FRISTART()` or by softkey on the control panel. OpenKC offers to remotely issue `FRISTART()` using the ToKRL variables of FRI, which get interpreted by a special KRL program. When in Command Mode, real-time control of the robot is possible. Exiting Command Mode is either possible through a call to `FRISTOP()` or if any error condition is met, i.e. violation of the timing constraints or any hard limit (velocity, acceleration). The states of the FRI are also reflected in Figure 29.

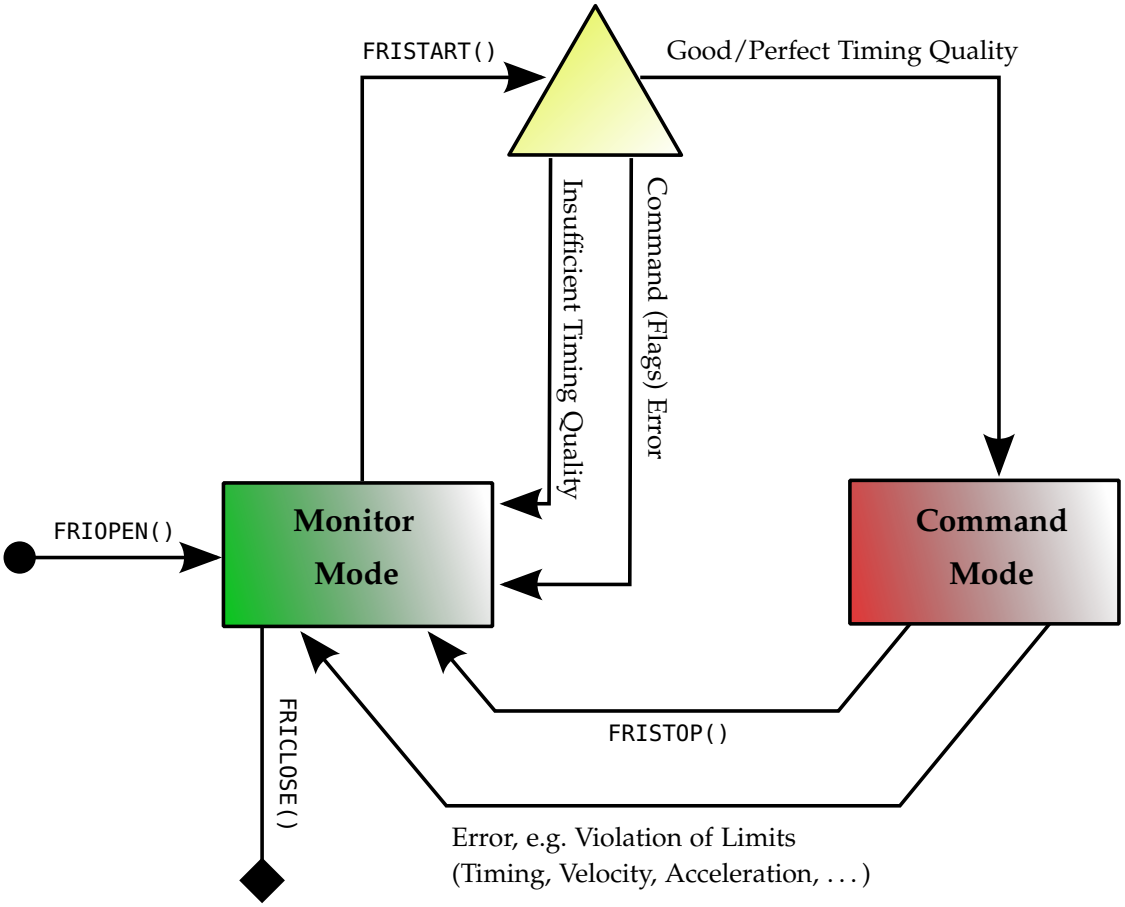

Figure 29: The control of the Kuka/DLR LWR via the Fast Research Interface (FRI) is subject to the transition of two modes. The Monitor Mode only allows the passive reading of the robots parameters and setting of control variables to the KRL level while the Command Mode allows the direct commanding of positions to the robot in real-time.

To change the control mode of the robot (e.g. from position to joint impedance control), the robot has to be in Monitor Mode. As its predecessor, the FRI version of OpenKC allows the switching of the control modes from within the API, i.e. on a mode switch, the framework enters Monitor Mode (if appropriate) and fulfills the change in the control mode and re-enters Command Mode (if appropriate). This functionality is also provided through a custom OpenKC KRL program that has to run on the robot controller.

Due to the use of POSIX real-time threads, the OpenKC FRI is

able to fulfill the timing constrains of ≤ 1 [ms] on recent hardware (e.g. Intel® Core™ 2 Quad CPU Q9550). Generally, the performance is above the OpenKC-RSI-XML version, since parsing and generation of XML-Messages are omitted.

Real-time Trajectory Planning

To actually move the robot, a path has to be planned and a trajectory has to be generated. To this end, we used a C++ implementation[29] of the Control Basis Framework (CBF) [109, 133, 286]. This framework provides flexible means to synthesize closed loop controllers from simple components: artificial potential functions, sensor transforms, effector transforms and resources[30].

[29] Written by Florian Schmidt

[30] A resource represents a robot control affordance. For example the joint angles of a robotic arm

Potential functions are a natural language for describing robotic tasks. The goal of the closed loop controller is to minimize the value of a scalar potential function defined on the task space at hand. Examples include a quadratic potential function on Cartesian end effector position space which takes a minimum at the desired goal position. In practice only the gradient of the potential function is of interest, as that is used to iteratively solve the problem of maximizing it.

Sensor transforms map actuator sensor readings into the desired task space. To stick with our previous example of Cartesian end-effector position control one example would be the forward kinematics mapping for a robotic arm.

An effector transform maps a task space update step into a actuator control affordance update step. Again, sticking with our previous example, this could be a (pseudo) inverse based mapping from Cartesian end-effector position space to the joint angle values of a robotic arm.

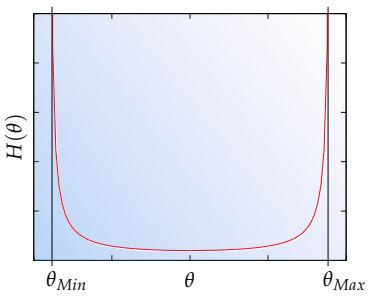

Figure 30: The potential function used to avoid joint limits within the null-space of the kinematic redundant Kuka/DLR LWR controlled via the CBF.

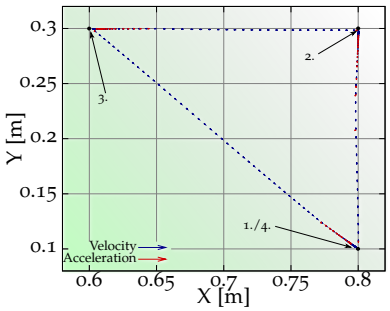

Figure 31: A trajectory in task space and projected to 2-D. The arrows indicate the measures velocities at sub-sampled positions of the trajectory.

Additionally the CBF allows for hierarchical composition of controllers. This is achieved by means of manipulator Jacobian null space projection [321]. The control affordance update step of a subordinate controller is projected into the null-space of the Jacobian of a higher priority controller. This enables us to flexibly combine tasks when strict prioritization is possible. Examples include optimizing manipulability measures [395] of a robotic manipulator and joint limit avoidance while at the same time reaching for a Cartesian end-effector position. In this case the reaching movement is the higher priority task and the joint limit avoidance is the lower priority task.

The framework is flexible enough to allow the composition of controllers for a wide range of tasks. The OpenKC framework facilitated very easy integration of the CBF approach into the bimanual robotic setup.

In our specific case, within the robots' null-space a controller with a potential function proposed by Zghal et al. [403] was used. The goal of this potential[31] is to exploit the null-space of the primary controller to avoid joint angle limits in an effective, yet diffident way. This is both achieved by this potential, which only has an impact on the trajectory when a joint limit is approached. It has to be mentioned that the functionality is dependent on a careful weighting of the controllers to avoid too little or too big movements in the null-space. In Figure 30 the potential in its qualitative course in a simple one-dimensional case is plotted. In all experiments, this potential function has shown to be very well behaved as the influence is negligible in a broad range of joint angles but through its steep flanks an effective avoidance of joint limits is achieved.

[31] The potential for joint angle θ and limits θ_{Min}, θ_{Max} is given as:

$$H(\vec{\theta}) = \sum_{i=1}^{N} \frac{(\theta_{i,Max} - \theta_{i,Min})^2}{(\theta_{i,Max} - \theta_i)(\theta_i - \theta_{i,Min})}$$

and the gradient step $\frac{\nabla H_i(\vec{\theta})}{\partial \theta_i}$ denotes to:

$$\frac{(\theta_{i,Max} - \theta_{i,Min})^2(2\theta_i - \theta_{i,Max} - \theta_{i,Min})}{(\theta_{i,Max} - \theta_i)^2(\theta_i - \theta_{i,Min})^2}$$

The potential field approach used within the CBF is stateless, i.e. agnostic to the last position the robot had. Only the current position and the goal are relevant for generating the gradient step towards the target. While the framework therefore offers the possibility to change the target position from one planning cycle to the next, which is a prerequisite for real-time trajectory control which again is needed for sensor guided motions, it does not take the last positions into account. It is hence neglecting the current velocity, acceleration and jerk of the robot. When the robot approaches a target, the potential field naturally flattens, and as a consequence, the length of the gradient decreases. So a gentle deceleration at the target point is implicitly given with this approach.

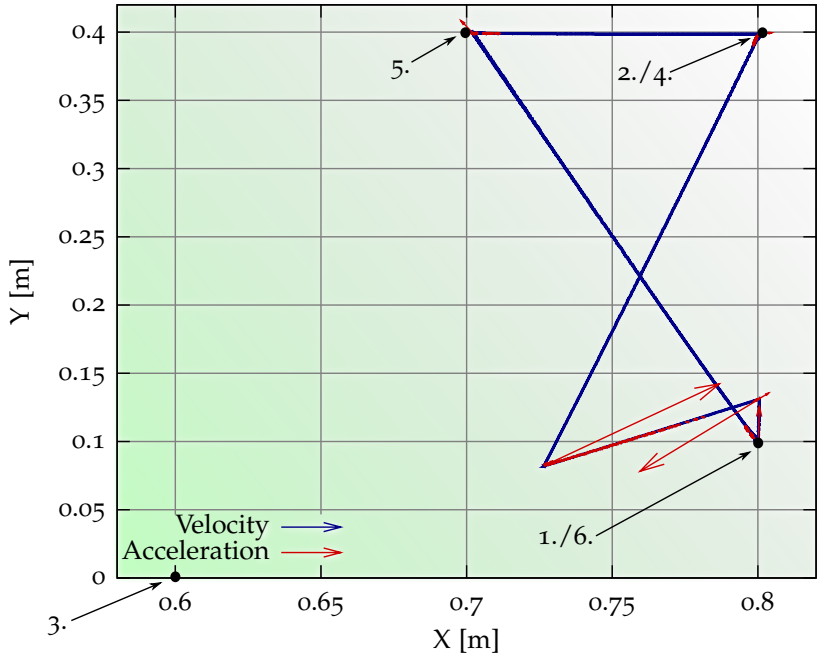

Figure 32: This figure shows an example trajectory without jerk limitation projected to 2-D, movement was also done on a plane in the task space. Motion started at point (1.). While in transit to the first target position (2.), a new target (3.) is set. Before reaching the target, the previous target is again set as goal (4.). The graph shows the measured position of the end-effector, trajectory points are sub-sampled (factor 8). High accelerations and therefore high jerks are found at the turning points.

This, however, is not the case when starting a motion or when changing the target position while the robot is on his way to a

different target. While velocities can be handled in capping the maximal length of the gradient steps, this does not hold true for acceleration and jerk. When a motion starts or on sudden changes of targets, the difference in the vectors of two successive gradient steps can become rather large, resulting in high accelerations and jerks (cf. Fig. 32). Accelerations have to be limited to obey the acceleration constraints of the individual joints, jerk needs to be limited to minimize the wear on the robot and to enhance the quality of the resulting movement. Or, to formulate the problem a little differently: we are looking for a dynamic filter which modifies the $\hat{v}(t)$ in a way that velocity, acceleration and jerk constraints are fulfilled and $v(t)$ is as similar to $\hat{v}(t)$ as possible. A dynamic limitation of acceleration and jerk is done through scaling and additive combining of gradient steps. The velocity and acceleration is restricted using these equations, given $|\hat{v}_i(t)| \neq 0$ and $\hat{v}_i(t) \neq v_i(t-1)$ respectively:

$$f_i^v(t) = \frac{v_i^{limit}}{|\hat{v}_i(t)|} \tag{2}$$

$$f_i^a(t) = \frac{a_i^{limit}}{|\hat{v}_i(t) - v_i(t-1)|} \tag{3}$$

where f_i is the scaling factor of the i^{th} joint, v_i^{limit} is the velocity limit of the i^{th} joint, a_i^{limit} is the acceleration limit of the i^{th} joint $v_i(t)$ is the velocity of the i^{th} joint at time t and $\hat{v}_i(t)$ denotes the gradient step of the i^{th} joint at time t as given by the CBF, hence unfiltered. If $f_i < 1.0$ for any joint, the velocity / acceleration constraints are violated. Through iteration over all joints, the minimal $f_i^{min} = \min_i(f_i)$ is determined and $v(t) \leftarrow f_i^{min}\hat{v}(t)$.

While the limitation of acceleration and velocity is a prerequisite to generate valid, drivable trajectories for the robot, the limitation of the jerk allows gentle, smooth movements with little wear on the robot. This, however, cannot be achieved without making allowances to the resulting path. The idea of a dynamic filter, similar to [92], shall therefore be introduced. Jerk is in the discrete case given as the difference or discrete derivative of acceleration:

$$j(t) = \dot{v}(t-1) - \dot{v}(t) \tag{4}$$

$$j(t) = \dot{v}(t-1) - (v(t-1) - v(t)) \tag{5}$$

Since $\dot{v}(t-1)$ and $v(t-1)$ are in the past and thus cannot be changed, $v(t)$ has to be modified in such a way that $j(t)$ can be bounded. Hence, $v(t)$ is substituted by

$$x \cdot v(t) + (1-x)(v(t-1) - \dot{v}(t-1))$$

with $0 \leq x \leq 1$. When taking a look a the limits, in the case $x = 1$, the original trajectory is followed precisely. In the contrary case that $x = 0$, the jerk becomes 0, but also the desired path is then not

taken into account at all. It is easy to see that

$$x = \frac{j^{limit}}{|v(t) - v(t-1) + \dot{v}(t-1)|} \tag{6}$$

given $v(t) \neq v(t-1) + \dot{v}(t-1)$, yields the optimal update step under the jerk and path constraints. In the case of $x > 1$, the original $v(t)$ is taken, because in this case the jerk limit j^{limit} is not violated. The formulas (2),(3) and (6) can then be rewritten into an algorithm (cf. Algorithm 1). This algorithm is run on every update step as a filter function and guarantees smooth movements. Its filter design enables real-time setting of targets, and since no complete planning of the trajectory is done but rather just the next update step, its run time behavior is also conforming to real-time constraints (<1 [ms] in our case).

Algorithm 1 Dynamic Acceleration and Jerk Limitation

Require: valid $\hat{v}(t)$, $\vec{v}(t-1)$, $\dot{\vec{v}}(t-1)$
  $f_{vel/acc} \leftarrow 1.0$
  $f_{jerk} \leftarrow 1.0$
  for all joints i **do**
    if $|\hat{v}_i(t)| \neq 0$ **then**
      $f_i^v(t) \leftarrow \frac{v_i^{limit}}{|\hat{v}_i(t)|}$
      if $f_i^v(t) < f_{vel/acc}$ **then**
        $f_{vel/acc} \leftarrow f_i^v(t)$
      end if
    end if
    if $\hat{v}_i(t) \neq v_i(t-1)$ **then**
      $f_i^a(t) = \frac{a_i^{limit}}{|\hat{v}_i(t) - v_i(t-1)|}$
      if $f_i^a(t) < f_{vel/acc}$ **then**
        $f_{vel/acc} \leftarrow f_i^a(t)$
      end if
    end if
  end for
  for all joints i **do**
    $v_i(t) \leftarrow f_{vel/acc} \cdot \hat{v}_i(t)$
    if $v_i(t) \neq v_i(t-1) + \dot{v}_i(t-1)$ **then**
      $x_i \leftarrow \frac{j_i^{limit}}{|v_i(t) - v_i(t-1) + \dot{v}_i(t-1)|}$
      if $x_i < f_{jerk}$ **then**
        $f_{jerk} \leftarrow x_i$
      end if
    end if
  end for
  for all joints i **do**
    $v_i(t) \leftarrow f_{jerk} \cdot v_i(t) + (1 - f_{jerk})(v_i(t-1) - \dot{v}_i(t-1))$
  end for

A TYPICAL TRAJECTORY (projected to 2-D) can be seen in the Figures 31, 32 and 33 respectively. In this example, different target

points on a plane in task space coordinates were given. In the first example (cf. Fig. 31), all target points are reached and the next target is only set when the potential function has already converged to the target position. In other words, only when the end-effector is close enough to the target, the next goal position is set. Due to the potential field approach, the target point may in theory never be reached. This, however, is in practice not significant, since this displacement is well beneath the position accuracy of the robot.

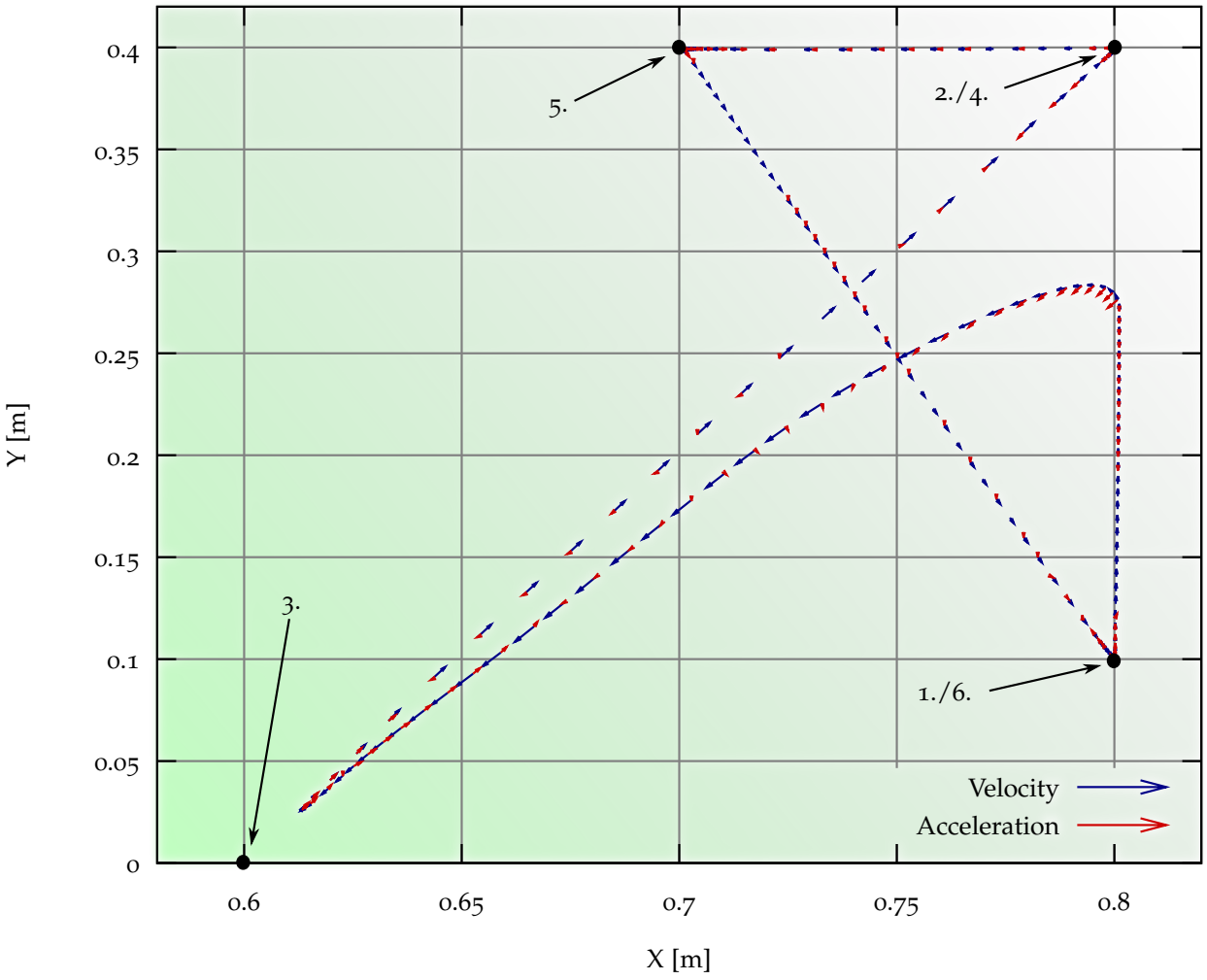

Figure 33: While in transit to target position (2.), a new target (3.) is set. Before reaching the target, the previous target is given (4.). The trajectory shows the measured position of the end-effector, trajectory points are sub-sampled (factor 8).

In Figure 32, while the robot is in transit to a target position, a new target is set. Here, velocity and acceleration limits (v^{limit} and a^{limit}) are enforced, without constraints on the jerk. While a very accurate tracking of the desired path $\hat{v}$ is achieved, high peaks in acceleration, and therefore high jerks, are noticeable. This limits the maximal velocities and accelerations that can safely be driven as high jerks put too much mechanical wear on the robot.

The same path as in Figure 32 is given in Figure 33. This time, however, jerk constraints (j^{limit}) are enforced in addition to velocity and acceleration. Much higher velocities can be achieved without the risk of violating any constraints of the robot. The trajectory

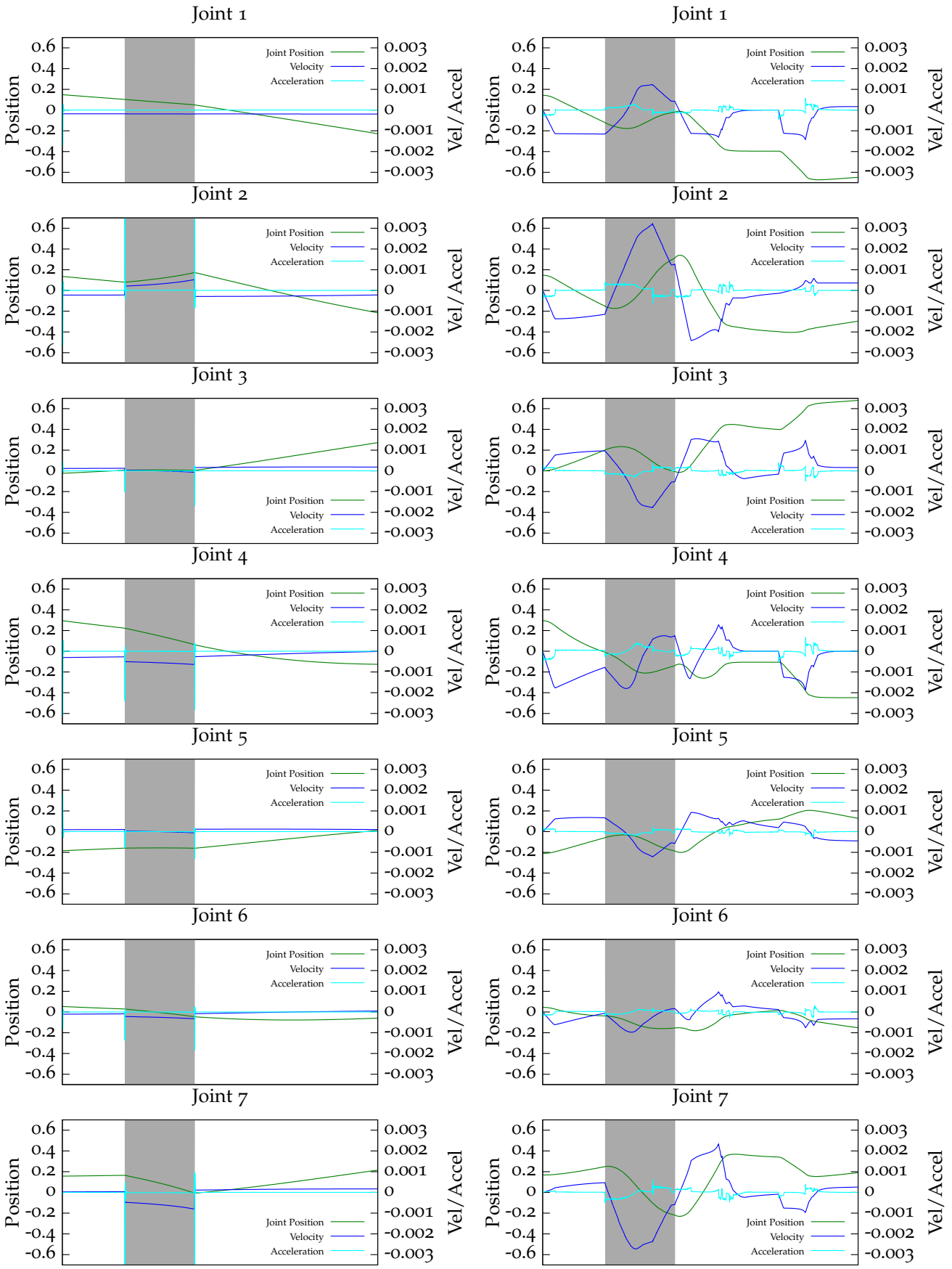

Figure 34: The Position, Velocity and Accelerations of each joint during the beginning of trajectory seen in Figure 32 and 33, on the left without jerk limitation, on the right side with jerk limitation.

does not accurately track the desired path $\hat{v}$, instead a new, smooth path is generated. On turning points, it is easy to see that the acceleration changes very gently. This approach allows for the safe exploitation of the maximal velocities and accelerations of the robot. Without jerk limitations, the trajectory took 9.712 [ms]. With jerk limitations, the trajectory took now only 3.512 [ms], due to the possibility to use higher acceleration and velocity limits.

Since the constraints are enforced on the individual joints, which also have different limits, in Figure 34 the different joint values, velocities and accelerations of the robot are plotted. In the left column, the values of the trajectory in Figure 32 are shown, while the right column shows the movement seen in Figure 33. The shaded area marks the period in time when the original target point (2.) was overwritten with point (3.).

THE METHODS THAT HAVE BEEN PRESENTED HERE provide the basis for sensor guided motions. Most of the work presented in the rest of this thesis are predicated on this control strategy for the robot. Thanks to the OpenKC software, the path planning, trajectory generation and dynamic filtering real-time sensor guided motion, including force guided motions, are possible.

Part III

Tactile Object Recognition

A classical example to motivate tactile sensing in a robotic setup is the blind grasp into a pocket or box. Humans can easily discriminate different objects in arbitrary containers and pick the desired object in an instant. Robots could, of course, try to boost object recognition by the use other abilities and sensor information to substitute for the lack of tactile sensing. This could be achieved for example through a high number of photometric sensors, especially eye-in-hand camera systems. Of course, one would sacrifice the vision of building an anthropomorphic system. In addition, tactile sensing provides data that can hardly be estimated by alternative means, like hardness and friction, besides giving information where most other sensors fail due to occlusions or interference, for example during a grasp. Therefore, the advantages of a sense of touch even in areas where other modalities would also contribute are easy to see.

Whilst for some task, tactile sensing can be substituted by special sensors, it seems more natural and sustainable to pursue the advancement of tactile sensing in robotics

Psychophysic experiments have shown the high, nearly perfect, recognition rate humans are capable of even when limited to the sense of touch [175]. During the classification task, usually a two stage exploration strategy consisting of a general action like enclosing the object followed by a specialized series of actions [192] are used. But the high recognition rates are only possible in certain domains, like common objects. When confronted with 2-D depictions of objects, the recognition rate drops significantly [177]. There are strong indications also in other experiments, that shape features are not primarily used. Instead material properties like texture or thermal conductivity are more important [171]. When tactile perception is constrained in one way or another, performance usually declines, although it is difficult to rule out certain aspects, for example texture perception without also impairing the tactile perception as such [196].

More results from the neurophysiology community can be found on pages 19 ff.

In this chapter the problem of robotic tactile object recognition is approached from different perspectives. The first question tackled here does not strictly focus on tactile object recognition but goes beyond and is approaching the question of how a tactile feature space could look. Dimension reduction is a key to the efficient use of many machine learning techniques. Tactile object recognition is in this context the exemplary task where the contribution of different tactile features is examined. We continue introducing grasping based on tactile sensing with the SDH-2 Hand, a dexterous 3-fingered robotic hand equipped with tactile sensors. It demonstrates how unknown objects are grasped in a simple pick and place task. It also shows how point clouds can be extracted by exploitation of the developed grasp primitive and how the acquired data can be used in a classification task. Although this approach to object recognition is biologically motivated, the proposed algorithm

To approaches are presented in this chapter:

I. Purely Tactile
II. Haptic, i.e. Tactile and Kinesthetic

uses mathematical algorithms to discriminate a number of objects.

Related Work

Tactile Object Recognition

Object recognition or classification of objects or object-categories has long been subject to research in the robotic community. It is not surprising that even very simple tactile sensors can be used to improve object recognition performance [255, 261]. It has been found that even very simple tactile sensing modules, in this case switches placed on a glove, can provide sufficient information to discriminate a small number of objects [242, 227, 226]. The glove is worn by a human, who uses his expertise to grasp different objects. An interesting result from these works is that only very few, about 20 out of 160, sensors are providing the information needed for the classification task.

Object classification through human worn gloves.

A more extensive study was done in [22]. Here, a cyberglove was equipped with 18 tactile sensor modules. With the use of hidden Markov model (HMM) about 90 % of the grasp sequences could be correctly recognized according to a grasp taxonomy.

A cyberglove with tactile sensors attached is also used in [26], where humans track the contour of objects. From the collected data from the cyberglove, tactile sensor and a tracked bracelet for position in space, a 3-D point cloud is acquired. In a next step, superquadric representations of the objects are generated.

In [305, 306] a theoretical background to tactile object recognition is given. Ideal and suboptimal paths (where information is gained, but the object may still not be recognized completely) can be analytically generated. This work provides a good starting point to a more model driven approach to object recognition, but is unfortunately based on planar 2-D objects. It is not straightforward to extend the ideas to 3-D, also, object models must exist. Although it is said that paths are given, the task of actual (collision free) robotic motion planning for tactile perception is not tackled.

Object and shape recognition and pose estimation in theory.

Accordingly, in [74], the problem of the next best view in terms of sensor placement is approached. Again, in 2-D, algorithms for polyhedral objects were found. The general problem in 3-D, also with a priori unknown object shapes remains, although some heuristics are given and evaluated in simulation.

Completely in the 2-D domain resides [136], where curves are

fitted to few tactile acquired contact points to estimate the shapes. Since only curves up to quadratic complexity are investigated, the applicability to real world scenarios, in particular since this work is limited to 2-D, is yet to be shown.

In the line of more theoretical work is also [41]. Based on previous findings [39, 40] the robustness of polyhedral modeling of objects is investigated. These models, of course, only apply to convex objects. Two approaches are used, one that refines a model from an upper bound, and the other that incrementally builds up a model from contact locations. These methods benefit from not only plain contact data but also from normal information to get more accurate faces. The types of inaccuracy tackled in this paper comprise incomplete knowledge about the object and imprecise object location. Also, outliers were pruned. It is shown that object translation has a great impact on the presented methods. Other than that, high recognition rates could be achieved, but only few models (max. 10) were used.

Starting with simulation but while continuing with conducting a real world experiment is presented in [238]. The reconstruction of an arbitrary convex object is done through estimation of the local curvature of the object which rests in two tactile equipped palms. The good results in simulation could partly be backed with a real world experiment, which left some important questions unanswered concerning how the object is deliberately and repeatably moved, since friction and dynamics were excluded from their 2-D model. Also it is not clear, if and how this work can be extended to 3-D.

Some hybrid systems for object recognition exist. Hybrids, however, are often comparatively bulky and complex. Since the recognition of objects held by a robotic manipulator is difficult due to occlusion and rather complicated object segmentation, the vision and the tactile exploration are carried out in sequence. One popular example is the work from Peter K. Allen [7], which has already been discussed in detail on page 36. In the follow up work [6], superquadric representations of the grasped objects were generated mostly from the haptic information. For more details on superquadrics refer to Fig. 13 on page 36.

Hybrid systems fuse vision and tactile data for object recognition.

In contrast to these model based approaches, in [166] another hybrid system is presented. Here, a neural network is used for sensor data fusion. The recognition rate of the fused input was at any time higher than when one modality was exclusively used. Tactile recognition was done with an artificial robot hand with 4 fingers. In test and training, different grasp positions were used. The classification results were above 93% for eleven objects in the set.

In a recent work, a bionic hand with one tactile sensor (combined stain gauge and PVDF film) at each phalanges is presented

[340]. The experimental section of this paper comprises only 4 objects, which may be to little to make general assumptions on the scalability of the approach. In addition, only sparse tactile sensing was provided. It is not clear if the results are repeatable given more objects. Especially since a self organizing map (SOM) was used, it would have been interesting to provide a much larger data-set to see if similar objects would be found in neighboring regions of the map. In previous work [341], the authors found that moving an object can reveal important information that help in the classification task.

Object recognition from grasping.

Consequently, [126] combines both findings. A bionic hand is used to differentiate between three classes of objects (prism, cylinder and ball). The work is distinct from most other works as it uses time series, which of course already have been successfully employed in [113]. The time series emerge from a regrasping algorithm, which also accounts for a good recognition even if objects are presented with great variance in posture and translation. To cope with the structure of data presented in time series, an artificial recurrent neural network is used.

In [102] a total of 7 different objects are passed to an anthropomorphic robot hand, equipped with tactile sensors at each phalanges. The results for classification with kinesthetic, tactile or fused data is compared. The central moments of the tactile image data is analyzed, also a principal component analysis (PCA) is done. The overall recognition rate is at approximately 75 %. A very interesting idea was to mount the tactile sensors on micro-joysticks. That way, the contact area was maximized and additional data from these passive joints was gained.

Experiments with a robotic hand equipped with (tactile) force sensors could distinguish 4 different containers [46] and also judge their internal state (empty/full and open/closed). The recognition rate of the containers was very high (93.9 %). Accounting for this rate was the different sizes of the container, as the gripper position of the first touch was primarily used for classification. The judgment of the internal state of the containers was much more difficult and dropped to 32.5% in one case. It was found that the recognition rate was highly dependent on the end state grasp force. This force was not adaptive, though, but predefined. This seriously constricts the general use of this special approach.

Judging the internal state of objects.

The work that is most closely related to this paragraph is the recent work found in [270]. Here, different feature sets from tactile images were compared in their classification performance. The general idea - to find an optimal set of features that help to interpret the tactile data apart from additional position data - is hence the same, yet many differences in the approach can be noted. First of all, the most of it is based on data obtained in simulation. The probing of the total of 10 objects was done employing the ideas of sampling based motion planing. This way the space of possible

Object recognition from tactile images.

robot end-effector poses was sampled, with a small tendency to favor nearby poses of recently made contacts. In case of contact, a special controller takes over to ensure for as uniform tactile imprints as possible. The sampling in simulation allows the use of such an algorithm, which would be much more difficult in the real world because collisions with unknown objects in unknown positions and translations would occur, which in turn would at least require special hardware. But still in such a case, tactile sampling in completely unconstrained settings remains a challenge. Nevertheless, the data acquired in simulation offers the possibility to change certain parameters with very few overhead, like the sensor resolution, signal noise, exploration strategy and object perturbation. The overall performance of the system was above 95 % when considering 60 samples or more. A small consecutive experiment with real world data was conducted, at lower recognition rates, yet proved the validity of the approach. Unfortunately the acquisition of the real world data is held very brief, a comparison to the work presented here therefore becomes difficult.

In a follow-up paper [271], the real world data experiment was extended to probe a set of five raised letters that were presented with different translations, i.e. variation in two dimensions. Since the letters are larger than the sensor, only small parts of the letter are displayed. Since the letters were presented to the tactile sensor with a special apparatus, the tactile sensor was used as an imaging device. The method used consists of sequential state estimation techniques, or occupancy grid mapping to be more precise, to gradually build up a mosaic map of the original letter. The results varied, according to the number of particles used, between 9 and 47 readings to successfully reconstruct the letter.

Grasping in a Tactile Context

To recognize objects with tactile sensors, one always has to think about how to make the contact to gather tactile data. In the case of an artificial hand, the use of grasping primitives seems reasonable. Grasping has been and still is a major topic in robotics. In this section, we present related work on grasping with special respect to tactile sensing.

The modeling of contacts and dynamics in grasping, manipulation and grasp planning has found wide attention in the research community [33, 24, 258, 236, 206, 394, 327, 97, 337]. These findings however either require explicit object models or have not yet been applied in a real world scenario. In the first case, one has to find means to acquire object data of unknown or previously unseen objects. Unquestionable methods to do this exist [30, 94, 209, 208, 222, 53], but of course these strongly benefit from rather structured environments (i.e. stable lighting conditions, uniform background or constrained object shapes). It is therefore

Traditional approaches to grasping are often model-based and neglect the tactile sensing modality.

preferential to also use haptic data to model objects and to improve manipulation performance [274, 234].

Although the idea to employ tactile sensors builds on a long tradition [255], still a wide area of applications in the context of manipulation has yet to be found. There is nothing vague about that according to [202], the development of tactile sensing devices remains the main focus of research in that area. Up until today there is need for further research on robust, flexible and sensitive tactile sensing technologies [350].

A tactile motor coordination with a artificial neural network was developed in [205], where two objects (both cylindrical) could be grasped with an artificial hand. In [186] as well as in [13], a SDH-2 hand is used to classify the expected stability of a previously simulated grasp. In contrast to the proposed approach, tactile sensing is primarily used to compensate for variations and errors in the visual perception of the system or inaccurate simulation results. Hence the provided feedback from the tactile sensors is used, but not in a tight control loop to form the grasp itself. Remarkable in this context are also [140, 391] which imposingly show the dexterity an artificial hand can gain from tactile feedback.

A comprehensive study on finding stable grasps using force and tactile sensing presents [76]. They could show that their proposed algorithm was able to grasp all test objects when the objects were perfectly aligned and outperformed a naive approach when errors in orientation and translation were introduced. They also suffer from inadequate sensitivity of the tactile sensors.

Grasping under uncertainty.

Recently, Toussaint et al. demonstrated a new approach to probabilistic planning in a real block world scenario [362]. In this work, which focuses on the reasoning part, a SDH-2 Hand grasps the objects facilitating a tactile feedback loop, therefore providing some feedback in the grasping process.

Although limited to simulation [68] shows that blind robot grasping, i.e. solely relying on tactile and kinesthetic feedback, offers great possibilities in the prediction of the stability of a grasp. This is done through a soft contact model, which is more advanced than previously frequently used point contact models. The analysis, however, focuses on form closure and supporting aspects of the grasp. Forces, or optimal grasp forces are not covered and real world experiments are also missing.

Compliance in grasping also comes more into focus. Passively compliant grippers can improve the grasping performance [71, 290, 163]. Likewise the actively compliant Robonault 2 hand is used in [57], where particle filtering is used to estimate the pose and shape of objects. In this very interesting work, not only contact but also the absence of contact is utilized to improve the performance of the system.

Feature Based Classification

Tactile Features

In modern robotic applications, and especially in the growing field of service robotics, the use of tactile sensors becomes more and more indispensable. Information gathered by tactile sensors can exploit object properties that are not accessible by other sensing modalities like photometric sensors. Texture, friction, weight as well as contact states or fine surface features of objects can be perceived and used in complex and unstructured environments.

To maximize the benefit of tactile sensing to the overall performance of the system, it is important to efficiently and effectively extract the relevant information from the tactile sensors and to fuse the gathered data with other modalities. This could be achieved by a detection and definition of relevant surface features during tactile exploration. In the field of computer vision, the research community has come up with a large number of different feature definitions which have shown to work well in the visual domain.

Finding the best feature-space for tactile sensing is important to boost the processing speed and to improve the information that can be gained from tactile sensing.

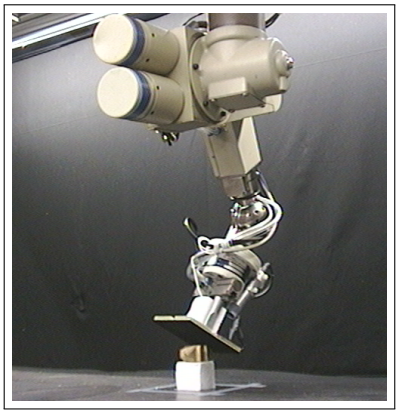

Figure 35: The tactile database was generated employing a Unimation PUMA 260 6-DOF Manipulator with a tactile sensor array mounted at the end-effector.

Here, we investigate different tactile features. Our approach is to do tactile based recognition of objects and evaluate the utility of various features during this task. These are extracted from a large tactile database. We employ unsupervised learning to cluster the continuous feature space into discrete classes, which are then further processed with the well-known C4.5 [281, 282] algorithm. The resulting decision trees are thoroughly analyzed and the different features are reviewed depending on the information gain provided by them in the classification task. It is therefore possible to analyze the contribution to the classification task of every examined feature.

Humans exhibit a remarkable ability to dexterously handle and manipulate known and unknown objects. This skill heavily relies on haptic input through the human skin [80, 147, 150]. Besides various social functions, this input modality is utilized for search, actuator positioning, object localization, handling and, last but not least, object recognition[175].

Some properties of tactile data, for example that the contact information only yields local information, is compensated through

the use of exploration strategies, or if available, other sensing modalities. One popular and - at least for humans - seemingly simple exploration strategy is a grasp. There are strong indications that humans do not reconstruct the complex 3-D shape of objects but rather do recognition of objects on a lower and more direct sensor input data level (cf. [170, 27] and pages 19 ff.).

Consider the task of recognizing an unknown object without using the visual sense; humans would do this by moving their hand around the object, combining information gathered from multiple touch experiences [192]. We seek to reproduce similar touch data for the robot using a large tactile database.

IN CONTRAST TO OTHER SENSING MODALITIES of service robots, the processing of tactile information has not yet brought up a considerable number of standard procedures. Often, tactile data is reduced to a binary contact/no contact information, and therefore putting aside many of the additional information that tactile data might be able to supply [181, 131, 362, 290, 326]. This is partly due to the unavailability of suitable and easy to use sensors that are able to closely resemble the qualities of human skin. Various efforts have been made in this direction [247, 152, 144, 336, 300, 157, 310]. Recent progress has been made on the hardware side, yielding sufficiently small and flexible tactile sensing arrays with an adequate resolution for object classification and recognition tasks [161, 391, 105]. However, some of these designs require sophisticated signal processing [61, 320, 264]. Some special designs even allow full body tactile sensing [111, 254]. In addition, the classification of tactile data into different tactile dimensions is shown [151]. This very interesting approach however, uses a special, custom made sensing apparatus, instead of standard hardware used here. For example, the hardness of a material was classified using a custom designed hardness sensor.

The optimization of tactile processing might be of importance for further developments in the field. If it would be possible to do efficient and loss-less compression of information through the processing of tactile data directly at the sensing elements, wiring problems and fast and reliable tactile processing might become possible even for large scale, i.e. full body tactile sensing.

Figure 36: These are the sixteen objects from the tactile database. The objects were sampled in different, yet stable positions.

NONETHELESS, THERE IS STILL A LARGE GAP from the availability of suitable sensors to the successful applications of tactile sensing in real-world setups. This may mainly be due to the lack of established methodologies, algorithms and features for tactile data processing. Various questions remain yet to be answered in a comprehensive manner: How to process tactile data efficiently and effectively? What will the overall architecture of a tactile system look like? What representations and algorithms to use? How to organize active tactile sensing systems? And finally, which features yield high information gains and should be used for further processing?

This section presents a dynamic tactile sensing system applying a pressure sensor array, mounted on a robot arm, that is moved around an unknown object while maintaining physical contact. Nonetheless, the focus lies on the processing of the tactile data and the application in the context of object recognition. To that end, an implicit object representation, based on various features extracted from the tactile time series, is developed. The features are used to classify previously learned objects applying a decision-tree method. Finally, we analyze the decision trees in order to assess the quality of each of the proposed features.

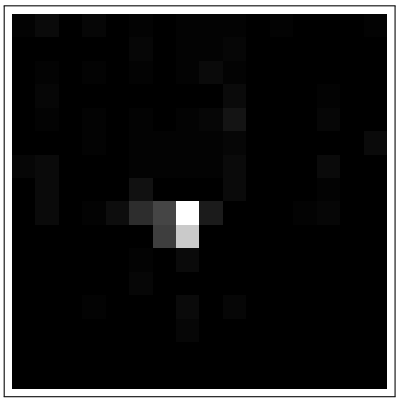

Figure 37: Tactile image data is often very sparse. Here an example is given, that is a good representative of the majority of tactile images in the database.

Architecture Description

To avoid the rather cumbersome work of data acquisition, while still using real world tactile data instead of simulation results, we decided to work on the tactile database previously developed [308]. We generated feature vectors, formed from attributes that seemed promising to us in some preliminary experiments with smaller data-sets. To be able to determine which features are contributing to a successful object and position classification, we used decision trees and the well known C4.5 algorithm. We analyzed the resulting decision trees to find out the features that contributed the most in this classification setup. The advantages of the C4.5 compared to other classification methods like artificial neural networks or support vector machines is that the process of a classification decision can be very easily understood, as it is very visual. That also seems to be why recently some classification work even in the tactile domain employed the C4.5 [46], as well as [304] used the fundamental concepts in C4.5, the entropy maximization.

Figure 38: The 16 test objects, which can be seen in Figure 36 where probed from different positions to a total of 42 object views. Only positions, where the object was stable were considered. Also the probing of symmetric poses was avoided. Here, a toy truck is given as an example. Unsteady positions (like making it stand on the driving cab) or symmetric poses (like probing the truck laying on both sides) are skipped.

Acquisition of the Data-Set

In the tactile database we used, 16 different objects (e.g. pencil sharpener, toy cars, etc. cf. Fig. 36) were probed from different positions and angles. All objects were probed from different stable position. Redundant positions were omitted. This resulted in a total of 42 different object classes, e.g. the toy truck was differentiated from the same truck lying upside down or sideways (cf. Fig. 38). The objects ranged in size and shape between 1 and 8 [cm]. A low cost 2-D tactile sensor of coarse spatial (16 $\times$ 16 'tactels' (tactile element), area: 10[cm] $\times$ 10[cm]) and temporal (10[Hz]) resolution was used. The sensor uses a piezo-resistive rubber foam for pressure sensing [161]. The foam showed to be robust throughout the experiments with comparably little hysteresis. The measured voltages are converted by a microprocessor with a resolution of 12-bit per sensing element.

The sensor was mounted on a Unimation Puma 260 6 DOF robot

A video sequence ("TactileDB") of the probing procedure is added on the enclosed/attached data storage.

manipulator (cf. Fig. 35). The robot was controlled utilizing RCCL, the Robot Control C Library [213]. All objects were smaller in size than the sensor area. The data-set is very well suited for our analysis because it represents all the little difficulties one has with real world data, let it be jitter or a less than optimal resolution. Also we had to often cope with very sparsely saturated tactile images, compare Fig. 37.

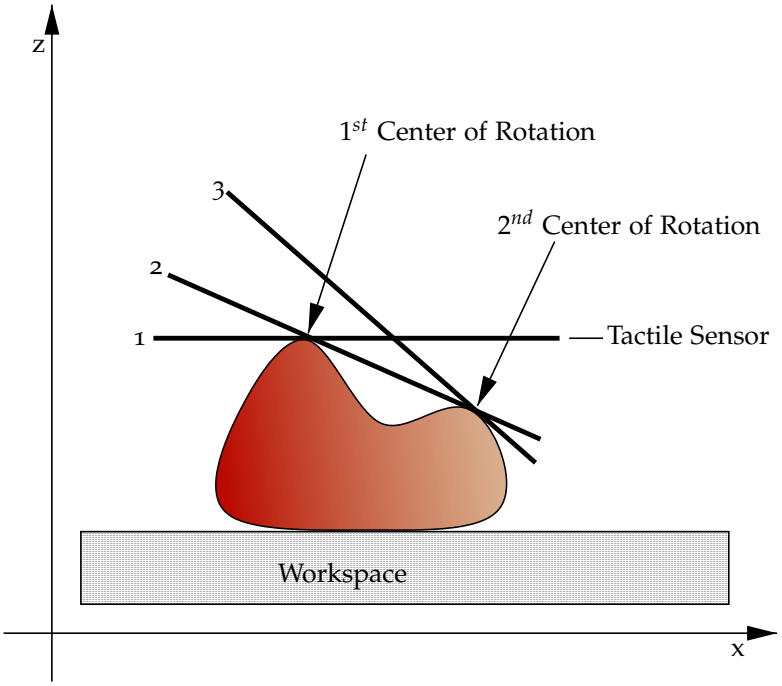

Figure 39: The object was probed in a straight line rolling, yet not sliding movement. This was guaranteed through pivoting movements around the point of contact, which is the last point on the path of probing.

AN IMPORTANT ASPECT OF OUR APPROACH IS that objects in the database were probed with a robot arm rolling the tactile pad over the object in a straight line (see Fig. 39). While rolling over the object, the pressure applied to the object was controlled through tactile feedback in real-time. This way it was guaranteed that the tactile output remained within a predefined threshold margin. In addition, a high reproducibility and reliability of the procedure could be achieved. The data from one run of probing generated a time series of tactile images. The features we propose were calculated on the full time series and parts of it respectively. Depending on the feature, more or less value was set on the special properties of the underlying time series.

EVERY OBJECT WAS SAMPLED FROM VARIOUS STABLE POSITIONS. The objects were probed from every angle and with four different translations of 3 [mm] in x and y direction. The probing from $0°, 45°, 90°$ and $135°$ (SA[32]) as illustrated in Fig. 40 was repeated with object rotations ranging from $0° \ldots 80°$ (OR[33]) with a step size of $10°$. The data is therefore well suited to check methods for robustness in both rotation and translation. The complete data-set

Every object was probed from different angles and translational offset. The data-set yields over 14 million frames, summing up to almost 7 [Gb] of raw data (approximately 5 [Gb] compressed).

[32] Scanning Angle

[33] Object Rotation

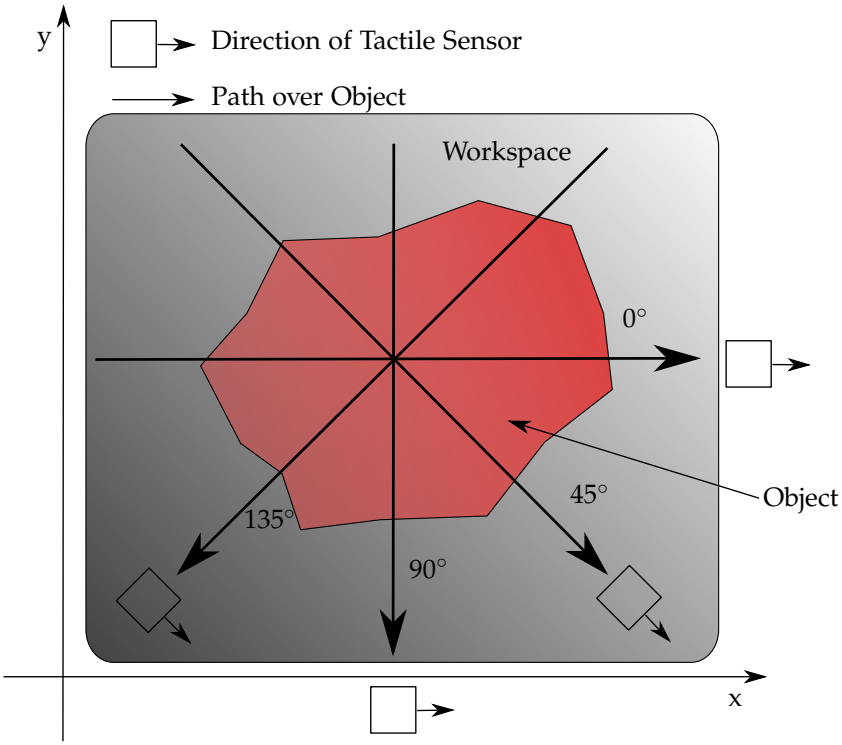

Figure 40: On this top view, the different angles of the probing process and the orientation of the sensor are presented.

has a total size of about 5 [Gb] compressed, using standard gzip compression or over 14.000.000 tactile and kinesthetic frames. If replayed in the original speed, this would be equivalent to more than 385 hours or 16 days of recordings.

It shall be mentioned that along with the tactile data, the position data from the robot was recorded as well. This allows 3-D reconstruction of the objects shape (cf. Fig. 41). Of course only convex shapes and only up to the resolution of the tactile sensor and the precision of the robot can be represented. We did not use any position data in the described experiments. Hence, only tactile data was used.

From the gathered data, two data-sets were used. The first data-set only contains the originally scanned 6048 time series[34]. Under the assumption that the process of scanning is approximately symmetric, i.e. the object rotated by 90° (OR) and scanning angle of 0° is equal to SA=0° and OR=90°. Furthermore, a scan of OR=340° and SA=0° can hence be approximated by reversing the scan OR=70° and SA=90°. Under the mentioned assumption, the data can be extrapolated to OR=0° . . . 350°, which quadruplicates the available data.

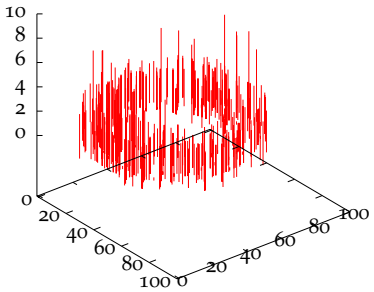

Figure 41: This is a visualization of the tactile data of approximately half a scan of an object (the orange tea light holder). Although the 3-D shape can be anticipated, there is a significant number of outliers and jitter, even though the shown data is already filtered.

[34] Number of time series:

$$4 \times 4 \times 9 \times 42 = 6048$$

- 4 Translations {(0,0),(0,3),(3,0),(3,3)}
- 4 Rotations 0°, 45°, 90° and 135°
- 9 starting angles (0° . . . 80°)
- 42 Objects

Architecture Description

The classification architecture used here consists of three stages. An overview of the complete architecture is depicted in Figure 42. In the first stage, a set of features is extracted. The details of the used features are explained in the following section. It shall

be noted that the time series are not of equal length. The length of the time series was determined by the object and the individual trajectories taken. The features, however, can be seen as an abstraction layer on the time series nature of the data.

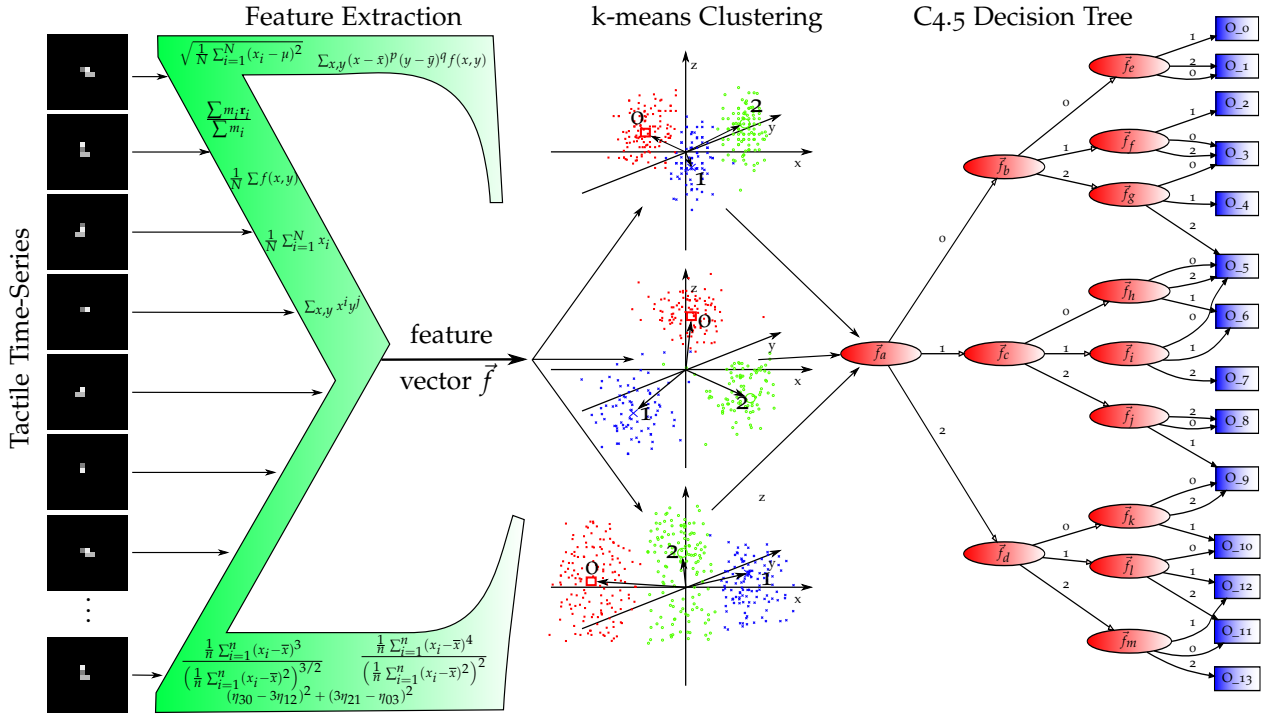

Figure 42: An overview of the classification architecture. From the tactile time series a set of continuous valued features is calculated. On these features, a discretization is performed. This is done through unsupervised learning (k-means). The number of clusters is the parameter of the system. Each feature is therefore transfered into N discrete classes and can hence be used with the C4.5 decision tree algorithm.

The second stage of the classification system is used to convert the continuous, and sometimes multi-dimensional features into discrete classes. Although the C4.5 algorithm is able to cope with continuous one dimensional signals, it only uses a simple threshold approach. Through unsupervised learning – the k-means EM-algorithm is used, more details on this is found in the section after next section – a finer separation into classes can be achieved, even in the multi-dimensional case.

The third stage consists of the C4.5 classification algorithm. The resulting decision tree can easily be analyzed, albeit the considerable sizes of the resulting trees. This is, however, a common challenge when trying to analyze and understand a classification problem of 42 classes.

Features

CONFORMING TO PRELIMINARY EXPERIMENTS with a limited object set done in the forerun of this work, particularly statistical features were computed from the tactile data. Statistical data is suited to give information on the contact without taking the absolute or relative position or the specific contact pattern into account. But it is possible, however, to discriminate contacts, how sharp peaked they are, or if it is a rather well distributed contact situation. The

Feature No.	Feature Description	Dim	FS	Q	C
1-6	Center of mass	$\mathbb{R}^2$	X	X	X
7 - 12	Distance center of mass $\leftrightarrow$ center of sensor	$\mathbb{R}^1$	X	X	X
13	Value Maximum tactel	$\mathbb{R}^1$	X		
14	Position Maximum tactel	$\mathbb{R}^2$	X		
15	Distance Maximum tactel $\leftrightarrow$ center of sensor	$\mathbb{R}^1$	X		
16	Value Minimum tactel	$\mathbb{R}^1$	X		
17	Position Minimum tactel	$\mathbb{R}^2$	X		
18	Distance Minimum tactel $\leftrightarrow$ center of sensor	$\mathbb{R}^1$	X		
19 - 24	Mean tactel	$\mathbb{R}^1$	X	X	X
25	Value median tactel	$\mathbb{R}^1$	X		
26 - 31	Standard deviation	$\mathbb{R}^1$	X	X	X
32 - 37	3^{rd} moment (skewness)	$\mathbb{R}^1$	X	X	X
38 - 43	4^{th} moment (kurtosis)	$\mathbb{R}^1$	X	X	X
44 - 49	Maximum in standard deviation of all frames	$\mathbb{R}^1$	X	X	X
50 - 55	Minimum in standard deviation of all frames	$\mathbb{R}^1$	X	X	X
56 - 61	Maximum of 3×3 windowed standard deviation	$\mathbb{R}^1$	X	X	X
62 - 67	Minimum of 3×3 windowed standard deviation	$\mathbb{R}^1$	X	X	X
68 - 73	Maximum of 3^{rd} moment	$\mathbb{R}^1$	X	X	X
74 - 79	Minimum of 3^{rd} moment	$\mathbb{R}^1$	X	X	X
80 - 85	Maximum of 3×3 windowed 3^{rd} moment	$\mathbb{R}^1$	X	X	X
86 - 91	Minimum of 3×3 windowed 3^{rd} moment	$\mathbb{R}^1$	X	X	X
92 - 97	Maximum of 4^{th} moment	$\mathbb{R}^1$	X	X	X
98 - 103	Minimum of 4^{th} moment	$\mathbb{R}^1$	X	X	X
104 - 109	Maximum of 3×3 windowed 4^{th} moment	$\mathbb{R}^1$	X	X	X
110 - 115	Minimum of 3×3 windowed 4^{th} moment	$\mathbb{R}^1$	X	X	X
116 - 121	Standard deviation of 3×3 window	$\mathbb{R}^1$	X	X	X
122 - 127	3^{rd} moment of 3×3 window	$\mathbb{R}^1$	X	X	X
128 - 133	4^{th} moment of 3×3 window	$\mathbb{R}^1$	X	X	X
134 - 139	Standard deviation of 3×3 window with most contact	$\mathbb{R}^1$	X	X	X
140 - 145	3^{rd} moment of 3×3 window with most contact	$\mathbb{R}^1$	X	X	X
146 - 151	4^{th} moment of 3×3 window with most contact	$\mathbb{R}^1$	X	X	X
152 - 158	Distance maximum tactel $\leftrightarrow$ center of sensor	$\mathbb{R}^1$	X	X	X
159	Number of tactels $>$ mean + 0.5(std.dev.)	$\mathbb{R}^1$	X		
160	Sum Powerspectrum	$\mathbb{R}^1$	X		
161 - 166	3×3 window of maximum contact area in time series	$\mathbb{R}^9$	X	X	X
167 - 172	5×5 window of maximum contact area in time series	$\mathbb{R}^{25}$	X	X	X
173 - 178	Averaged 3×3 window of maximum contact (see Fig. 43)	$\mathbb{R}^9$	X	X	X
179 - 184	Averaged 5×5 window of maximum contact (see Fig. 44)	$\mathbb{R}^{25}$	X	X	X
185	Hu rotation invariant moment I_1, cf. eq. (7)	$\mathbb{R}^1$	X		
186	Hu rotation invariant moment I_2, cf. eq. (8)	$\mathbb{R}^1$	X		
187	Hu rotation invariant moment I_3, cf. eq. (9)	$\mathbb{R}^1$	X		
188	Hu rotation invariant moment I_4, cf. eq. (10)	$\mathbb{R}^1$	X		
189	Hu rotation invariant moment I_5, cf. eq. (11)	$\mathbb{R}^1$	X		
190	Hu rotation invariant moment I_6, cf. eq. (12)	$\mathbb{R}^1$	X		
191	Hu rotation invariant moment I_7, cf. eq. (13)	$\mathbb{R}^1$	X		
192 - 196	Hu rotation invariant moment I_1, cf. eq. (7)	$\mathbb{R}^1$		X	X
197 - 201	Hu rotation invariant moment I_2, cf. eq. (8)	$\mathbb{R}^1$		X	X
202 - 206	Hu rotation invariant moment I_3, cf. eq. (9)	$\mathbb{R}^1$		X	X
207 - 211	Hu rotation invariant moment I_4, cf. eq. (10)	$\mathbb{R}^1$		X	X
212 - 216	Hu rotation invariant moment I_5, cf. eq. (11)	$\mathbb{R}^1$		X	X
217 - 221	Hu rotation invariant moment I_6, cf. eq. (12)	$\mathbb{R}^1$		X	X
222 - 226	Hu rotation invariant moment I_7, cf. eq. (13)	$\mathbb{R}^1$		X	X

Table 6: Table of Features Used: On Full Time Series (FS), On Quarters (Q) and on a Composite (C) of the Quarters

standard deviation, skewness and the kurtosis are therefore the basis of many suggested features.

Some features are based on the whole time series, while others considered only parts of the series or worked on the results of those features from parts of the time series. For example, some of the used features include positions and distances of the center of mass[35], maximum, minimum and mean pressures, as well as standard deviation, third and forth stochastic moments. In addition, the power spectrum (through discrete Fourier transformation) as well as the raw, unprocessed 3×3 (see Fig. 43) and 5×5 windows (see Fig. 44) centered at the points with the highest contact force (both total and averaged over the windowed areas) were chosen.

From the area of computer vision, different variations of the scale-invariant feature transform (SIFT) have been very popular and successful in a number of tasks [216]. In preliminary experiments with tactile data, we were not able to show that these features also are applicable to tactile data. This is very easy to understand as the strength of the SIFT features is to generate features that are robust against the scale of the object (close or far away from the camera). This problem is not existent with tactile data. On the contrary, different scales are important to discriminate different objects. Also it has to be taken into account, that the tactile resolution is much coarser than a digital image. One set of features well known from computer vision was, however, added to the list of tested features: the rotational invariant moments by Hu [132]. Given:

$$\eta_{ij} = \frac{\mu_{ij}}{\mu_{00}^{\left(1+\frac{i+j}{2}\right)}}$$

with:

$$\mu_{pq} = \sum_x \sum_y (x - \bar{x})^p (y - \bar{y})^q f(x, y)$$

and $f(x, y)$ is the value of the tactile image at coordinates x, y. Then, the rotational invariant moments used denote to:

$$I_1 = \eta_{20} + \eta_{02} \tag{7}$$

$$I_2 = (\eta_{20} - \eta_{02})^2 + (2\eta_{11})^2 \tag{8}$$

$$I_3 = (\eta_{30} - 3\eta_{12})^2 + (3\eta_{21} - \eta_{03})^2 \tag{9}$$

$$I_4 = (\eta_{30} + \eta_{12})^2 + (\eta_{21} + \eta_{03})^2 \tag{10}$$

$$\begin{aligned} I_5 = {} & (\eta_{30} - 3\eta_{12})(\eta_{30} + \eta_{12})[(\eta_{30} + \eta_{12})^2 - 3(\eta_{21} + \eta_{03})^2] + \\ & (3\eta_{21} - \eta_{03})(\eta_{21} + \eta_{03})[3(\eta_{30} + \eta_{12})^2 - (\eta_{21} + \eta_{03})^2] \end{aligned} \tag{11}$$

$$\begin{aligned} I_6 = {} & (\eta_{20} - \eta_{02})[(\eta_{30} + \eta_{12})^2 - (\eta_{21} + \eta_{03})^2] + \\ & 4\eta_{11}(\eta_{30} + \eta_{12})(\eta_{21} + \eta_{03}) \end{aligned} \tag{12}$$

$$\begin{aligned} I_7 = {} & (3\eta_{21} - \eta_{03})(\eta_{30} + \eta_{12})[(\eta_{30} + \eta_{12})^2 - 3(\eta_{21} + \eta_{03})^2] - \\ & (\eta_{30} - 3\eta_{12})(\eta_{21} + \eta_{03})[3(\eta_{30} + \eta_{12})^2 - (\eta_{21} + \eta_{03})^2]. \end{aligned} \tag{13}$$

While most of the features are rotationally invariant, some exceptions exist. We will go into detail on this in the results and discussion section. The idea, however, is to also use some features,

[35] The center of mass of a tactile image is given as $C = \frac{\sum m_i r_i}{\sum m_i}$ and is not to be confused with the (physical) center of mass of a probed object

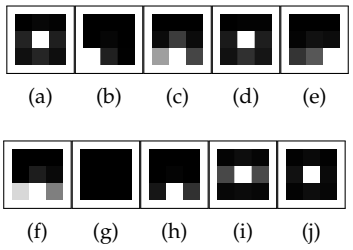

Figure 43: The 10 cluster centroids of the 3×3 windowed area. The images here are visually enhanced, i.e. normalized.

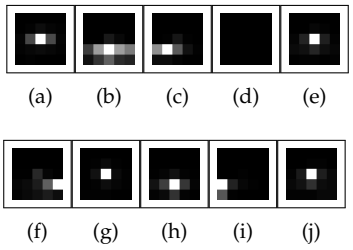

Figure 44: The cluster centroids of the 5 x 5 windowed area (N = 10). As can already be noticed in Fig. 43, prototypes with a point of contact in the center with no or few other active tactels are overrepresented. These images are visually enhanced (normalized).

that one would expect not to generalize well and look how they got used in the approach.

To clarify some expressions used here and thereafter: When the minimum or maximum is used, it means that the minimal or maximal value of this category in the relevant section of the time series is used. If neither minimum or maximum is used, it implicitly means that the average value is taken, i.e. it is averaged over all frames in the corresponding section of the time series.

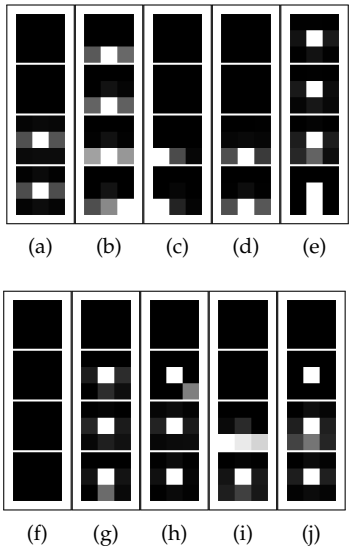

Figure 45: The cluster prototypes of the composition of the 3×3 window over the four parts of the time series. Due to the inhomogeneous length of the time series, the representative of the first quarter has a high tendency to show no or only few contact. The images are arranged from top to bottom.

Dealing with the time series structure of the data different strategies are employed. A special property of the time series used here is that consecutive frames are very similar (cf. Fig. 47). It is therefore an important aspect to find good representatives in the data. To give an example of the processing: one feature would be the mean pressure over all tactile elements of the full time series (FS), while the next feature would then be the mean pressure over all tactels of just a quarter of the time series (Q). A composite (C) feature consists of the mean pressures of all four quarters of the time series. The composite features therefore represent for the relative changes in the course of a time series. From this also follows that the composite version of a feature has four times the dimensionality of the feature has alone. Examples of composite features can be seen in Fig. 45 and 46, which are the composite extensions of Fig. 43 and 44 respectively.

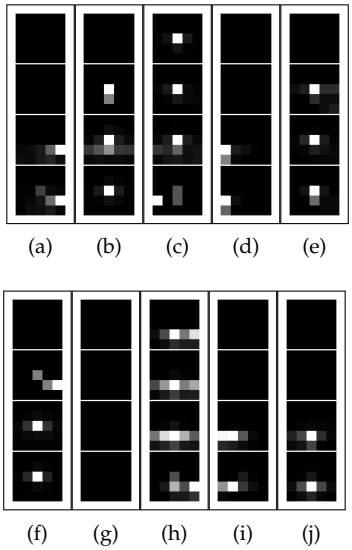

Figure 46: Similar to Fig. 45, the prototypes of the 5×5 windows are shown here. The images are normalized to improve the visual quality, ergo the difference between contact and no contact is enhanced.

Applying all these features on the time series resulted in 226 different attributes with a total dimensionality of $x \in \mathbb{R}^{920}$ before subsequent processing steps. Please note, that in this collection some dimensions are being partly redundant (i.e. mean pressure of a single quarter of the series and the composite mean pressure of all four quarters is redundant). Nevertheless, despite the redundant information, there is already a significant dimension reduction done, since a single tactile frame already has dimension $\mathbb{R}^{16\times16} = \mathbb{R}^{256}$.

A typical time series consists of about 2,200 frames, so we are reducing from approximately 500,000 dimensions to 920, and after a further processing step (discretization, see the next section) to only 226 attributes (see Table 6). This reduction has a great impact on the size of the data, the processing speed and a successful learning process. In other words, this does not only reduce the computational effort, but also the training samples needed if one was to adopt the feature selection to different learning methods and goals.

Discretization

Since all of the features are at a real value, a discretization step is needed. Despite the fact, that the C4.5 is able to handle continuous valued attributes, it might not be the optimal choice for

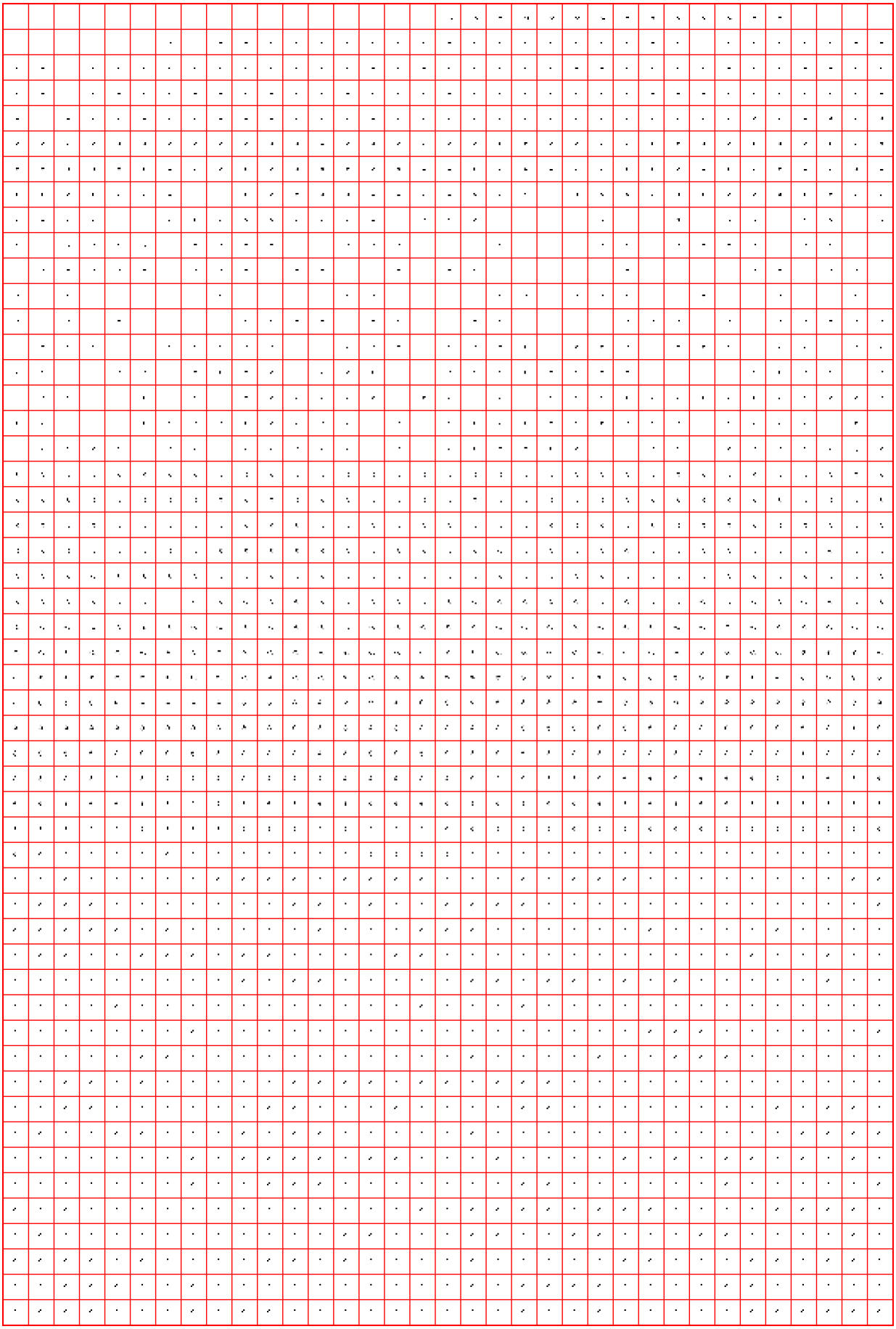

Figure 47: A full time series shown as tactile images from left to right and top to bottom. The images are visually enhanced (threshold & normalized).

our classification scenario, since C4.5 uses a simple threshold mechanism on continuously valued attributes. Therefore, one would be limited to binary decision trees, which would in turn need to be considerably deeper to perform adequately and to be able to discriminate the 42 different object classes (minimal theoretic minimum depth is 6). Also, the information gain per feature would have a natural limit to it. So to be more flexible, the different attributes are clustered into N different bins. This parameter happens to be the only true parameter in our approach. The authors used the k-means clustering algorithm [220] proposed by MacQueen and implemented by Michael B. Eisen, and improved by de Hoon [70]. Through this unsupervised clustering method, the continuous features are mapped into discrete bins.

Algorithm 2 k-means EM-Algorithm

Require: data-set $\{x_1, \ldots, x_N\}$
Require: number of cluster-centers k
Require: $N \geq k$
{Random Initialization of Cluster Prototypes}
for i=1 **to** k **do**
  $\mu_i = x_{random()}$
end for
repeat
  {Assignment of Data Points to Cluster Prototypes}
  for i=1 **to** N **do**
    for j=1 **to** k **do**
      $$r_{ij} = \begin{cases} 1 & \text{if } k = \underset{l}{\operatorname{argmin}}(||x_i - \mu_l||^2) \\ 0 & \text{otherwise} \end{cases}$$
    end for
  end for
  {Adjustment of Cluster Prototypes to Cluster Centroid}
  for j=1 **to** k **do**
    $\mu_j = \frac{\sum_i r_{ij} x_i}{\sum_i r_{ij}}$
  end for
until convergence

The core k-means procedure is sketched in algorithm 2. Since the adjustment step is in its nature that it always reduces the overall error $J = \sum_{i=1}^{N} \sum_{j=1}^{k} r_{ij} ||x_i - \mu_k||^2$, convergence is guaranteed. This does not mean, however, that the algorithm will converge to a global minimum. As a matter of fact, the k-means algorithm is sensitive to its initialization and therefore can get stuck in local minimums. Therefore, the algorithm is repeatedly run for 10,000 repetitions, the solution which minimizes J the most is picked.

The k-means algorithm is unsupervised, yet the number of cluster prototypes must be set in advance. So either knowledge of the underlying data must be used or a heuristic must be applied to guess how many true clusters are in the data-set. Methods for the

latter exist (e.g. [330, 377]) but have intentionally not been used up to this point since this would cause inhomogeneities in the further processing steps.

C4.5

THE LAST PROCESSING STAGE is used to find features that provide the most information gain. To this end, the well known C4.5 algorithm was employed. Being the improved version of ID3 (Iterative Dichotomiser 3) [280], the C4.5 algorithm builds up a decision tree on the presented data through supervised learning.

A decision tree is a graph which can be used to model different processes, of course including, but not limited to, decision making. Starting at the root node, different path depending on the value of the nodes are taken. The leaf or bottom node yields the result or decision. In Figure 48, a simple, binary tree is shown. Here, a decision tree is used for classification, at each node, a property or attribute is queried. Depending of the value, a path through the tree is taken with the classification result at the leaf node.

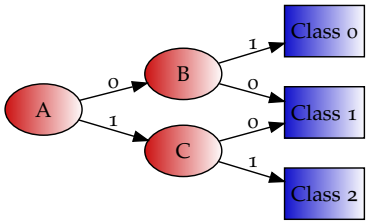

Figure 48: A simple binary decision tree. A, B and C are attributes that describe an object. Depending on their attributes, the leaf nodes are labeled with the results.

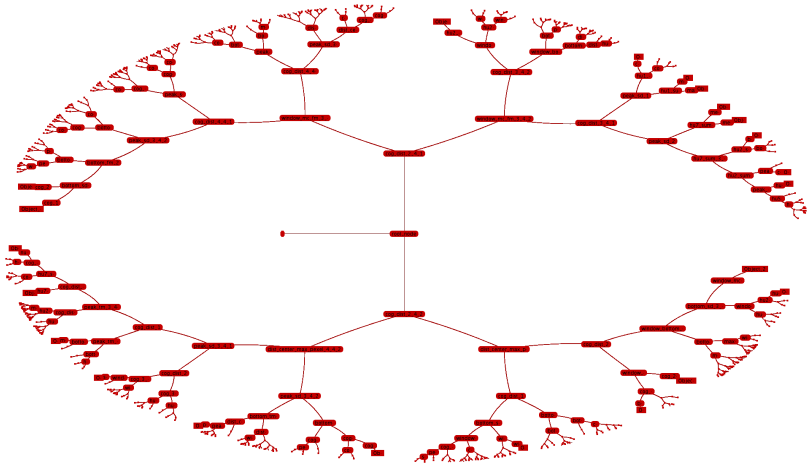

Figure 49: The resulting decision trees can be rather large (>4,000 Nodes). Therefore, hyperbolic tree representations as seen here can help to visualize the tree and allow convenient interactive browsing.

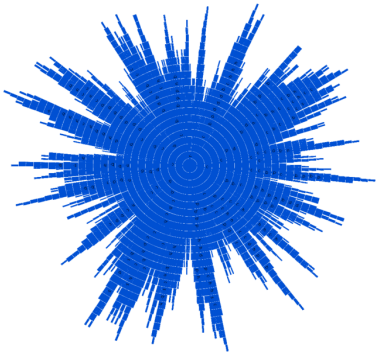

Figure 50: A different form of visualizing trees is a sunburst diagram as seen in this figure.

To generate the tree, C4.5 algorithm calculates the information gain obtained by branching on all available attributes. It then selects the attribute with the most information gain as a node. The information gain is defined as:

$$IG(X,a) \stackrel{\text{def}}{=} H(X) - H(X|a) \tag{14}$$

where X is the set of all training samples and $a \in Attr$, with $Attr$ being the set of all (remaining, unused) attributes. $H(.)$ is the information entropy, first proposed by Shannon [315]:

$$H(X) \stackrel{\text{def}}{=} -\sum_{i=1}^{N} p(x_i) log_2(p(x_i)) \tag{15}$$

where $p(.)$ denotes a probability mass function. Since the probability density function of the underlying process is unknown, it was

estimated using a simple maximum likelihood estimator [36] on the training set. A brief description of the tree building process in the C4.5 algorithm is given below in Algorithm 3.

[36]
$$\widehat{\mu}_m = \frac{1}{N}\sum_{i=1}^{N} x_i$$

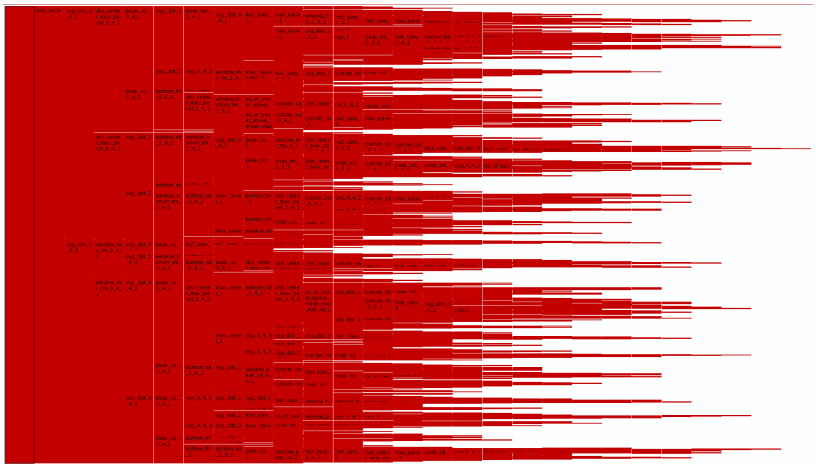

Figure 51: The rectangular tree representation shows the quantitative distribution of the classes. It can be seen, that at the highest level, the different classes are almost evenly distributed, which is not always the case at the consecutive levels.

The results of the proposed procedure are decision trees asking for a specific feature at each inner node and having the object class at its leaves. The branching level per node is at most the number N of clusters from the previous discretization step.

Algorithm 3 C4.5 Tree Generation

1: Create a root node T.
2: **if** all X at node T give the same output y **then**
3: $T \leftarrow$ terminal node with label "y"
4: terminate algorithm
5: **else**
6: $a_{best} \leftarrow \underset{a}{\text{argmax}}(IG(X, a))$
7: Create node labeled a_{best}
8: Create child nodes T_j to that node
9: **for all** T_j **do**
10: Recurse into line 2.
11: **end for**
12: **end if**

In this form, (batch mode) the building of the tree is deterministic. The C4.5, however, builds the tree by choosing a random subset of the data and successive expanding it by adding falsely classified data samples from the training set (iterative mode). The latter mode seems to produce smaller trees that perform slightly better that those in batch mode. Therefore, through all experiments, iterative mode was used. Since the iterative mode is no longer deterministic, due to the randomly chosen set at start, twenty runs were done and the best performing tree on the training set was selected.

Evaluation Parameters

To tackle various questions concerning the significance of the proposed features as well as the performance and the dependence on different parameters of the presented system, the resulting decision trees were analyzed.

Since the central parameter N, the number of discretization steps, and therefore the maximal branching factor for the resulting trees, was assumed to have influence on the resulting trees, a broad variety of different values (range 2 – 60) was tested. For each feature or attribute, a statistical analysis was done, including:

- The level the feature appeared in (an attribute may appear more than once on different levels in different branches of the tree).
- The number of cases in training data, that were (partly) classified by this feature.
- The class entropy:
$$\sum_{i=1}^{n} p(x_i) \log_b p(x_i) \tag{16}$$
where $p(x)$ is the (estimated) probability density function of class x at the node.
- The mutual information.

The mutual information [60] of an attribute is defined as:

$$MI(X;Y) \stackrel{\text{def}}{=} \sum_{y \in Y} \sum_{x \in X} p(x,y) log_2 \left(\frac{p(x,y)}{p(x)p(y)} \right) \tag{17}$$

and it is considered to be well suited for this analysis because it allows the comparison of attributes at different levels of the tree. Again, a naive maximum likelihood estimator for $p(.)$ was used.

Results

The classification results can be found in Figure 52 and 53 respectively. In these figures, the shown results were 100-fold cross-validated. The best classification results on the test set with the original data can be found at $N = 6$ (35% error), while the worst classification is at $N = 2$ (45.7%). With values for $N > 30$, the classification rate gradually, yet non-monotonically declines. A possible explanation for this may be the effect of over fitting. Larger trees are getting generated (see Fig. 54). This effect, however, does not seem to be as evident in the extended data-set.

As has already been mentioned, perfect classification is not the foremost goal of this experiment. It is evident on the other hand, that the test error is considerable, while the training error stays in the range of approximately 6 – 7.2 %, which is a quite reasonable

The low test classification performance can be accounted to the over fitting phenomenon in decision trees when not enough examples are presented.

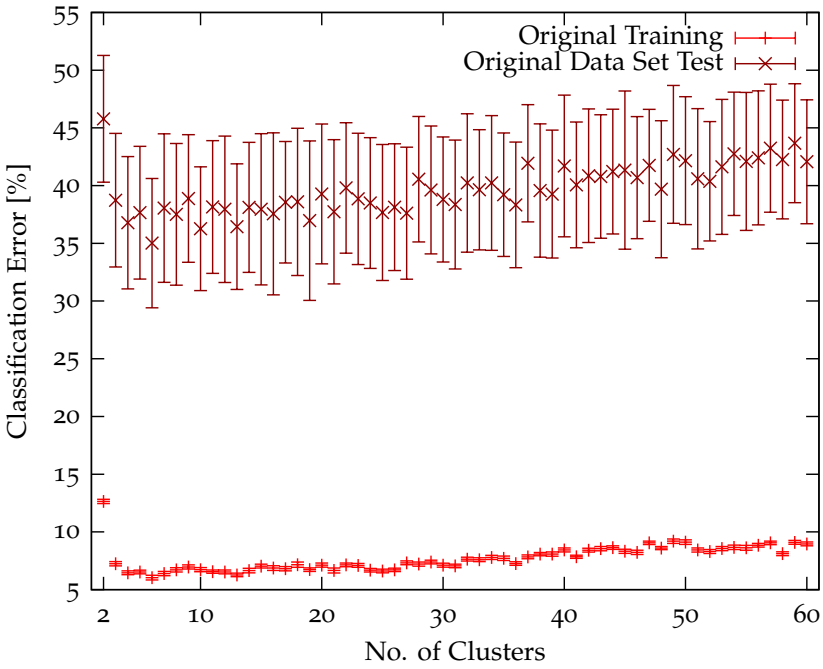

Figure 52: The classification results for the original set of 6048 time series is shown. While the training error is in a range that can be expected, the test error discloses poor generalization of the architecture on this data-set.

outcome considering the type and amount of data and the level of difficulty of the task at hand. See also earlier work [308] with this data-set with a neural motivated classification architecture.

It is a known behavior of decision trees that if the number of training examples is too low, especially with respect to noise in the data, that trees are generated, that seem to be over fitting the data and perform low on the test set (cf. [237], pp. 66). In this case, the algorithm grows the tree as deep as necessary on the training data and learns the noise rather than the variance in the training data which represents the difference in the object classes. This may lead to a poor generalization on the test set.

The extended data-set where the data from the experiments was extrapolated to different scanning angles performs better, both on training and testing. The testing error stays below 2 % (peak), averaging around approximately 0.15 %. The best classification rate in test is 0.079 % error at $N = 13$ and 16 respectively. The best training error is found to be 0.002 % at $N = 59$.

Influence of N

With the exception of $N = 2$, small values of N already show quite satisfying results. In the case of the original data-set, after reaching the best classification rate, the performance decreases with higher values of N ($N > 20$).

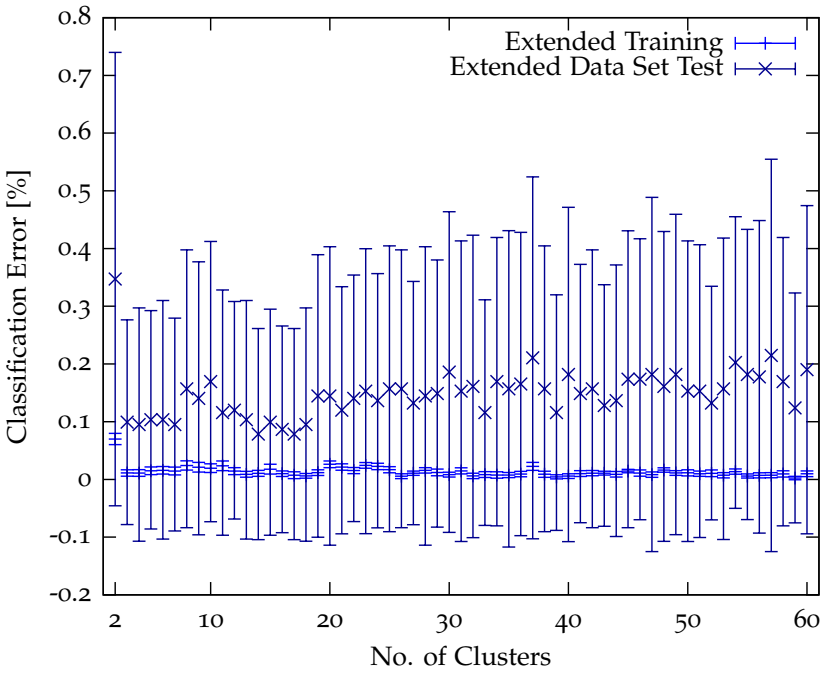

Figure 53: The classification results in case of the extended data-set are several orders of magnitude improved. The higher number of examples has shown positive effect, both on the training and the test error. While the best results are in the range < 20, it cannot be assumed that a tendency towards a clear inclination in the error rate at higher values of N is to be expected.

In the extended data set, it can be assumed that over fitting occurs with higher values of N, although with very minor impact on the classification performance. But nevertheless, training error (slightly) decreases accompanied by an (also slight) increase in the testing error.

The size of the trees seems to almost linearly increase with N. Also the number of features that contribute to the classification, i.e. with mutual information $MI(X;Y) > 0$, are decreasing with N in the original set. In the extended data-set, a limit at approximately 160 used features seems to exist. This is interesting, as we are looking for as few features as possible with a high information value attached. We therefore investigate the distribution of used features at different values of N.

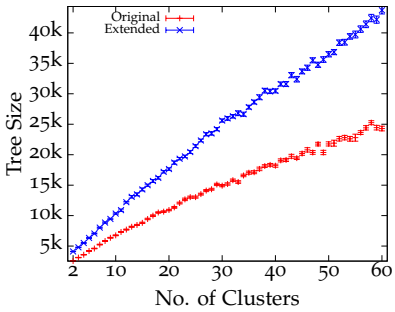

Figure 54: Tree Sizes increase with the parameter N. Higher values of N allow higher branching factors at the nodes. In certain cases may be possible for almost redundant branches to emerge, which adds to the complexity of the tree but does neither improve classification nor information gained from the additional branches.

To subsume the capabilities of the architecture for classification with respect to N: although the over fitting phenomenon increases when N is set to a large value, the approach seems to be quite robust in the parameter, as the classification results are only marginally effected.

Feature Analysis

To analyze the contribution of the different features, the mutual information and the class entropy yielded by the features are examined. Since the k-means as well as the C4.5 algorithm are not deterministic due to random initialization, some variation in the results is logical.

This effect is also present in Fig. 55, where the number of fea-

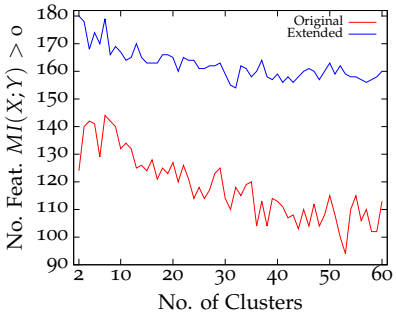

Figure 55: With growing N, and therefore higher branching factors in the tree, less features are used in the classification.

tures used in the classification process, i.e. $MI(X;Y) > 0$, are shown. In Fig. 56, which is a kind of a sorted histogram of the mutual information of the features, the change in the distribution of the mutual information at different values of N can be seen. With the extended data-set, the decrement in the mutual information seems to occur almost linearly at N=5, but changes to a cotangent like function. This cotangent like behavior can also be noted for all plots of the original data-set.

To give an impression of the jitter in the results, and therefore broadly propagated information values from the features used, in Fig. 57 a sparkline-like plot is used to represent parts of this very extensive data-set and results. Here, the mutual information of the features from left to right are represented by small bar graphs. Each line represents the results of one cross-validated set for N - the red lines represent the original data-set, the blue lines incorporate the extended data-set. What can easily be seen here is the considerable jitter between subsequent runs of the classification system. Also that there are features which get used quite regularly in the original, but not the extended data-set and vice versa.

Albeit the high variance in the usage and mutual information between the two data-sets and the different runs (varying N), in the accumulated class entropy and mutual information graph (cf. Fig. 58 and 59) a high conformity on two extremes is noted. The feature with the most information gain is agreed upon in both data-sets. Also, there are areas of unused, ergo not information yielding, features that have a large overlap. Especially in Fig. 59 a large number of features of the extended data-set only contribute very sparsely to the classification. This may be a hint as to why the number of features is quite constant with the extended data-set (cf. Fig. 55).

As can be seen in Table 7, certain features do not get used at all (e.g. # 173 - 184), while others are only used very sparsely (e.g. # 104 - 109). There are, at times, differences between the two data-sets but also coincidences, for example that features scored low in both data-sets. This has been taken into account in the chosen table representation.

In the original data-set, features that operate on the first quarter of the time series (Q1) are noticeably often completely unused. Also it is apparent, that the Hu invariant moments are not used both in the Q1 and the composed (C) versions in the original data-set. This is, however, not the case with the extended data-set, where the Hu rotation invariant moments are much more popular.

Of course, not only looking at the features not contributing to the classification task is of interest, but also the features contributing the most to the classification task. The fifteen features with the highest mutual information are listed in Table 8. There are a number of differences in the two data-sets. Most noticeably, in the

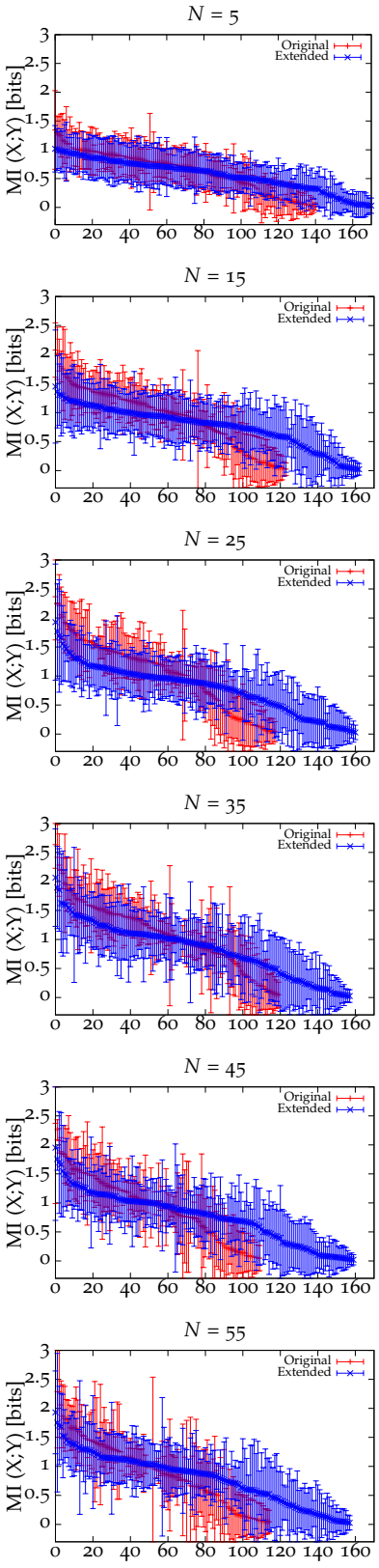

Figure 56: A quantitative evaluation of the distribution of the mutual information is shown in this figure. The features are sorted, therefore the feature with the most mutual information is leftmost. Features with $MI(X;Y) = 0$ are not displayed.

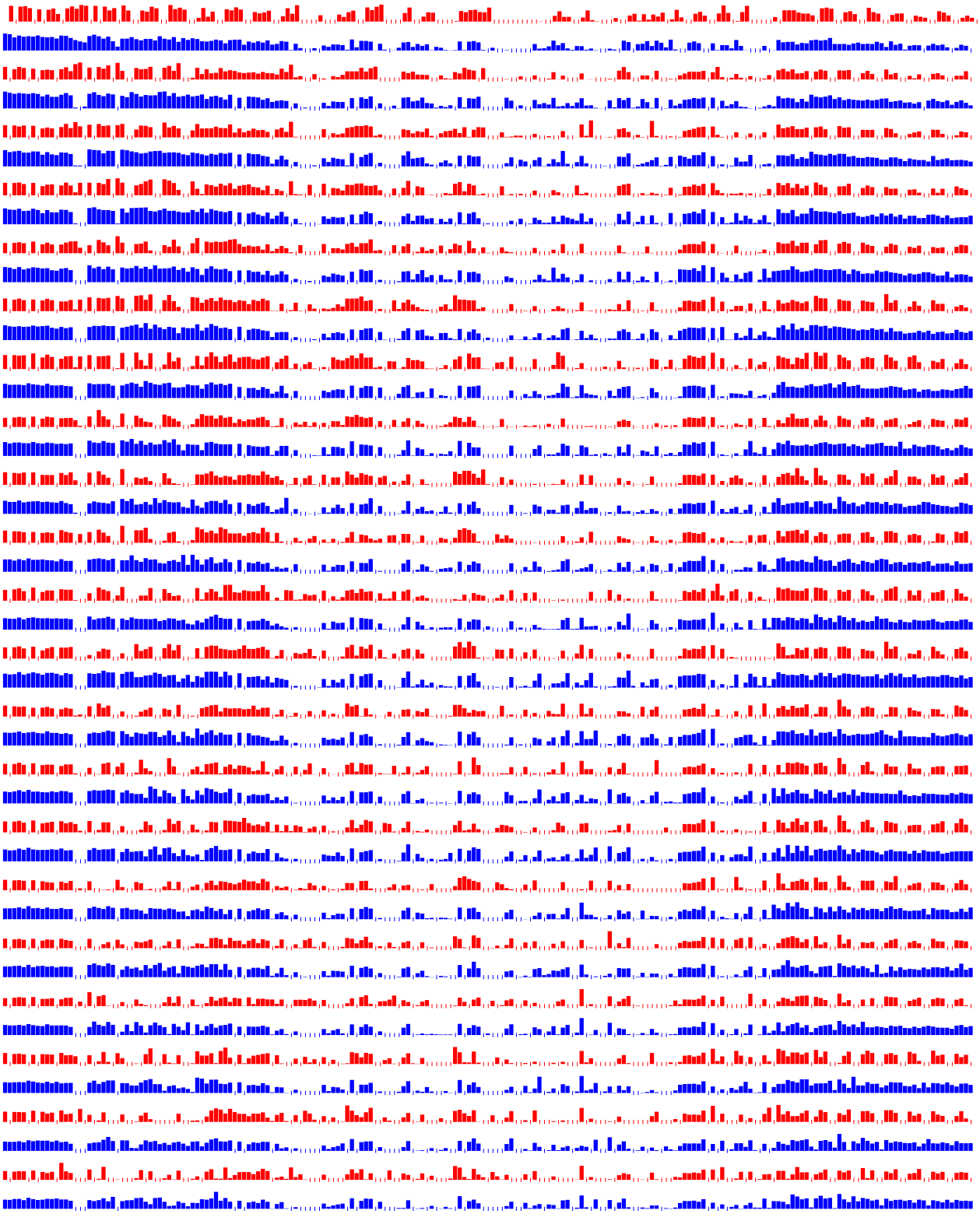

Figure 57: The entropy of the different features vary with N as well as the generated trees. Here, from top to bottom, sparklines from $N = 2 \ldots 22$ of the best trees is shown. The red sparklines originate from the extended data-set, the blue sparklines are from the original 6048 time series set.

No.	Description	F	Q1	Q2	Q3	Q4	C
2, 6	Center of mass		O				O
8	Dist. center of mass ↔ center of sensor		O				
12	Value Maximum tactel	O					
16	Value Minimum tactel	B					
17	Position Minimum tactel	B					
18	Distance Minimum tactel ↔ center of sensor	Z					
20, 24	Mean tactel		O				O
25	Value median tactel	B					
27, 28	Standard deviation		O	O			
33, 34	3^{rd} moment		O	O			
39, 40	4^{th} moment		O	O			
50, 52	Minimum in standard deviation of all frames	B		B			
62, 64 - 67	Minimum of 3×3 windowed standard deviation	B		B	B	B	B
68, 70	Maximum of 3^{rd} moment	Z		A			
74, 76	Minimum of 3^{rd} moment	B		B			
80, 82 - 85	Maximum of 3×3 windowed 3^{rd} moment	B		B	E	B	Z
88	Minimum of 3×3 windowed 3^{rd} moment			B			
92, 94	Maximum of 4^{th} moment	X		Y			
96, 97	Maximum of 4^{th} moment					A	Z
98, 100	Minimum of 4^{th} moment	B		B			
104 - 109	Maximum of 3×3 windowed 4^{th} moment	B	Z	B	B	B	Y
112, 113, 115	Minimum of 3×3 windowed 4^{th} moment			B	Z		B
117 - 119	Standard deviation of 3×3 window		Y	O	A		
123 - 125, 127	3^{rd} moment of 3×3 window		O	Y	A		A
129 - 131, 133	4^{th} moment of 3×3 window		O	O	A		Z
134 - 137, 139	Std. dev. of 3×3 window with most contact	X	X	X	X		X
142	3^{rd} moment of 3×3 window with most contact			Z			
148 - 151	4^{th} moment of 3×3 window with most contact			Z	B	A	B
158	Distance maximum tactel ↔ center of sensor						Z
160	Sum Powerspectrum	B					
162, 163, 166	3×3 window of maximum contact area in time series		O	A			O
168, 172	5×5 window of maximum contact area in time series		O				O
173 - 178	Averaged 3×3 window of maximal contact	X	X	X	X	X	X
179 - 184	Averaged 5×5 window of maximal contact	X	X	X	X	X	X
192, 196	Hu rotation invariant moment I_1		O				O
197, 201	Hu rotation invariant moment I_2		O				O
202, 206	Hu rotation invariant moment I_3		O				O
207, 211	Hu rotation invariant moment I_4		O				O
212, 216	Hu rotation invariant moment I_5		O				O
217, 221	Hu rotation invariant moment I_6		O				O
222, 226	Hu rotation invariant moment I_7		O				O

Key	Description
A	$MI(X;Y) < 0.1$ [bits] in Original Data-Set
B	$MI(X;Y) < 0.1$ [bits] in Extended Data-Set
E	$MI(X;Y) = 0$ [bits] in Extended Data-Set
O	$MI(X;Y) = 0$ [bits] in Original Data-Set
X	$MI(X;Y) = 0$ in both Data-Sets
Y	$MI(X;Y) = 0$ in Original Data-Set & $MI(X;Y) < 0.1$ [bits] in Extended Data-Set
Z	$MI(X;Y) = 0$ in Extended Data-Set & $MI(X;Y) < 0.1$ [bits] in Original Data-Set

Table 7: In this Table all features that have a weak or no contribution at all to the classification task are listed. The evaluation was done on $N \in \{2, \ldots, 60\}$.

original data-set the "center of mass" is facilitated quite often. This feature is neither translational nor rotational invariant and may therefore not generalize well.

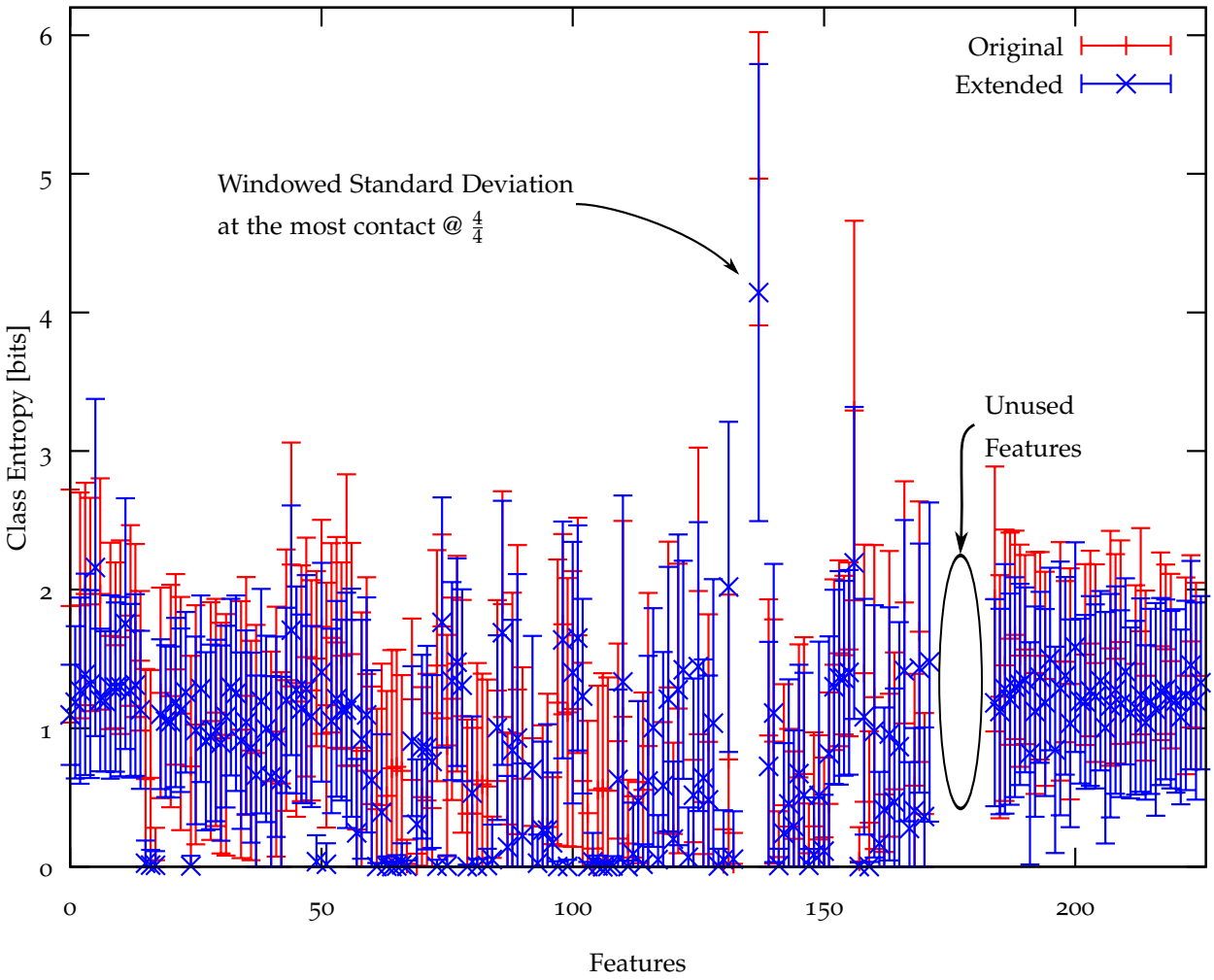

Figure 58: The class entropy of all features is shown here for both data-sets. The variance is mostly quite high, this is also due to the very large range of N from 2 to 60.

In the extended data-set, some of the Hu invariant rotations show high values for the mutual information. In both results, statistical measures, especially the 3^{rd} moment, are widespread. Not overly surprising, but noticeable is feature # 157, which scores in all data-sets high values, both class entropy and mutual information wise. This feature, however, like the features # 1 - 6, is to be interpreted as a representative for the geometric properties of the object.

THE FEATURES WITH THE HIGHEST class entropy (cf. Equation 16) are listed in Table 9. The obviously largest difference here is feature # 138, which has in both data-sets the highest class entropy, while the mutual information of this feature is at approximately 0.7 [bits], a rather mediocre value. However, this feature is at $N > 18$ always at the root node, which results in a high class entropy.

A difference in the listing of the top class entropy and mutual

information features between the original and the extended data-set is that features that were calculated on the full time series (marked with F) are quite common with the original data but not so with the extended data-set.

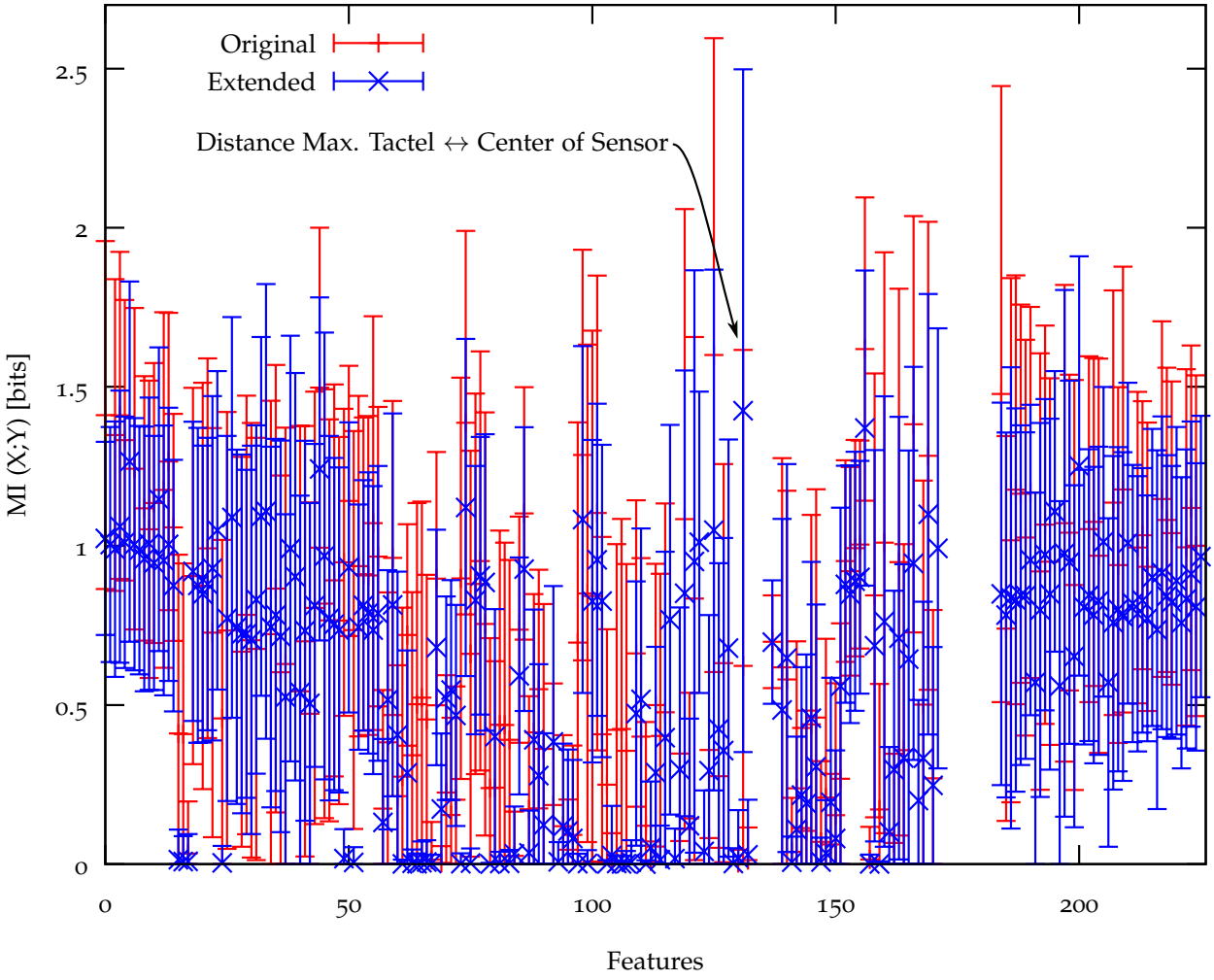

Figure 59: The Mutual Information of the different features, again, as in Fig. 58, a significant variance can be seen.

Discussion

The proposed method showed to be well behaved in its main parameter N, the number of discretization steps. All other parameters in k-means clustering and C4.5 were mostly left at default values. Variation of these parameters within reasonable ranges had no significant influence on the classification results. While the tree size is growing with N, the classification error remains almost constant. Choosing a higher than optimal value for N will therefore mainly have an impact on run time and memory consumption, but will not significantly affect the classification results. The proposed three stage architecture is therefore a feasible approach to the classification task.

No.	$MI \pm$ SD	Short Descr.	Type
157	1.62 ± 0.48	Max. tactel ↔ Center	Q4
126	1.60 ± 1.00	3^{rd} Mom. 3×3	Q4
45	1.50 ± 0.50	Max. Std.Dev.	Q1
185	1.48 ± 0.97	Hu I_1	F
1	1.41 ± 0.55	Center of mass	F
4	1.41 ± 0.51	Center of mass	Q3
75	1.39 ± 0.60	Min. 3^{rd} moment	Q1
167	1.38 ± 0.65	5×5 window	F
3	1.35 ± 0.49	Center of mass	Q2
5	1.33 ± 0.44	Center of mass	Q4
99	1.29 ± 0.65	Min. 4^{th} moment	Q1
170	1.28 ± 0.74	5×5 window	Q3
14	1.27 ± 0.47	Position Max. tactel	F
7	1.24 ± 0.51	Center of mass ↔ Center	F
210	1.18 ± 0.70	Hu I_4	Q4

(a) Original Data-Set

No.	$MI \pm$ SD	Short Descr.	Type
132	1.42 ± 1.07	4^{th} Mom. 3×3	Q4
157	1.37 ± 0.50	Max. tactel ↔ Center	Q4
6	1.26 ± 0.57	Center of mass	C
201	1.25 ± 0.66	Hu I_2	C
45	1.24 ± 0.54	Max. Std.Dev.	Q1
12	1.15 ± 0.48	Center of mass ↔ Center	C
75	1.12 ± 0.53	Min. 3^{rd} moment	Q1
34	1.11 ± 0.71	3^{rd} moment	Q2
196	1.11 ± 0.44	Hu I_1	C
170	1.10 ± 0.69	5×5 window	Q3
33	1.09 ± 0.56	3^{rd} moment	Q1
27	1.09 ± 0.63	SD	Q1
99	1.08 ± 0.55	Min. 4^{th} moment	Q1
4	1.06 ± 0.43	Center of mass	Q3
126	1.05 ± 0.82	3^{rd} Mom. 3×3	Q4

(b) Extended Data-Set

Table 8: A listing of the fifteen features with the most Mutual Information $MI(X;Y)$ accumulated over all $N \in \{2,\ldots,60\}$.

Over all, the performance of the system is at the same level or better as a completely different approach using an artificial neural VPL [112] classifier.

Although the results in the classification task are quite satisfying, the outcome of the feature analysis is at times inconclusive. For example, feature # 138, the standard deviation of the 3 × 3 window at the point of maximal force in the third quarter of the time series, is found by the C4.5 algorithm to yield the most information gain, at least at $N > 18$. Similar features (e.g. # 134 - 137), however, do not contribute at all, or show only a weak contribution (e.g. # 117-119).

Generally, and this holds true for both data-sets, the information is very broadly propagated onto quite some features. This is, of course, due to the complexity of the task (42 object classes, high dimensional data space, limited set of samples). It would have been desirable to get a small set of five to fifteen features that allow good classification.

No.	$CE \pm$ SD	Short Descr.	Type
138	4.96 ± 1.06	SD 3×3 window	Q4
157	3.29 ± 1.37	Max. tactel ↔ Center	Q4
45	2.18 ± 0.88	Max. Std.Dev.	Q1
126	1.99 ± 1.03	3^{rd} Mom. 3×3	Q4
4	1.97 ± 0.80	Center of mass	Q3
7	1.97 ± 0.83	Center of mass ↔ Center	F
185	1.93 ± 0.96	Hu I_1	F
167	1.91 ± 0.87	5×5 window	F
87	1.89 ± 0.81	Min. 3^{rd} moment 3×3	Q1
5	1.89 ± 0.77	Center of mass	Q4
3	1.89 ± 0.81	Center of mass	Q2
1	1.88 ± 0.84	Center of mass	F
13	1.81 ± 0.65	Value Max. tactel	F
56	1.78 ± 1.05	Max. SD 3×3	F
99	1.75 ± 0.65	Min. 4^{th} moment	Q1

(a) Original Data-Set

No.	$CE \pm$ SD	Short Descr.	Type
138	4.14 ± 1.65	SD 3×3 window	Q4
157	2.19 ± 1.13	Max. tactel ↔ Center	Q4
6	2.16 ± 1.22	Center of mass	C
132	2.02 ± 1.19	4^{th} Mom. 3×3	Q4
75	1.76 ± 0.90	Min. 3^{rd} moment	Q1
12	1.75 ± 0.90	Center of mass ↔ Center	C
45	1.71 ± 0.90	Max. Std.Dev.	Q1
87	1.69 ± 0.95	Min. 3^{rd} moment 3×3	Q1
102	1.65 ± 0.81	Min. 4^{th} moment	Q4
99	1.64 ± 0.85	Min. 4^{th} moment	Q1
201	1.58 ± 0.76	Hu I_2	C
196	1.50 ± 0.66	Hu I_1	C
172	1.48 ± 1.15	5×5 window	C
78	1.48 ± 0.75	Min. 3^{rd} moment	Q4
224	1.46 ± 0.75	Hu I_7	Q3

(b) Extended Data-Set

Table 9: For all $N \in \{2,\ldots,60\}$, the features with the best class entropy are shown for both data-sets.

The results (cf. Fig. 56) do not, however, indicate a clear threshold. This does not mean that the suggested features are all inapt to generate such results. It also has to be considered that the under-

lying data is not free from challenges. The resolution of the sensor is coarse, the jitter in the data is considerable, also due to the difficult control of contact based trajectory planning. The data-set is therefore by no means comparable to the data used in [270], where the data was generated from simulation. All experiments that the authors have conducted show that real world tactile data is almost never alike those found in [270] or even [304], at least not with the sensors available to the authors and without heavy object fixation.

Some features, like # 17, the position of the minimum tactel, were intentionally added although it cannot be assumed that such a feature is of any use in this task. Basically, features like this comprise noise from the data acquisition. In the original data-set, the feature is used often, while in the extended set, it is almost not used at all. This is coherent with the poor generalization on the original data-set. Therefore, one result from the feature analysis is that features that have high scores in the original data-set, but low scores in the extended set are features of low quality.

The use of statistical moments showed promising results and may be a valid method to discriminate different tactile contact situations exclusive of their location, pattern and intensity. To validate the expected usefulness of the suggested features[37] further investigations with different data-sets and with state of the art tactile technology are indicated.

[37] namely statistical moments, but also Hu moments

Object Recognition on Haptic 3-D Point Clouds

The work presented in the remainder of this chapter describes work that, in parts, derives from collaboration with Martin Meier during the supervision of his diploma thesis on the adaption of the FastSLAM algorithm for the processing of tactile data. Therefore, an extensive reflection of these methods and results can also be found in [233]. For a short paper version, refer to [234]. While the implementation of the grasping procedure and data acquisition were done by the author of this thesis, the implementation and refinement of the methods on the data processing, as well as the evaluation of the results, originates from Martin Meier's work. In the next section, the hardware setup and the algorithm for data acquisition are presented. The algorithm allows the "blindfolded"[38], haptic grasping and placing of object, but can also be used for the haptic scanning of objects. This section is followed by a section on object recognition on the resulting point clouds.

Grasping Based on Tactile Sensing

In the following experiments an industrially manufactured three-fingered hand, the Schunk Dexterous Hand 2 (SDH-2), is used (see Figure 60). The hand is equipped with tactile sensors, which we employ to grasp previously unknown objects. Two types of grasps were developed and were integrated in a robotic setup so far. We show the feasibility of our approach with a common pick and place task. The grasp primitive will also be used to gather 3-D point information from the object through haptic[39] information. Since no vision sensors are used, the system solely relies on its tactile and internal sensors when grasping the objects, or when establishing a grip. The latter is for example repeatedly done to gather as much complete haptic data from the object as possible. Through the use of haptic data failed grasps are also detected. During a pick and place task, the prehension of an object pose that might possibly lead to a failed grasp is detected. In this case, the grip is released and a corrective movement is performed. The grasp is then repeated.

All grasps are feedback-controlled in real-time through the hands' tactile sensors. Finally, uncertainties when placing ob-

[38] Blindfolded refers here to the fact that no photometric sensors are used. The robot solely relies on tactile and kinesthetic senses

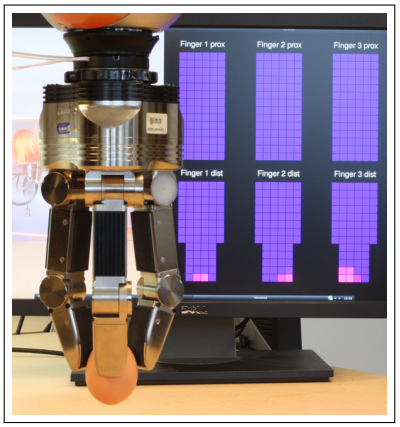

Figure 60: The SDH-2 hand is grasping a raw egg. In the background, the data from the tactile sensors is visualized.

[39] tactile and kinesthetic

jects are compensated with the use of the internal sensors of the Kuka/DLR LWR, which for example allows very gentle object disposal.

Motivation

AUTONOMOUS GRASPING CAN BE SEEN AS A CORNERSTONE for many robotic applications, from the already well established field of automation in the manufacturing industry to the emerging field of service and domestic robots. The research effort on this area is accordingly considerable. Although noticeable progress could be achieved, especially in unconstrained and unstructured environments certain challenges remain [160]. One of the main difficulties in grasping is that the robot approaches a task that cannot generally be solved without interaction and contact-based perception of the environment. Vision based object modeling and localization is prone to errors, which is of growing importance in fine manipulation task where feedback is needed. Also photometric sensors will most probably never be able to expose all aspects of the object that are important for grasping and manipulation, like for example the weight, friction, stiffness and deformability.

Tactile sensing is indispensable for grasping and manipulation. If the task is moderately constrained it is even possible to relinquish the use of computer vision.

We therefore propagate a more haptic sight into grasping. Hence we renounce to make use of any kind of optical sensor. To keep the task at hand still viable, we provide some higher level knowledge (e.g. hints on the position of the objects and pre-grasp posture) or, as an alternative, direct physical human-robot interaction. We show the power of using tactile and intrinsic sensors by solving a pick and place task. We employ the intrinsic sensing modalities of the used hardware to handle unknown objects with the appropriate care. The situations in which uncertainty needs to be dealt with are not limited to the grasping phase, where much greater variations are handled than normally would occur with a state of the art vision system. Also when placing the objects, uncertainties must be taken into account, since no assumptions on the height of the table are made, and thus, for example the stacking of objects comes for free without the need of any higher level reasoning or scene analysis.

In the interactive case, the robot will ask the user to guide the robots end-effector to a new pre-grasp position. When in scanning mode, the robot proceeds to the next position.

Experimental Setup

THE SETUP CONSISTS OF A KUKA/DLR LWR IV, which is based on a development of the DLR [117]. The robot has 7 DOF and torque sensors in every joint. The robot features active compliance in joint or Cartesian space, i.e. it allows to set stiffness and damping in a virtual spring-damper system $\ddot{x} + \frac{c}{m}\dot{x} + \frac{k}{m}x = 0$, with x being the displacement, m the mass, k is the spring constant and c is the damping coefficient. To control the robot, the open source software developed in [309] was used. It controls the robot at 1 [ms] cycle

time. The whole system was controlled with a single PC (Xeon E5530 CPU, Gentoo Linux, low latency kernel with preemtion). More details on the control of the robot arm have already been given in Part II.

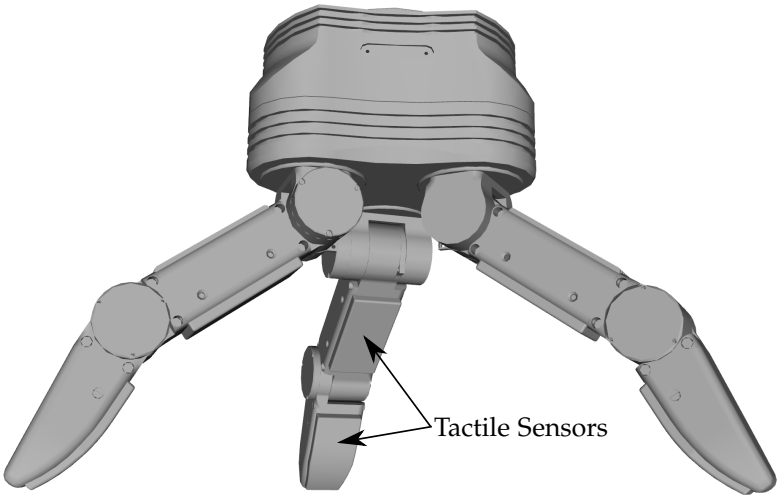

Figure 61: A Model of the Schunk SDH-2 hand with the tactile sensing elements, two elements per finger.

Mounted on the end-effector of the LWR is a three-fingered, 7 DOF SDH-2 hand (cf. Fig. 61). It is originally equipped with six tactile sensor arrays like those presented in [161], manufactured by Weiss Robotics. The sensors at the proximal phalanges consist of a 6 $\times$ 14 array, while the sensors at the distal phalanges have a dimension of 6 $\times$ 13. Every tactel has a sensing area of 3.4 [mm] $\times$ 3.4 [mm]. The SDH-2 has two RS-232 serial bus interfaces. One interface is used to control the motors and get the values from the joint encoders, the other is used to get the tactile data from the sensing elements. When polling all sensor interfaces, an approximate frame rate of 30 [Hz] can be achieved. The hand receives commanded joint velocities and provides current joint angles. The control loop operates at approximately 35-40 [Hz]. The data transfer rates are limited by the bus interface and the command processing respectively. The highest frame rate possible for the tactile sensors is approximately 100 [Hz] when the scanning is restricted to a single sensor or areas thereof.

Description of the Grasping Algorithm

The strategy to grasp an object is to start from a pre-grasp posture. The grasp type (i.e. a cylindrical or a parallel jaw grip) is given as a priori knowledge in the pick and place task. Then, starting from the pre-grasp posture, the grasp is executed. As soon as a tactile sensors report contact, the movement of the corresponding finger is interrupted. When all finger movements have stopped, the object should be embraced by the hand. At this point, the grasp is analyzed. To this end, we evaluate the distance and the centroid of

the contact points, which are in turn computed from the forward kinematics of the robot and the tactile sensor readings. If, for example, the distance of contact points drops below a fixed threshold[40] of 0.2 [mm], the grasp is considered to have failed and the contact is classified as a self-contact of the fingertips. In this case the robot initiates a user interaction to clarify the situation or resumes the scanning at the next position respectively. In the case when no predefined scanning pattern is given, i.e. the pick and place task, the robot asks for physical guidance to a more promising position and initiates the pre-grasp to grasp procedure from there. The physical human-robot interaction is started and stopped by the user. When the user touches one of the tactile pads, the robot will become completely compliant and the user can easily direct the robot and correct the position of the end-effector (see Fig. 62). When the interaction has finished,i.e. the user has released the robot, it will continue with the grasping process.

[40] A threshold has to be used due to the low resolution of the tactile sensors, the curvature of the fingertip and the elasticity of the resistive foam

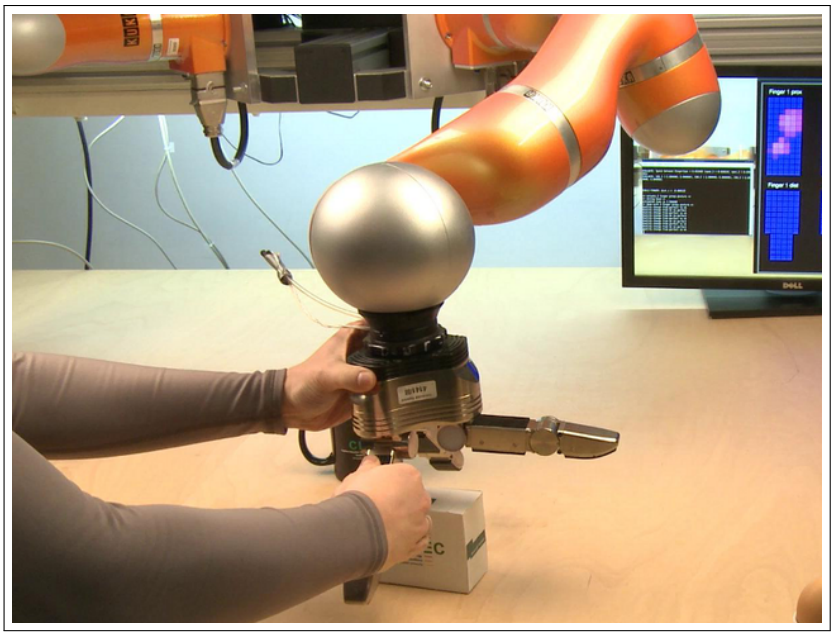

Figure 62: In case of a failed grasp, the robot asks for user interaction. The operator can initiate physical interaction with the robot through touching the tactile sensors. The robot will become compliant and can then be guided closer to the object.

In the case where the grasp posture was classified as suboptimal, which is the case when the perceived centroid of the object is significantly away from the center of the hand, the grasp is repeated and the position of the end-effector is corrected to the sensed object center. We employ an analytical straight forward approach to calculate the new grasping position.

When the evaluation of the grasp posture reports a good grasp posture, the actual grasp is conducted. To maximize tactile information from the object (e.g. for object classification or contact maximization, see [234, 307]), the object is lifted by rolling the fingertips upwards. The position of the fingers normal to the object (i.e. the grasp force) is controlled through the tactile feedback from the sensors. Since the employed tactile sensing principle is not well suited

A video showing the tactile grasping and placement of objects ("Tactile-Grasping") is available on the enclosed disk.

for very precise force measurement, controlling the grasp force of each finger separately is not feasible. Errors in the estimation of the force on the fingers would most probably lead to a pushing movement by one of the fingers, while the other(s) would be repelled. This would eventually end up in a failed or at least very unstable grasp. To overcome this situation, a global strategy is employed. The sensor values of all tactels are accumulated and normalized:

$$f = \frac{\sum_{i=1}^{\#tactels} p_i}{1 + (\#tactels > 0)} \tag{18}$$

where p_i is the reading from the i-th tactel. During the grasp a proportional controller adjusts the normal position of the fingers with respect to f.

To compensate for the amendable first touch sensitivity and since the hand has neither passive compliance nor force/torque sensing, the maximal motor currents during the phase of establishing contact to the object is reduced. This prevents accidental pushing of objects. In addition, if the finger stops because it touches the object but the tactile sensor has failed to detect that contact, the described algorithm will still work, even though no contact is reported by the tactile sensors. To this end, the positions of the fingers are used to evaluate the situation. Hence, if it is not possible to drive the fingers in a way to produce a self-contact, it is assumed that an external cause, i.e. an object between the fingers, is present.

Placement

To carefully place the object in hand the internal sensors of the Kuka/DLR robot are used, which provide not only the acting torques at each of its joints but also estimates the forces that are applied to its end-effector. Since the obtained forces are subject to noise from the sensor readings and errors in the modeling of the robots dynamics, we apply the method of a moving average to get a valid estimate of the weight of the object. This serves as calibration to the unknown object. This way, we are able to improve the perception of external forces on the end-effector. When placing the object, the robot is set to a low Cartesian stiffness in the direction of the table top. The movement towards the table is stopped at a threshold of 5 [N] and the hand is opened. Looking at this procedure qualitatively this method to place objects reaches the order of the performance of humans, who usually also start to release objects when contact with the supporting table is sensed.

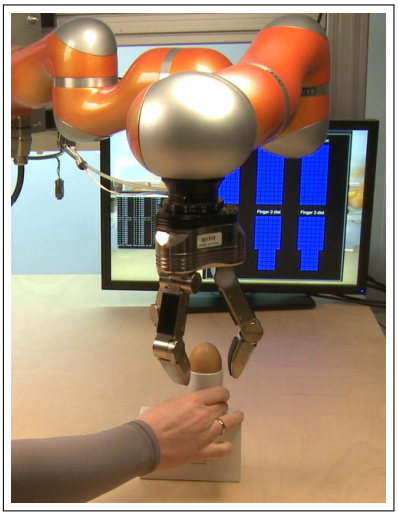

Figure 63: With the intrinsic perception of the system, the placement of a fragile object without knowledge about the height or exact position of the egg cup is possible.

Discussion of the Pick & Place System

Up to this point, no extensive quantitative analysis of the proposed "blind" pick and place system was done. It can be said, however, that a wide range of box-sized and cylindrical objects

were successfully grasped by the robot. Of course, the dimensions of the objects in question have to suit the size and agility of the SDH-2 hand. It must also be mentioned that the system has limitations in *autonomously* resolving failed grasps. This is especially true if contact conditions on different fingers are caused by different objects, which basically means, that right now the system lacks strategies to cope with cluttered and very unstructured scenes.

In addition, the robot relies at this point more on a priori knowledge as absolutely necessary. For example, the height as well as the shape (and as a consequence the preferred grasp) of objects could be sensed.

Generation of Point Clouds

The most convenient way to generate point clouds from objects is the use of photometric sensors[41]. In comparison, sequentially palpating the object seems cumbersome and inefficient. Nevertheless, the use of tactile sensors in point cloud generation can easily be justified. First of all, if a complete and precise point cloud is to be generated, the use of laser scanners is necessary. It is possible to produce very fine grained 3-D information this way, but requires a complex apparatus and a time consuming scanning process. On the other end of the scale are low cost camera systems that work with structured light to produce a depth image of the scene with precisions in the order of approximately 1 [cm] [328]. While photometric sensing has the advantage of providing many points at high data rates, difficulties arise with reflections, transparency or occlusions. Acquiring point cloud data is therefore feasible to enrich photometric acquired data, resolve ambiguities or punctually improve the precision in special situations. We take this to the extreme by solely generating point cloud data from tactile sensing and using this data in a classification task.

[41] Time-of-Flight Cameras, Stereo Vision, Structured Light Cameras, Laser Scanners, ...

Methods

Tactile sensors provide at times very high frame rates of up to 1.9 [kHz] [312]. In addition, multiple readings will result in redundant data. It is therefore worthwhile to find a representation of the data that both compacts the data, while at the same time using the redundancy to increase the precision of the data. We hence propose to use a nearest neighbor approach to assign to each newly acquired contact point m_n to an already existing point μ_k in the reduced point cloud set $X = \{\mu_k\}$, which is concurrently updated to new contact points.

This update process can be done in different ways. We compare a simple sliding average approach to a more elaborate, discrete Kalman filtering method [156], which allows to explicitly model the

uncertainty of the measurement.

Kalman filter A discrete Kalman filter is a set of equations that allows us to predict values from noisy and inaccurate measurements. Here, in addition to the mean μ_k a covariance matrix Σ_k is used to model the uncertainty of the represented contact points. The Kalman filter consists of two steps: the predictor and the update step, which will be explained below.

The contact points are noted in Cartesian space coordinates with respect to a fixed world coordinate frame. Observations are obtained from the spatial location m_n of responsive tactels, i.e. single tactile elements of the sensor array. Due to their fixed size, a contact point can be only localized up to a given precision, which we model by using Gaussian noise with covariance Q, resembling the physical dimensions of a tactel.

To compute the world coordinates m_n of a contact point, we have to transform the sensor position z_n given with respect to a coordinate frame attached to the tactile sensing array, i.e. the finger segment $f_{i(n)}$, into the world coordinate reference frame. This operation is done by facilitating the forward kinematics of the robot arm and the affected finger f_i:

$$m_n = T(z_n) = T_{tool}(\theta_{arm}) \cdot T_{f_i}(\theta_{f_i}) \cdot \bar{z}_n = R \cdot z_n + p\,. \tag{19}$$

The homogeneous transformations $T_{tool}(\theta_{arm})$ and $T_{f_i}(\theta_{f_i})$ define the forward kinematics of the robot arm (up to the tool mount) and the finger f_i respectively and depend on the actual joint angles θ. R and p denote the rotational and positional parts of the respective transformations.

A newly created Kalman filter model is initialized with μ equal to the observed tactel position and the measurement covariance Q, both expressed in world coordinates:

$$\mu^0 = m_n\,, \tag{20}$$
$$\Sigma_k^0 = R\,Q\,R^T\,. \tag{21}$$

The rotational part R of the forward kinematics transform in Equation 19 converts the measurement covariance Q from local finger-segment coordinates to world coordinates.

The update rule of the k-th Kalman filter for a new measurement m_n is given as:

$$\mu_k' = \mu_k + K \cdot (m_n - \mu_k) \tag{22}$$
$$\Sigma_k' = \Sigma_k - K\,S\,K^T = \Sigma \cdot (\mathbf{1} - K^t) \tag{23}$$

where S and K express the residual covariance and Kalman gain respectively:

$$S = \Sigma + R\,Q\,R^T \tag{24}$$
$$K = \Sigma \cdot S^{-1}\,. \tag{25}$$

It shall be noted that the general Kalman equations are simplified in this special case, because we can assume (i) no object motion, i.e. no inherent system evolution, and (ii) the observation function, which maps the internal state to the observation mean, is the identity function.

Space partitioning The most frequently used operation is the association of a freshly sensed contact point m_n to the corresponding Kalman filter μ_{k^*} already represented in the tactile point cloud. To this end, the Mahalanobis distance is employed as follows:

$$k^* = \underset{k=1\ldots M}{\operatorname{argmin}} \, d^2(m_n, \mu_k) \tag{26}$$

$$= \underset{k=1\ldots M}{\operatorname{argmin}} \, (m_n - \mu_k)\Sigma_k^{-1}(m_n - \mu_k) \tag{27}$$

Searching linearly for the best matching filter would lead to a complexity of $\mathcal{O}(NM)$ to assign N newly gathered contact points to M already existent filters. This search time can be reduced with the use of kd-trees [21]. These trees build up a binary space partitioning in a k-dimensional space (here, $k = 3$). This reduces the average time for the nearest-neighbor search to $\mathcal{O}(\log M)$. Together with the update of the Kalman filter, which has a constant run-time, the overall complexity of this approach is $\mathcal{O}(N \log M)$.

The decision, whether an existing Kalman filter is updated or a new filter is created, is made by simply applying a threshold. This threshold is based on the Mahalanobis distance $d(m_n, \mu_{k^*})$ as defined in equation 26. In case a new filter has to be created, the initialization equations (see Eq. 20 –21) are used.

Iterative Closest Point Algorithm To evaluate the acquired point clouds, a method to compare two shape representations has to be used. The Iterative Closest Point (ICP) algorithm [125, 23] is able to transform two point clouds X and P in a way that minimizes the mean square error:

$$E(q_r, q_t) = \frac{1}{|\mathrm{P}|} \sum_{i=1}^{|\mathrm{P}|} ||x_i - (R(q_r)p_i + q_t)||^2, \tag{28}$$

with q_r and q_t are the rotational and translational parameters of the transformation respectively.

The required correspondence between points p_i to points x_i is established by a nearest neighbor match. Subsequently, the point set P is aligned to X, applying the minimizing transformation $T(R(q_r), q_t)$. This procedure is iteratively repeated until a limiting number of iterations is reached or the residual error drops below a predefined threshold. In general, this approach is prone to get stuck in local minima, especially when applied to visually obtained point clouds, which are restricted to the front view of an object. However, due to the holistic tactile exploration used here, we did not observe

any problems with local minima. Therefore, in favor of a real-time performance, we have chosen not to use more complex variants of the ICP algorithm, like an expectation-maximization version [103].

After aligning both tactile point clouds by ICP, we can compute the distance of the test model P to the reference model X – both representing tactile point clouds – using the average minimal distance of points p_i to X:

$$E(\mathrm{X},\mathrm{P}) = \frac{1}{|\mathrm{P}|}\sum_{p\in\mathrm{P}}\min_{x\in\mathrm{X}}||x-p|| \tag{29}$$

Notice, that this distance measure is not symmetric.

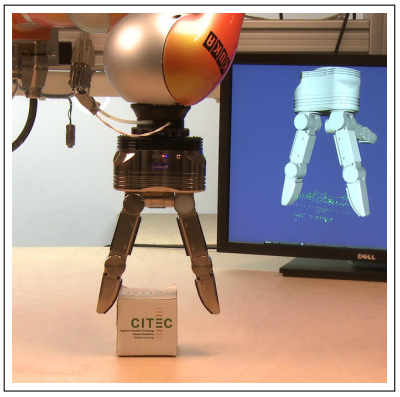

(a)

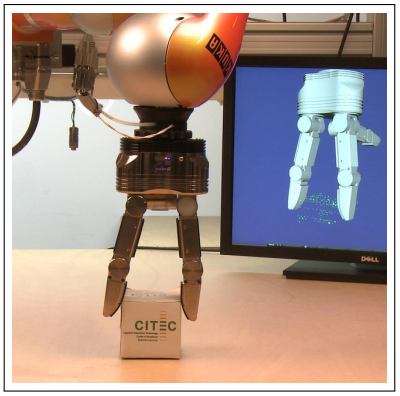

(b)

Figure 64: The first finger has reached the object and has established a contact (a). The second finger continues the grasp until contact is established as well (b). In the display in the background, the acquired point cloud up to that point can be seen.

The scanning of an object is recorded on a video ("TactileScan") as well as the recognition task ("TactileRecog").

Data Acquisition

For the generation of tactile point clouds, the SDH-2 hand was used to systematically scan the test set of eight objects. Since the object geometry is previously unknown, a predefined scanning pattern was used. The scanning was done along a horizontal scan line, with ten grasps at a distance of 1 [cm]. This scanning was repeated five times with a vertical spacing of 1.5 [cm]. The distance in the vertical dimension is higher since the dimensions of the fingers are larger in that direction. This procedure was then repeated with a rotation of 90° along the vertical object axis. Hence, a complete scan of the object consists of $10 \cdot 5 \cdot 2 = 100$ grasps. The complete volume scanned is little larger than $9[cm] \times 9[cm] \times 6[cm]$, since the size of the fingers is not taken into account and may roughly add about 1 - 2 [cm] in width and height.

For the grasping process, the strategy already described in detail on page 109 is employed. We use a prismatic precision grasp [63]. Starting from a pre-grasp posture, the hand is closed until contact is found. Once, both distal phalanges have established contact with the object, a firm grip is done to acquire rich tactile data from the interaction with the object. In case no object contact can be recognized at a scanning point, ergo a detectable self-contact occurred, the contact points are not passed through to the point cloud generation process.

The repetitive accuracy for each of the finger joints is 0.01°. The positional repetitive accuracy of the arm's end-effector is around $0.1[mm]$. Hence, the spatial dimensions of one tactel with $3.4[mm] \times 3.4[mm]$ are one magnitude above the other possible sources of measurement uncertainty. Accordingly, the covariance matrix to model the uncertainty as Gaussian white noise is chosen as $Q = \mathrm{diag}(3.4^2, 3.4^2, 0.4^2)$ (cf. Eq. (21)). The standard deviation $\sigma_z = 0.4$ along the surface normal axis is chosen to account for the softness of the sensor material at the fingertip.

Each of the eight objects was scanned five times. With this real world example data we want to show that our approach has a low

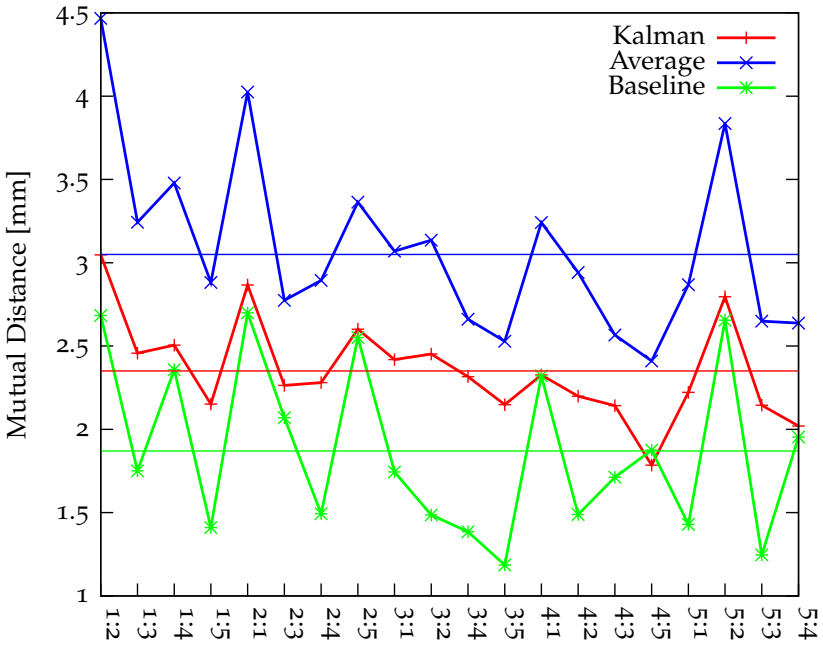

Figure 65: Mutual distances of the five scans of the jam can. All trials have been compared to one another. Since the used distance measure is not symmetric, all permutations have been considered.

variance and inter-model error within an object and a high variance and error when comparing different objects.

Evaluation

Since no real ground truth data is available, we use a point cloud comprising all acquired contact points as a baseline. This approach is as a general method not feasible because of the large amounts of mostly redundant data, which is not only more memory intense, but also slows down the processing. The sliding average is calculated with the following equation:

$$\mu'_k = \lambda \mu_k + (1 - \lambda) m_n \tag{30}$$

where a decay factor $\lambda = 0.8$ was chosen to match the typical data rate of one acquired contact frame per grasp.

To assess the quality of the tactile point clouds generated by these three methods, we evaluate the mutual distances (cf. Eq. 29) of all possible pairings formed from the set of five scans performed for each object. Exemplary, this is shown in Figure 65 for object # 5, the 'Jam Can'.

The figure demonstrates that the alignment error of the proposed Kalman filter representation is always smaller than the error generated by the sliding average method. The absolute value is slightly larger than half of the edge length of a tactile element, which would be the maximum possible distance assuming optimal alignment. A possible cause for this divergence lies in the softness of objects and their motion between trials.

As can be seen from Figure 66 this superior performance of the Kalman filter approach generalizes well, which holds true also

for the other objects. Here, the figure shows for each object the mean mutual distance obtained from all data-set pairings possible for an object, i.e. the mean of all data points. The performance is also comparable to the baseline, i.e. there is only a slight loss of precision due to the much more compacted centroid representation.

To determine if the Kalman filter converges towards the true value, we investigate the the associated covariance matrices Σ_k. If the filter converges, the determinant of the covariance matrix should converge towards zero. In Figure 67 the determinants of all objects and all contact points are shown what has had at least 10 update steps. In general, already after very few updates (2 – 4) good quality is achieved.

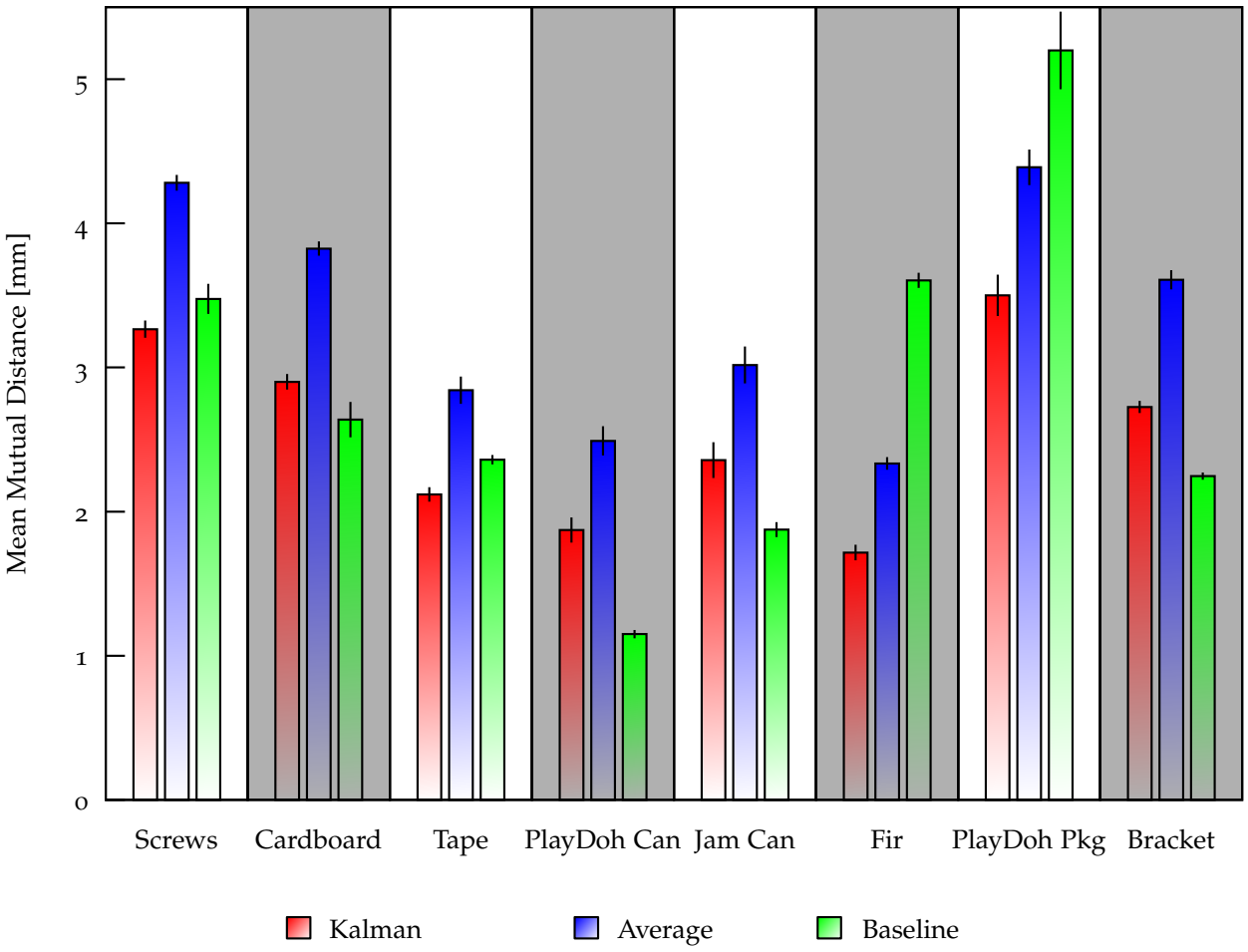

Figure 66: Mean mutual distances of all objects and all passes. All possible pairings within an object were calculated and are summarized in this plot.

The computational time for aligning the generated representations via ICP and calculating the error margin for one test object against one set of training objects amounts to an average of 6.7 [ms] for the Kalman approach. The averaging approach takes 6.3 [ms] and the baseline 46.4 [ms] on a Core2@2.8 GHz. Using only a single sensor frame per successful contact, the tactile models generated by the Kalman and averaging approach consist of 600-700 data points compared to the raw data-set comprising around 2,000 points.

Classification

The presented data, as up to this point has been shown, has a low inter-trial modeling error within one object. If the inter-object error on the other hand would be big, then the data can simply be used for object classification. This is a good example application to demonstrate the usefulness of the tactile data and the validity of the approach. We therefore again employ the ICP algorithm to align the data. We calculate the mutual distance. The object model with the smallest mutual distance is then chosen as the output class by the classifier. To evaluate the performance of this classification approach, we divided the set of tactile scans into a test and a training set. While the test set comprises the first obtained scan for every object, the training set comprises the remaining four scans (leave one out cross-validation).

When doing classification the described way, admittedly on a small set of objects, which are none the less not trivial to discriminate, the success rate is 100 %. We therefore seek to explore the limits of this classification architecture by randomly removing data points from the data-set. This also adds more realism to the task since it is desirable to successfully recognize objects with possibly one or at least very few grasps. To this end, we hence remove a certain percentage of successful grasp attempts at random from the test set and performed the classification with the reduced tactile point clouds.

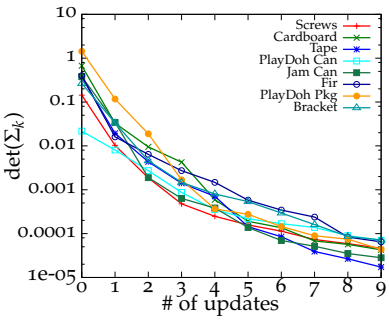

Figure 67: The determinants of Σ_k of the Kalman filter is shown here in dependency of the updates made to the filter. The values rapidly converge towards small values. The scale is logarithmic.

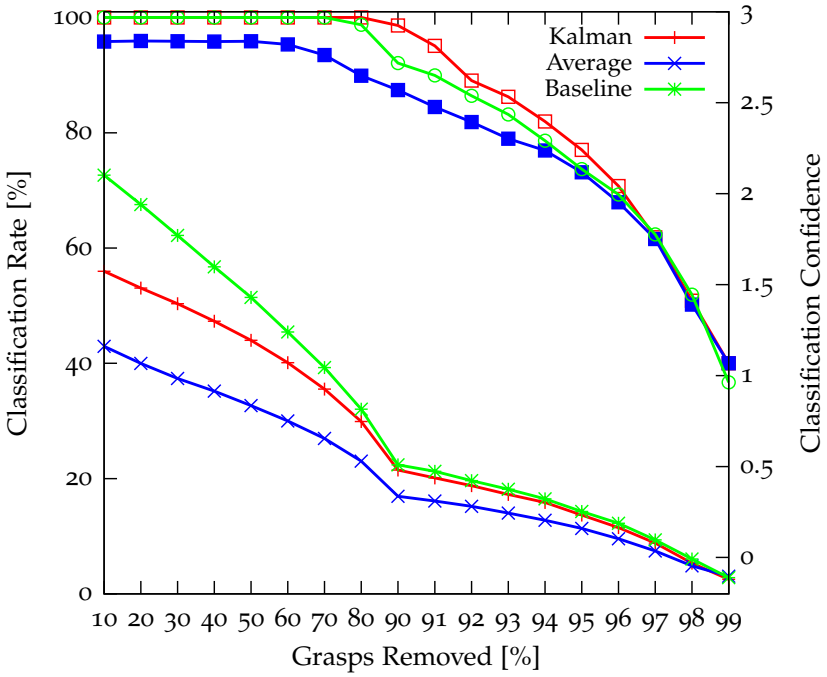

Figure 68: Classification results and confidence level of the classification. The upper curves (boxes and circle marks) present the classification rate, the lower curves (crosses) denote the classification confidence.

To obtain statistically relevant results, we compute the mean over 100 random sets (100 fold cross-validation) drawn for every given set size. We compare the classification capabilities for all three

discussed methods, i.e. the Kalman filter, the sliding average, and the baseline, which is the raw data without any processing. The corresponding classification results are shown in the upper half of Fig. 68, which indicates that the proposed Kalman filter approach performs best with a significant collapse of classification rate only well above 90% removal rate.

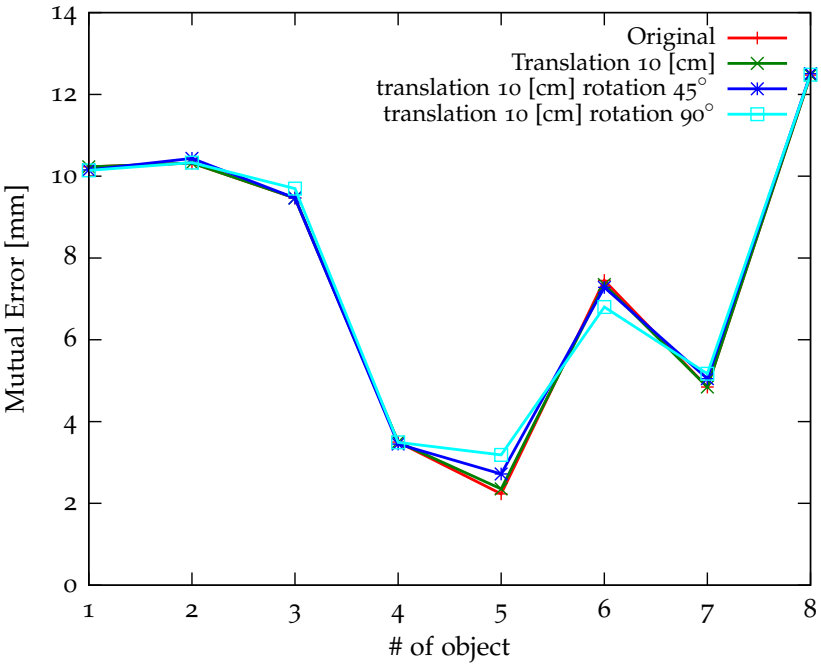

Figure 69: The approach is - most probably accountant to the ICP algorithm - very robust against translation and rotation. Here, as an example, the mutual distances for object # 5 ('Jam Can') are shown.

To further validate the robustness of the classification results we employ the normalized confidence margin defined as follows:

$$M = \frac{1}{E_1} \times \begin{cases} E_2 - E_1 & \text{if } E_1 = E^* \text{ (correct result)} \\ E_1 - E^* & \text{else, i.e. false classification} \end{cases} \tag{31}$$

In the case of a correct classification, this value measures the (positive) margin $E_2 - E_1$ of residual errors belonging to the second-best and best matching object representations X_2 and X_1, i.e. $E_1 = \min_X E(X, P)$ and $E_2 = \min_{X \neq X_1} E(X, P)$. Otherwise, the value resembles the (negative) margin $E_1 - E^*$ of residual errors belonging to the false best matching and correct object representations X_1 and X^*. This robustness margin, shown in the lower half of Fig. 68 , slowly decreases towards zero, with the values of the Kalman filter approach located between the baseline and simple averaging.

The baseline has a higher confidence margin than the other approaches but also performs weaker in the total classification performance. The larger noise level in the raw data could account for this thereby causing the ICP to run into local minimums.

To evaluate the effect of object displacements on the classification performance, a sparse representation of all objects (with 90% of grasps removed) was translated by 10 [cm] and/or rotated before comparison with training objects. As shown in Fig. 69, ICP achieves

slightly worse alignment results, thus decreasing the confidence margin. However, classification remains correct.

Summary

In this section, we have shown a "blindfolded" robotic setup that is able to grasp box-shaped and cylindrical objects relying mainly on intrinsic sensors and tactile feedback. The presented robot is able to react to uncertainty in object position (i.e. adjusts to a more promising position) and handles failed grasps through user interaction. Furthermore, the robot is able to place objects gently and does not rely on a fixed height of the placement position. The proposed algorithm is suited to get a greater extent of tactile feedback from the object, thus enabling further processing of the acquired data.

We employed the grasping part to systematically scan a set of eight everyday objects and generated point clouds from the haptic data. We compared three approaches: a simple moving average approach, a Kalman filter and, as a baseline, the raw, unprocessed data. We could show, that the Kalman filter gives the best performance when considering sparing of data points as well as processing time. We also proposed the use of kd-trees to efficiently partition the point cloud and to speed up processing for high speed, real-time tactile perception.

Discussion

In this chapter, two completely different approaches to tactile object classification have been shown. The goal of the first approach, although yielding good performance, was not only to show the producibility of an object recognition system which is solely based on tactile data, but also to find out relevant features for future applications, possibly also beyond object recognition tasks. This high demanding objective, however, could only partly be reached. The results, nevertheless, point us into directions that are worth further investigating. The used data-set is extensive and certainly offers a "real world" level of difficulty. But one also has to admit that the data-set also suffers from problems that are all-around in the tactile robotics world, let it be the low spatial and temporal resolution, the non-linear behavior of the sensing material or a considerable amount of jitter. The development of new tactile sensors is moving at a fast pace right now. Further experiments with different sensors and different objects or a completely different application employing the most promising tactile features should be on the list of roboticists in this field.

The used architecture showed to be well behaved and suitable for the purpose at hand. It may be possible to further enhance the classification performance of the system by replacing or improving the k-means clustering part, either with another clustering method, or for example by optimizing for a specific k on a per feature base.

The Kalman filter based processing of tactile data into haptic point clouds has not only proven to be robust, but also economically efficient concerning memory and processing power without making any trade-offs on the effectiveness of the method. Although model acquisition with tactile sensors is elaborate, it may be required in special cases, and may become significantly faster and therefore more convenient with the advent of better, more sensitive sensors and faster actuators.

The best application for the method right now seems to be a hybrid system with a photometric 3-D device, which will be able to acquire an initial point cloud of the scene. This data may be further segmented into sub-point clouds that supposedly belong to a single object. A hand equipped with tactile sensors would then be able to enhance the internal world model by dissolving

ambiguities. It would be possible to harden or disprove hypothesis if two object bodies belong to one object. Also the precision of the existing models can be refined, since the precision of the method was shown to be very high (in the order of $3 - 4$ [mm]).

A further extension would be to build surfaces from the acquired points, which could also be enriched with tactile available data like friction and texture. This would eventually lead to a new quality of object representations that reaches beyond the Euclidean view of objects just having physical extensions in space or colors, but also material properties.

Part IV

Tactile Determined Grasp Force Adaption

The detection of incipient slip is an important cornerstone in tactile based grasping. In this section, an approach to detect incipient slip using a fast, piezo-resistive, yet static[42] tactile sensor pad is presented. The proposed approach renders special slip sensors obsolete and therefore enables static and dynamic sensing with one sensing mechanism. For the detection of the slip, a fast fourier transform is used to pre-process the data. In a subsequent step, a standard artificial neural network is trained on the data from the frequency domain to detect slippage.

[42] Static opposed to dynamic sensors that measure changes in the force

Once incipient slippage is detectable, it is straightforward to use this information to dynamically adapt the grasp force to objects of unknown weight and friction, and even furthermore, the object is allowed to change its weight and friction coefficients, due to loading and unloading, or because the object became wet.

In addition, experiments were done to test if it is possible to discriminate different surface textures with this approach. The interesting question here is, if the frequency domain and dynamic active sensing can be used to discriminate fine surface structures far beyond the spatial sensor resolution.

Related Work

A great challenge in robotics research today is human like grasping. Humans are able to grasp unknown objects, matching the applied force carefully to the load needed to lift, handle and manipulate the object. This is done through the detection of micro-slips of the object. These micro-slips produce vibrations which the human skin is able to sense and use in the active motor control of the fingers. These vibrations are amplified through the structure of the skin, i.e. the ridges. During the transition between a stick condition and a slip condition, the state changes non-linearly until a plain slip condition is reached. It would be of great help to detect the beginning phase, i.e. incipient slip of objects.

One factor to the dexterity of humans is the adaption to different and changing friction and weight conditions. This skill is not inborn, but acquired and learned and slightly varies amongst individuals.

With the information of incipient slip, the optimal force for objects can easily be determined and a force closure grasp can be established, which is strongly supported by human studies [147, 381]. For details, see also the section on grasp force control on page 24.

To detect these micro-slips with artificial systems, special dynamic tactile sensors have been designed using the piezo-electric effect (e.g. [365, 323, 51]) or stain gauges measuring shear forces (e.g. [388, 178, 296], or both (e.g. [335]). Those sensors yield a good dynamic response and good results for the purpose of slip detection. Unfortunately though, the downside of these sensors is, that they sometimes can be easily damaged and above all, are not suited for measuring static and constant forces respectively. While the human skin uses four different kinds of mechanoreceptors for different aspects of tactile sensing submodalities, it remains a challenge to integrate static and dynamic sensors in an artificial sensing device. The avoidance of blind spots, minituarisation and a feasible amount of cabling are main challenges in the tactile sensor design. Stacking of dynamic and static sensors impairs the perception of, sometimes, already not very sensitive devices further.

Piezo-electric sensing devices offer a good dynamic response and hence have been successfully used to detect object slip.

Depending on dynamic PVDF sensors and with experiments added, the building of an artificial skin, i.e. with ridges, can be found in [389, 87]. Here, the signal was band pass filtered at a peak frequency of 200 [Hz]. The signal was fed into an artificial neural network to determine the stick/slip condition. It was claimed that an artificial hand was used to experiment with it. It is not mentioned, if different materials/textures have been used, and it is not said if the constructed skin is able to detect slippage if the sliding

motion is not perpendicular to the ridges. Also it is not clear, if the frequency is related to the speed of the motion.

A similar design, i.e. facilitating ridges, can be found in [67] with the exception that FSR sensors are used. This naturally limits the temporal resolution and therefore the range of detectable frequencies. The authors, however, give a good analysis in which the approach works and when not, i.e. when objects are sliding parallel to the ridges, if the velocity is too high or the object is too heavy. Ridges are probably a good measure to improve detection quality, but must be carefully used as magnification measure, not as the measurement principle as such.

Slip can also be detected in changes in the pressure distribution. This has been done for example in [368]. This method, however might produce false positives (e.g. a rolling object) and false negatives (e.g. an object that slides but maintains an even pressure distribution, cf. Fig. 70). Other than that the method is computationally inexpensive and simple and therefore as an additional source of information is a good choice.

Pursuing the changes in the center of pressure was also employed in grasping experiments with four different objects [338]. A three fingered, 12 DOF hand was used for the experiments. The results are quite promising, albeit the time to find the optimal grasp force is with 12 [s] rather long.

Combinations of static and dynamic sensors (e.g. [48]) have even been successfully integrated into robotic hands [96, 58] providing slip detection and force measurement. Recently, new sensors which specifically addresses the problem of detecting slippage have been designed [397, 201]. A learning architecture facilitating neural networks with the learning signal coming from a vision system is evaluated in [334]. The tactile sensing system provides frequency and pressure information, while the vision system is used to report if object and robot are moving relative to one another. This works well especially with macro slips, but the authors see improvement on the sensitivity to micro slips which are harder to detect due to the minimal relative movement, albeit most micro slips were detected.

Special optical sensor designs also exist, either in the form of an hemispherical fingertip [369, 141] or as a device especially for the detection of human fingertip slippage [185]. The latter depends on the softness of the tissue of the human fingertip. In addition, in [386] ridges are used to detect the shear force with which it is possible to infer slippage. If the ridge is bent due to shear force, it can be detected due to optical interference. An optic approach that uses photometric sensor to detect movement of the object is presented in [200, 201], in this case the area of application was a moving conveyor. Hence, this approach is interesting in cases where no true tactile sensor can be used.

Some sensors use additional force information as shear forces to detect sliding motions. The additional information is valuable,

Slip detection using simple FSR sensors can be accomplished, albeit restrictions apply.

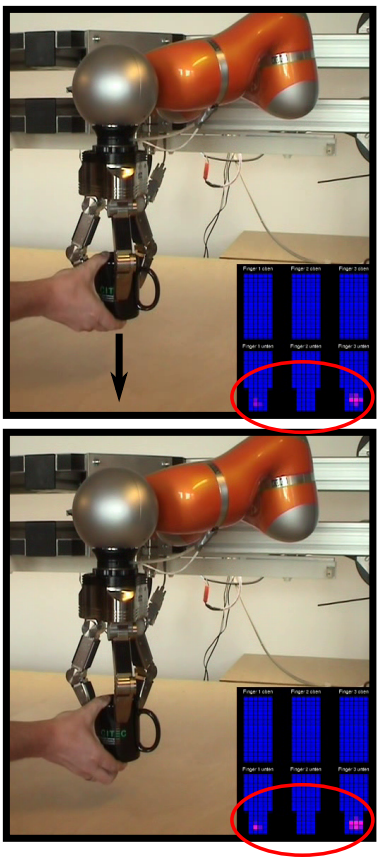

Figure 70: Object slippage can occur without changes in the center of pressure of the tactile sensor, especially if the sensibility and spatial acuity of the sensor is limited.

Using static pressure distributions can be used to detect slippage of objects, with limited performance.

Pairing dynamic and static sensor yields the best of both worlds at the price of a higher complexity and possible interference of the two sensing principles.

Various optical sensors can be used to detect the movement of objects. They often lack tactile sensing capabilities.

of course, especially in the case where friction coefficients, and therefore the maximal shear force until static friction is exceeded, is known. Sensors tend to be more complex though [167, 398].

Several other designs can be used for slip detection, e.g. shear information or pressure distribution in fluids.

The idea of a tactile retina is proposed and implemented in [224, 223]. Basically, the processing of the tactile information is done within the tactile element, which only passes the processed information upstream, thereby dramatically reducing the information and wiring complexity.

A fingertip filled with a fluid was also successfully used for the detection of incipient slippage. A microphone was used to record high frequency variations in the pressure [78].

Besides neural networks, also support vector machines were successfully used for slip classification.

An artificial neural network was used in [228] to determine the optimal grasp force of objects. The accuracy was, however, not satisfactory with 51-63 %. The experiments that were conducted are unfortunately only poorly described. It is not possible to compare the results to the findings in this work here. In a follow-up work a combined dynamic and static (FSR) sensor was used [229]. This time, 104 samples were used to train a support vector machine. Only the surface roughness is used as input parameter, i.e. knowledge of the object weight must still be known. This time, a higher accuracy was obtained, but not validated in an experiment with grasping.

A 4-D micro-force sensor (F_z,M_x,M_y,M_z) with strain gauges was used with a soft fingertip for slip detection and grasp force adaption [119, 118, 120]. A model for the soft fingertip is presented to improve the results, since the force sensor is covered by the soft material. The sensor is quite fragile for one, also the soft fingertip improves of course the friction and compliance of the finger. The force sensor yields a high temporal resolution and enables slip detection through the measurement of moments and the model of the fingertip.

Texture classification has been done with dynamic sensors with good response to fine surface features.

On the question of texture detection and classification, good progress was recently made combining visual and tactile information through weak pairing of the two modalities [183]. A tactile sensor consisting of a needle mounted at the membrane of a microphone was used which gives a high temporal resolution, albeit with very limited sensing area. Also, the exact measurement of contact heights was difficult due to the compliance of the needle. Hence it can be said that the sensor was tuned for texture classification. Apart from the specialized setup, the combination of the different modalities as well as the good classification results are noticeable. Similar to that design is also the whisker tactile sensor found in [300] and [322].

The work that is probably closest to what is presented in this chapter emerged in the group of Makoto Shimojo. Quite some publications [357, 355, 354, 356, 353] deal with the development of a tactile slip sensor and its application to force control in a high

speed robot hand [110, 313, 392, 391, 140]. In the earlier work [352, 351, 105], a specialized slip sensor design was chosen, which allowed the detection of slip due to a high temporal resolution of about 1 [kHz]. The limitation of the sensor was that only a single, absolute value of pressure could be detected, i.e. the sensor only consisted of a single cell. This shortcoming, however, was removed in later designs, where two layers of different tactile sensors were stacked.

Application of slip detection for grasp force adaption can very recently be found in a high-speed robotic hand.

While the detection of the incipient slip is done in a similar fashion as will be presented here, as sliding window discrete fourier transforms and discrete wavelet transform (DWT) are being used, the implementation and also the methodology differs. In the cited work the object is moved and ground truth data is acquired with a laser range finder to measure the displacement of the object. Also, the on-board electronics of the tactile sensor are modified on the basis of the data from the experiments that the output is an analog voltage signal in the range of $0 \ldots 5$ [V], where 0 [V] is the stable, and 5 [V] is the slip case. The algorithm is tuned to detect a prototypical curve in the raw signal with the DWT. It is not mentioned if the curve is also dependent on the material/texture of the object. In the test of the grasp force adaption, 53 [g] of rather light material is filled into a cup.

A novel, state-of-the-art high performance system for automatic grasp force adaption to unknown objects is presented here.

In contrast to some of the related work, in this chapter a piezo-resistive, and therefore static tactile sensor is used to detect incipient slippage. Hence, no extra hardware that serves the sole purpose of detecting slip, vibrations or movement is used. The data acquisition is done with the sensor mounted on the robot, we therefore are able to differentiate between vibrations induces by the robots own control cycle and object slippage. We successfully employ a neural network, i.e. learn the desired behavior. To this end, we use different object textures. We prove the usefulness in an experiment where dynamic adaption of the grasp force is necessary.

Experimental Setup

Our tactile robotic setup consists of two Kuka/DLR LWR arms in a bi-manual setup, as can be seen in Fig. 71. This way, grasping with the tactile pads is possible. The initial data acquisition for this experiment was done mono-manual and consisted of a tactile sensor module as seen in Fig. 72.

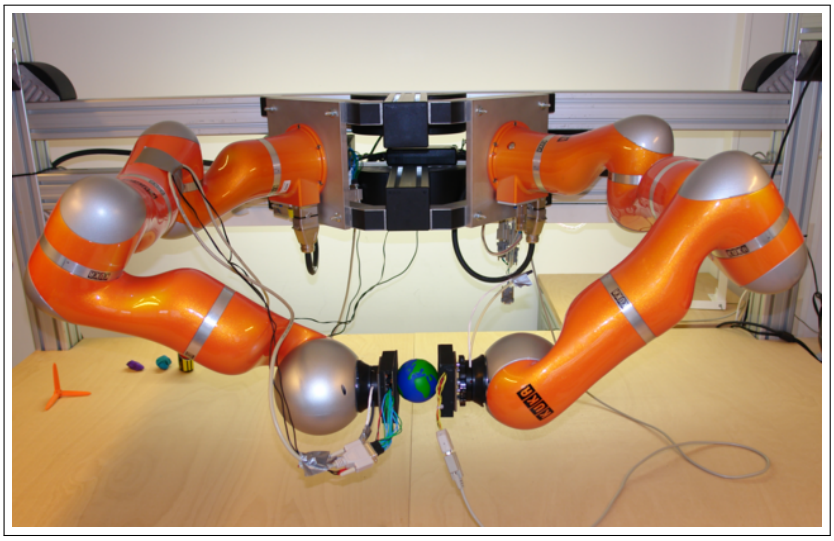

Figure 71: The bi-manual setup in the tactile lab. Both Kuka/DLR LWRs have a myrmex tactile sensor mounted on their end-effectors.

Tactile Sensor

The tactile sensor employed here is named "myrmex"[43] and was developed to enable very high speed data acquisition in hand with high sensibility for low contact forces [312, 311]. A myrmex sensor is a square module of dimensions 80 [mm] x 80 [mm] with a height of 15 [mm]. The sensor's working principle is based on the resistive method to measure pressure on a surface. For this method a conductive elastomer is used which changes its resistance proportional to the pressure applied to it. The change in resistance behaves well over a large range (almost linear in its responsiveness), with non-linear responses only at both low and very high pressures. Each myrmex sensor has a matrix of 16 x 16 sensor cells on its surface, resulting in a spatial resolution of 5 [mm]

[43] Made by Carsten Schürmann

x 5 [mm]. These sensor cells get covered with a carbonized foam which functions as the conductive elastomer. One strength of this approach is that there are no measurement gaps between the sensor cells. Thus, the complete sensor area is sensitive to contact forces.

The sensitivity and range of pressure detected is very dependent on the properties of the foam which is used. It is possible to detect forces below 0.1 $[\frac{g}{mm^2}]$ and as high as 20 $[\frac{g}{mm^2}]$ with the appropriate foam. The myrmex sensors are designed to also function in a big array of modules. It is possible to enlarge the sensing area by simply sticking two modules together. Arbitrary configurations can be used this way. However, in this paper, the sensor was used in the standalone mode.

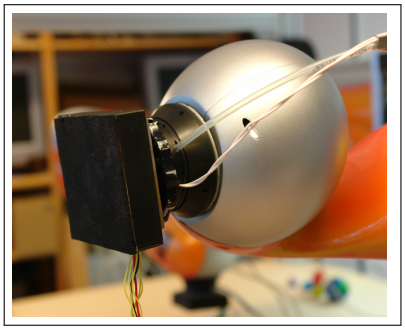

Figure 72: The myrmex sensor mounted on the Kuka/DLR LWR end-effector. The internal cabling (air and power) that can be seen in the picture are not used in this setup.

In this single or standalone operation, it can sample its surface at about 1,800 [Hz]. Each of the 256 sensor cells on a module returns a digital value with a resolution of 12 Bit. Each sensor module is equipped with a PIC32 micro-controller which is responsible for acquiring the data from each cell and storing it prior to transmission. The modules are normally interconnected with pin headers and use a custom made parallel protocol to transmit the data between each other. This protocol handles the identification of the connections between the units and is able to determine the module's location inside a matrix of such modules. This implementation was chosen so that an array of these modules can be arranged with a varying number of modules and different rectangular shapes without modifying the hard- or firmware. Because there are no compatible or standardized versions of this protocol for standard PCs, a module array or single module gets connected to a mediator unit which then transfers the tactile data to a PC. This mediator unit is equipped with an AVR32 micro-controller which communicates with the sensor(s) via the sensors own parallel protocol. The mediator uses an USB 2.0 high speed controller to communicate with a PC. The USB connection was chosen because it provides high enough bandwidth for high speed data acquisition even with many modules, and offers a standardized protocol which is very suitable for the task: the USB Video Class. By making use of the USB video protocol, the data from the modules is packaged in a video frame with the sensor cell values encoded as pixel data. This allows a very convenient translation to the variable array sizes into the frame dimensions which then can be easily be interpreted by the PC software. The biggest advantage of the USB video protocol is its standardization and the availability of low level drivers for this device class.

Features of the myrmex tactile sensor:

- High Temporal Resolution
- High Sensitivity
- USB Interface
- Modular Design
- Robust

A set of five different objects with different surface texture is used as a test and training set. For the data acquisition, the objects are fixated and the sensor is moved in a sliding motion over the object. To ensure a precise motion, the sensor is mounted on a Kuka/DLR LWR. The recorded data is used to learn the detection of slippage as well as to distinguish between different object surfaces.

Kuka/DLR LWR

The Kuka/DLR LWRs have torque sensors in every joint. The Kuka/DLR robot facilitates these torque readings to allow different modes of impedance control. For the task at hand, one robot was set into axis impedance control, where it is possible to set different stiffness and damping parameters for each of the seven joints.

Also the robot provides a force estimation for the end-effector. The forces on the end-effector are calculated with the use of a dynamic model of the robot and the torque readings within the Kuka controller [4]. The force estimation is used to establish an ongoing contact force between the myrmex sensor (which is mounted on the end-effector) and the material probe. To this end, a force controller was implemented with the software described in great detail in chapter II. A PD-Controller[44] [49] is used to maintain a set force at the end-effector in a Cartesian direction. To avoid unwanted, abundant movements, a boundary box can be set so that the end-effector will not leave.

[44] Proportional-Derivative

The robot arm is controlled in real-time using Kuka's FRI interface on the robots side and our own implementation of the provided interface of the controlling server, the OpenKC software package (for details, see Part II). The communication between the robot controller and, in our case, a standard PC running a highly preemptive Linux kernel, is done via UDP/IP over Ethernet. The robot sends a binary message with its actual positions, torques and estimated forces, the server software reads out the transmitted data and will send a response packet to the robot controller. In the response packet, a correction for either the joint values or the Cartesian position is sent to the robot. The robot will generate packets in a 2 [ms] interval, and the server needs to answer within this time period.

The robot arm is force controlled at a cycle of 2 [ms] by using the OpenKC framework and FRI Interface.

Experiments

To have a sound data basis for the slip detection algorithm, the described setup was used to record a number of stick/slip conditions. A total of five different surfaces (cf. Fig. 73) were probed: a fabric, a wooden surface, a ceramic cup, the smooth, upside surface of a mouse pad and the rather rough, downside rubber side of the mouse pad.

Each of the five objects was sampled five times with the robot, which maintained a contact force of 6 [N].

Each object was sampled five times. During the sampling procedure, at first, contact with the object was established and a contact force of 6 [N] was maintained. Afterward, the end-effector was moved to four further positions on the material. The positions were aligned in a square with a short resting phase of approximately one second at each corner. During the run, the tactile data from the myrmex sensor as well as the position and force information of the robot were recorded. The recording frequency was running asynchronous to the robots control cycle at 100 [Hz]. The robot itself was controlled at a frequency of 500 [Hz], the myrmex sensor produced samples at approximately 1,800 [Hz]. The software to record the myrmex tactile data run in a parallel thread saving all tactile frames coming from the sensor. It was therefore possible, using the ring buffer recording, described in Part II, to save the last 1,800 tactile samples as well as the current end-effector position, velocity and acceleration. The robot movement data provides the ground truth for the classification.

Data Processing

To analyze the data samples, a transformation from the time domain to the frequency domain is done. To this end, a one dimensional discrete fast Fourier transform (FFT) is used. The FFT is an efficient way to compute the discrete Fourier transform:

$$X_k = \sum_{n=0}^{W-1} x_n \cdot e^{-i2\pi \frac{k}{W} n} \tag{32}$$

with x_n being the data samples A data sample consists of the sum of all tactels at a given frame n. The frames represent the recorded time series.

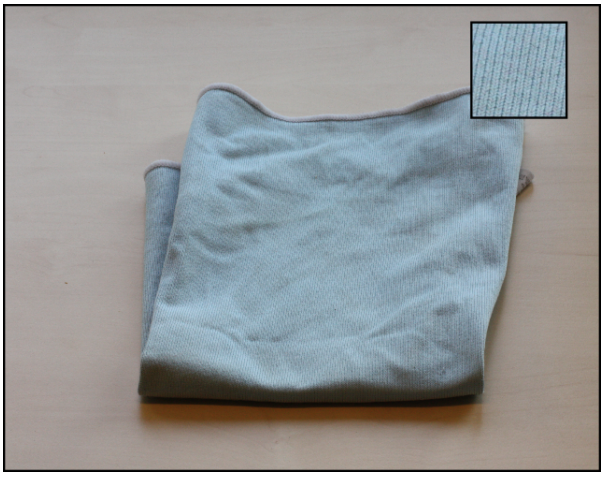

(a) Fabric

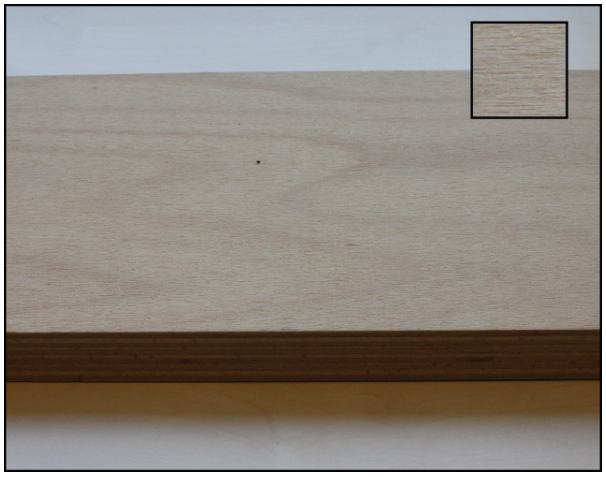

(b) Wood

(c) Cup

(d) Mousepad Top Side

(e) Mousepad Bottom Side

Figure 73: These different objects were probed. The texture and roughness of the objects' surfaces differs. A closeup is shown in the upper right corner to give an impression of the textures.

The squared magnitude of the FFT represents the spectrogram of the function:

$$\text{spectrogram}\{x(t)\} = |X_t|^2 \tag{33}$$

The different spectrograms with $W = 1792$ of the different materials can be seen in 74.

A trade-off regarding latency and accuracy has to be made regarding the input size to the fourier transform.

Here, W, the window size is a parameter of the method that is going to be investigated thoroughly. A small W will enhance the responsiveness but due to limitation of the Nyquist frequency, places a boundary to the highest frequency. Nevertheless, leakage and aliasing effects have to be taken into account anyhow. Also the rubber foam of the myrmex sensor impairs the analysis of the "true" spectrum [319]. It must be assumed that higher frequencies, albeit probably damped by the sensor material, occur during probing but cannot be specifically detected. Despite these limitations, a qualitative and quantitative difference in the spectrum between slip and stick conditions can be found.

The frequency spectra of the different materials during slip give cause to the assumption that a material classification of the surface, although a challenge, may be worth investigating closely. This is a special challenge because the surface of the sensor, which surely has an impact on the measured vibrations, is, because of the open-cell foam, in its character quite random. Nevertheless, it will reveal the value of the vibratory information that can be retrieved from the static sensor.

Classification Architecture

To show the feasibility of our approach and the ability of the tactile sensor pad to serve as a conjunction of a static and a dynamic tactile sensing device, a standard artificial neural network was trained to detect slippage. A first parameter of this approach is the window size W of the FFT as it has impact on the frequencies that are detectable and the possible input dimension. In a subsequent step, the resulting spectrum was divided into N frequency bands of equal size, with the exception of the DC part of the Fourier transform, which gets mapped directly to the zero band. The absolute value of the complex frequency information was squared, thus eliminating the phase information. Also the logarithm was taken to compensate for lower power levels at higher frequencies. The recipe for converting the FFT output to the frequency band can be seen in Algorithm 4. The resulting frequency bands were normalized to the interval $[0 \ldots 1]$ to be suitable for further processing.

Parameters of the system:

- W Window size of the sliding FFT
- N Number of frequency bands or areas that are summed up as input for the neural network
- H The number of hidden neurons in the artificial neural network

For both tasks, slip detection and material classification, a three layered artificial neural network was employed. The architecture of the network for the slip detection task is W–H–1 while for the

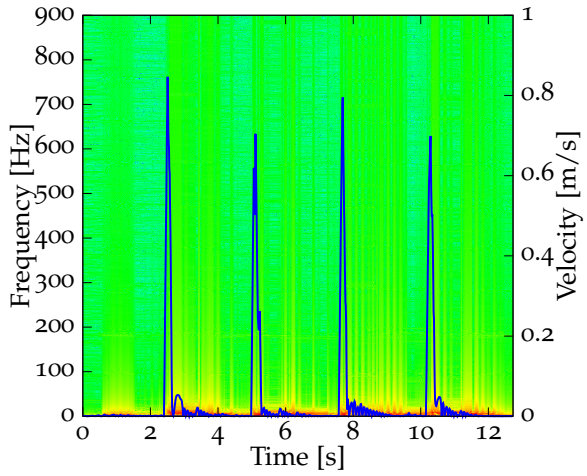

(a) Fabric

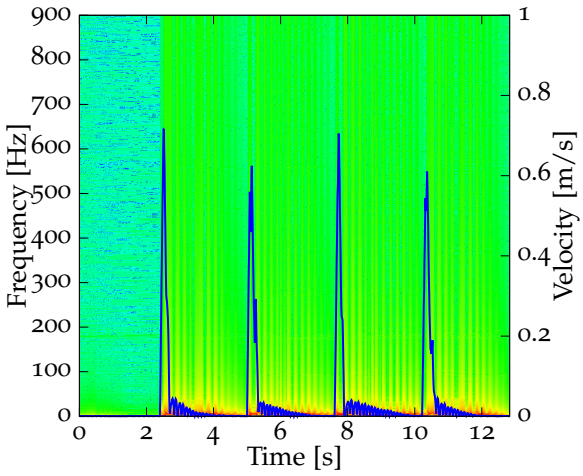

(b) Wood

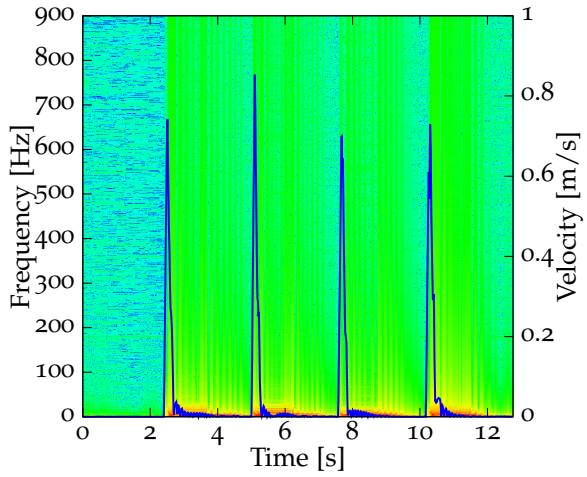

(c) Cup

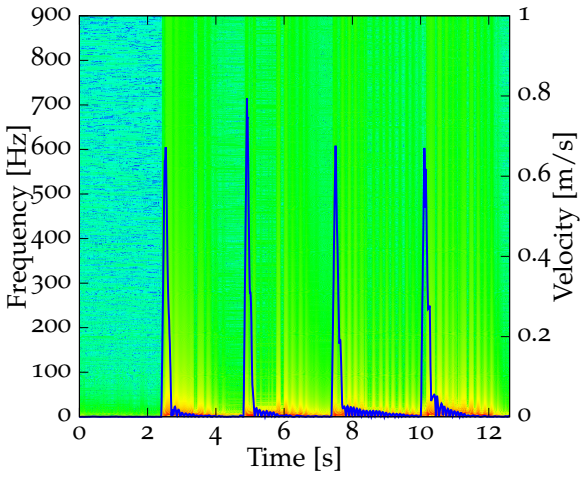

(d) Mousepad Top Side

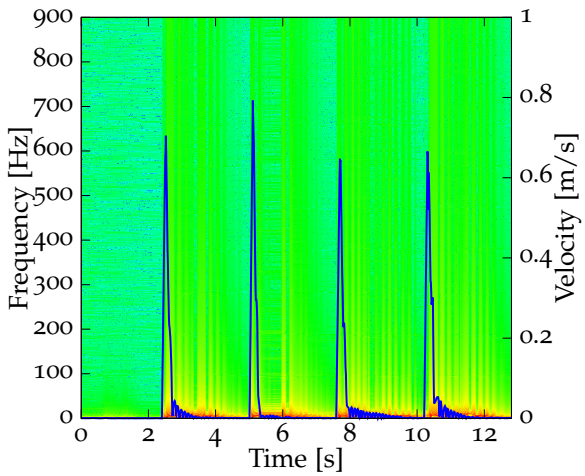

(e) Mousepad Bottom Side

Figure 74: For each texture, a single try is plotted. The blue line depicts the velocity of the end-effector parallel to the object surface, i.e. $v = |v_x| + |v_y|$. A spectrogram of the frequencies is shown.

Algorithm 4 Partitioning of the Frequency Data

Require: No. of Bands N
Require: Window Size $W > N$
Require: Complex Result of FFT x_n
Ensure: B_n holds n-th band frequency powerspectrum

{Init to zero}
for i=1 **to** N **do**
  $B_i \leftarrow 0$
end for
{Treat the DC component special}
$B_0 \leftarrow log(|x_0|^2)$
{Iterate over the frequencies}
for i=1 **to** N **do**
  for k=$\frac{((\mathrm{i}-1)\cdot\frac{W}{2}+1)}{N-1}$ **to** $\frac{i\cdot(\frac{W}{2}+1)}{N-1}$ **do**
    $B_i \leftarrow B_i + log(|x_k|^2)$
  end for
end for

material classification task the networks layout was W–H–5, with H being the number of neurons in the hidden layer of the network.

For the neural networks, the free and open source software Fast Artificial Neural Net Library (FANN)[45] was employed. The network was trained using the resilient backpropagation algorithm [283]. The training was limited to 6,000 epochs. As activation function the standard sigmoid function[46] was used.

[45] http://leenissen.dk/fann/wp/

[46] $y = \frac{1}{(1+\exp(-2*x))}$

Results

Slip Detection Task

The recorded data was divided into a training and a test set for cross-validation. From a total of 25 data-sets, one data-set was left out for testing (leave one out cross-validation). The data of each of the 25 trials was partitioned into a stick and a slip set. If the velocity was above 0.005 $[\frac{m}{s}]$, the sample was considered to be in the slip set. If the velocity was below 0.00125 $[\frac{m}{s}]$, a stick condition was assumed. For the window size W, the values 256, 512, 768, 1024, 1280, 1536 and 1792 were tested. For the number of frequency bands, and therefore the parameter N of inputs, a total of 22 different values for N in the range $[2 \ldots 100]$ were used.

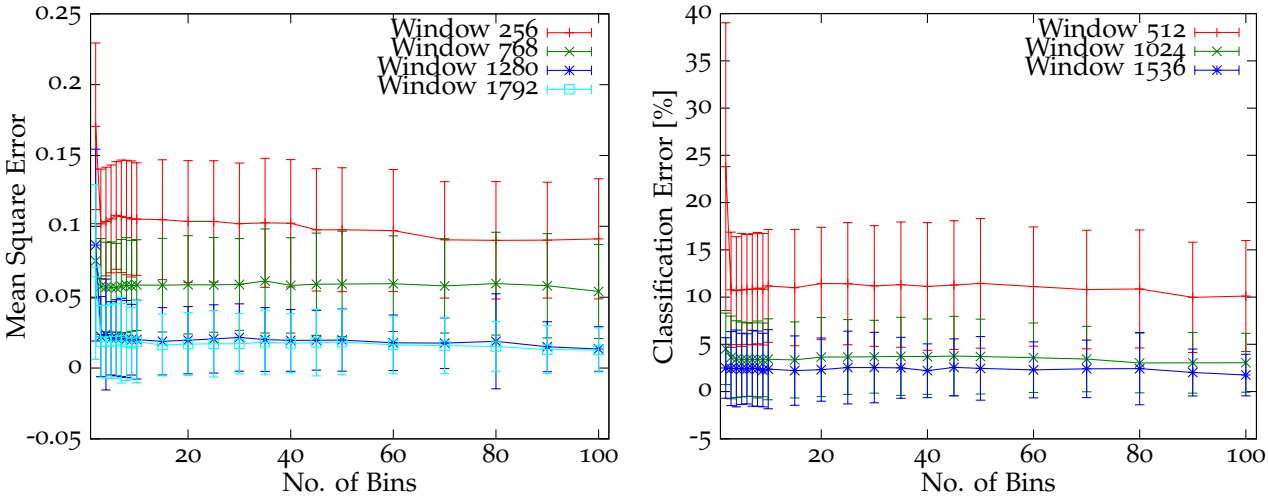

Figure 75: Classification results for different window sizes W and number of input neurons N. Both, the mean square error and the classification error are shown. The number of hidden neurons (H) is 6.

The number of neurons in the hidden layer (H) was probed within $[4 \ldots 16]$ with a granularity of 2. For each set of parameters, eight randomly initialized neural networks were trained and then tested. For all results, the mean square error (MSE) was calculated:

$$MSE(\overline{X}) \stackrel{\text{def}}{=} \frac{1}{n} \sum_{i=1}^{n} (f(x_i) - y_i)^2 \tag{34}$$

In addition to the MSE, the classification error was calculated, with stick/slip threshold at 0.5 (cf. Fig. 75). Since the number of true stick conditions was, due to the fast movement and time

needed to completely stop the movement, much larger than the number of stick conditions, additional measures were used. The ratio between slip and stick was approximately 3:1. Hence, the overall classification error alone does not yield a good standalone measure. To overcome this, both sensitivity[47] and specificity[48] are also evaluated (see Fig. 76). The results indicate that both stick and slip conditions are detected adequately.

The error on the test data-set did not significantly benefit from values $N \geq 10$. From the results and the spectrograms (Fig. 74) it can be inferred that very few different frequency bands are involved and a simple classification architecture is sufficient to get a well performing system.

[47] $\frac{\text{\# true positives}}{\text{\# true positives} + \text{\# false negatives}}$

[48] $\frac{\text{\# true negatives}}{\text{\# true negatives} + \text{\# false positives}}$

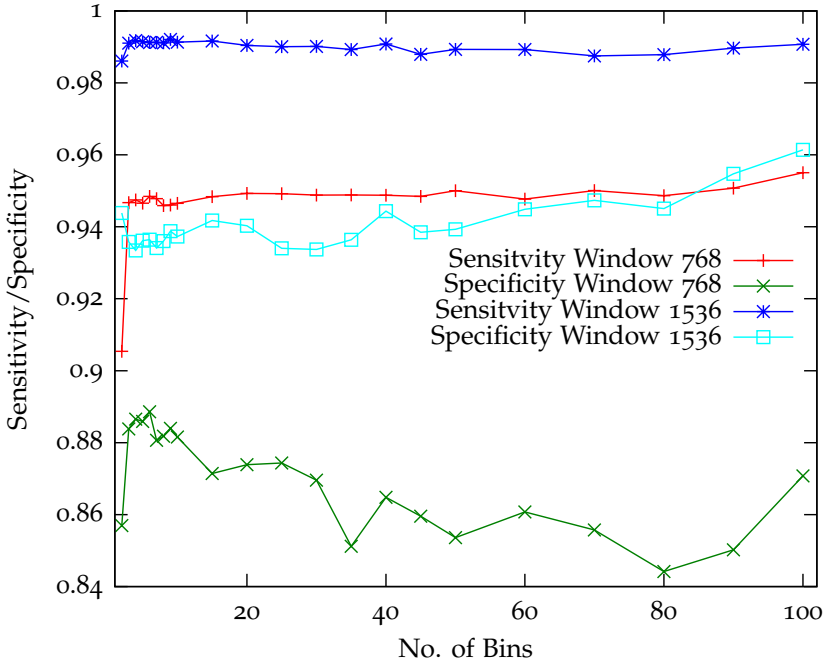

Figure 76: Exemplary the sensitivity and specificity for two different window sizes W are shown. H, the number of neurons in the hidden layer, is 6. Generally, the performance is satisfactory and well behaved in all parameters.

The remaining question is, how the number of hidden neurons influence the performance and generalization of the approach. With Figure 77 the influence of different numbers of neurons in the middle layer of the multi-layer perceptron. In regards to the numbers, a significant influence of the parameter H within the tested range could not be verified. This means, neither clear degrade in performance nor an over fitting could be noted, thus the system is well behaved within the tested parameter range.

For the application of the approach, it makes sense to use a system that minimizes the parameters W, N and H, as they add to the computational complexity of the system. The results indicate that to this end, a window size of 1280, 4 hidden neurons and N in the range of 4 – 6 would yield optimal results in this respect. The best results[49] are not that much better than those considered optimal[50].

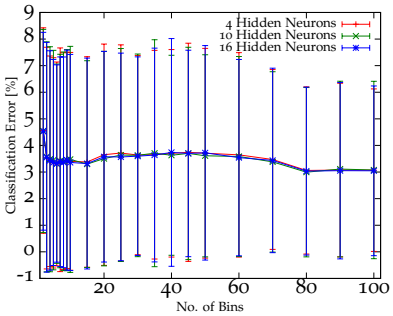

Figure 77: The number of neurons in the hidden layer has no significant impact on the performance of the classification architecture. Exemplary, the classification test error is shown for $W = 1024$.

[49] Best results for $W = 1792$, $N = 90$, $W = 16$ is a classification error of 1.62 % $\pm$ 2.14.

[50] 2.64 % $\pm$ 3.41

Surface Material Classification Task

For the material classification task an almost identical set of parameters was tested, the ranges for W[51] and N[52] are identical to the slip detection task, while the number of hidden neurons H was in the range $[4 \dots 16]$, again at a granularity of 2. Again, the data-set was divided into training and test set, honoring the leave one out cross-validation principle.

[51] $\{256, 512, 768, 1024, 1280, 1536, 1792\}$
[52] $[2 \dots 100]$

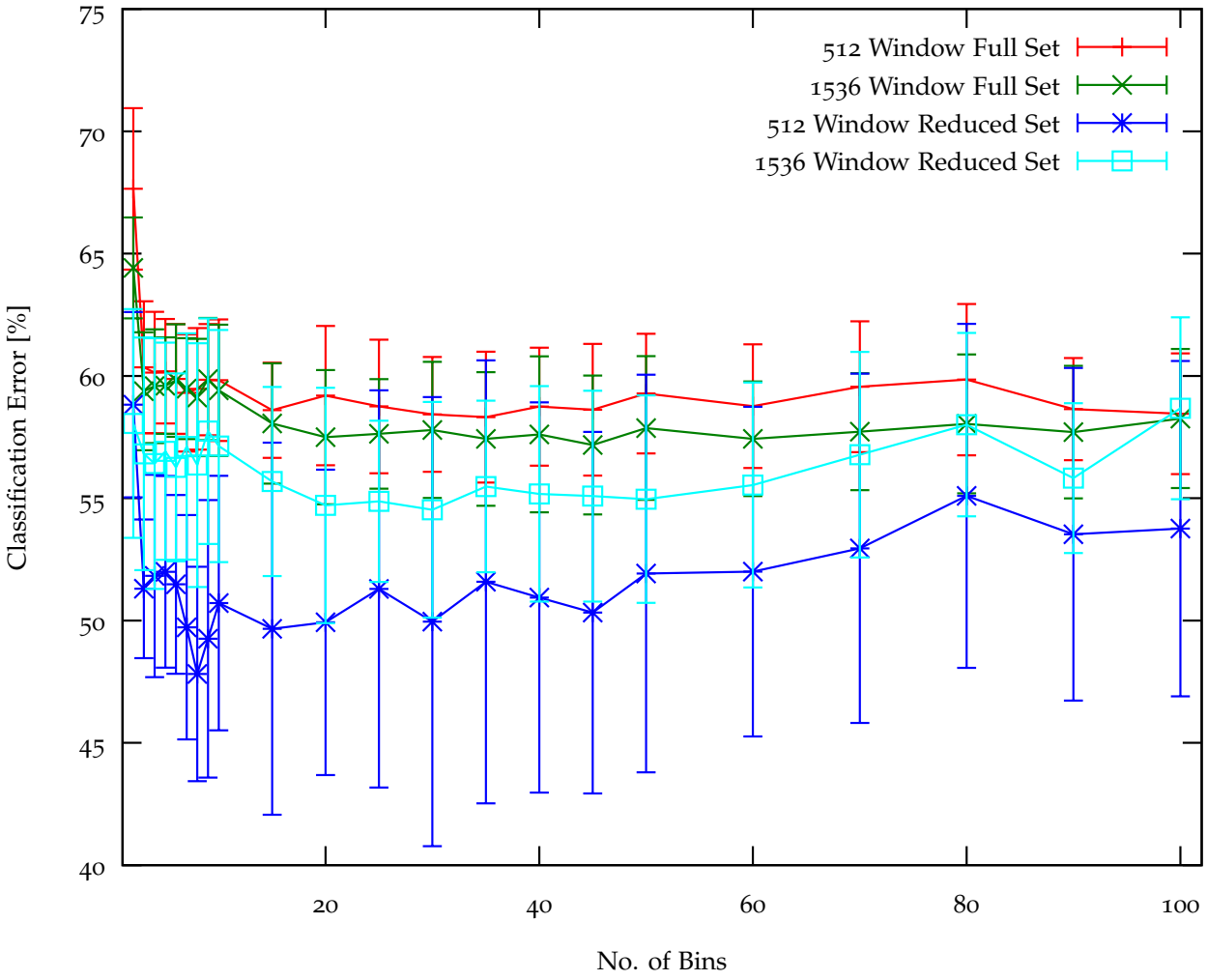

Figure 78: The surface texture classification task shows to be much more difficult with the proposed approach. The Reduced set only regards data samples where the velocity of the end-effector exceeded 0.02 $[\frac{m}{s}]$.

Because the frequency spectrum is quite different when the end-effector is in rest or moving, two data-sets were evaluated: One is respecting all gathered data samples while the reduced set only respects those where the end-effector was moving at least at a speed of 0.02 $[\frac{m}{s}]$.

The classification of the surface textures shows to be much more difficult than the previous presented slip detection task. In Figure 78 some of the results are shown. The best classification results (error of 47.81 % $\pm$ 4.38) were obtained at $W = 512$, $N = 8$ and $H = 16$.

The classification does benefit from more neurons in the hidden layer (cf. Fig. 79). At the same time, high values of N hurt the performance, an indication of possible over-fitting.

When taking a closer look at the confusion matrix, which can be found in Table 10, one can find that very distinct surfaces like the ceramic cup, that is significantly smoother than all the other surfaces, or the fabric, which has a totally different hardness, are classified to satisfactory degree. On the other hand, the wooden surface has a rather high chance of being confused with any of the other classes.

Albeit the much higher variances in the results across the tested parameters, no satisfactory set of parameters could be found. Assuming that the approach is not highly non-linear in its parameters, a significantly better performance with a different set of parameters other than the ones tested is not probable.

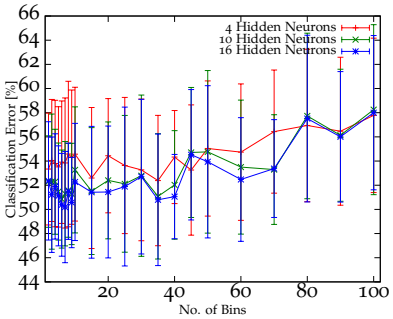

Figure 79: The number of neurons in the hidden layer has no significant impact on the performance of the classification architecture. Exemplary, the classification test error is shown for $W = 1024$.

		Answer Neural Classifier				
		MP Top	MP Bot.	Fabric	Cup	Wood
True Class	MP Top	31.66%	29.81%	1.57 %	11.20 %	25.76 %
	MP Bottom	33.34%	42.17 %	2.34 %	1.37 %	20.69 %
	Fabric	12.70 %	9.90 %	61.48 %	0.36 %	15.57 %
	Cup	9.30 %	6.19 %	2.42 %	66.93%	15.17 %
	Wood	22.44 %	17.14 %	18.20 %	4.68 %	37.54 %

Table 10: Confusion matrix of the material classification task. The columns represent the answer from the neural network whereas the rows stand for the true class. Hence, the diagonal entries are the correct classifications.

The detection and classification of material textures or fine surface features showed to be difficult. While a rough estimate seems possible, the gap between robot and human performance is quite large and obvious. The most probable reasons for this will be discussed in the Discussion section.

Grasp Force Adaption

With the results from the slip detection, a simple, yet effective algorithm to control the grasp force of unknown objects with the help of tactile sensing is composed. Humans exhibit a remarkable skill of controlling the grasp force such that it is enough to prevent the object from slipping. At the same time, they maintain a close to minimal force to prevent the object from breaking and the muscles from exhaustion. Hence, an optimal solution between the two conflicting constraints, maintaining a minimal force and avoiding slippage, is found.

Two versions of the slip detection are enclosed on the data storage attached to this thesis: "SlipDetection" and "SlipDetectionLong".

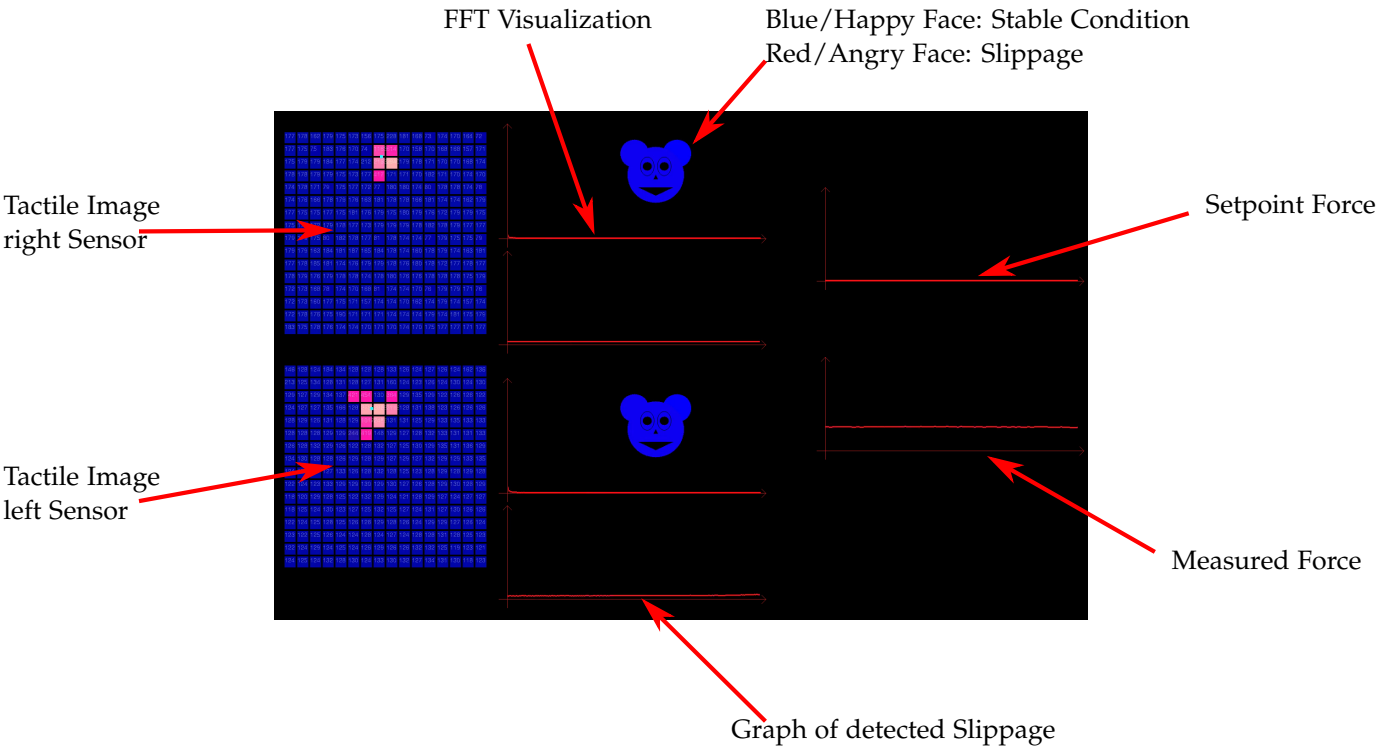

Figure 80: The visualization shows the state of the algorithm in real-time on a display during the experiments.

If the friction coefficient and the weight of the object are known beforehand, the necessary grasp force can be pre-computed of course. This possibility should not be neglected but used as a heuristic starting point, as it is the case when humans are grasping [99, 101, 100, 239, 98, 150, 83, 79, 85, 84, 73]. But determining the friction coefficient may not always be possible or feasible, also this strategy alone is not sufficient. In addition, the friction coefficient

can dynamically change, for example when the object gets wet, or any other substance is interfering (e.g. sand, water, oil). In addition, the weight of the object might change, think of a container that gets filled or emptied, or when external forces are exerted onto the object. In this context, slip detection can be brought into a new light, for example when the robot is handing over objects. In this case, slippage caused by external forces may triggering the handing over of the object.

Algorithm 5 Grasp Force Adaption

```
1:  while Grasping Object do
2:    s ← is_slip_detected()
3:    if s == SLIP then
4:      graspforce ← graspforce + Δ_f
5:      slipcount ← 0
6:      wait t_f
7:    else
8:      slipcount ← slipount + 1
9:      if slipcount > threshold then
10:       graspforce ← graspforce − Δ_f/4
11:       slipcount ← 0
12:       wait t_r
13:     end if
14:   end if
15: end while
```

THE SHOWN ALGORITHM FOR THE ADAPTION of the grasp force will simply increase the force if slippage is detected. If, for a certain period of time, no slippage is observed the grasp force is slightly decreased. This will lead eventually to a slippage event. The force, that is necessary to avoid that slip is the force at the time the slippage occurred plus a safety margin (e.g. +5 %). After adjustment of the force, a refractory period is forced, i.e. the algorithm will allow the robot controller to adjust the force, since during the force adaption, signals very similar to those emerging from slips may falsely be interpreted as another slip event. Therefore, the wait term is important as it inhibits the self-excitation of the system.

Simplified algorithm:
On Slip Increase Force
On Stable Condition Reduce Force

The Algorithm 5 implements the described behavior with exception of the fixation of the final, safe grasp force. This can easily be added with another variable but was left out to reduce the complexity of the algorithm without any true gain of insights.

Experiment

TO VERIFY THE VALIDITY OF THE PRESENTED method, a simple experiment is conducted. A plastic cup with the weight of 1-2 [g], is filled with approximately 250 [g] of gravel. The tactile data, the

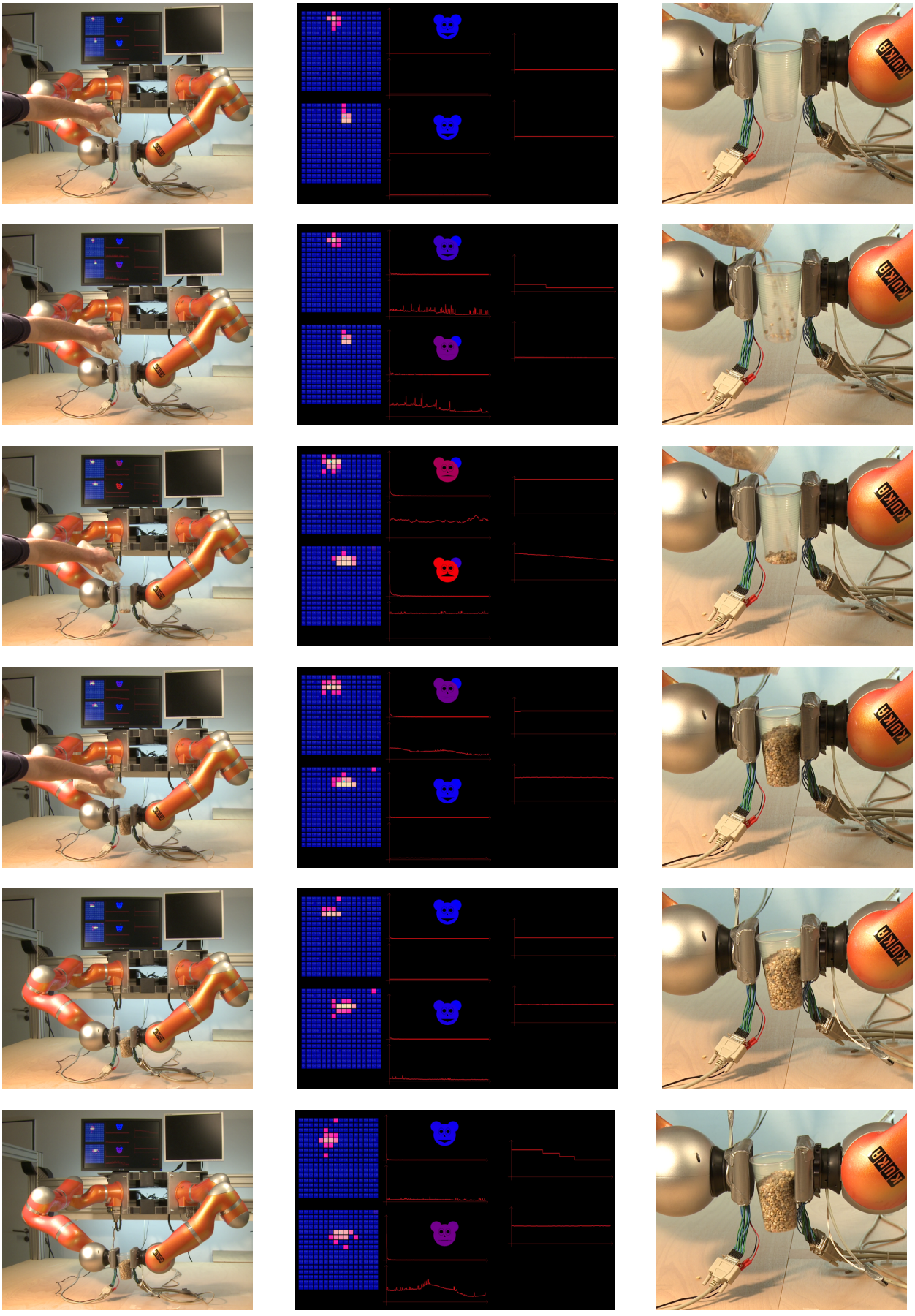

Figure 81: In this sequence, the grasp force adaption algorithm is shown. The first slippage takes place when the cup is filled. After a gradual decrease in the force, a second slip event is detected.

fast fourier transformation, the output of the neural network as well as the measured and setpoint grasping force is visualized as can be seen in Fig. 80. At the point when the gravel hits the bottom of the plastic cup, micro slips are detected (see Fig. 81). Immediately, the grasp force is increased and a noticeable movement of the cup is prevented.

Due to the excessive slip events, the resulting grasp force may be above the optimal value. Hence, the grasp force is successively decreased until yet another slip event is noted. Now, the final grasp force can be determined by adding a safety margin onto the force value at which the slippage had occurred.

Albeit no quantitative study has been done as this has already been conducted with the slip detection algorithm, the result is a qualitatively well operating system that has shown to be able to adapt to different objects, i.e. no degradations in performance has been noted on different sizes, friction coefficients and contact areas.

All task were run on a single PC (Intel Xeon E5530 CPU, 6 [Gb] Memory)

THANKS TO THE EFFICIENT IMPLEMENTATION of the OpenKC-framework, the real-time path planning and trajectory components it was possible to do real-time control of both arms, both sensors and calculation of the fast fourier transforms on a single PC, which greatly helped to reduce the complexity of the system. The cycle time of the robots was 2 [ms], tactile data was received and processed, including slip detection, at 1.8 [kHz]. The visualization, as can be seen in Figure 80 also ran on the same computer in a low priority thread at approximately 70 [Hz].

Discussion

Different aspects to dynamical tactile sensing with a high-speed static tactile sensor were analyzed. Even though the detection of incipient slip has been the focus of previous work by a number of authors, this approach here is unique as it uses strictly static sensor data. In addition, the manner of getting training data for the neural classification architecture is with that respect novel. The advantage of this method is, that controlled systems like robotic end-effectors are themselves not free from vibrations that emerge from the joint controllers, which may manifest, due to leakage and aliasing effects, in different frequencies. For a window size of 1,800 samples, a peak at approximately 190 [Hz] can be noted due to the vibrations at the end-effector.

This vibration is part of the input to the neural network and is therefore learned and hence filtered out respectively. The different materials and different speeds further add to a good generalization behavior. The extensive study which investigated the space of parameters very thoroughly yielded very stable and reasonable results. The experiments in a setup for grasp force adaption showed that the approach is real-time capable and has a high impact area of application.

Important conclusions can be drawn from the results of the material texture classification. The processing of the gathered data or the data itself do not seem to be sufficient for the aspired task. Since the features are clearly far beyond the spatial resolution of the sensor, the task itself is ambitious. The vibrations that are hoped to be characteristic for each material turn out to be very similar. Probable reasons for this are:

I. The frequency damping of the piezo-resistive foam which has a verifiable low-pass filter function. It can be assumed that medium to high frequencies may be very specific for the different materials, especially for the very structured surfaces like the mousepad.

II. The random structure of the foam will also randomize the exerted vibrations, i.e. the vibrations are not only dependent on the texture of the probed material but also on the parts of the sensor that happen to be in contact with the object. Having

structured ridges therefore might improve the performance significantly, if the movement is perpendicular to the ridges.

III. Due to the control structure which comprises a real-time force control algorithm and the potential based path planning, a movement with uniform velocity is difficult to accomplish. Results would have been better if more uniform movements would have been possible. Admittedly this would have had an impact on the generalization and applicability of the results.

IV. The spatial resolution of the sensor is - compared to human performance - quite low. It can therefore not be expected that a level in the magnitude of human recognition can be accomplished.

The latest aspect should be further investigated by a new experiment with surface textures that differentiate on a coarser level.

Part V

Haptic Handling of Deformable Material

Still today, most robotic applications are limited to rigid objects. This poses a significant constriction on possible areas of application. Humans are permanently working with all kinds of deformable material like cloth, strings, food and paper, or in the very extreme case, liquids. If it is the goal to have robots really enter the human workspace, for example in service robotics, then those robots must be able to deal with different hardness of objects. This also poses new challenges to the intern representation of objects, since a piece of paper remains the same object, although it may assume quite different shapes and appearances. This calls for a high degree of sensors and a good strategy for sensor fusion. While the operation of tactile sensors is still not very common in robotic applications and research, tactile sensing is often being used in addition to well known and established input channels like (3-D) vision, laser scanners or time-of-flight cameras [186, 362]. It is not uncommon to reduce the application of the tactile sensors to report the success of a previously calculated grasp. This is a reduction to a simple binary information (object in hand or not) and does not reflect the complex data that are to be gained from tactile sensing.

While there are without dispute interaction tasks where tactile sensors can be substituted by other modalities, tactile sensing is virtually indispensable when deformable objects come into play. It shall be mentioned, that in the presented experiments, we are aiming towards truly deformable (viscoelastic, rheological) materials, as opposed to anelastic material like a sponge. It shall be mentioned that the field of Rheology is concerned with the flow and deformation behavior of materials. It is out of the scope of this document to give a thorough aggregation though.

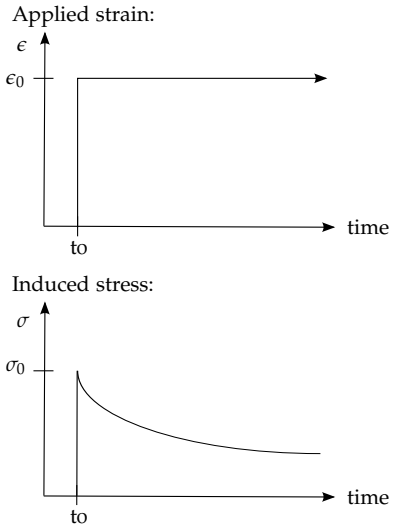

Figure 82: Schematic drawing of a viscoelastic material when strain is applied. The nonlinear change in the stress result from a deformation of the material.

Theoretic Background

Generally, viscoelasticity is described as either being linear or non-linear. For small deformations the linear viscoelasticity applies and can be described by this function:

$$\epsilon(t) = \frac{\sigma(t)}{E_{\text{inst,creep}}} + \int_0^t K(t-t')\dot{\sigma}(t')dt'$$

where:

- t is time
- $\sigma(t)$ is stress
- $\epsilon(t)$ is strain
- $E_{\text{inst,creep}}$ is the elasic modul for creep and relaxation, thus a material dependent parameter
- $K(t)$ is the creep function[53]

The nonlinear type of viscoelasticity is found at large deformations or especially, when the material changes its properties under deformations. Several models of the behavior of viscoelastic material exist and shall be briefly introduced:

Maxwell model The Maxwell model is constructed of a purely viscous damper and a purely elastic spring and can be described by the following equation:

$$\frac{d\epsilon_{Total}}{dt} = \frac{d\epsilon_D}{dt} + \frac{d\epsilon_S}{dt} = \frac{\sigma(t)}{\eta} + \frac{1}{\mathrm{E}}\frac{d\sigma}{dt}$$

The model seems especially well suited to metals and polymers close to their melting point. An extension to the model is the Maxwell–Wiechert model, which puts an arbitrary number of Maxwell models (i.e. spring-damper in series) in parallel to a spring. This allows a more fine grained simulation of viscoelastic behavior.

Kelvin–Voigt model The Kelvin-Voigt model is suited to describe the creep response in polymers. The relation is composed of a

[53] There are several functions for creep, the general creep equation denotes to $\frac{d\varepsilon}{dt} = \frac{C\sigma^m}{d^b}e^{\frac{-Q}{kT}}$, with C being a material dependent constant, m and b are dependent on the creep mechanism, Q denotes the activation energy, d is the grain size, k is the Boltzmann's constant, while T denotes the absolute temperature

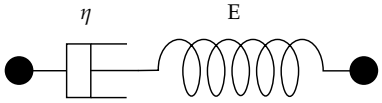

Figure 83: Schematic drawing of the Maxwell model composed of a damper and a spring.

damper and a spring in parallel and can be expressed as a linear first-order differential equation:

$$\sigma(t) = \mathrm{E}\epsilon(t) + \eta\frac{d\epsilon(t)}{dt}$$

This model has its strength in anelastic materials, i.e. when the process of deformation is reversed, when the stress is removed. It is therefore well suited for materials like rubber.

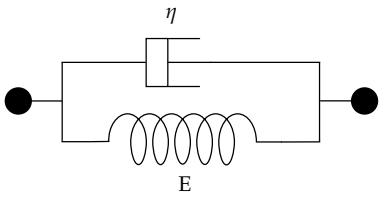

Figure 84: In the Kelvin-Voigt model, a damper and a spring a placed in parallel.

Standard linear solid model This model is the simplest model that somewhat overcomes the greatest shortcomings of the Maxwell and the Kelvin-Voigt model (i.e. regarding creep and stress relaxation). For that purpose, a spring and a spring-damper are placed in parallel:

$$\frac{d\epsilon}{dt} = \frac{\frac{\mathrm{E}_1}{\eta}\left(\frac{\eta}{\mathrm{E}_1}\frac{d\sigma}{dt} + \sigma(t) - \mathrm{E}_2\epsilon(t)\right)}{\mathrm{E}_1 + \mathrm{E}_2}$$

Amongst other things, the number of parameters make it difficult to calculate, although its results are more accurate than the previous mentioned models.

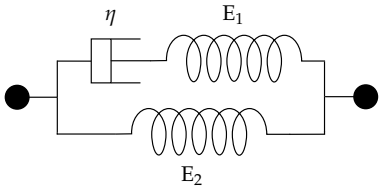

Figure 85: The Standard linear solid model offers a spring and a spring-damper in parallel for a higher model accuracy at the cost of a more complicated calculation.

IT IS VITAL TO MANY TASKS to identify the intrinsic properties of the material of the object that has to be handled or maybe deformed in a goal-directed manner. To be able to apply one of the afore mentioned models, for example, one has to find out which model suits best the material at hand as well as determine the parameters of the model as accurate as possible. As a step towards this goal, in the following, an apace and simple approach to determine the character of the material (rigid, (an-)elastic or deformable) is presented. Also, an algorithm to perform a directed deformation of plasticine is presented and qualitatively evaluated. Both task are done in a bi-manual robot setup with a high frequency tactile sensor pad mounted on each robot manipulator.

Related Work

Handling of deformable materials is a rather sparsely populated area in the current research, especially within the robotic community. One branch in the area of computer graphics is working on modeling deformable material, mostly soft tissue like the liver, to provide simulation environments for example for surgical training applications. Sometimes, accuracy is sacrificed to just realistic/plausible behavior. In the robotic context, and therefore working with real objects, some achievements could be made.

Probing and haptic displaying of elastic material

A complete system for the probing and haptic simulation of elastic material has recently been implemented by Fong [82]. In this work, a custom implemented structured light approach is taken to get 3-D information about the object that is to be simulated. The object is probed by a PHANTOM 1.5, a 3 degree of freedom haptic device, that is also used to display the simulated object after the probing process. The PHANTOM is able to exert a defined force, but has no tactile sensing and therefore this device cannot be used to detect contact with the object. But for accurate modeling, this would be important. To achieve a most authentic simulation, the contact with the object is detected with the self-developed structured light 3-D vision system. Also slippage of the probe relative to the object is detected with visual cues, which seemingly yielded good results, but the use of an additional sensors would clearly have improved the quality of the acquired data. Nevertheless, from the measured data, a force field was constructed. The interpolation between the probed points was done with radial basis functions. This also allowed a real-time rendering of the data at 1 [ms].

In that line, but with partly more elaborate equipment, is [86] to be filed. The general idea - to use a robotic manipulator to probe the parameters for a model of the deformable object - is similar to [82]. Yet, a force sensor is used at the tip of a robotic arm. Instead of a custom structured light approach, an off the shelf time-of-flight 3-D camera is used. The point clouds are aligned using the Iterative Closest Point (ICP) algorithm [23, 292]. The major difference is the employed model. A Finite Element Method (FEM) is used for simulation of the object. With the number of vertices in the model of n, the global force displacement equation set to

$$f = \mathrm{K}(\mathrm{E}, v)q$$

where $f \in \mathbb{R}^{3n}$ is the internal force induced by the displacement $q \in \mathbb{R}^{3n}$ of the vertices of the tetrahedral mesh and the stiffness-matrix K, depending on the Young's modulus[54] E and the Poisson's ratio[55] v. A gradient decent on the error returned by the ICP of the probed and simulated object was used to estimate both the Young modulus and the Poisson's ratio. The approach was experimentally verified with three elastic objects (foam cube, plush teddy, inflated balloon).

On the refinement of the FEM simulation for rheological objects, recent progress could be made [378]. The finite elements were also used in a grasping experiment of planar objects with two robotic fingers [143]. This work, which presented some preliminary results, of course has to be extended to 3-D objects.

A more extensive paper deals with the parametrization of linear and non-linear shell theories for elastic objects [360, 359]. The theories are presented in detail and an experimental comparison is made. The non-linear model is according to the authors more suited for larger deformations that may occur during grasping.

In [366] a latency model is introduced which explains the time-dependent behavior of viscoelastic materials during grasping. Both theory and experiments are presented.

In [219] the focus lies on realistic haptic rendering of elastic material. Here, a non-linear spring-damper-restorer model is used. The primary goal is plausible behavior of elastic material in contact with a rigid object, and therefore to a lesser extend the accurate modeling of probed material.

NOT CLOSELY RELATED TO THE WORK HERE, BUT very interesting is recent progress in the handling of cloth [317, 243, 169, 15, 392, 14, 376, 339] as well as manipulating paper [11, 344, 343]. The mentioned work is on the one hand offering very advanced solutions to hard problems, are on the other hand seemingly very restricted to a narrow domain (e.g. special cloth, custom folding mechanism). This may be interpreted as a further indication on the novelty of the research in this area. Also the large number of different models and the experiments to parametrize them supports this presumption [366, 359, 94, 82, 399, 159, 361, 294, 219].

THE ROBOTIC DETERMINATION OF THE VISCOELASTIC AND PLASTIC elements in a over all four component model, which is then used to do a guided deformation of the previously unknown rheological object is the work probably most closely related to the one here [116]. Although no parametrization of a model is done in the work presented in the remainder of the chapter, also guided plastic deformation is done, even though on a much coarser scale.

[54] Young's modulus is the ratio of stress (pressure) to strain, i.e. $E = \frac{\sigma}{\epsilon}$

[55] Poisson's ratio describes the contraction of an isotropic linearly elastic material when stretched. The width change is defined to

$$v = \frac{L\Delta d}{d\Delta L}$$

with d being the thickness and $\frac{\Delta d}{d}$ the relative change in thickness

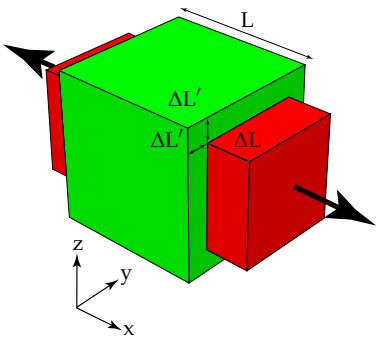

Figure 86: In this example, a cube with sides of length L is subject to tensile stress. The green cube represents the cube in without influence of external forces. The red cube is under tension and expands in x direction while contracting in y and z direction by ΔL.

Haptic Deformation of Plasticine

Experimental Setup

The tactile sensors used here are the myrmex sensors [311, 312], i.e. the same sensors as were used in part IV. The sensors show a remarkable first touch sensitivity and enable the sensing of static and dynamic touch through a high sampling rate of up to 1.8 [kHz] and are therefore well suited for the task at hand. The pad has a size of 8 x 8 [cm] and a resolution of 16 x 16 tactile elements. The pads are mounted on two 7 degrees-of-freedom Kuka/DLR lightweight robot arms. For end-effector position and orientation control we used an implementation of the control basis framework proposed by Grupen et. al. [133, 109] which allows the synthesis of closed loop controllers from simple components like sensor and effector transforms, artificial potentials and robot resources. Additionally it allows hierarchical composition of controllers by means of null space composition. This approach is very flexible and generalizes rapidly to a wide range of applications. The fusion of the kinesthetic sensors of the robot arm and the tactile sensor pads allow a very fast and precise control of the pressure applied to the object, which is vital for the exploration of deformable objects, as too much force would render exploratory movements useless. For more details on the hard- and software setup, please refer to part II.

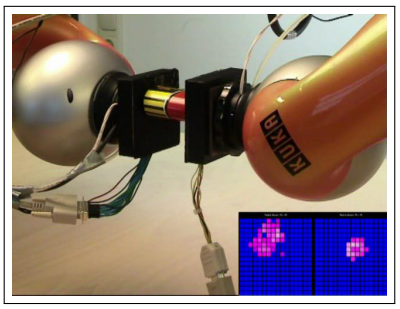

Figure 87: The Kuka/DLR LWR with the myrmex tactile sensors are testing the elasticity and plasticity of the object. The tactile data can also be seen.

A video showing the test procedure for elasticity and plasticity is enclosed on the attached storage device ("Material-Test").

Classification Hardness and Deformability

In a first experiment, the type elasticity and plasticity of the object is determined. The step response from applying a force to the object can easily be used to determine the plasticity (distance of the sensor pads before and after) and the elasticity (distance of the sensor pads when pressure is applied) of the material. To this end, the robots closes the end-effectors until a contact at the tactile sensing pads was registered. Once both arms have establish a contact to the object, the robots are switched from position control to force control mode. It is thus possible to apply a force to the object. A force of approximately 8 [N] was exerted. After one second of constant force, the robot is switched back to position control mode. A new position away from the objects center is commanded. The distance is one half of the distance between the point when

first contact was noted to the position at which the force was applied. The movement is driven very slowly, unless, of course, loss of contact impended, in which case the movement was halted.

With the results of the measurements, it was possible to train an artificial neural network that is able to distinguish solid, inelastic objects from elastic objects and also to determine if the material is showing plasticity or not. The network has been tested on previously unseen objects (cf. Fig. 88). The network has been trained before with solid objects, elastic foam and various plasticine that differed in regards to the elasticity and volume from the test set.

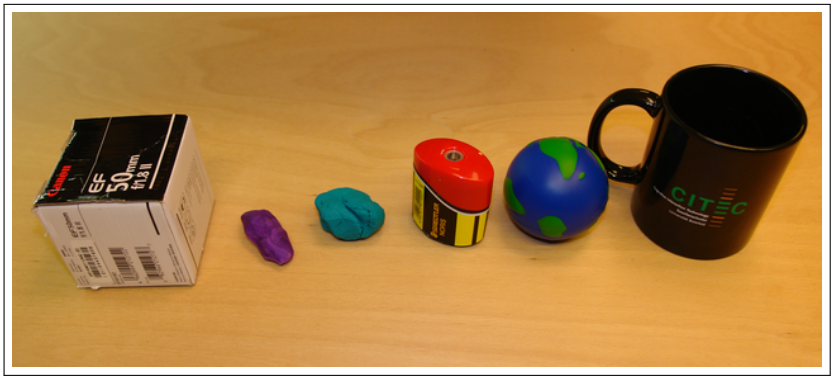

Figure 88: These objects were tested for elasticity and plasticity. From left to right, a solid cardboard box, a piece of plasticine, a piece of softer plasticine, a solid pencil sharpener, an elastic ball, a solid cup.

All objects were successfully classified using simple thresholds on the output of the neural network. A challenge still remains the handling of objects that will only permanently deform if a certain force threshold is exceeded (think of paper folds). If this threshold is not met in the material testing, this material property might be undiscovered. On the other hand, this applies to almost all objects: If to much pressure is applied, they will deform in some way or break.

Forming a Ball

THE GOAL-ORIENTED DEFORMATION OF PLASTICINE has many challenges. When humans take a piece of plasticine and form a ball, the geometry is usually acquired through vision. If the plasticine has an elongation, it is often the starting point of the kneading process. The palms of the hands are ideal for the deformation, one hand is generally used as supporting area. The palms are flexible, so a little cavity is formed to both avoid the rolling out of hands and to improve the shaping of the plasticine.

THE ROBOT GENERALLY LACKS MUCH OF THE DEXTERITY of a human hand. In our case, not even a vision system was used to get the initial geometry of the material. The only tool used is a tactile sensor with a plane surface. Therefore, the risk of the plasticine to roll away is much higher than in a human hand. Even if the plasticine does not completely roll off the tactile sensor, it might not be

Challenges:

- Unknown geometry
- Grasp force critical
- Friction unknown
- Static tool

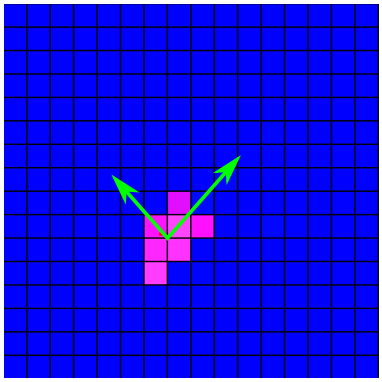

Figure 89: A tactile sensor image and the two principal axis of the 2-D distribution.

possible to continue the process of deforming, e.g. in case of a very flat object. This has also an impact on the strategy of deforming. If the robot was to use one tactile pad as a supporting plane, the risk for the object to fall down is much higher than the potential gain from a probably easier configuration regarding gravity. We therefore follow the idea of using the tactile pads perpendicular with regard to the gravitational pull, hence the precise control of the grasp force is important. Unintentional deformations and object slippage is to be avoided.

The ability to roll the plasticine object (and manipulability in this sense) is tested because if the object is in a position that rolling is impossible, a re-grasp has to be initiated. To this end, the object is carefully moved in the directions of the two principal axis of the sensor image (cf. Fig. 89). If the object is not roll-able, which can easily be verified by the tactile data, a re-grasp is necessary. In this case, the friction between the object and the sensor pad is just not sufficient to explore the object thoroughly. We have been investigating strategies to turn the plasticine, which under certain circumstances might be usable (cf. Fig. 90).

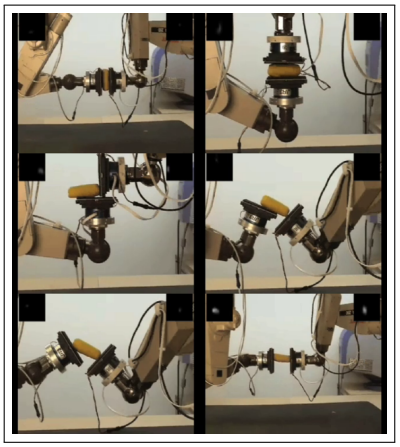

Figure 90: A possibility for a re-grasp if the object is in a position such that the goal-oriented deformation is not possible.

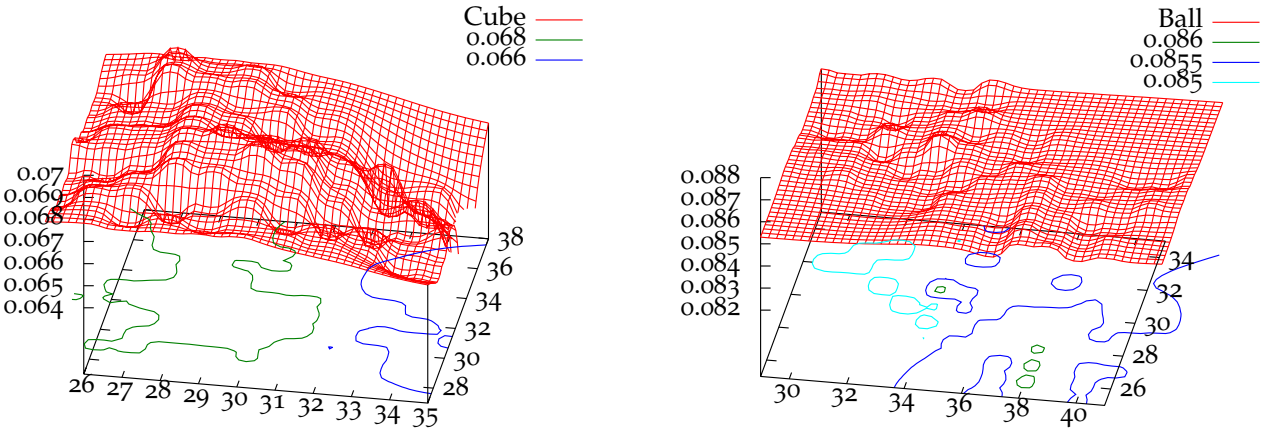

Figure 91: Two grid patterns that emerged from an exploratory movement of two different plasticine objects. On the left side, a cube is explored, on the right side, the process of deforming is almost finished. Please note, the different scales in the plots.

If the object, however, moves as expected, the exploration is started. During exploration, a map of the objects is build up. The map is a 2-D projection of the surface in a grid pattern with a grid size of 1.5 [mm]. To every node of the grid, the diameter of the object is measured, hence a 3-D map is build up little by little. For the purpose of measuring the diameter, a constant pressure has to be maintained when the object is rolled to different positions. The distance of the tactile pads is then assumed to be the objects' diameter.

The path planning through the grid follows a greedy strategy, i.e. the exploration is directed towards unknown areas and into the direction of the largest measured elongation. To reach the goal of forming a ball, prominent edges are thus searched and, when found, eventually gently kneaded away using a spiral movement of the pads. Two examples of such a grid pattern – a cube and a ball – can be seen in Figure 91.

A video of the goal-directed deforming of plasticine is enclosed ("Deforming").

During the kneading, the previously acquired data of the geometry of the object becomes invalid due to the constant, creeping deformation of the plasticine. Therefore, the explored data becomes void after a certain time has passed, i.e. the algorithm is actively forgetting older data. If the explored surface of the object has reached a uniform diameter and the seen and remembered surface area is larger than 60 % of the assumed surface size[56], the task is considered completed.

[56] $A = 4\pi r^2$, r is inferred from the distance of the tactile pads

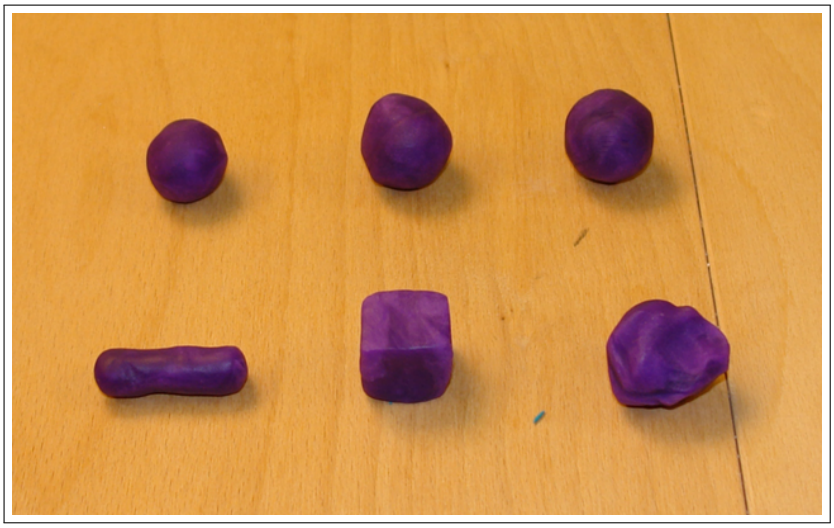

Figure 92: In the top row the results from plasticine objects like those in the bottom row are shown after the goal-oriented deforming into a ball.

The validity of this approach is shown only qualitatively. A number of different starting shapes have been used, some of them are shown in Figure 92. The results, also shown in the same figure, look quite promising.

Important for all described tasks is the very precise control of the applied pressure. Through a combination of the internal sensing of the Kuka/DLR LWR and the tactile sensors, this control could be managed through a PD-controller. Because of the small size of the plasticine, very low derivations in the applied force can either lead to an unwanted deformation or, on the contrary, the object may be dropped. To avoid this, the movement speed has been limited. This, however, leads to quite long processing times. An average object takes approximately 20 minutes to finish. A picture sequence of the deforming is shown in Figure 93.

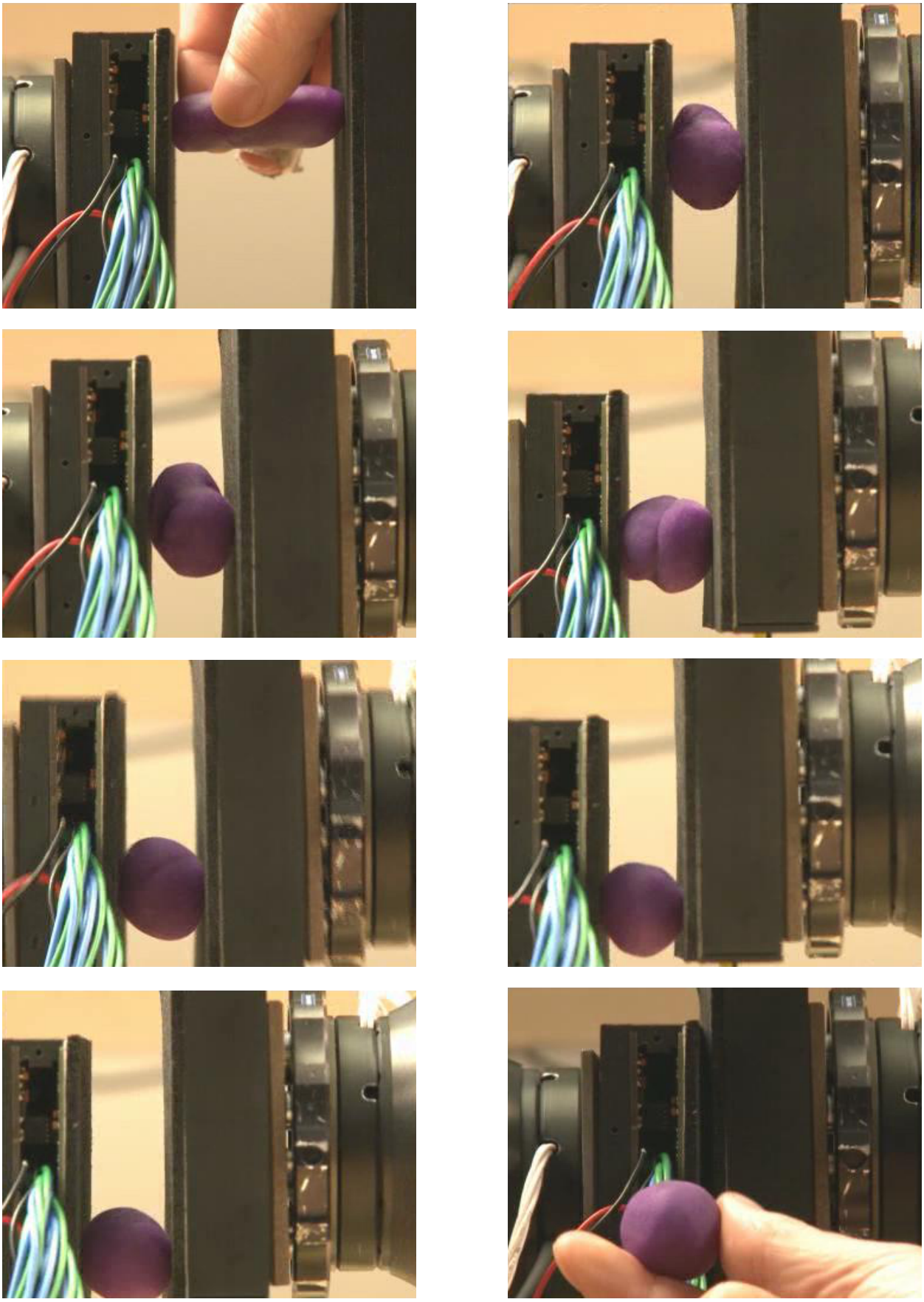

Figure 93: From left to right and top to bottom the goal-oriented deformation of a cylindrical object into a ball.

Discussion

The novelty of the research question and the complexity of the problem requires the floating of trail balloons to get an impression of the magnitude of the expected and unexpected difficulties. Although the term might suggest otherwise, the engineering problems associated with any experiment with deformable material are considerable. In our case, this investigation would not have been possible without sensitive, high-speed tactile sensors, real-time trajectory planning and the availability of the frameworks developed for and mentioned throughout this thesis.

Much of the theoretic background mentioned here and the recently developed models have been neglected in the presented experiments. The reasons to do so are:

I. The complexity of the models. The more precise a model is, the number of parameters increases. Automatic parametrization is yet out of reach.

II. While the 1-D behavior of a elastic of plastic object can be described quite well, the approach to 3-D objects is yet extremely difficult, not only because the internal state of a 3-D object is usually unknown. Learning and probabilistic methods may improve the results obtained so far.

III. From a biological standpoint, the extensive use of complex models seems to miss the mark. A simple, adaptive feedback mechanism might prove to be more powerful than overly complex modeling.

IV. Having a model is only half way to handling deformable material. It does not answer the question how the material has to be handled to reach a desired goal.

A quantitative study is missing for a number of reasons. For one, ground truth data for a good quantization is rather hard to obtain. Then, the presented work is meant to be a jump start for further, more extensive research in that direction. It serves also as a proof-of-concept, hence this study has a strong exploratory character. The results, albeit qualitative, comprise a significant scientific innovation in the field of tactile guided robotics.

Part VI

Conclusion

Concluding Remarks

The core of this thesis deals with the processing of artificial tactile signals in a robotic context. The subject is approached from different directions, covering several aspects of tactile and haptic perception and exploiting the potential of the tactile sensing hardware that is available to researchers today. Also, beyond that, prospects of what can be expected to come in the future we postulated. Human tactile sensing is used for grasping, manipulation and recognition, and indeed facilitates learning and understanding. The sense of touch, unlike hearing or sight, cannot easily be suspended, for example by closing the eyes. It is therefore hard to imagine a world without tactile sensation. It may be because of this, that tactile perception has long been underappreciated. Recent and important result regarding human tactile perception were therefore presented in this thesis and are an important pillar for directing research in artificial tactile sensing.

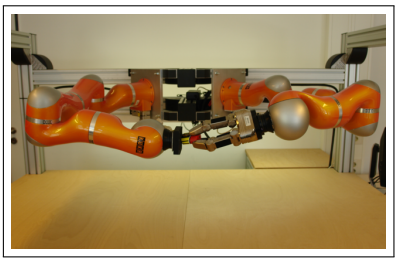

Figure 94: Major hardware components for which the framework was developed for. The tactile sensing devices, a myrmex sensor and a SDH-2 hand, are mounted on the end-effector of two Kuka/DLR LWR.

While researching tactile robotics, new possibilities emerged with new robotic hardware[57] that had become available in our working group. This allowed the possibility to look in new and very interesting directions of research, but at the price of integrating new hardware and developing methods to take advantage of the available features. A framework for tactile robotics research originated from this pursuit for optimal hardware utilization. Important building blocks have consequently been reported in Part II and will hopefully serve as a basis for further research. Specifically, a software library for the acquisition of data from three different types of tactile sensors with a unified API was written. Real-time buffering and recording, as well as formats for writing and reading tactile data complete this package.

In addition, an open source software framework for the control of the Kuka/DLR LWR facilitating two different interfaces, RSI-XML and FRI, was implemented, tested and evaluated. For path planning, a realization[58] of the control basis framework was used. For real-time trajectory planning a method for limiting velocity, acceleration and jerk in real-time was presented and evaluated. This framework allows sensor guided motions, which is the building block for all of the presented research here.

Implementation of Software for convenient real-time tactile data acquisition, robot control and trajectory jerk limitation

[57] New Hardware:

- Myrmex tactile sensor
- Kuka/DLR LWR
- Schunk SDH-2

[58] written by Florian Schmidt

TACTILE OBJECT RECOGNITION HAS been the subject of many publications in the past and the potential of tactile sensing has already been proven to a reasonable degree. Hence, one could argue that further research in this direction is not warranted. However, we were able to present two novel approaches that emphasize aspects that have so far been neglected in tactile object recognition. Both methods penetrate into uncovered slots in tactile research and address questions beyond the original recognition task. To this end, the first presented architecture aims to reveal the relevant structures of tactile data. With higher data rates and resolutions, efficient representations and key features of tactile patterns have to be identified. Classification based on the information gain of a broad range of tactile features gives insights and hints for future tactile processing, although further investigation in different settings may be appropriate for final conclusions in this matter. Even so, the extensive analysis in the first half of part III provides more than just a solid basis for additional work in this promising direction to a thus far not completely answered question.

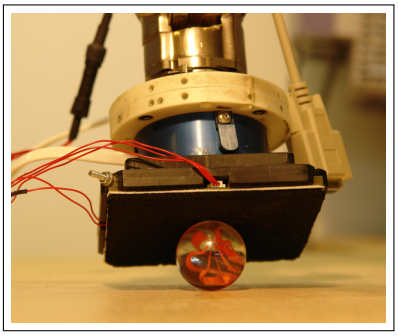

Figure 95: Closeup of the robots end-effector during tactile probing of a marble.

A COMPLETELY DIFFERENT APPROACH to object recognition is presented in the second half of part III. Here, a Kalman filter is used to consolidate and aggregate haptic input into object representations. The proposed method was shown to be robust, memory and computational efficient and integrates well with other modalities, i.e. any 3-D point cloud can easily be fused and altered with haptically acquired data facilitating the presented findings. The validity of the method, which in the main was elaborated upon Martin Meier's diploma thesis [233], has been verified in an experiment carried out on the Schunk Dexterous Hand 2, which is equipped with tactile sensors. To this end, a tactile based grasping algorithm was developed and used for a pick and place task in order to make tactile scans of arbitrary objects. To quantify the quality of the acquired and processed data, an object recognition task was decided upon. The proposed method facilitates the iterative closest point algorithm and displayed excellent classification results and a very good run-time behavior that allows real-time classification of objects.

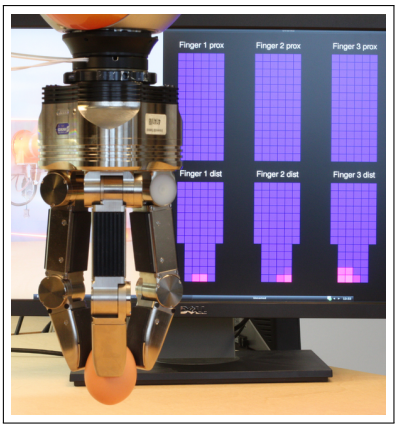

Figure 96: The tactile based grasping algorithm is, amongst other purposes, able to handle fragile objects without detailed object shape information.

AFTER STATIC TACTILE DATA PROCESSING IN PART III, the analysis of dynamic tactile data was the subject of part IV. Static, yet high-speed, tactile sensors were used to detect and process highly dynamic events like incipient slip, i.e. the beginning of slippage. For this purpose, different objects were probed with a tactile sensor, which was mounted to the robot's end-effector. This way, data samples for both stick and slip conditions could be gathered and were used to train an artificial neural network. Due to the high temporal resolution of the tactile sensors, the gathered data was converted to the frequency domain in a preprocessing step. The approach was showen to work very reliably and generalized well among the

different surfaces used for training and testing.

As an application for incipient slip detection, a simple, yet effective algorithm for optimal grasp force adaption was proposed and implemented. In an experiment, a container was filled while the robot automatically adjusts the grasp force to the novel weight condition. The automatic adaption of the grasp force to unknown objects and physical conditions has numerous applications in grasping and pick and place tasks, especially in domains which deal with intrinsically irregular objects like for example agricultural products.

The frontiers of dynamic sensing with static sensors to characterize various materials was also explored. The detection of fine surface features like the texture of materials could only be roughly approximated. While very smooth and plain surfaces could be distinguished from very rough and sticky, whereas the discrimination of intermediate textures could not be done to a satisfactory degree. Probable reasons include the sensor material, which does not only damp higher frequencies, but due to the random structure of the material will not generate typical frequency footprints.

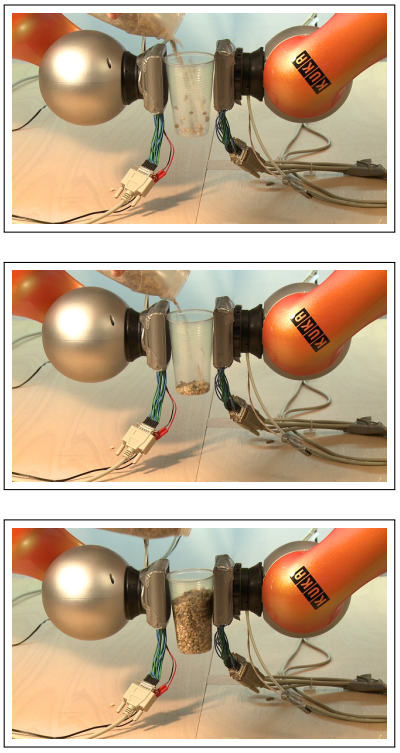

Figure 97: Grasp force adaption in a dynamic loading situation.

Finally, in part V a most intriguing facet of tactile robotics was addressed: the handling of deformable material. Deformable objects open up new dimensions (e.g. elasticity, plasticity) which have to be explored and mastered. As a matter of fact, a single ductile object may span a greater configuration variety in terms of position, forms and folds, than a large set of rigid objects. Since there are no agreed general approaches to handling of deformable material, we started by a explorative rather than quantitative study. In a small experiment, different objects were probed for their rheological behavior, i.e. deformable, soft or inherently stable. In addition, the target-oriented deformation of plasticine was shown. Different geometric forms were successfully converted into a sphere by the robot. Despire the difficult feedback control task accomplished here, a holistic theory is still lacking and should be the focus of further research.

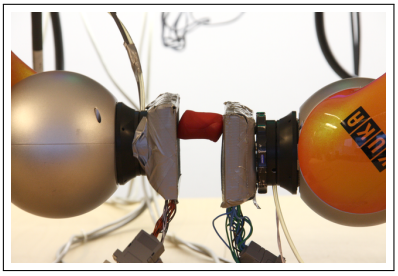

Figure 98: A piece of plasticine of unknown shape is presented to the robots tactile sensors. It is explored and converted to a sphere.

A main conclusion of this thesis is the finding that there is an absolute need for tactile sensing for robots in unstructured environments. Apart from being biologically motivated, the necessity of tactile sensing during tasks like grasping, dexterous manipulation and, an aspect not covered here, safety in human-robot interaction, is underpinned by this work. The application of tactile sensing was shown in object recognition, grasping and manipulation tasks.

As better sensing devices become available in the future, restrictions encountered during this thesis will disappear and tactile sensing will become as common as camera devices are today, and indeed fully equipped tactile robots may soon become standard.

Bibliography

[1] A. Ababou, N. Ababou, S. Chadli, and R. Dabou. Accuracy improvement of large area flexible piezoresistive digital tactile array sensing system. In *2008 IEEE Sensors*, pages 1048–1051. IEEE, Oct. 2008. doi:10.1109/ICSENS.2008.4716623.

[2] D. Accoto, F. Damiani, R. Sahai, D. Campolo, E. Guglielmelli, and P. Dario. A thermal slip sensor for biorobotic applications. In *Proceedings 2007 IEEE International Conference on Robotics and Automation*, number April, pages 1523–1528. IEEE, Apr. 2007. doi:10.1109/ROBOT.2007.363540.

[3] R. Ahmadi, J. Dargahi, M. Packirisamy, and R. Cecere. A new hybrid catheter-tip tactile sensor with relative hardness measuring capability for use in catheter-based heart surgery. In *2010 IEEE Sensors*, pages 1592–1595. IEEE, Nov. 2010. doi:10.1109/ICSENS.2010.5690287.

[4] A. Albu-Schäffer and G. Hirzinger. Parameter Identification and Passivity Based Joint Control for a 7DOF Torque Controlled Light Weight Robot. In *Proc. IEEE Int'l Conf. on Robotics and Automation 2001*, pages 2852–2858, 2001.

[5] P. K. Allen. *Robotic Object Recognition Using Vision and Touch*. Springer Berlin / Heidelberg, Berlin, 1987.

[6] P. K. Allen and P. Michelman. Acquisition and interpretation of 3-d sensor data from touch. *IEEE Trans. on Robotics and Automation*, 6(4):397–404, 1990.

[7] P. K. Allen and K. Roberts. Haptic object recognition using a multi-fingered dextrous hand. In *Proceedings, 1989 International Conference on Robotics and Automation*, pages 342–347. IEEE Comput. Soc. Press, 1989. doi:10.1109/ROBOT.1989.100011.

[8] E. L. Amazeen and M. T. Turvey. Weight perception and the haptic size-weight illusion are functions of the inertia tensor. *Journal of experimental psychology. Human perception and performance*, 22(1):213–32, Feb. 1996.

[9] A. Ataollahi, P. Polygerinos, P. Puangmali, L. D. Seneviratne, and K. A. Althoefer. Tactile sensor array using prismatic-tip optical fibers for dexterous robotic hands. In *2010 IEEE/RSJ International Conference on Intelligent Robots and Systems*, pages 910–915. IEEE, Oct. 2010. doi:10.1109/IROS.2010.5649109.

[10] R. Bajcsy and F. Solina. Three Dimensional Object Representations Revisited. In *First International Conference on Computer Vision*, pages 231–240, London, England, 1987.

[11] D. J. Balkcom and M. T. Mason. Robotic origami folding. *The International Journal of Robotics Research*, 27(5):613–627, May 2008. doi:10.1177/0278364908090235.

[12] A. Barr. Superquadrics and Angle-Preserving Transformations. *IEEE Computer Graphics and Applications*, 1(1):11–23, Jan. 1981. doi:10.1109/MCG.1981.1673799.

[13] Y. Bekiroglu, K. Huebner, and D. Kragic. Integrating grasp planning with online stability assessment using tactile sensing. In *2011 IEEE International Conference on Robotics and Automation*, pages 4750–4755. IEEE, May 2011. doi:10.1109/ICRA.2011.5980049.

[14] M. Bell and D. J. Balkcom. Knot tying with single piece fixtures. In *2008 IEEE International Conference on Robotics and Automation*, pages 379–384. Ieee, May 2008. doi:10.1109/ROBOT.2008.4543237.

[15] M. Bell and D. J. Balkcom. Grasping Non-stretchable Cloth Polygons. *The International Journal of Robotics Research*, 29(6):775–784, Aug. 2009. doi:10.1177/0278364909344634.

[16] S. J. Bensmaïa, J. C. Craig, and K. O. Johnson. Temporal factors in tactile spatial acuity: evidence for RA interference in fine spatial processing. *Journal of neurophysiology*, 95(3):1783–91, Mar. 2006. doi:10.1152/jn.00878.2005.

[17] S. J. Bensmaïa, J. C. Craig, T. Yoshioka, and K. O. Johnson. SA1 and RA afferent responses to static and vibrating gratings. *Journal of neurophysiology*, 95(3):1771–82, Mar. 2006. doi:10.1152/jn.00877.2005.

[18] S. J. Bensmaïa and M. Hollins. The vibrations of texture. *Somatosensory & motor research*, 20(1):33–43, Jan. 2003. doi:10.1080/0899022031000083825.

[19] S. J. Bensmaïa and M. Hollins. Pacinian representations of fine surface texture. *Perception & psychophysics*, 67(5):842–54, July 2005.

[20] S. J. Bensmaïa, M. Hollins, and J. Yau. Vibrotactile intensity and frequency information in the pacinian system: a psychophysical model. *Perception & psychophysics*, 67(5):828–41, July 2005.

[21] J. L. Bentley. Multidimensional binary search trees used for associative searching. *Communications of the ACM*, 18(9):509–517, Sept. 1975. doi:10.1145/361002.361007.

[22] K. Bernardin, K. Ogawara, K. Ikeuchi, and R. Dillmann. A sensor fusion approach for recognizing continuous human grasping sequences using hidden Markov models. *IEEE Transactions on Robotics*, 21(1):47–57, Feb. 2005. doi:10.1109/TRO.2004.833816.

[23] P. J. Besl and N. D. McKay. A method for registration of 3-D shapes. *IEEE Transactions on pattern analysis and machine intelligence*, pages 239–256, 1992.

[24] A. Bicchi and V. Kumar. Robotic grasping and contact: A review. In *Proceedings of the IEEE International Conference on Robotics and Automation*, 2000.

[25] A. Bicchi, K. J. Salisbury, and D. Brock. *Experimental evaluation of friction characteristics with an articulated robotic hand*, pages 153–167. Springer Berlin / Heidelberg, 1993. doi:10.1007/BFb0036137.

[26] A. Bierbaum, K. Welke, D. Burger, T. Asfour, and R. Dillmann. Haptic exploration for 3D shape reconstruction using five-finger hands. In *2007 7th IEEE-RAS International Conference on Humanoid Robots*, pages 616–621. IEEE, Nov. 2007. doi:10.1109/ICHR.2007.4813935.

[27] A. E. Bigelow. Children's tactile identification of miniaturized common objects. *Developmental Psychology*, 17(1):111–114, 1981. doi:10.1037/0012-1649.17.1.111.

[28] R. Black, K. Chau, B. Moslehi, and M. R. Cutkosky. Exoskeletal Force-Sensing End-Effectors With Embedded Optical Fiber-Bragg-Grating Sensors. *IEEE Transactions on Robotics*, 25(6):1319–1331, Dec. 2009. doi:10.1109/TRO.2009.2032965.

[29] S. J. Bolanowski, G. A. Gescheider, R. T. Verrillo, and C. M. Checkosky. Four channels mediate the mechanical aspects of touch. *The Journal of the Acoustical Society of America*, 84(5):1680–94, Nov. 1988.

[30] G. M. Bone, A. Lambert, and M. Edwards. Automated modeling and robotic grasping of unknown three-dimensional objects. In *2008 IEEE International Conference on Robotics and Automation*, pages 292–298. Ieee, May 2008. doi:10.1109/ROBOT.2008.4543223.

[31] R. M. Bracewell, A. S. Wimperis, and A. M. Wing. *Brain Mechanism of Haptic Perception*, chapter Psychophys, pages 25–37. Springer Berlin / Heidelberg, Berlin, Heidelberg, 2008.

[32] H. Bruyninckx. Open robot control software: the OROCOS project. In *Proceedings 2001 ICRA. IEEE International Conference on Robotics and Automation (Cat. No.01CH37164)*, pages 2523–2528. IEEE, 2001. doi:10.1109/ROBOT.2001.933002.

[33] M. Buss, H. Hashimoto, and J. B. Moore. Dextrous hand grasping force optimization. *IEEE Transactions on Robotics and Automation*, 12(3):406–418, 1996. doi:10.1109/70.499823.

[34] G. Canepa, M. Campanella, and D. De Rossi. Slip detection by a tactile neural network. In *Proceedings of IEEE/RSJ International Conference on Intelligent Robots and Systems (IROS'94)*, volume 1, pages 224–231. IEEE, 1994. doi:10.1109/IROS.1994.407387.

[35] G. Canepa, R. Petrigliano, M. Campanella, and D. De Rossi. Detection of incipient object slippage by skin-like sensing and neural network processing. *IEEE transactions on systems, man, and cybernetics. Part B, Cybernetics : a publication of the IEEE Systems, Man, and Cybernetics Society*, 28(3):348–56, Jan. 1998. doi:10.1109/3477.678629.

[36] G. Cannata and M. Maggiali. Processing of an Embedded Tactile Matrix Sensor. In *2006 IEEE International Conference on Robotics and Biomimetics*, pages 170–175. IEEE, 2006. doi:10.1109/ROBIO.2006.340353.

[37] G. Cannata, M. Maggiali, G. Metta, and G. Sandini. An embedded artificial skin for humanoid robots. In *2008 IEEE International Conference on Multisensor Fusion and Integration for Intelligent Systems*, pages 434–438. IEEE, Aug. 2008. doi:10.1109/MFI.2008.4648033.

[38] C. J. Cascio and K. Sathian. Temporal cues contribute to tactile perception of roughness. *The Journal of neuroscience : the official journal of the Society for Neuroscience*, 21(14):5289–96, July 2001.

[39] S. Caselli, C. Magnanini, and F. Zanichelli. Haptic object recognition with a dextrous hand based on volumetric shape representations. In *Proceedings of 1994 IEEE International Conference on MFI '94. Multisensor Fusion and Integration for Intelligent Systems*, pages 280–287. IEEE, 1994. doi:10.1109/MFI.1994.398442.

[40] S. Caselli, C. Magnanini, and F. Zanichelli. Investigation of polyhedral shape representations and connectionist techniques in haptic object recognition. In *Proceedings of IEEE/RSJ International Conference on Intelligent Robots and Systems (IROS'94)*, pages 232–239. IEEE, 1994. doi:10.1109/IROS.1994.407386.

[41] S. Casselli, C. Magnanini, and F. Zanichelli. On the robustness of haptic object recognition based on polyhedral shape representations. In *Proceedings 1995 IEEE/RSJ International Conference on Intelligent Robots and Systems. Human Robot Interaction and Cooperative Robots*, pages 200–206. IEEE Comput. Soc. Press, 1995. doi:10.1109/IROS.1995.526160.

[42] F. Castelli. An integrated tactile-thermal robot sensor with capacitive tactile array. *IEEE Transactions on Industry Applications*, 38(1):85–90, 2002. doi:10.1109/28.980361.

[43] N. N. Chen and R. Rink. Touch-driven robot control using a tactile Jacobian. In *Proceedings of International Conference on Robotics and Automation*, number April, pages 1737–1742. IEEE, 1997. doi:10.1109/ROBOT.1997.614400.

[44] M.-Y. Cheng, B.-T. Liao, X.-H. Huang, and Y.-J. Yang. A flexible tactile sensing array based on novel capacitance mechanism. In *TRANSDUCERS 2009 - 2009 International Solid-State Sensors, Actuators and Microsystems Conference*, pages 2182–2185. IEEE, June 2009. doi:10.1109/SENSOR.2009.5285609.

[45] M.-Y. Cheng, C.-L. Lin, and Y.-J. Yang. Tactile and shear stress sensing array using capacitive mechanisms with floating electrodes. In *2010 IEEE 23rd International Conference on Micro Electro Mechanical Systems (MEMS)*, volume 2, pages 228–231. IEEE, Jan. 2010. doi:10.1109/MEMSYS.2010.5442525.

[46] S. Chitta, M. Piccoli, and J. Sturm. Tactile object class and internal state recognition for mobile manipulation. In *2010 IEEE International Conference on Robotics and Automation*, pages 2342–2348. IEEE, May 2010. doi:10.1109/ROBOT.2010.5509923.

[47] B. Choi, S. Lee, H. Choi, and S. Kang. Development of Anthropomorphic Robot Hand with Tactile Sensor : SKKU Hand II. In *2006 IEEE/RSJ International Conference on Intelligent Robots and Systems*, pages 3779–3784. IEEE, Oct. 2006. doi:10.1109/IROS.2006.281763.

[48] B.-J. Choi, S.-C. Kang, and H.-R. Choi. Development of Tactile Sensor for Detecting Contact Force and Slip. In *2005 IEEE/RSJ International Conference on Intelligent Robots and Systems*, volume 30, pages 1977–1982. IEEE, Apr. 2005. doi:10.1109/IROS.2005.1545267.

[49] G. Chong. PID control system analysis, design, and technology. *IEEE Transactions on Control Systems Technology*, 13(4):559–576, July 2005. doi:10.1109/TCST.2005.847331.

[50] C. Chuang. 3D capacitive tactile sensor using DRIE micromachining. In *Proceedings of SPIE*, volume 5836, pages 719–726. SPIE, 2005. doi:10.1117/12.608621.

[51] C.-H. Chuang, C.-T. Lu, and T.-H. Fang. Slippage and direction sensing based on a flexible tactile sensor with structural electrodes. In *2009 IEEE Sensors*, pages 958–962. Ieee, Oct. 2009. doi:10.1109/ICSENS.2009.5398192.

[52] C. Cinel, G. W. Humphreys, and R. Poli. Cross-modal illusory conjunctions between vision and touch. *Journal of experimental psychology. Human perception and performance*, 28(5):1243–66, Oct. 2002. doi:10.1037/0096-1523.28.5.1243.

[53] S. C. Colbert, R. Alqasemi, and R. V. Dubey. Efficient Shape and Pose Recovery of Unknown Objects from Three Camera Views. In *Proceeding of the 7th International Symposium on Mechatronics and its Applications (ISMA10)*, page In Press, 2010. doi:10.

[54] T. R. Coles, D. Meglan, and N. W. John. The Role of Haptics in Medical Training Simulators: A Survey of the State-of-the-art. *IEEE Transactions on Haptics*, (June 2009):51–66, 2010. doi:10.1109/TOH.2010.19.

[55] T. Cooke, F. Jäkel, C. Wallraven, and H. H. Bülthoff. Multimodal similarity and categorization of novel, three-dimensional objects. *Neuropsychologia*, 45(3):484–95, Feb. 2007. doi:10.1016/j.neuropsychologia.2006.02.009.

[56] T. Cooke, C. Wallraven, and H. H. Bülthoff. Multidimensional scaling analysis of haptic exploratory procedures. *ACM Transactions on Applied Perception*, 7(1):1–17, Jan. 2010. doi:10.1145/1658349.1658356.

[57] C. Corcoran and R. Platt. A measurement model for tracking hand-object state during dexterous manipulation. In *2010 IEEE International Conference on Robotics and Automation*, pages 4302–4308. IEEE, May 2010. doi:10.1109/ROBOT.2010.5509194.

[58] D. P. J. Cotton, P. H. Chappell, A. Cranny, N. M. White, and S. P. Beeby. A Novel Thick-Film Piezoelectric Slip Sensor for a Prosthetic Hand. *IEEE Sensors Journal*, 7(5):752–761, May 2007. doi:10.1109/JSEN.2007.894912.

[59] D. P. J. Cotton, I. M. Graz, and S. P. Lacour. A Multifunctional Capacitive Sensor for Stretchable Electronic Skins. *IEEE Sensors Journal*, 9(12):2008–2009, Dec. 2009. doi:10.1109/JSEN.2009.2030709.

[60] T. M. Cover and J. A. Thomas. *Elements of information theory*. John Wiley & Sons, Inc., 2006.

[61] B. M. Cowie, D. J. Webb, B. Tam, P. Slack, and P. N. Brett. Fibre Bragg grating sensors for distributive tactile sensing. *Measurement Science and Technology*, 18(1):138–146, Jan. 2007. doi:10.1088/0957-0233/18/1/017.

[62] J. C. Craig. Grating orientation as a measure of tactile spatial acuity. *Somatosensory & motor research*, 16(3):197–206, Jan. 1999.

[63] M. R. Cutkosky. On grasp choice, grasp models, and the design of hands for manufacturing tasks. *IEEE Transactions on Robotics and Automation*, 5(3):269–279, June 1989. doi:10.1109/70.34763.

[64] M. R. Cutkosky, R. D. Howe, and W. R. Provancher. *Force and Tactile Sensing*, chapter 19.1, page 1611. Springer Berlin / Heidelberg, Berlin, Heidelberg, 2008.

[65] M. R. Cutkosky and J. M. Hyde. Manipulation Control with Dynamic Tactile Sensing. In *International Symposium on Robotics Research*, volume 8, pages 245–261, 1993.

[66] R. S. Dahiya, M. Valle, G. Metta, L. Lorenzelli, and C. Collini. Tactile sensing arrays for humanoid robots. In *2007 Ph.D Research in Microelectronics and Electronics Conference*, pages 201–204. IEEE, July 2007. doi:10.1109/RME.2007.4401847.

[67] D. D. Damian, H. Martinez, K. Dermitzakis, A. Hernandez-Arieta, and R. Pfeifer. Artificial ridged skin for slippage speed detection in prosthetic hand applications. In *2010 IEEE/RSJ International Conference on Intelligent Robots and Systems*, pages 904–909. IEEE, Oct. 2010. doi:10.1109/IROS.2010.5652094.

[68] H. Dang, J. Weisz, and P. K. Allen. Blind grasping: Stable robotic grasping using tactile feedback and hand kinematics. In *2011 IEEE International Conference on Robotics and Automation*, pages 5917–5922. IEEE, May 2011. doi:10.1109/ICRA.2011.5979679.

[69] J. Dargahi and S. Najarian. Human tactile perception as a standard for artificial tactile sensing–a review. *The international journal of medical robotics + computer assisted surgery : MRCAS*, 1(1):23–35, June 2004. doi:10.1002/rcs.3.

[70] M. J. L. de Hoon, S. Imoto, J. Nolan, and S. Miyano. Open source clustering software. *Bioinformatics (Oxford, England)*, 20(9):1453–4, June 2004. doi:10.1093/bioinformatics/bth078.

[71] A. M. Dollar and R. D. Howe. Towards grasping in unstructured environments: grasper compliance and configuration optimization. *Advanced Robotics*, 19(5):523–543, June 2005. doi:10.1163/156855305323383785.

[72] J. M. Ehrich, M. Flanders, and J. F. Soechting. Factors Influencing Haptic Perception of Complex Shapes. *IEEE transactions on haptics*, 1(1):19–26, Jan. 2008. doi:10.1109/ToH.2008.4.

[73] A.-C. Eliasson, H. Forssberg, K. Ikuta, I. Apel, G. Westling, and R. S. Johansson. Development of human precision grip V: Anticipatory and triggered grip actions during sudden loading. *Experimental Brain Research*, 106(3):323–330, 1995. doi:10.1007/BF00231065.

[74] R. Ellis. Planning Tactile Recognition Paths in Two and Three Dimensions. *The International Journal of Robotics Research*, 11(2):87–111, Apr. 1992. doi:10.1177/027836499201100201.

[75] J. Engel, N. Chen, C. Tucker, C. Liu, S.-H. Kim, and D. Jones. Flexible Multimodal Tactile Sensing System for Object Identification. In *2006 5th IEEE Conference on Sensors*, pages 563–566. IEEE, Oct. 2007. doi:10.1109/ICSENS.2007.355530.

[76] J. Felip and A. Morales. Robust sensor-based grasp primitive for a three-finger robot hand. In *2009 IEEE/RSJ International Conference on Intelligent Robots and Systems*, pages 1811–1816. IEEE, Oct. 2009. doi:10.1109/IROS.2009.5354760.

[77] A. Fenko, J. J. Otten, and H. N. Schifferstein. Describing product experience in different languages: The role of sensory modalities. *Journal of Pragmatics*, 42(12):3314–3327, Dec. 2010. doi:10.1016/j.pragma.2010.05.010.

[78] J. a. Fishel, V. J. Santos, and G. E. Loeb. A robust micro-vibration sensor for biomimetic fingertips. In *2008 2nd IEEE RAS & EMBS International Conference on Biomedical Robotics and Biomechatronics*, volume 6106, pages 659–663. IEEE, Oct. 2008. doi:10.1109/BIOROB.2008.4762917.

[79] J. R. Flanagan and M. A. Beltzner. Independence of perceptual and sensorimotor predictions in the size-weight illusion. *Nature neuroscience*, 3(7):737–41, July 2000. doi:10.1038/76701.

[80] J. R. Flanagan, M. K. Burstedt, and R. S. Johansson. Control of fingertip forces in multidigit manipulation. *Journal of neurophysiology*, 81(4):1706–17, Apr. 1999.

[81] J. R. Flanagan and R. S. Johansson. *Hand Movements*, pages 399–414. Academic Press, 2002.

[82] P. Fong. Sensing, Acquisition, and Interactive Playback of Data-based Models for Elastic Deformable Objects. *The International Journal of Robotics Research*, 28(5):630–655, May 2009. doi:10.1177/0278364908100326.

[83] H. Forssberg, A. Eliasson, H. Kinoshita, R. S. Johansson, and G. Westling. Development of human precision grip I: Basic coordination of force. *Experimental Brain Research*, 85(2):451–457, June 1991. doi:10.1007/BF00229422.

[84] H. Forssberg, A. Eliasson, H. Kinoshita, G. Westling, and R. S. Johansson. Development of human precision grip IV:Tactile adaptation of isometric finger forces to the frictional condition. *Experimental Brain Research*, 104(2):323–330, May 1995. doi:10.1007/BF00242017.

[85] H. Forssberg, H. Kinoshita, A. Eliasson, R. S. Johansson, G. Westling, and A. Gordon. Development of human precision grip II: Anticipatory control of isometric forces targeted for object's weight. *Experimental Brain Research*, 90(2):393–398, Aug. 1992. doi:10.1007/BF00227253.

[86] B. Frank, R. Schmedding, C. Stachniss, M. Teschner, and W. Burgard. Learning the elasticity parameters of deformable objects with a manipulation robot. In *2010 IEEE/RSJ International Conference on Intelligent Robots and Systems*, pages 1877–1883. IEEE, Oct. 2010. doi:10.1109/IROS.2010.5653949.

[87] I. Fujimoto, Y. Yamada, T. Morizono, Y. Umetani, and T. Maeno. Development of artificial finger skin to detect incipient slip for realization of static friction sensation. In *Proceedings of IEEE International Conference on Multisensor Fusion and Integration for Intelligent Systems, MFI2003.*, pages 15–20. IEEE, 2003. doi:10.1109/MFI-2003.2003.1232571.

[88] W. Fujisaki and S. Nishida. Audio-tactile superiority over visuo-tactile and audio-visual combinations in the temporal resolution of synchrony perception. *Experimental brain research. Experimentelle Hirnforschung. Expérimentation cérébrale*, 198(2-3):245–59, Sept. 2009. doi:10.1007/s00221-009-1870-x.

[89] N. Gaissert and C. Wallraven. Perceptual representations of parametrically-defined and natural objects comparing vision and haptics. In *2010 IEEE Haptics Symposium*, pages 35–42. IEEE, Mar. 2010. doi:10.1109/HAPTIC.2010.5444683.

[90] A. Gallace and C. Spence. The science of interpersonal touch: an overview. *Neuroscience and biobehavioral reviews*, 34(2):246–59, Feb. 2010. doi:10.1016/j.neubiorev.2008.10.004.

[91] E. Gamzu and E. Ahissar. Importance of temporal cues for tactile spatial- frequency discrimination. *The Journal of neuroscience : the official journal of the Society for Neuroscience*, 21(18):7416–27, Sept. 2001.

[92] O. Gerelli and C. G. L. Bianco. A discrete-time filter for the on-line generation of trajectories with bounded velocity, acceleration, and jerk. In *2010 IEEE International Conference on Robotics and Automation*, pages 3989–3994. IEEE, May 2010. doi:10.1109/ROBOT.2010.5509712.

[93] G. A. Gescheider. Auditory and Cutaneous Temporal Resolution of Successive Brief Stimuli. *Journal of Experimental Psychology*, 75(4):570–572, 1967. doi:10.1037/h0025113.

[94] J. Glover, D. Rus, and N. Roy. Probabilistic Models of Object Geometry with Application to Grasping. *The International Journal of Robotics Research*, 28(8):999–1019, June 2009. doi:10.1177/0278364909340332.

[95] D. Goeger, M. Blankertz, and H. Woern. A tactile proximity sensor. In *2010 IEEE Sensors*, pages 589–594. IEEE, Nov. 2010. doi:10.1109/ICSENS.2010.5690450.

[96] D. Goger, N. Gorges, and H. Woern. Tactile sensing for an anthropomorphic robotic hand: Hardware and signal processing. In *2009 IEEE International Conference on Robotics and Automation*, pages 895–901. IEEE, May 2009. doi:10.1109/ROBOT.2009.5152650.

[97] C. Goldfeder, M. T. Ciocarlie, and P. K. Allen. The Columbia grasp database. In *2009 IEEE International Conference on Robotics and Automation*, pages 1710–1716. IEEE, May 2009. doi:10.1109/ROBOT.2009.5152709.

[98] A. Gordon, H. Forssberg, R. S. Johansson, A. Eliasson, and G. Westling. Development of human precision grip III: Integration of visual size cues during the programming of isometric forces A. *Experimental Brain Research*, 90(2):399–403, Aug. 1992. doi:10.1007/BF00227254.

[99] A. Gordon, H. Forssberg, R. S. Johansson, and G. Westling. Integration of sensory information during the programming of precision grip: comments on the contributions of size cues. *Experimental Brain Research*, 85(1):226–229, May 1991. doi:10.1007/BF00230004.

[100] A. Gordon, H. Forssberg, R. S. Johansson, and G. Westling. The integration of haptically acquired size information in the programming of precision grip. *Experimental Brain Research*, 83(3):483–488, Feb. 1991. doi:10.1007/BF00229825.

[101] A. Gordon, H. Forssberg, R. S. Johansson, and G. Westling. Visual size cues in the programming of manipulative forces during precision grip. *Experimental Brain Research*, 83(3):477–482, Feb. 1991. doi:10.1007/BF00229824.

[102] N. Gorges, S. E. Navarro, D. Goeger, and H. Woern. Haptic object recognition using passive joints and haptic key features. In *2010 IEEE International Conference on Robotics and Automation*, pages 2349–2355. IEEE, May 2010. doi:10.1109/ROBOT.2010.5509553.

[103] S. Granger and X. Pennec. Multi-scale EM-ICP: A Fast and Robust Approach for Surface Registration. In *Computer Vision — ECCV 2002*, pages 418–432. Springer Berlin / Heidelberg, 2002. doi:10.1007/3-540-47979-1_28.

[104] H. Gray, P. L. Williams, and L. H. Bannister. *Gray's anatomy: the anatomical basis of medicine and surgery*. Churchill Livingstone, 1995.

[105] D. Gunji, Y. Mizoguchi, S. Teshigawara, A. Ming, A. Namiki, M. Ishikawaand, and M. Shimojo. Grasping force control of multi-fingered robot hand based on slip detection using tactile sensor. In *2008 IEEE International Conference on Robotics and Automation*, pages 2605–2610. IEEE, May 2008. doi:10.1109/ROBOT.2008.4543605.

[106] J. Han and M. A. Shannon. Smooth Contact Capacitive Pressure Sensors in Touch- and Peeling-Mode Operation. *IEEE Sensors Journal*, 9(3):199–206, Mar. 2009. doi:10.1109/JSEN.2008.2011090.

[107] J. Han, J. Yeom, J. Lee, M. A. Shannon, and R. I. Masel. Smooth Contact Mode Capacitive Pressure Sensor with Polyimide Diaphragm. In *2007 IEEE Sensors*, pages 1468–1471. IEEE, 2007. doi:10.1109/ICSENS.2007.4388691.

[108] L. D. Harmon. Automated Tactile Sensing. *International Journal Of Robotics Research*, 1(2):3–32, 1982. doi:10.1177/027836498200100201.

[109] S. Hart and R. A. Grupen. Natural task decomposition with intrinsic potential fields. In *2007 IEEE/RSJ International Conference on Intelligent Robots and Systems*, pages 2507–2512. IEEE, Oct. 2007. doi:10.1109/IROS.2007.4399481.

[110] H. Hasegawa, Y. Mizoguchi, K. Tadakuma, M. Ishikawa, and M. Shimojo. Development of intelligent robot hand using proximity, contact and slip sensing. In *2010 IEEE International Conference on Robotics and Automation*, pages 777–784. IEEE, May 2010. doi:10.1109/ROBOT.2010.5509243.

[111] M. Hayashi, T. Sagisaka, Y. Ishizaka, T. Yoshikai, and M. Inaba. Development of functional whole-body flesh with distributed three-axis force sensors to enable close interaction by humanoids. In

2007 IEEE/RSJ International Conference on Intelligent Robots and Systems, pages 3610–3615. IEEE, Oct. 2007. doi:10.1109/IROS.2007.4399360.

[112] G. Heidemann and H. J. Ritter. *Visual Checking of Grasping Positions of a Three-Fingered Robot Hand*, pages 891–898. Springer Berlin / Heidelberg, 2001. doi:10.1007/3-540-44668-0_123.

[113] G. Heidemann and M. Schöpfer. Dynamic tactile sensing for object identification. In *IEEE International Conference on Robotics and Automation, 2004. Proceedings. ICRA '04. 2004*, number April, pages 813–818 Vol.1, New Orleans, 2004. IEEE. doi:10.1109/ROBOT.2004.1307249.

[114] J.-s. Heo, C.-H. Han, and J.-J. Lee. System Design and Evaluation of the Robot Tactile Sensor Using the Microbending Fiber Optic Sensors. In *RO-MAN 2007 - The 16th IEEE International Symposium on Robot and Human Interactive Communication*, pages 14–18. IEEE, 2007. doi:10.1109/ROMAN.2007.4415046.

[115] M. J. Hertenstein, R. Holmes, M. McCullough, and D. Keltner. The communication of emotion via touch. *Emotion (Washington, D.C.)*, 9(4):566–73, Aug. 2009. doi:10.1037/a0016108.

[116] M. Higashimori, K. Yoshimoto, and M. Kaneko. Active shaping of an unknown rheological object based on deformation decomposition into elasticity and plasticity. In *2010 IEEE International Conference on Robotics and Automation*, pages 5120–5126. IEEE, May 2010. doi:10.1109/ROBOT.2010.5509462.

[117] G. Hirzinger, N. Sporer, A. Albu-Schäffer, M. Hahnle, R. Krenn, A. Pascucci, and M. Schedl. DLR's Torque-Controlled Light Weight Robot III - Are We Reaching the Technological Limits Now? In *Proc. IEEE Int'l Conf. on Robotics and Automation 2002*, pages 1710–1716, 2002.

[118] V. A. Ho, D. V. Dao, S. Sugiyama, and S. Hirai. Development and Analysis of a Sliding Tactile Soft Fingertip Embedded With a Microforce/Moment Sensor. *IEEE Transactions on Robotics*, 27(3):411 – 424, 2011. doi:10.1109/TRO.2010.2103470.

[119] V. A. Ho and S. Hirai. Two-dimensional dynamic modeling of a sliding motion of a soft fingertip focusing on stick-to-slip transition. In *2010 IEEE International Conference on Robotics and Automation*, pages 4315–4321. IEEE, May 2010. doi:10.1109/ROBOT.2010.5509330.

[120] V. A. Ho and S. Hirai. Three-dimensional modeling and simulation of the sliding motion of a soft fingertip with friction, focusing on stick-slip transition. In *2011 IEEE International Conference on Robotics and Automation*, pages 5233–5239. IEEE, May 2011. doi:10.1109/ICRA.2011.5979901.

[121] M. A. Hoepflinger, C. D. Remy, M. Hutter, L. Spinello, and R. Siegwart. Haptic terrain classification for legged robots. In *2010 IEEE International Conference on Robotics and Automation*, pages 2828–2833. IEEE, May 2010. doi:10.1109/ROBOT.2010.5509309.

[122] M. Hollins and S. J. Bensmaïa. The coding of roughness. *Canadian journal of experimental psychology = Revue canadienne de psychologie expérimentale*, 61(3):184–95, Oct. 2007.

[123] M. Hollins, S. J. Bensmaïa, and S. Washburn. Vibrotactile adaptation impairs discrimination of fine, but not coarse, textures. *Somatosensory & motor research*, 18(4):253–62, Jan. 2001. doi:10.1080/01421590120089 64.

[124] E. Holweg, H. Hoeve, W. Jongkind, L. Marconi, C. Melchiorri, and C. Bonivento. Slip detection by tactile sensors: algorithms and experimental results. In *Proceedings of IEEE International Conference on Robotics and Automation*, number April, pages 3234–3239. IEEE, 1996. doi:10.1109/ROBOT.1996.509205.

[125] B. K. P. Horn. Closed-form solution of absolute orientation using unit quaternions. *Journal of the Optical Society of America A*, 4(4):629, Apr. 1987. doi:10.1364/JOSAA.4.000629.

[126] K. Hosoda and T. Iwase. Robust haptic recognition by anthropomorphic bionic hand through dynamic interaction. In *2010 IEEE/RSJ International Conference on Intelligent Robots and Systems*, pages 1236–1241. IEEE, Oct. 2010. doi:10.1109/IROS.2010.5649297.

[127] R. Howe and M. R. Cutkosky. Sensing skin acceleration for slip and texture perception. In *Proceedings, 1989 International Conference on Robotics and Automation*, pages 145–150. IEEE Comput. Soc. Press, 1989. doi:10.1109/ROBOT.1989.99981.

[128] R. D. Howe. Tactile sensing and control of robotic manipulation. *Advanced Robotics*, 8(3):245–261, Jan. 1993. doi:10.1163/156855394X00356.

[129] R. D. Howe and M. R. Cutkosky. Dynamic Tactile Sensing: Perception of Fine Surface Features with Stress Rate Sensing. *IEEE Transactions on Robotics and Automation*, (Vol.9, No. 2):140–150, 1993.

[130] R. D. Howe, I. Kao, and M. R. Cutkosky. The Sliding of Robot Fingers Under Combined Torsion and Shear Loading. In *IEEE International Conference on Robotics and Automation*, pages 103–105, 1988. doi:10.1109/ROBOT.1988.12032.

[131] K. Hsiao, S. Chitta, M. T. Ciocarlie, and E. G. Jones. Contact-reactive grasping of objects with partial shape information. In *2010 IEEE/RSJ International Conference on Intelligent Robots and Systems*, pages 1228–1235. IEEE, Oct. 2010. doi:10.1109/IROS.2010.5649494.

[132] M.-K. Hu. Visual pattern recognition by moment invariants. *IEEE Transactions on Information Theory*, 8(2):179–187, Feb. 1962. doi:10.1109/TIT.1962.1057692.

[133] M. Huber and R. A. Grupen. Learning to coordinate controllers - reinforcement learning on a control basis. In *In Proceedings of the International Joint Conference on Artificial Intelligence*, pages 1366–1371, 1997.

[134] L. E. Humes, T. A. Busey, J. C. Craig, and D. Kewley-Port. The effects of age on sensory thresholds and temporal gap detection in hearing, vision, and touch. *Attention, perception & psychophysics*, 71(4):860–71, May 2009. doi:10.3758/APP.71.4.860.

[135] S. Hyun, L. Pei, J.-F. Molinari, and M. Robbins. Finite-element analysis of contact between elastic self-affine surfaces. *Physical Review E*, 70(2):1–12, Aug. 2004. doi:10.1103/PhysRevE.70.026117.

[136] R. Ibrayev. Tactile recognition of algebraic shapes using differential invariants. In *IEEE International Conference on Robotics and Automation, 2004. Proceedings. ICRA '04. 2004*, pages 1548–1553 Vol.2. IEEE, IEEE, 2004. doi:10.1109/ROBOT.2004.1308044.

[137] IEEE. *Standards in Information technology - Portable Operating System Interface (POSIX)*. IEEE, 2001.

[138] E. In. A Capacitive Proximity Sensor in Dual Implementation with Tactile Imaging Capability on a Single Flexible Platform For Robot Assistant Applications. In *19th IEEE International Conference on Micro Electro Mechanical Systems*, number January, pages 606–609. IEEE, 2006. doi:10.1109/MEMSYS.2006.1627872.

[139] D. Inoue, M. Konyo, and S. Tadokoro. Distributed Tactile Sensors for Tracked Robots. In *2006 5th IEEE Conference on Sensors*, pages 1309–1312. IEEE, Oct. 2006. doi:10.1109/ICSENS.2007.355870.

[140] T. Ishihara, A. Namiki, M. Ishikawa, and M. Shimojo. Dynamic Pen Spinning Using a High-speed Multifingered Hand with High-speed Tactile Sensor. In *2006 6th IEEE-RAS International Conference on Humanoid Robots*, pages 258–263. IEEE, Dec. 2006. doi:10.1109/ICHR.2006.321394.

[141] Y. Ito, Y. Kim, and G. Obinata. Slippage degree estimation for dexterous handling of vision-based tactile sensor. In *2009 IEEE Sensors*, pages 449–452. Ieee, Oct. 2009. doi:10.1109/ICSENS.2009.5398268.

[142] P. Jenmalm, S. Dahlstedt, and R. S. Johansson. Visual and tactile information about object-curvature control fingertip forces and grasp kinematics in human dexterous manipulation. *Journal of neurophysiology*, 84(6):2984–97, Dec. 2000.

[143] Y.-b. Jia and J. Tian. On two-finger grasping of deformable planar objects. In *2011 IEEE International Conference on Robotics and Automation*, pages 5261–5266. IEEE, May 2011. doi:10.1109/ICRA.2011.5980565.

[144] J. Jockusch, J. Walter, and H. Ritter. A tactile sensor system for a three-fingered robot manipulator. In *Proceedings of International Conference on Robotics and Automation*, pages 3080–3086. IEEE, IEEE, 1997. doi:10.1109/ROBOT.1997.606756.

[145] R. S. Johansson. *Sensory Control of Dexterous Manipulation in Humans*, chapter 19, pages 381–414. Academic Press, 1996.

[146] R. S. Johansson. Sensory input and control of grip. In *Novartis Foundation symposium*, volume 218, pages 45–59; discussion 59–63, Jan. 1998.

[147] R. S. Johansson and G. Westling. Roles of glabrous skin receptors and sensorimotor memory in automatic control of precision grip when lifting rougher or more slippery objects. *Experimental brain research. Experimentelle Hirnforschung. Expérimentation cérébrale*, 56(3):550–64, Jan. 1984.

[148] R. S. Johansson and G. Westling. Roles of glabrous skin receptors and sensorimotor memory in automatic control of precision grip when lifting rougher or more slippery objects. *Experimental Brain Research*, 56(3):550–564, Oct. 1984. doi:10.1007/BF00237997.

[149] R. S. Johansson and G. Westling. Signals in tactile afferents from the fingers eliciting adaptive motor responses during precision grip. *Experimental Brain Research*, 66(1):141–154, Mar. 1987. doi:10.1007/BF00236210.

[150] R. S. Johansson and G. Westling. Coordinated isometric muscle commands adequately and erroneously programmed for the weight during lifting task with precision grip. *Experimental brain research. Experimentelle Hirnforschung. Expérimentation cérébrale*, 71(1):59–71, Jan. 1988.

[151] M. Johnsson and C. Balkenius. Recognizing texture and hardness by touch. In *2008 IEEE/RSJ International Conference on Intelligent Robots and Systems*, pages 482–487. IEEE, Sept. 2008. doi:10.1109/IROS.2008.4650676.

[152] D. Johnston, J. Hollerbach, and S. Jacobsen. A full tactile sensing suite for dextrous robot hands and use in contact force control. In *Proceedings of IEEE International Conference on Robotics and Automation*, number April, pages 3222–3227. IEEE, 1996. doi:10.1109/ROBOT.1996.509203.

[153] L. A. Jones and S. J. Lederman. *Human Hand Function*, volume 32. Oxford University Press, 2006.

[154] R. Joshi and A. Sanderson. Shape matching from grasp using a minimal representation size criterion. In *[1993] Proceedings IEEE International Conference on Robotics and Automation*, pages 442–449. IEEE Comput. Soc. Press, 1993. doi:10.1109/ROBOT.1993.292020.

[155] A. Kadowaki, T. Yoshikai, M. Hayashi, and M. Inaba. Development of soft sensor exterior embedded with multi-axis deformable tactile sensor system. In *RO-MAN 2009 - The 18th IEEE International Symposium on Robot and Human Interactive Communication*, pages 1093–1098. IEEE, Sept. 2009. doi:10.1109/ROMAN.2009.5326073.

[156] R. E. Kalman. A new approach to linear filtering and prediction problems. *Journal Of Basic Engineering*, 82(Series D):35–45, 1960. doi:10.1109/ICASSP.1982.1171734.

[157] K. Kamiyama, H. Kajimoto, N. Kawakami, and S. Tachi. Evaluation of a vision-based tactile sensor. In *IEEE International Conference on Robotics and Automation, 2004. Proceedings. ICRA '04. 2004*, pages 1542–1547 Vol.2. IEEE, IEEE, 2004. doi:10.1109/ROBOT.2004.1308043.

[158] C. Kane, E. Repetto, M. Ortiz, and J. Marsden. Finite element analysis of nonsmooth contact. *Computer Methods in Applied Mechanics and Engineering*, 180(1-2):1–26, Nov. 1999. doi:10.1016/S0045-7825(99)00034-1.

[159] I. Kao, N. Sakamoto, M. Higashimori, and M. Kaneko. Applying viscoelastic contact modeling to grasping task: An experimental case study. In *2008 IEEE/RSJ International Conference on Intelligent Robots and Systems*, number 1, pages 1790–1795. Ieee, Sept. 2008. doi:10.1109/IROS.2008.4651030.

[160] C. Kemp, A. Edsinger, and E. Torres-Jara. Challenges for robot manipulation in human environments [Grand Challenges of Robotics]. *IEEE Robotics & Automation Magazine*, 14(1):20–29, Mar. 2007. doi:10.1109/MRA.2007.339604.

[161] O. Kerpa, K. Weiss, and H. Wörn. Development of a flexible tactile sensor system for a humanoid robot. In *Proceedings 2003 IEEE/RSJ International Conference on Intelligent Robots and Systems (IROS 2003) (Cat. No.03CH37453)*, number October, pages 1–6. IEEE, 2003. doi:10.1109/IROS.2003.1250596.

[162] R. Kikuuwe, A. Sano, H. Mochiyama, N. Takesue, and H. Fujimoto. A tactile sensor capable of mechanical adaptation and its use as a surface deflection detector. In *Proceedings of IEEE Sensors, 2004.*, pages 256–259. IEEE, 2004. doi:10.1109/ICSENS.2004.1426150.

[163] B.-s. Kim and J.-b. Song. Object grasping using a 1 DOF variable stiffness gripper actuated by a hybrid variable stiffness actuator. In *2011 IEEE International Conference on Robotics and Automation*, pages 4620–4625. IEEE, May 2011. doi:10.1109/ICRA.2011.5979864.

[164] H.-K. Kim, S.-G. Lee, J.-E. Han, T.-R. Kim, S.-U. Hwang, S. D. Ahn, I.-K. You, K.-I. Cho, T.-K. Song, and K.-S. Yun. Transparent and flexible tactile sensor for multi touch screen application with force sensing. In *TRANSDUCERS 2009 - 2009 International Solid-State Sensors, Actuators and Microsystems Conference*, pages 1146–1149. Ieee, June 2009. doi:10.1109/SENSOR.2009.5285933.

[165] J.-h. Kim, W.-c. Choi, H.-j. Kwon, and D.-i. Kang. Development of tactile sensor with functions of contact force and thermal sensing for attachment to intelligent robot finger tip. In *2006 5th IEEE Conference on Sensors*, pages 1468–1472. IEEE, Oct. 2006. doi:10.1109/ICSENS.2007.355911.

[166] J. K. Kim, J. W. Wee, and C. H. Lee. Sensor fusion system for improving the recognition of 3D object. In *IEEE Conference on Cybernetics and Intelligent Systems, 2004.*, pages 1207–1212. IEEE, 2004. doi:10.1109/ICCIS.2004.1460763.

[167] K. Kim, K. Lee, Y. Kim, D. Lee, N. Cho, W. Kim, K. Park, H. Park, Y. Park, J. Kim, and J. Pak. 3-Axes Flexible Tactile Sensor Fabricated by Si Micromachining and Packaging Technology. In *19th IEEE International Conference on Micro Electro Mechanical Systems*, number January, pages 678–681. IEEE, 2006. doi:10.1109/MEMSYS.2006.1627890.

[168] G.-I. Kinoshita, S. Aida, and M. Mori. A pattern classification by dynamic tactile sense information processing. *Pattern Recognition*, 7(4):243–251, Dec. 1975. doi:10.1016/0031-3203(75)90009-6.

[169] Y. Kita, T. Ueshiba, E. S. Neo, and N. Kita. A method for handling a specific part of clothing by dual arms. In *2009 IEEE/RSJ International Conference on Intelligent Robots and Systems*, volume 1, pages 4180–4185. IEEE, Oct. 2009. doi:10.1109/IROS.2009.5354213.

[170] R. L. Klatzky, S. Lederman, and C. Reed. Haptic integration of object properties: texture, hardness, and planar contour. *Journal of experimental psychology. Human perception and performance*, 15(1):45–57, Feb. 1989.

[171] R. L. Klatzky and S. J. Lederman. Identifying objects from a haptic glance. *Perception & psychophysics*, 57(8):1111–23, Nov. 1995.

[172] R. L. Klatzky and S. J. Lederman. Touch. In A. F. Healy and R. W. Proctor, editors, *Experimental Psychology*, pages 147–176. John Wiley & Sons, Inc., New York, 2002.

[173] R. L. Klatzky, S. J. Lederman, and J. Mankinen. Visual and haptic exploratory procedures in children's judgments about tool function. *Infant Behavior and Development*, 28(3):240–249, Sept. 2005. doi:10.1016/j.infbeh.2005.05.002.

[174] R. L. Klatzky, S. J. Lederman, and D. E. Matula. Haptic exploration in the presence of vision. *Journal of experimental psychology. Human perception and performance*, 19(4):726–43, Aug. 1993.

[175] R. L. Klatzky, S. J. Lederman, and V. A. Metzger. Identifying objects by touch: An "expert system". *Perception & Psychophysics*, 37(4):299–302, July 1985. doi:10.3758/BF03211351.

[176] R. L. Klatzky, S. J. Lederman, and C. Reed. There's More to Touch Than Meets the Eye: The Salience of Object Attributes for Haptics With and Without Vision. *J. of Experimental Psychology: General*, 116(4):356–369, 1987.

[177] R. L. Klatzky, J. M. Loomis, S. J. Lederman, H. Wake, and N. Fujita. Haptic identification of objects and their depictions. *Perception & psychophysics*, 54(2):170–8, Aug. 1993.

[178] Y. Koda and T. Maeno. Grasping Force Control in Master-Slave System with Partial Slip Sensor. In *2006 IEEE/RSJ International Conference on Intelligent Robots and Systems*, volume 19, pages 4641–4646. IEEE, Oct. 2006. doi:10.1109/IROS.2006.282173.

[179] L. Kogut and I. Etsion. A Finite Element Based Elastic-Plastic Model for the Contact of Rough Surfaces. *Tribology Transactions*, 46(3):383–390, July 2003. doi:10.1080/10402000308982641.

[180] K. Kokjer. The Information Capacity of the Human Fingertip. *IEEE Transactions on Systems, Man, and Cybernetics*, 17(1):100–102, Jan. 1987. doi:10.1109/TSMC.1987.289337.

[181] D. Kragic, S. Crinier, D. Brunn, and H. Christensen. Vision and tactile sensing for real world tasks. In *2003 IEEE International Conference on Robotics and Automation (Cat. No.03CH37422)*, pages 1545–1550. IEEE, 2003. doi:10.1109/ROBOT.2003.1241811.

[182] R. K. Kramer, C. Majidi, and R. J. Wood. Wearable tactile keypad with stretchable artificial skin. In *2011 IEEE International Conference on Robotics and Automation*, pages 1103–1107. IEEE, May 2011. doi:10.1109/ICRA.2011.5980082.

[183] O. Kroemer, C. H. Lampert, and J. Peters. Learning Dynamic Tactile Sensing With Robust Vision-Based Training. *IEEE Transactions on Robotics*, 27(3):545–557, June 2011. doi:10.1109/TRO.2011.2121130.

[184] J. J. Kulikowski. Some stimulus parameters affecting spatial and temporal resolution of human vision. *Vision research*, 11(1):83–93, Jan. 1971. doi:10.1016/0042-6989(71)90206-9.

[185] Y. Kurita, A. Ikeda, and T. Ogasawara. A fingerprint pointing device utilizing the deformation of the fingertip during the incipient slip. *IEEE Transactions on Robotics*, 21(5):801–811, Oct. 2005. doi:10.1109/TRO.2005.847568.

[186] J. Laaksonen, V. Kyrki, and D. Kragic. Evaluation of feature representation and machine learning methods in grasp stability learning. In *IEEE International Conference on Humanoid Robots*, pages 112–117, 2010.

[187] Y.-T. Lai, C.-L. Lin, X.-H. Huang, M.-Y. Cheng, and Y.-J. Yang. A flexible tactile sensing array for robot applications. In *2010 IEEE Sensors*, pages 2599–2602. IEEE, Nov. 2010. doi:10.1109/ICSENS.2010.5690188.

[188] C. Lebosse, P. Renaud, B. Bayle, and M. de Mathelin. Modeling and Evaluation of Low-Cost Force Sensors. *IEEE Transactions on Robotics*, 27(4):815–822, 2011. doi:10.1109/TRO.2011.2119850.

[189] S. J. Lederman. Skin and touch. Encyclopedia of human biology, 1991.

[190] S. J. Lederman and L. A. Jones. Tactile and Haptic Illusions. *IEEE Transactions on Haptics*, pages 1–22, 2011. doi:10.1109/TOH.2011.2.

[191] S. J. Lederman and R. L. Klatzky. Hand movements: a window into haptic object recognition. *Cognitive psychology*, 19(3):342–68, July 1987. doi:10.1016/0010-0285(87)90008-9.

[192] S. J. Lederman and R. L. Klatzky. Haptic classification of common objects: Knowledge-driven exploration*1. *Cognitive Psychology*, 22(4):421–459, Oct. 1990. doi:10.1016/0010-0285(90)90009-S.

[193] S. J. Lederman and R. L. Klatzky. Extracting object properties through haptic exploration. *Acta Psychologica*, 84(1):29–40, Oct. 1993. doi:10.1016/0001-6918(93)90070-8.

[194] S. J. Lederman and R. L. Klatzky. The Intelligent Hand: An Experimental Approach to Human Object Recognition and Implications for Robotics and AI. *AI Magazine*, 15(1):26–38, 1994.

[195] S. J. Lederman and R. L. Klatzky. Relative availability of surface and object properties during early haptic processing. *Journal of experimental psychology. Human perception and performance*, 23(6):1680–1707, Dec. 1997.

[196] S. J. Lederman and R. L. Klatzky. Haptic identification of common objects: effects of constraining the manual exploration process. *Perception & psychophysics*, 66(4):618–28, May 2004.

[197] S. J. Lederman and R. L. Klatzky. Haptic perception: a tutorial. *Attention, perception & psychophysics*, 71(7):1439–59, Oct. 2009. doi:10.3758/APP.71.7.1439.

[198] S. J. Lederman, J. M. Loomis, and D. A. Williams. The role of vibration in the tactual perception of roughness. *Perception & psychophysics*, 32(2):109–16, Aug. 1982.

[199] H.-k. Lee, S.-i. Chang, and E. Yoon. Dual-Mode Capacitive Proximity Sensor for Robot Application: Implementation of Tactile and Proximity Sensing Capability on a Single Polymer Platform Using Shared Electrodes. *IEEE Sensors Journal*, 9(12):1748–1755, Dec. 2009. doi:10.1109/JSEN.2009.2030660.

[200] K.-m. Lee and S. Foong. Lateral optical sensor with slip detection of natural objects on moving conveyor. In *2008 IEEE International Conference on Robotics and Automation*, pages 329–334. IEEE, May 2008. doi:10.1109/ROBOT.2008.4543229.

[201] K.-m. Lee and S. Foong. Lateral Optical Sensor With Slip Detection for Locating Live Products on Moving Conveyor. *IEEE Transactions on Automation Science and Engineering*, 7(1):123–132, Jan. 2010. doi:10.1109/TASE.2009.2025505.

[202] M. Lee. Review Article Tactile sensing for mechatronics—a state of the art survey. *Mechatronics*, 9(1):1–31, Feb. 1999. doi:10.1016/S0957-4158(98)00045-2.

[203] M. H. Lee. Tactile Sensing: New Directions, New Challenges. *The International Journal of Robotics Research*, 19(7):636–643, July 2000. doi:10.1177/027836490001900702.

[204] G. E. Legge, C. Madison, B. N. Vaughn, A. M. Y. Cheong, and J. C. Miller. Retention of high tactile acuity throughout the life span in blindness. *Perception & psychophysics*, 70(8):1471–88, Nov. 2008. doi:10.3758/PP.70.8.1471.

[205] F. Leoni, M. Guerrini, C. Laschi, D. Taddeucci, P. Dario, and A. Starita. Implementing robotic grasping tasks using a biological approach. In *Proceedings. 1998 IEEE International Conference on Robotics and Automation*, pages 2274–2280. IEEE, IEEE, 1998. doi:10.1109/ROBOT.1998.680662.

[206] Y. Li and I. Kao. A review of modeling of soft-contact fingers and stiffness control for dextrous manipulation in robotics. In *Proceedings 2001 ICRA. IEEE International Conference on Robotics and Automation*, pages 3055–3060. IEEE, 2001. doi:10.1109/ROBOT.2001.933086.

[207] X. Libouton, O. Barbier, L. Plaghki, and J.-L. Thonnard. Tactile roughness discrimination threshold is unrelated to tactile spatial acuity. *Behavioural brain research*, 208(2):473–8, Apr. 2010. doi:10.1016/j.bbr.2009.12.017.

[208] V. Lippiello, F. Ruggiero, B. Siciliano, and L. Villani. Preshaped visual grasp of unknown objects with a multi-fingered hand. In *2010 IEEE/RSJ International Conference on Intelligent Robots and Systems*, pages 5894–5899. IEEE, Oct. 2010. doi:10.1109/IROS.2010.5650680.

[209] V. Lippiello, F. Ruggiero, and L. Villani. Floating visual grasp of unknown objects. In *2009 IEEE/RSJ International Conference on Intelligent Robots and Systems*, pages 1290–1295. IEEE, Oct. 2009. doi:10.1109/IROS.2009.5354350.

[210] Y. Liu, N. Mechbal, J.-p. Nikolovski, M. Hafez, and M. Verge. Thin shell tactile sensing by acoustic wave diffraction patterns. In *2011 IEEE International Conference on Robotics and Automation*, pages 5929–5934. IEEE, May 2011. doi:10.1109/ICRA.2011.5979883.

[211] Y.-C. Liu, C.-M. Sun, L.-Y. Lin, M.-H. Tsai, and W. Fang. A tunable range/sensitivity CMOS-MEMS capacitive tactile sensor with polymer fill-in technique. In *TRANSDUCERS 2009 - 2009 International Solid-State Sensors, Actuators and Microsystems Conference*, number c, pages 2190–2193. Ieee, June 2009. doi:10.1109/SENSOR.2009.5285611.

[212] J. Lloyd and M. Parker. Real Time Control Under UNIX for RCCL. In *Robotics and Manufacturing ISRAM '90*, pages 237—-242, 1990.

[213] J. Lloyd, M. Parker, and R. McClain. Extending the RCCL programming environment to multiple robots and processors. In *Proceedings. 1988 IEEE International Conference on Robotics and Automation*, pages 465–469, Philadelphia, PA, 1988. IEEE, IEEE Comput. Soc. Press. doi:10.1109/ROBOT.1988.12095.

[214] J. M. Loomis. Counterexample to the hypothesis of functional similarity between tactile and visual pattern perception. *Perception & psychophysics*, 54(2):179–84, Aug. 1993.

[215] J. M. Loomis and S. J. Lederman. Tactual perception. In K. R. Boff, L. Kaufman, and J. P. Thomas, editors, *Handbook of Perception and Human Performance: Volume II*, chapter 31, pages 1–41. John Wiley & Sons, Inc., New York, 1986.

[216] D. Lowe. Object recognition from local scale-invariant features. In *Proceedings of the Seventh IEEE International Conference on Computer Vision*, pages 1150–1157 vol.2. IEEE, 1999. doi:10.1109/ICCV.1999.790410.

[217] M.-C. Lu. A Highly Sensitive CMOS-MEMS Capacitive Tactile Sensor. In *19th IEEE International Conference on Micro Electro Mechanical Systems*, volume 1, pages 642–645. IEEE, 2006. doi:10.1109/MEMSYS.2006.1627881.

[218] V. Lumelsky and E. Cheung. Real-time collision avoidance in teleoperated whole-sensitive robot arm manipulators. *IEEE Transactions on Systems, Man, and Cybernetics*, 23(1):194–203, 1993. doi:10.1109/21.214777.

[219] Q. Luo and J. Xiao. Contact and Deformation Modeling for Interactive Environments. *IEEE Transactions on Robotics*, 23(3):416–430, June 2007. doi:10.1109/TRO.2007.895058.

[220] J. Macqueen. Some methods for classification and analysis of multivariate observations. In *Proc. Fifth Berkeley Symp. on Math. Statist. and Prob.*, volume 233, pages 281–297, 1967.

[221] J. C. Makous, R. M. Friedman, and C. J. Vierck. A critical band filter in touch. *The Journal of neuroscience : the official journal of the Society for Neuroscience*, 15(4):2808–18, Apr. 1995. doi:7722630.

[222] A. Maldonado, U. Klank, and M. Beetz. Robotic grasping of unmodeled objects using time-of-flight range data and finger torque information. In *2010 IEEE/RSJ International Conference on Intelligent Robots and Systems*, pages 2586–2591. IEEE, Oct. 2010. doi:10.1109/IROS.2010.5649185.

[223] R. Maldonado-López, F. Vidal-Verdú, G. Liñán, E. Roca, and A. Rodríguez-Vázquez. Early slip detection with a tactile sensor based on retina. *Analog Integrated Circuits and Signal Processing*, 53(2):97–108, 2007. doi:10.1007/s10470-007-9059-3.

[224] R. Maldonado-Lopez, F. Vidal-Verdu, G. Linan, E. Roca, and A. Rodriguez-Vazquez. Tactile Retina for Slip Detection. In *2006 IEEE Symposium on Virtual Environments, Human-Computer Interfaces and Measurement Systems*, number July, pages 96–101. IEEE, July 2006. doi:10.1109/VECIMS.2006.250799.

[225] N. Masataka, M. Konyo, T. Maeno, and S. Tadokoro. Reflective grasp force control of humans induced by distributed vibration stimuli on finger skin with ICPF actuators. In *Proceedings 2006 IEEE International Conference on Robotics and Automation, 2006. ICRA 2006.*, number May, pages 3899–3904. IEEE, 2006. doi:10.1109/ROBOT.2006.1642299.

[226] K. Matsuo, K. Murakami, T. Hasegawa, and R. Kurazume. A decision method for the placement of mechanical tactile elements for grasp type recognition. In *2008 IEEE Sensors*, pages 1472–1475. IEEE, Oct. 2008. doi:10.1109/ICSENS.2008.4716723.

[227] K. Matsuo, K. Murakami, T. Hasegawa, and R. Kurazume. A decision method for the placement of tactile sensors for manipulation task recognition. In *2008 IEEE International Conference on Robotics and Automation*, pages 1641–1646. IEEE, May 2008. doi:10.1109/ROBOT.2008.4543436.

[228] A. M. Mazid and M. F. Islam. Grasping Force Estimation Recognizing Object Slippage by Tactile Data Using Neural Network. In *2008 IEEE Conference on Robotics, Automation and Mechatronics*, pages 935–940. IEEE, Sept. 2008. doi:10.1109/RAMECH.2008.4681378.

[229] A. M. Mazid and A. B. M. Shawkat Ali. Grasping force estimation detecting slip by tactile sensor adopting machine learning techniques. In *TENCON 2008 - 2008 IEEE Region 10 Conference*, pages 1–6. IEEE, Nov. 2008. doi:10.1109/TENCON.2008.4766846.

[230] F. McGlone and D. Reilly. The cutaneous sensory system. *Neuroscience and biobehavioral reviews*, 34(2):148–59, Feb. 2010. doi:10.1016/j.neubiorev.2009.08.004.

[231] F. McGlone, A. B. Vallbo, H. Olausson, L. Loken, and J. Wessberg. Discriminative touch and emotional touch. *Canadian journal of experimental psychology = Revue canadienne de psychologie expérimentale*, 61(3):173–83, Sept. 2007. doi:10.1037/cjep2007019.

[232] H. McGurk and J. MacDonald. Hearing lips and seeing voices. *Nature*, 264(5588):746–748, 1976. doi:10.1038/264746a0.

[233] M. Meier. *Adaption des FastSLAM Algorithmus zur Verarbeitung taktiler Sensordaten*. Diploma thesis, University of Bielefeld, 2009.

[234] M. Meier, M. Schöpfer, R. Haschke, and H. Ritter. A Probabilistic Approach to Tactile Shape Reconstruction. *IEEE Transactions on Robotics*, 27(3):630–635, June 2011. doi:10.1109/TRO.2011.2120830.

[235] G. Milighetti, S. Burger, and H.-B. Kuntze. On the robot based surface finishing of moving unknown parts by means of a new slip and force control concept. In *Proceedings 2007 IEEE International Conference on Robotics and Automation*, number April, pages 4752–4757. IEEE, Apr. 2007. doi:10.1109/ROBOT.2007.364211.

[236] A. Miller and P. K. Allen. GraspIt! *IEEE Robotics & Automation Magazine*, 11(4):110–122, Dec. 2004. doi:10.1109/MRA.2004.1371616.

[237] T. M. Mitchell. *Machine Learning*, volume 4 of *McGraw-Hill Series in Computer Science*. McGraw-Hill, 1997. doi:10.1146/annurev.cs.04.060190.001351.

[238] M. Moll and M. Erdmann. Reconstructing shape from motion using tactile sensors. In *Proceedings 2001 IEEE/RSJ International Conference on Intelligent Robots and Systems. Expanding the Societal Role of Robotics in the the Next Millennium (Cat. No.01CH37180)*, pages 692–700, Maui, HI, 2001. IEEE. doi:10.1109/IROS.2001.976250.

[239] M. Mon-Williams and A. H. Murray. The size of the visual size cue used for programming manipulative forces during precision grip. *Experimental brain research. Experimentelle Hirnforschung. Expérimentation cérébrale*, 135(3):405–10, Dec. 2000.

[240] L. Moss-Salentijn. The Human Tactile System. In H. R. Nicholls, editor, *Advanced tactile sensing for robotics*, chapter 7, pages 123–150. Worl Scientific Publishing Co. Pte. Ltd., PO Box 128, Farrer Road, Singapore 9128, 1992.

[241] H. Mühe, A. Angerer, A. Hoffmann, and W. Reif. On reverse-engineering the KUKA Robot Language. 2010.

[242] K. Murakami, K. Matsuo, T. Hasegawa, and R. Kurazume. A Decision Method for Placement of Tactile Elements on a Sensor Glove for the Recognition of Grasp Types. *IEEE/ASME Transactions on Mechatronics*, 15(1):157–162, Feb. 2010. doi:10.1109/TMECH.2009.2023647.

[243] K. Nagata and N. Yamanobe. Picking up a towel by cooperation of functional finger actions. In *2009 IEEE/RSJ International Conference on Intelligent Robots and Systems*, pages 1785–1790. IEEE, Oct. 2009. doi:10.1109/IROS.2009.5354783.

[244] S. Najarian, J. Dargahi, and A. Merizi. *Artificial Tactile Sensing in Biomedical Engineering*. McGraw-Hill, 2009.

[245] T. Nguyen, R. Heslin, and M. L. Nguyen. The Meanings of Touch: Sex Differences. *Journal of Communication*, 25(3):92–103, Sept. 1975. doi:10.1111/j.1460-2466.1975.tb00610.x.

[246] H. R. Nicholls. *Advances Tactile Sensing for Robotics*. World Scientific Publishing Co., Inc., 1992.

[247] H. R. Nicholls. Tactile Sensor Designs. In H. R. Nicholls, editor, *Advanced tactile sensing for robotics*, chapter 2, pages 13–48. Worl Scientific Publishing Co. Pte. Ltd., PO Box 128, Farrer Road, Singapore 9128, 1992.

[248] H. R. Nicholls and M. H. Lee. A Survey of Robot Tactile Sensing Technology. *The International Journal of Robotics Research*, 8(3):3–30, June 1989. doi:10.1177/027836498900800301.

[249] S. B. Niku. *Introduction to Robotics*. Pearson, New Jersey, 2001.

[250] J. Nishiyama, C.-h. D. Tsai, M. Quigley, I. Kao, A. Shibata, M. Higashimori, and M. Kaneko. An experimental study of biologically inspired artificial skin sensor under static loading and dynamic stimuli. In *2011 IEEE International Conference on Robotics and Automation*, pages 1778–1783. IEEE, May 2011. doi:10.1109/ICRA.2011.5980511.

[251] J. F. Norman and A. N. Bartholomew. Blindness enhances tactile acuity and haptic 3-D shape discrimination. *Attention, perception & psychophysics*, June 2011. doi:10.3758/s13414-011-0160-4.

[252] M. Ohka, H. Kobayashi, and Y. Mitsuya. Sensing characteristics of an optical three-axis tactile sensor mounted on a multi-fingered robotic hand. In *2005 IEEE/RSJ International Conference on Intelligent Robots and Systems*, pages 493–498. IEEE, 2005. doi:10.1109/IROS.2005.1545264.

[253] M. Ohka, N. Morisawa, H. Suzuki, J. Takata, H. Koboyashi, and H. B. Yussof. A robotic finger equipped with an optical three-axis tactile sensor. In *2008 IEEE International Conference on Robotics and Automation*, pages 3425–3430. IEEE, May 2008. doi:10.1109/ROBOT.2008.4543734.

[254] Y. Ohmura and Y. Kuniyoshi. Humanoid robot which can lift a 30kg box by whole body contact and tactile feedback. In *2007 IEEE/RSJ International Conference on Intelligent Robots and Systems*, pages 1136–1141. IEEE, Oct. 2007. doi:10.1109/IROS.2007.4399592.

[255] T. Okada and S. Tsuchiya. Object recognition by grasping. *Pattern Recognition*, 9(3):111–119, Oct. 1977. doi:10.1016/0031-3203(77)90008-5.

[256] A. M. Okamura. Feature Detection for Haptic Exploration with Robotic Fingers. *The International Journal of Robotics Research*, 20(12):925–938, Dec. 2001. doi:10.1177/02783640122068191.

[257] A. M. Okamura, M. A. Costa, M. L. Turner, C. Richard, and M. R. Cutkosky. Haptic Surface Exploration. In P. Corke and J. Trevelyan, editors, *Experimental Robotics VI*, volume 250, pages 423–432. Springer-Verlag, 2000. doi:10.1007/BFb0119420.

[258] A. M. Okamura, N. Smaby, and M. R. Cutkosky. An overview of dexterous manipulation. In *Proceedings 2000 ICRA. Millennium Conference. IEEE International Conference on Robotics and Automation. Symposia Proceedings (Cat. No.00CH37065)*, number April, pages 255–262. IEEE, 2000. doi:10.1109/ROBOT.2000.844067.

[259] C. Ott. *Cartesian Impedance Control of Redundant and Flexible-Joint Robots*, volume 49 of *Springer Tracts in Advanced Robotics*. Springer Berlin Heidelberg, Berlin, Heidelberg, 2008. doi:10.1007/978-3-540-69255-3.

[260] K. E. Overvliet, J. B. J. Smeets, and E. Brenner. The use of proprioception and tactile information in haptic search. *Acta psychologica*, 129(1):83–90, Sept. 2008. doi:10.1016/j.actpsy.2008.04.011.

[261] H. Ozaki, S. Waku, A. Mohri, and M. Takata. Pattern Recognition of a Grasped Object by Unit-Vector Distribution. *IEEE Transactions on Systems, Man, and Cybernetics*, 12(3):315–324, 1982. doi:10.1109/TSMC.1982.4308821.

[262] G. Palli and S. Pirozzi. Miniaturized optical-based force sensors for tendon-driven robots. In *2011 IEEE International Conference on Robotics and Automation*, pages 5344–5349. IEEE, May 2011. doi:10.1109/ICRA.2011.5979970.

[263] L. Paredes-Madrid, P. Torruella, P. Solaeche, I. Galiana, and P. Gonzalez de Santos. Accurate modeling of low-cost piezoresistive force sensors for haptic interfaces, May 2010. doi:10.1109/ROBOT.2010.5509436.

[264] Y.-L. Park, R. J. Black, B. Moslehi, and M. R. Cutkosky. Fingertip force control with embedded fiber Bragg grating sensors. In *2008 IEEE International Conference on Robotics and Automation*, pages 3431–3436. IEEE, May 2008. doi:10.1109/ROBOT.2008.4543735.

[265] D. Pawluk, R. Kitada, A. Abramowicz, C. Hamilton, and S. J. Lederman. Figure/Ground Segmentation via a Haptic Glance: Attributing Initial Finger Contacts to Objects or their Supporting Surfaces. *IEEE Transactions on Haptics*, (March 2011):2–13, 2010. doi:10.1109/TOH.2010.25.

[266] D. Pawluk, R. Kitada, A. Abramowicz, C. Hamilton, and S. J. Lederman. Haptic figure-ground differentation via a haptic glance. In *2010 IEEE Haptics Symposium*, pages 63–66. IEEE, Mar. 2010. doi:10.1109/HAPTIC.2010.5444676.

[267] W. Penfield and H. Jasper. *Epilepsy and the Functional Anatomy of the Human Brain*, volume 155. Little, Brown, and Company, 1954. doi:10.1001/jama.1954.03690190092039.

[268] R. M. Peters, E. Hackeman, and D. Goldreich. Diminutive digits discern delicate details: fingertip size and the sex difference in tactile spatial acuity. *The Journal of neuroscience : the official journal of the Society for Neuroscience*, 29(50):15756–61, Dec. 2009. doi:10.1523/JNEUROSCI.3684-09.2009.

[269] L. Petrosino and D. Fucci. Temporal resolution of the aging tactile sensory system. *Perceptual and motor skills*, 68(1):288–90, Feb. 1989.

[270] Z. Pezzementi, E. Plaku, C. Reyda, and G. D. Hager. Tactile-Object Recognition From Appearance Information. *IEEE Transactions on Robotics*, 27(3):473–487, June 2011. doi:10.1109/TRO.2011.2125350.

[271] Z. Pezzementi, C. Reyda, and G. D. Hager. Object mapping, recognition, and localization from tactile geometry. In *2011 IEEE International Conference on Robotics and Automation*, pages 5942–5948. IEEE, May 2011. doi:10.1109/ICRA.2011.5980363.

[272] D. Picard, C. Dacremont, D. Valentin, and A. Giboreau. Perceptual dimensions of tactile textures. *Acta psychologica*, 114(2):165–84, Oct. 2003.

[273] R. Platt, C. Ihrke, L. Bridgewater, D. Linn, R. Diftler, M. Abdallah, S. Askew, and F. Permenter. A miniature load cell suitable for mounting on the phalanges of human-sized robot fingers. In *2011 IEEE International Conference on Robotics and Automation*, pages 5357–5362. IEEE, May 2011. doi:10.1109/ICRA.2011.5980169.

[274] M. Popović, D. Kraft, L. Bodenhagen, E. Başeski, N. Pugeault, D. Kragic, T. Asfour, and N. Krüger. A strategy for grasping unknown objects based on co-planarity and colour information. *Robotics and Autonomous Systems*, 58(5):551–565, May 2010. doi:10.1016/j.robot.2010.01.003.

[275] E. Pritchard, M. Mahfouz, B. Evans, S. Eliza, and M. Haider. Flexible capacitive sensors for high resolution pressure measurement. In *2008 IEEE Sensors*, pages 1484–1487. IEEE, Oct. 2008. doi:10.1109/ICSENS.2008.4716726.

[276] P. Puangmali, H. Liu, K. A. Althoefer, and L. D. Seneviratne. Optical fiber sensor for soft tissue investigation during minimally invasive surgery. In *2008 IEEE International Conference on Robotics and Automation*, pages 2934–2939. Ieee, May 2008. doi:10.1109/ROBOT.2008.4543655.

[277] P. Puangmali, H. Liu, L. D. Seneviratne, P. Dasgupta, and K. Althoefer. Miniature 3-Axis Distal Force Sensor for Minimally Invasive Surgical Palpation. *IEEE/ASME Transactions on Mechatronics*, pages 1–11, 2011. doi:10.1109/TMECH.2011.2116033.

[278] K. A. Purdy, S. J. Lederman, and R. L. Klatzky. Manipulation with no or partial vision. *Journal of experimental psychology. Human perception and performance*, 25(3):755–74, June 1999.

[279] M. Quigley, B. Gerkey, K. Conley, J. Faust, T. Foote, J. Leibs, E. Berger, R. Wheeler, and A. Ng. ROS: an open-source Robot Operating System. In *Program*, number Figure 1 in Open-Source Software workshop. IEEE, 2009.

[280] J. Quinlan. Induction of Decision Trees. *Machine Learning*, 1(1):81–106, 1986. doi:10.1023/A:1022643204877.

[281] J. Quinlan. Learning With Continuous Classes. In *5th Australian Joint Conference on Artificial Intelligence*, volume 92, pages 343–348, Singapore, 1992.

[282] J. R. Quinlan. Improved Use of Continuous Attributes in C 4.5. *Journal of Artificial Intelligence Research*, 4:77–90, 1996. doi:10.1613/jair.279.

[283] M. Riedmiller and H. Braun. A direct adaptive method for faster backpropagation learning: the RPROP algorithm. *IEEE International Conference on Neural Networks*, 1993(3):586–591, 1993. doi:10.1109/ICNN.1993.298623.

[284] B. Robins, F. Amirabdollahian, Z. Ji, and K. Dautenhahn. Tactile interaction with a humanoid robot for children with autism: A case study analysis involving user requirements and results of an initial implementation. In *19th International Symposium in Robot and Human Interactive Communication*, pages 704–711. IEEE, Sept. 2010. doi:10.1109/ROMAN.2010.5598641.

[285] I. Rock and J. Victor. Vision and Touch: An Experimentally Created Conflict Between The Two Senses. *Science (New York, N.Y.)*, 143:594–596, Feb. 1964.

[286] M. H. Roderic A. Grupen. A Framework for the Development of Robot Behavior. *In AAAI Spring Symposium Series: Developmental Robotics*, 2(3), Sept. 2005.

[287] S. a. Rose, J. F. Feldman, J. J. Jankowski, and L. R. Futterweit. Visual and auditory temporal processing, cross-modal transfer, and reading. *Journal of learning disabilities*, 32(3):256–66, May 1999. doi:10.1177/002221949903200307.

[288] J. Rossiter and T. Mukai. A Novel Tactile Sensor Using a Matrix of LEDs Operating in Both Photoemitter and Photodetector Modes. In *IEEE Sensors, 2005.*, pages 994–997. IEEE, 2005. doi:10.1109/ICSENS.2005.1597869.

[289] J. Rossiter and T. Mukai. An LED-based Tactile Sensor for Multi-sensing over Large Areas. In *2006 5th IEEE Conference on Sensors*, pages 835–838. IEEE, Oct. 2006. doi:10.1109/ICSENS.2007.355597.

[290] F. Rothling, R. Haschke, J. J. Steil, and H. Ritter. Platform portable anthropomorphic grasping with the bielefeld 20-DOF shadow and 9-DOF TUM hand. In *2007 IEEE/RSJ International Conference on Intelligent Robots and Systems*, pages 2951–2956, San Diego, California, USA, Oct. 2007. IEEE, IEEE. doi:10.1109/IROS.2007.4398963.

[291] M. Rucci and R. Bajcsy. Learning visuo-tactile coordination in robotic systems. In *Proceedings of 1995 IEEE International Conference on Robotics and Automation*, pages 2678–2683. IEEE, 1995. doi:10.1109/ROBOT.1995.525661.

[292] S. Rusinkiewicz and M. Levoy. Efficient variants of the ICP algorithm. *Proceedings Third International Conference on 3-D Digital Imaging and Modeling*, 0:145–152, 2001. doi:10.1109/IM.2001.924423.

[293] S. Saga, M. Konyo, and K. Deguchi. Comparison of spatial and temporal characteristic between reflection-type tactile sensor and human cutaneous sensation. In *RO-MAN 2009 - The 18th IEEE International Symposium on Robot and Human Interactive Communication*, pages 22–27. IEEE, Sept. 2009. doi:10.1109/ROMAN.2009.5326297.

[294] N. Sakamoto, M. Higashimori, T. Tsuji, and M. Kaneko. An Optimum Design of Robotic Hand for Handling a Visco-elastic Object Based on Maxwell Model. In *Proceedings 2007 IEEE International Conference on Robotics and Automation*, number April, pages 1219–1225. IEEE, Apr. 2007. doi:10.1109/ROBOT.2007.363151.

[295] G. Sandini, G. Metta, and D. Vernon. *The iCub Cognitive Humanoid Robot: An Open-System Research Platform for Enactive Cognition*, volume 4850/2007 of *Lecture Notes in Computer Science*, pages 358–369. Springer Berlin / Heidelberg, 2007. doi:10.1007/978-3-540-77296-5_32.

[296] A. Sano, R. Kikuuwe, H. Mochiyama, N. Takesue, and H. Fujimoto. A Tactile Sensing for Human-Centered Robotics. In *2006 5th IEEE Conference on Sensors*, pages 819–822. IEEE, Oct. 2006. doi:10.1109/ICSENS.2007.355593.

[297] K. Sathian and A. Zangaladze. Tactile spatial acuity at the human fingertip and lip: bilateral symmetry and interdigit variability. *Neurology*, 46(5):1464–6, May 1996.

[298] K. Sato, H. Shinoda, and S. Tachi. Finger-shaped thermal sensor using thermo-sensitive paint and camera for telexistence. In *2011 IEEE International Conference on Robotics and Automation*, pages 1120–1125. IEEE, May 2011. doi:10.1109/ICRA.2011.5980271.

[299] H. N. Schifferstein. The perceived importance of sensory modalities in product usage: a study of self-reports. *Acta psychologica*, 121(1):41–64, Jan. 2006. doi:10.1016/j.actpsy.2005.06.004.

[300] P. A. Schmidt, E. Mael, and R. P. Würtz. A sensor for dynamic tactile information with applications in human–robot interaction and object exploration. *Robotics and Autonomous Systems*, 54(12):1005–1014, Dec. 2006. doi:10.1016/j.robot.2006.05.013.

[301] A. Schmitz, M. Maggiali, L. Natale, B. Bonino, and G. Metta. A tactile sensor for the fingertips of the humanoid robot iCub. In *2010 IEEE/RSJ International Conference on Intelligent Robots and Systems*, pages 2212–2217. IEEE, Oct. 2010. doi:10.1109/IROS.2010.5648838.

[302] A. Schmitz, M. Maggiali, L. Natale, and G. Metta. Touch sensors for humanoid hands. In *19th International Symposium in Robot and Human Interactive Communication*, pages 691–697. IEEE, Sept. 2010. doi:10.1109/ROMAN.2010.5598609.

[303] A. Schmitz, P. Maiolino, M. Maggiali, L. Natale, G. Cannata, and G. Metta. Methods and Technologies for the Implementation of Large-Scale Robot Tactile Sensors. *IEEE Transactions on Robotics*, 27(3):389–400, June 2011. doi:10.1109/TRO.2011.2132930.

[304] A. Schneider, J. Sturm, C. Stachniss, M. Reisert, H. Burkhardt, and W. Burgard. Object identification with tactile sensors using bag-of-features. In *2009 IEEE/RSJ International Conference on Intelligent Robots and Systems*, pages 243–248. IEEE, Oct. 2009. doi:10.1109/IROS.2009.5354648.

[305] J. Schneiter. An objective tactile sensing strategy for object recognition and localization. In *Proceedings. 1986 IEEE International Conference on Robotics and Automation*, pages 1262–1267. Institute of Electrical and Electronics Engineers, 1986. doi:10.1109/ROBOT.1986.1087542.

[306] J. Schneiter and T. Sheridan. An automated tactile sensing strategy for planar object recognition and localization. *IEEE Transactions on Pattern Analysis and Machine Intelligence*, 12(8):775–786, 1990. doi:10.1109/34.57668.

[307] M. Schöpfer, M. Pardowitz, and H. J. Ritter. Using Entropy for Dimension Reduction of Tactile Data. In *14th International Conference on Advanced Robotics*, Proceedings of the ICAR 2009, pages 1 – 6, Munich, Germany, 2009. IEEE, IEEE.

[308] M. Schöpfer, H. J. Ritter, and G. Heidemann. Acquisition and Application of a Tactile Database. In *Proceedings 2007 IEEE International Conference on Robotics and Automation*, number April, pages 1517–1522, Roma, Italy, Apr. 2007. IEEE. doi:10.1109/ROBOT.2007.363539.

[309] M. Schöpfer, F. Schmidt, M. Pardowitz, and H. J. Ritter. Open source real-time control software for the Kuka light weight robot. In *2010 8th World Congress on Intelligent Control and Automation*, pages 444–449, Jinan, China, July 2010. IEEE. doi:10.1109/WCICA.2010.5553773.

[310] A. Schultz, J. Solomon, M. Peshkin, and M. Hartmann. Multifunctional Whisker Arrays for Distance Detection, Terrain Mapping, and Object Feature Extraction. In *Proceedings of the 2005 IEEE International Conference on Robotics and Automation*, pages 2588–2593. IEEE, 2005. doi:10.1109/ROBOT.2005.1570503.

[311] C. Schürmann, R. Haschke, and H. J. Ritter. Modular high speed tactile sensor system with video interface. In *Tactile sensing in Humanoids {\textendash} Tactile Sensors and beyond @ IEEE-Ras Conference on Humanoid Robots (Humanoids)*, Paris, France, 2009.

[312] C. Schürmann, R. Koiva, R. Haschke, and H. Ritter. A Modular High-Speed Tactile Sensor for Human Manipulation Research. In *Proceedings of the 2011 IEEE World Haptics Conference (WHC)*, 2011.

[313] T. Senoo, Y. Yamakawa, S. Mizusawa, A. Namiki, M. Ishikawa, and M. Shimojo. Skillful manipulation based on high-speed sensory-motor fusion. In *2009 IEEE International Conference on Robotics and Automation*, pages 1611–1612. IEEE, May 2009. doi:10.1109/ROBOT.2009.5152852.

[314] A. Serino and P. Haggard. Touch and the body. *Neuroscience and biobehavioral reviews*, 34(2):224–36, Feb. 2010. doi:10.1016/j.neubiorev.2009.04.004.

[315] C. E. Shannon. A mathematical theory of communication. *ACM SIGMOBILE Mobile Computing and Communications Review*, 5(1):3, Jan. 2001. doi:10.1145/584091.584093.

[316] C. E. Sherrick and R. W. Cholewiak. Cutaneous Sensitivity. In K. R. Boff, L. Kaufman, and J. P. Thomas, editors, *Handbook of Perception and Human Performance: Volume I*, chapter 12, pages 1–58. John Wiley & Sons, Inc., New York, 1986.

[317] M. Shibata, T. Ota, and S. Hirai. Wiping motion for deformable object handling. In *2009 IEEE International Conference on Robotics and Automation*, pages 134–139. IEEE, May 2009. doi:10.1109/ROBOT.2009.5152448.

[318] T. Shimizu, M. Shikida, K. Sato, and K. Itoigawa. A new type of tactile sensor detecting contact force and hardness of an object. In *Technical Digest. MEMS 2002 IEEE International Conference. Fifteenth IEEE International Conference on Micro Electro Mechanical Systems (Cat. No.02CH37266)*, pages 344–347. IEEE, 2002. doi:10.1109/MEMSYS.2002.984273.

[319] M. Shimojo. Mechanical filtering effect of elastic cover for tactile sensor. *IEEE Transactions on Robotics and Automation*, 13(1):128–132, 1997. doi:10.1109/70.554353.

[320] M. Shimojo, T. Araki, S. Teshigawara, and A. Ming. A net-structure tactile sensor covering free-form surface and ensuring high-speed response. In *2007 IEEE/RSJ International Conference on Intelligent Robots and Systems*, pages 670–675. IEEE, Oct. 2007. doi:10.1109/IROS.2007.4399084.

[321] B. Siciliano. *Springer Handbook of Robotics*. Springer Berlin Heidelberg, Berlin, Heidelberg, 2008. doi:10.1007/978-3-540-30301-5.

[322] J. Solomon and M. Hartmann. Artificial Whiskers Suitable for Array Implementation: Accounting for Lateral Slip and Surface Friction. *IEEE Transactions on Robotics*, 24(5):1157–1167, Oct. 2008. doi:10.1109/TRO.2008.2002562.

[323] J. Son, E. Monteverde, and R. D. Howe. A tactile sensor for localizing transient events in manipulation. In *Proceedings of the 1994 IEEE International Conference on Robotics and Automation*, pages 471–476. IEEE Comput. Soc. Press, 1994. doi:10.1109/ROBOT.1994.351253.

[324] C. Sonoda, T. Miki, and Y. Tateishi. Fuzzy inference based subjective material-recognition system employing a multi-modal tactile sensor. In *2009 IEEE International Conference on Fuzzy Systems*, pages 245–250. IEEE, Aug. 2009. doi:10.1109/FUZZY.2009.5277178.

[325] M. W. Spong, S. Hutchinson, and M. Vidyasagar. *Robot Modeling and Control*. John Wiley & Sons, Inc., New Jersey, 2006.

[326] J. Steffen, R. Haschke, and H. Ritter. Experience-based and tactile-driven dynamic grasp control. In *2007 IEEE/RSJ International Conference on Intelligent Robots and Systems*, pages 2938–2943. IEEE, Oct. 2007. doi:10.1109/IROS.2007.4398960.

[327] J. Steffen, R. Haschke, and H. Ritter. Towards dextrous manipulation using manipulation manifolds. *2008 IEEERSJ International Conference on Intelligent Robots and Systems*, pages 2738–2743, 2008. doi:10.1109/IROS.2008.4650720.

[328] T. Stoyanov, A. Louloudi, H. Andreasson, and A. J. Lilienthal. Comparative Evaluation of Range Sensor Accuracy in Indoor Environments. In *Proceedings of the European Conference on Mobile Robots (ECMR)*, Örebro, Sweden, 2011.

[329] M. W. Strohmayr, H. P. Saal, A. H. Potdar, and P. van der Smagt. The DLR touch sensor I: A flexible tactile sensor for robotic hands based on a crossed-wire approach. In *2010 IEEE/RSJ International Conference on Intelligent Robots and Systems*, number 028056, pages 897–903. IEEE, Oct. 2010. doi:10.1109/IROS.2010.5650191.

[330] C. a. Sugar and G. M. James. Finding the Number of Clusters in a Dataset. *Journal of the American Statistical Association*, 98(463):750–763, Sept. 2003. doi:10.1198/016214503000000666.

[331] S. Sugiyama and S. Hirai. Analysis of sliding of a soft fingertip embedded with a novel micro force/moment sensor: Simulation, experiment, and application. In *2009 IEEE International Conference on Robotics and Automation*, pages 889–894. IEEE, May 2009. doi:10.1109/ROBOT.2009.5152458.

[332] J. Sullivan, B. Mitchinson, M. Pearson, M. Evans, N. Lepora, C. Fox, C. Melhuish, and T. Prescott. Tactile Discrimination using Active Whisker Sensors. *IEEE Sensors Journal*, (c):1–12, 2011. doi:10.1109/JSEN.2011.2148114.

[333] M. Suzuki, Y. Ikejiri, T. Fukutani, and S. Aoyagi. Tactile sensor using gelled polyurethane ultrathin film. In *2009 IEEE Sensors*, number 2, pages 1297–1300. Ieee, Oct. 2009. doi:10.1109/ICSENS.2009.5398395.

[334] Y. Tada and K. Hosoda. Acquisition of Multi-Modal Expression of Slip through Pick-Up Experiences. In *2006 IEEE/RSJ International Conference on Intelligent Robots and Systems*, pages 5810–5815. IEEE, Oct. 2006. doi:10.1109/IROS.2006.282392.

[335] Y. Tada, K. Hosoda, and M. Asada. Learn to grasp utilizing anthropomorphic fingertips together with a vision sensor. In *2005 IEEE/RSJ International Conference on Intelligent Robots and Systems*, pages 3323–3328. IEEE, 2005. doi:10.1109/IROS.2005.1545028.

[336] D. Taddeucci, C. Laschi, R. Lazzarini, R. Magni, P. Dario, and A. Starita. An approach to integrated tactile perception. In *Proceedings of International Conference on Robotics and Automation*, pages 3100–3105. IEEE, IEEE, 1997. doi:10.1109/ROBOT.1997.606759.

[337] K. Tahara, S. Arimoto, and M. Yoshida. Dynamic object manipulation using a virtual frame by a triple soft-fingered robotic hand. In *2010 IEEE International Conference on Robotics and Automation*, pages 4322–4327. IEEE, May 2010. doi:10.1109/ROBOT.2010.5509372.

[338] T. Takahashi, T. Tsuboi, T. Kishida, Y. Kawanami, S. Shimizu, M. Iribe, T. Fukushima, and M. Fujita. Adaptive grasping by multi fingered hand with tactile sensor based on robust force and position control. In *2008 IEEE International Conference on Robotics and Automation*, pages 264–271. Ieee, May 2008. doi:10.1109/ROBOT.2008.4543219.

[339] J. Takamatsu, T. Morita, K. Ogawara, H. Kimura, and K. Ikeuchi. Representation for knot-tying tasks. *IEEE Transactions on Robotics*, 22(1):65–78, Feb. 2006. doi:10.1109/TRO.2005.855988.

[340] S. Takamuku, A. Fukuda, and K. Hosoda. Repetitive grasping with anthropomorphic skin-covered hand enables robust haptic recognition. In *2008 IEEE/RSJ International Conference on Intelligent Robots and Systems*, pages 3212–3217. IEEE, Sept. 2008. doi:10.1109/IROS.2008.4651175.

[341] S. Takamuku, K. Hosoda, and M. Asada. Shaking eases Object Category Acquisition: Experiments with a Robot Arm. In L. Berthouze, C. G. Prince, M. Littman, H. Kozima, and C. Balkenius, editors, *Proceedings of the Seventh International Conference on Epigenetic Robotics: Modeling Cognitive Development in Robotic Systems*. Lund University Cognitive Studies, 2007.

[342] S. Takamuku, T. Iwase, and K. Hosoda. Robust material discrimination by a soft anthropomorphic finger with tactile and thermal sense. In *2008 IEEE/RSJ International Conference on Intelligent Robots and Systems*, pages 3977–3982. Ieee, Sept. 2008. doi:10.1109/IROS.2008.4651156.

[343] K. Tanaka, Y. Kamotani, and Y. Yokokohji. Origami folding by a robotic hand. In *2007 IEEE/RSJ International Conference on Intelligent Robots and Systems*, pages 2540–2547. IEEE, Oct. 2007. doi:10.1109/IROS.2007.4399358.

[344] K. Tanaka, Y. Kihara, and Y. Yokokohji. Synthesizing a desired trajectory and sensory feedback control laws for an origami-folding robot based on the statistical characteristics of direct teaching by a human. In *2009 IEEE International Conference on Robotics and Automation*, pages 126–133. IEEE, May 2009. doi:10.1109/ROBOT.2009.5152368.

[345] Y. Tanaka, K. Doumoto, A. Sano, and H. Fujimoto. Active tactile sensing of stiffness and surface condition using balloon expansion. In *2009 2nd Conference on Human System Interactions*, pages 54–59. IEEE, May 2009. doi:10.1109/HSI.2009.5090953.

[346] Y. Tanaka, K. Doumoto, A. Sano, and H. Fujimoto. Development of a sensor system with syringe based on tactile sensing using balloon expansion, May 2010. doi:10.1109/ROBOT.2010.5509877.

[347] Y. Tanaka, R. Sugimura, A. Sano, and H. Fujimoto. An active tactile sensor using fluid for body tissue. In *2008 IEEE/RSJ International Conference on Intelligent Robots and Systems*, pages 71–76. IEEE, Sept. 2008. doi:10.1109/IROS.2008.4651136.

[348] Y. Tanaka, M. Tanaka, and S. Chonan. Development of a sensor system for collecting tactile information. *Microsystem Technologies*, 13(8-10):1005–1013, Nov. 2006. doi:10.1007/s00542-006-0307-8.

[349] M. M. Taylor and S. J. Lederman. Tactile roughness of grooved surfaces: A model and the effect of friction. *Perception & Psychophysics*, 17(1):23–36, Jan. 1975. doi:10.3758/BF03203993.

[350] J. Tegin and J. Wikander. Tactile sensing in intelligent robotic manipulation – a review. *Industrial Robot: An International Journal*, 32(1):64–70, 2005. doi:10.1108/01439910510573318.

[351] S. Teshigawara, M. Ishikawa, and M. Shimojo. Development of high speed and high sensitivity slip sensor. In *2008 IEEE/RSJ International Conference on Intelligent Robots and Systems*, pages 47–52. IEEE, Sept. 2008. doi:10.1109/IROS.2008.4650688.

[352] S. Teshigawara, M. Ishikawa, and M. Shimojo. Study of high speed and high sensitivity slip sensor characteristic of conductive material. In *2008 SICE Annual Conference*, pages 900–903. IEEE, Aug. 2008. doi:10.1109/SICE.2008.4654782.

[353] S. Teshigawara, S. Shimizu, K. Tadakuma, M. Aiguo, M. Shimojo, and M. Ishikawa. High sensitivity slip sensor using pressure conductive rubber. In *2009 IEEE Sensors*, pages 988–991. Ieee, Oct. 2009. doi:10.1109/ICSENS.2009.5398213.

[354] S. Teshigawara, S. Shimizu, T. Tsutsumi, Y. Suzuki, A. Ming, M. Shimojo, and M. Ishikawa. High sensitivity slip sensor using pressure conductive rubber for dexterous grasp and manipulation. In *2010 IEEE Sensors*, pages 570–574. IEEE, Nov. 2010. doi:10.1109/ICSENS.2010.5690469.

[355] S. Teshigawara, K. Tadakuma, M. Ishikawa, and M. Shimojo. High sensitivity initial slip sensor for dexterous grasp. In *2010 IEEE International Conference on Robotics and Automation*, pages 4867–4872. IEEE, May 2010. doi:10.1109/ROBOT.2010.5509288.

[356] S. Teshigawara, K. Tadakuma, A. Ming, M. Ishikawa, and M. Shimojo. Development of high-sensitivity slip sensor using special characteristics of pressure conductive rubber. In *2009 IEEE International Conference on Robotics and Automation*, pages 3289–3294. IEEE, May 2009. doi:10.1109/ROBOT.2009.5152388.

[357] S. Teshigawara, T. Tsutsumi, S. Shimizu, Y. Suzuki, A. Ming, M. Ishikawa, and M. Shimojo. Highly sensitive sensor for detection of initial slip and its application in a multi-fingered robot hand. In *2011 IEEE International Conference on Robotics and Automation*, pages 1097–1102. IEEE, May 2011. doi:10.1109/ICRA.2011.5979750.

[358] G. Tholey and J. P. Desai. A Modular, Automated Laparoscopic Grasper with Three-Dimensional Force Measurement Capability. In *Proceedings 2007 IEEE International Conference on Robotics and Automation*, number April, pages 250–255. IEEE, Apr. 2007. doi:10.1109/ROBOT.2007.363795.

[359] J. Tian and Y.-b. Jia. Modeling deformable shell-like objects grasped by a robot hand. In *2009 IEEE International Conference on Robotics and Automation*, pages 1297–1302. IEEE, May 2009. doi:10.1109/ROBOT.2009.5152736.

[360] J. Tian and Y.-b. Jia. Modeling Deformations of General Parametric Shells Grasped by a Robot Hand. *IEEE Transactions on Robotics*, 26(5):837–852, Oct. 2010. doi:10.1109/TRO.2010.2050350.

[361] P. Tiezzi and I. Kao. Modeling of Viscoelastic Contacts and Evolution of Limit Surface for Robotic Contact Interface. *IEEE Transactions on Robotics*, 23(2):206–217, Apr. 2007. doi:10.1109/TRO.2006.889494.

[362] M. Toussaint, N. Plath, T. Lang, and N. Jetchev. Integrated motor control, planning, grasping and high-level reasoning in a blocks world using probabilistic inference. In *2010 IEEE International Conference on Robotics and Automation*, pages 385–391. IEEE, May 2010. doi:10.1109/ROBOT.2010.5509831.

[363] F. Tremblay, A.-C. Mireault, L. Dessureault, H. Manning, and H. Sveistrup. Postural stabilization from fingertip contact: I. Variations in sway attenuation, perceived stability and contact forces with aging. *Experimental brain research. Experimentelle Hirnforschung. Expérimentation cérébrale*, 157(3):275–85, Aug. 2004. doi:10.1007/s00221-004-1830-4.

[364] F. Tremblay, A.-C. Mireault, L. Dessureault, H. Manning, and H. Sveistrup. Postural stabilization from fingertip contact II. Relationships between age, tactile sensibility and magnitude of contact forces. *Experimental brain research. Experimentelle Hirnforschung. Expérimentation cérébrale*, 164(2):155–64, July 2005. doi:10.1007/s00221-005-2238-5.

[365] M. Tremblay and M. R. Cutkosky. Estimating friction using incipient slip sensing during a manipulation task. In *[1993] Proceedings IEEE International Conference on Robotics and Automation*, volume 1, pages 429–434. IEEE Comput. Soc. Press, 1993. doi:10.1109/ROBOT.1993.292018.

[366] C.-h. D. Tsai and I. Kao. The latency model for viscoelastic contact interface in robotics: Theory and experiments. In *2009 IEEE International Conference on Robotics and Automation*, pages 1291–1296. IEEE, May 2009. doi:10.1109/ROBOT.2009.5152679.

[367] L.-C. Tsao, M.-Y. Cheng, I.-L. Chen, W.-P. Shih, Y.-J. Yang, F.-Y. Chang, K.-C. Fan, and S.-H. Chang. Flexible Temperature Sensor Array using Electro-Resistive Polymer Forhumanoid Artificial Skin. In *TRANSDUCERS 2007 - 2007 International Solid-State Sensors, Actuators and Microsystems Conference*, pages 2287–2290. IEEE, 2007. doi:10.1109/SENSOR.2007.4300626.

[368] N. Tsujiuchi, T. Koizumi, A. Ito, H. Oshima, Y. Nojiri, Y. Tsuchiya, and S. Kurogi. Slip Detection with Distributed-Type Tactile Sensor. *2004 IEEERSJ International Conference on Intelligent Robots and Systems IROS IEEE Cat No04CH37566*, pages 331–336, 2004. doi:10.1109/IROS.2004.1389373.

[369] J. Ueda, A. Ikeda, and T. Ogasawara. Grip-force control of an elastic object by vision-based slip-margin feedback during the incipient slip. *IEEE Transactions on Robotics*, 21(6):1139–1147, Dec. 2005. doi:10.1109/TRO.2005.853496.

[370] J. Ulmen and M. R. Cutkosky. A robust, low-cost and low-noise artificial skin for human-friendly robots. In *2010 IEEE International Conference on Robotics and Automation*, pages 4836–4841, Anchorage, Alaska, USA, May 2010. IEEE. doi:10.1109/ROBOT.2010.5509295.

[371] A. B. Vallbo and R. S. Johansson. Properties of cutaneous mechanoreceptors in the human hand related to touch sensation. *Human neurobiology*, 3(1):3–14, Jan. 1984.

[372] R. W. Van Boven, R. H. Hamilton, T. Kauffman, J. P. Keenan, and A. Pascual-Leone. Tactile spatial resolution in blind braille readers. *Neurology*, 54(12):2230–6, June 2000.

[373] D. J. van den Heever, K. Schreve, and C. Scheffer. Tactile Sensing Using Force Sensing Resistors and a Super-Resolution Algorithm. *IEEE Sensors Journal*, 9(1):29–35, Jan. 2009. doi:10.1109/JSEN.2008.2008891.

[374] F. Vega-Bermudez and K. O. Johnson. Differences in spatial acuity between digits. *Neurology*, 56(10):1389–91, May 2001.

[375] F. Vidal-Verdu, M. J. Barquero, J. Seron, and A. Garcia-Cerezo. Large area smart tactile sensor for rescue robot. In *2009 IEEE International Workshop on Robotic and Sensors Environments*, pages 6–10. IEEE, Nov. 2009. doi:10.1109/ROSE.2009.5355985.

[376] H. Wakamatsu. Knotting/Unknotting Manipulation of Deformable Linear Objects. *The International Journal of Robotics Research*, 25(4):371–395, Apr. 2006. doi:10.1177/0278364906064819.

[377] J. Wang. Consistent selection of the number of clusters via crossvalidation. *Biometrika*, 97(4):893–904, Dec. 2010. doi:10.1093/biomet/asq061.

[378] Z. Wang and S. Hirai. Green strain based FE modeling of rheological objects for handling large deformation and rotation. In *2011 IEEE International Conference on Robotics and Automation*, number 1, pages 4762–4767. IEEE, May 2011. doi:10.1109/ICRA.2011.5979732.

[379] A. B. Watson. *Temporal sensitivity*, volume 1 of *Handbook of Perception and Human Performance*, chapter 6, pages 1–43. Wiley, 1986.

[380] K. Weiss and H. Worn. The working principle of resistive tactile sensor cells. In *IEEE International Conference Mechatronics and Automation, 2005*, number July, pages 471–476. IEEE, 2005. doi:10.1109/ICMA.2005.1626593.

[381] G. Westling and R. S. Johansson. Factors influencing the force control during precision grip. *Experimental Brain Research*, 53(2):277–284, Jan. 1984. doi:10.1007/BF00238156.

[382] G. Westling and R. S. Johansson. Responses in glabrous skin mechanoreceptors during precision grip in humans. *Experimental brain research. Experimentelle Hirnforschung. Expérimentation cérébrale*, 66(1):128–40, Jan. 1987.

[383] N. Wettels, A. Parnandi, G. Loeb, and G. Sukhatme. Grip Control Using Biomimetic Tactile Sensing Systems. *IEEE/ASME Transactions on Mechatronics*, 14(6):718–723, Dec. 2009. doi:10.1109/TMECH.2009.2032686.

[384] N. Wettels, V. J. Santos, R. S. Johansson, and G. E. Loeb. Biomimetic Tactile Sensor Array. *Advanced Robotics*, 22(8):829–849, Aug. 2008. doi:10.1163/156855308X314533.

[385] T. A. Whitaker, C. Simões Franklin, and F. N. Newell. Vision and touch: independent or integrated systems for the perception of texture? *Brain research*, 1242:59–72, Nov. 2008. doi:10.1016/j.brainres.2008.05.037.

[386] H. William, Y. Ibrahim, and B. Richardson. A Tactile Sensor for Incipient Slip Detection. *International Journal of Optomechatronics*, 1(1):46–62, Jan. 2007. doi:10.1080/15599610701232655.

[387] N. Wirth. The programming language pascal. *Acta Informatica*, 1(1):35–63, 1971. doi:10.1007/BF00264291.

[388] D. Yamada, T. Maeno, and Y. Yamada. Artificial finger skin having ridges and distributed tactile sensors used for grasp force control. In *Proceedings 2001 IEEE/RSJ International Conference on Intelligent Robots and Systems. Expanding the Societal Role of Robotics in the the Next Millennium (Cat. No.01CH37180)*, pages 686–691. IEEE, 2001. doi:10.1109/IROS.2001.976249.

[389] Y. Yamada, I. Fujimoto, T. Morizono, Y. Umetani, T. Maeno, and D. Yamada. Development of artificial skin surface ridges with vibrotactile sensing elements for incipient slip detection. In *Conference Documentation International Conference on Multisensor Fusion and Integration for Intelligent Systems. MFI 2001 (Cat. No.01TH8590)*, pages 251–257. VDI/VDE Soc. Meas. & Autom. Control, 2001. doi:10.1109/MFI.2001.1013543.

[390] Y. Yamada, A. Ishiguro, and Y. Uchikawa. A method of 3D object reconstruction by fusing vision with touch using internal models with global and local deformations. In *Proceedings IEEE International Conference on Robotics and Automation*, pages 782–787. IEEE Comput. Soc. Press, 1993. doi:10.1109/ROBOT.1993.291939.

[391] Y. Yamakawa, A. Namiki, M. Ishikawa, and M. Shimojo. One-handed knotting of a flexible rope with a high-speed multifingered hand having tactile sensors. In *2007 IEEE/RSJ International Conference on Intelligent Robots and Systems*, pages 703–708. IEEE, Oct. 2007. doi:10.1109/IROS.2007.4399379.

[392] Y. Yamakawa, A. Namiki, M. Ishikawa, and M. Shimojo. Knotting manipulation of a flexible rope by a multifingered hand system based on skill synthesis. In *2008 IEEE/RSJ International Conference on Intelligent Robots and Systems*, pages 2691–2696. IEEE, Sept. 2008. doi:10.1109/IROS.2008.4650802.

[393] Y.-J. Yang, M.-Y. Cheng, S.-C. Shih, X.-H. Huang, C.-M. Tsao, F.-Y. Chang, and K.-C. Fan. A 32 × 32 temperature and tactile sensing array using PI-copper films. *The International Journal of Advanced Manufacturing Technology*, 46(9-12):945–956, Feb. 2009. doi:10.1007/s00170-009-1940-z.

[394] M. Yoshida, S. Arimoto, and J.-h. Bae. Blind Grasp and Manipulation of a Rigid Object by a Pair of Robot Fingers with Soft Tips. In *Proceedings 2007 IEEE International Conference on Robotics and Automation*, number April, pages 4707–4714. IEEE, Apr. 2007. doi:10.1109/ROBOT.2007.364204.

[395] T. Yoshikawa. Manipulability of Robotic Mechanisms. *The International Journal of Robotics Research*, 4(2):3–9, June 1985. doi:10.1177/027836498500400201.

[396] J.-i. Yuji and C. Sonoda. A PVDF Tactile Sensor for Static Contact Force and Contact Temperature. In *2006 5th IEEE Conference on Sensors*, pages 738–741. IEEE, Oct. 2006. doi:10.1109/ICSENS.2007.355574.

[397] H. Yussof, N. Morisawa, J. Wada, and M. Ohka. Handling capabilities of two robot hands equipped with optical three-axis tactile sensor. In *RO-MAN 2009 - The 18th IEEE International Symposium on Robot and Human Interactive Communication*, pages 165–170. IEEE, Sept. 2009. doi:10.1109/ROMAN.2009.5326224.

[398] H. Yussof and M. Ohka. Grasp synthesis based on tactile sensation in robot manipulation of arbitrary located object. In *2009 IEEE/ASME International Conference on Advanced Intelligent Mechatronics*, pages 560–565. IEEE, July 2009. doi:10.1109/AIM.2009.5229954.

[399] H. Yussof, M. Ohka, A. R. Omar, and M. A. Ayub. Determination of object stiffness control parameters in robot manipulation using a prototype optical three-axis tactile sensor. In *2008 IEEE Sensors*, pages 992–995. IEEE, Oct. 2008. doi:10.1109/ICSENS.2008.4716609.

[400] H. Yussof, J. Wada, and M. Ohka. A New Control Algorithm Based on Tactile and Slippage Sensation for Robotic Hand. In *World Automation Congress (WAC), 2010*, pages 1–6, 2010.

[401] D. Zbyszewski, A. Bhaumik, K. A. Althoefer, and L. D. Seneviratne. Tactile sensing using a novel air cushion sensor: A feasibility study. In *2008 IEEE/RSJ International Conference on Intelligent Robots and Systems*, pages 41–46. IEEE, Sept. 2008. doi:10.1109/IROS.2008.4651070.

[402] D. Zbyszewski, P. Polygerinos, L. D. Seneviratne, and K. A. Althoefer. A novel MRI compatible air-cushion tactile sensor for Minimally Invasive Surgery. In *2009 IEEE/RSJ International Conference on Intelligent Robots and Systems*, pages 2647–2652. IEEE, Oct. 2009. doi:10.1109/IROS.2009.5354140.

[403] H. Zghal, R. Dubey, and J. Euler. Efficient gradient projection optimization for manipulators with multiple degrees of redundancy. In *Proceedings., IEEE International Conference on Robotics and Automation*, pages 1006–1011. IEEE Comput. Soc. Press, 1990. doi:10.1109/ROBOT.1990.126123.

[404] H. Zhang and N. N. Chen. Control of contact via tactile sensing. *IEEE Transactions on Robotics and Automation*, 16(5):482–495, 2000. doi:10.1109/70.880799.